

Some pages of this thesis may have been removed for copyright restrictions.

If you have discovered material in Aston Research Explorer which is unlawful e.g. breaches copyright, (either yours or that of a third party) or any other law, including but not limited to those relating to patent, trademark, confidentiality, data protection, obscenity, defamation, libel, then please read our [Takedown policy](#) and contact the service immediately (openaccess@aston.ac.uk)

"THE DRYING OF SMALL DROPS OF PARTICULATE SLURRIES"

by

HOE WAI CHEONG

A Thesis submitted to
The University of Aston in Birmingham
for the Degree of
Doctor of Philosophy

September

1983

To my wife KO LEE
for bringing our son BENJAMIN
into this world.

SUMMARY

"THE DRYING OF SMALL DROPS OF PARTICULATE SLURRIES"

HOE WAI CHEONG

Ph.D.

September 1983

The literature on the evaporation of drops of pure liquids, drops containing solids and droplet sprays has been critically reviewed.

An experimental study was undertaken on the drying of suspended drops of pure water and aqueous sodium sulphate decahydrate with concentrations varying from 5 to 54.1 wt.%.

Individual drops were suspended from a glass filament balance in a 26 mm I.D. vertical wind tunnel, designed and constructed to supply hot de-humidified air, to simulate conditions encountered in commercial spray driers. A novel thin film thermocouple was developed to facilitate the simultaneous measurement of drop weight and core temperature. The heat conduction through the thermocouple was reduced because of its unique design; using essentially a single 50 μ diameter nickel wire.

For pure water drops, the Nusselt number was found to be a function of the Reynolds, Prandtl and Transfer numbers for a temperature range between 19 to 79°C.

$$Nu = 2 + 0.19 (1/B)^{0.24} Re^{0.5} Pr^{0.33}$$

Two distinct periods were observed during the drying of aqueous sodium sulphate decahydrate. The first period was characterised by the evaporation from a free liquid surface, whilst drying in the second period was controlled by the crust resistance. Fracturing of the crust occurred randomly but was more frequent at higher concentrations and temperatures.

A model was proposed for the drying of slurry drops, based on a receding evaporation interface. The model was solved numerically for the variation of core temperature, drop weight and crust thickness as a function of time. Experimental results were in excellent agreement with the model predictions although at higher temperatures modifications to the model had to be made to accommodate the unusual behaviour of sodium sulphate slurries, i.e. the formation of hydrates.

Key Words: Thin Film Thermocouple
Receding Evaporation Interface
Slurry Drop Drying

ACKNOWLEDGEMENTS

The author wishes to express his gratitude to Professor G V Jeffreys for his dedicated supervision and encouragement throughout the course of this research programme.

The author also wishes to thank the following:

Dr C J Mumford, for his encouragement and helpful advice;

Mr N Roberts and his staff, for their advice and co-operation;

The Department of Physics, for the use of their vacuum coating equipment;

The Department of Metallurgy, for the use of their Scanning Electron Microscope;

Mrs A Davies, for diligently typing this thesis;

My parents, for their continual encouragement; and

The University of Aston in Birmingham and the Science and Engineering Research Council, for funding the research project.

LIST OF FIGURES

<u>Figure</u>	<u>Title</u>	<u>Page</u>
4.1	Characteristics of drying droplets at air temperatures below the boiling point (72).	47
4.2	Characteristics of drying droplets at air temperatures above the boiling point (72).	47
4.3	Drying curves for aqueous sodium sulphate drops.	48
4.4	Drying rate curves for aqueous sodium sulphate drops with an initial moisture content of 9.6 kg water/kg solute (83).	48
6.1	Drop temperature history for reconstituted dried whole milk (15).	65
6.2	Drop temperature histories for aqueous sodium sulphate (68, 72).	65
6.3	Drop temperature histories of aqueous sodium sulphate at initial moisture content of 9.6 kg water/kg solute (83).	69

<u>Figure</u>	<u>Title</u>	<u>Page</u>
6.4	Comparison between experimental and calculated drop temperatures for a drop containing skimmed milk (83).	69
8.1	Schematic Diagram of Wind Tunnel.	96
8.2	Air reservoir - Schematic Diagram of Pipework.	98
8.3	Pipework Assembly into Gas Cylinder.	99
8.4	Air Drier Assembly	101
8.5	Air Heater Assembly	101
8.6	Working Section and Viewing Window Assembly.	104
8.7	Typical velocity profile across the working section.	105
8.8	Filament Holder Assembly	108
8.9	Procedure for insertion of Nickel Wire into the Hollow Filament.	110
8.10	Threaded Filament Ready for Coating.	110
8.11	Mild Steel Frame	112

<u>Figure</u>	<u>Title</u>	<u>Page</u>
8.12	Thin Film Thermocouple Holder Assembly	114
8.13	The Cold Junction and its location in the Ice Container.	115
9.1	Glass Filament Calibration Curve (C4,5,6).	120
9.2	Thin Film Glass Filament Thermocouple Calibration Curve for $V \leq 1.1$ mV.	124
9.3	Thin Film Glass Filament Thermocouple Calibration Curve for $1.1 \text{ mV} < V < 2.65$ mV.	125
10.1	Plot of Nu against $Re^{0.5} Pr^{0.33}$ at Ambient Temperature (21°C).	133
10.2	Plot of Nu against $Re^{0.5} Pr^{0.33}$ for T_g at 33.5 and 34°C.	136
10.3	Plot of Nu against $Re^{0.5} Pr^{0.33}$ for T_g at 46.25°C.	136
10.4	Plot of Nu against $Re^{0.5} Pr^{0.33}$ for T_g at 63°C.	137
10.5	Plot of Nu against $Re^{0.5} Pr^{0.33}$ for T_g at 79°C.	137

<u>Figure</u>	<u>Title</u>	<u>Page</u>
10.6	Plot of Nu against $(1/B)^{0.24} Re^{0.5} Pr^{0.33}$ for T_g between 19.5 - 79°C.	139
10.7	Drying of drops of aqueous sodium sulphate decahydrate (5 wt.%) at varying velocities.	142
10.8	Drying of drops of aqueous sodium sulphate decahydrate (5 wt.%) at high temperatures.	144
10.9	Drying of drops of aqueous sodium sulphate decahydrate (15 wt.%) at varying velocities.	147
10.10	Drying of drops of aqueous sodium sulphate decahydrate (15 wt.%) at high temperatures.	149
10.11	Drying of drops of aqueous sodium sulphate decahydrate with varying initial concen- trations ($v = 1.08 \text{ ms}^{-1}$)	150
10.12	Simultaneous Drop Weight and Core Temperature Measurements at $T_g = 20^\circ\text{C}$.	153
10.13	Simulatneous Drop Weight and Core Temperature Measurements at $T_g = 40.7^\circ\text{C}$.	155
10.14	Simultaneous Drop Weight and Core Temperature Measurements at $T_g = 59.3^\circ\text{C}$.	156

<u>Figure</u>	<u>Title</u>	<u>Page</u>
10.15	Simultaneous Drop Weight and Core Temperature Measurements at $T_g = 78.3^\circ\text{C}$.	157
10.16	Comparison of Experimental Core Temper- atures with Model Predictions at $T_g = 20^\circ\text{C}$.	163
10.17	Comparison of Experimental Core Temper- atures with Model Predictions at $T_g = 40.7^\circ\text{C}$.	164
10.18	Comparison of Experimental Core Temper- atures with Model Predictions at $T_g = 59.3^\circ\text{C}$.	165
10.19	Comparison of Experimental Core Temper- atures with Model Predictions at $T_g = 78.3^\circ\text{C}$.	166
10.20	Model Predictions of Crust Thickness as a function of time for $C_o = 40 \text{ wt.}\%$.	167

LIST OF TABLES

<u>Table</u>	<u>Title</u>	<u>Page</u>
5.1	Droplet Size Distribution Functions.	56
10.1	Evaporation of Water Drops at Ambient Temperature.	132
10.2	Values of ϕ at Elevated Temperatures.	138
A1-A35	Water Drops at Ambient Temperatures.	208-225
A36-A39	Water Drops at Elevated Temperatures.	227-230
B1-B19	Drops of Aqueous Sodium Sulphate Decahydrate ($C_0 = 5-54.1$ wt.%)	233-242
C1-C7	Drops of Aqueous Sodium Sulphate Decahydrate ($C_0 = 40$ wt.%)	245-248
C8-C11	Experimental Core Temperature Measurements.	250-253
D1-D4	Model Predictions	262-265

LIST OF PLATES

<u>Plate</u>	<u>Title</u>	<u>Page</u>
8.1	Layout of the Wind Tunnel	95
10.1	Decrease in drop diameter of a suspended drop of water at ambient temperature and an air velocity of 0.5 ms^{-1} .	134
10.2	Crust surface of a particle dried with an air velocity of 0.50 ms^{-1} ($C_O = 5 \text{ wt.}\%$, $T_g = 18^\circ\text{C}$).	143
10.3	Crust surface of a particle dried with an air velocity of 2.92 ms^{-1} ($C_O = 5 \text{ wt.}\%$, $T_g = 19.5^\circ\text{C}$).	143
10.4	Crust surface of a particle dried at $T_g = 66.5^\circ\text{C}$ ($C_O = 5 \text{ wt.}\%$, $v = 1.10 \text{ ms}^{-1}$).	145
10.5	Crust surface of a particle dried at $T_g = 110^\circ\text{C}$ ($C_O = 5 \text{ wt.}\%$, $v = 1.09 \text{ ms}^{-1}$)	145
10.6	Crust surface of a particle dried at an air velocity of 3.0 ms^{-1} ($C_O = 15 \text{ wt.}\%$, $T_g = 22^\circ\text{C}$)	148
10.7	Crust surface showing a 'blow hole' at an air velocity of 3.0 ms^{-1} ($C_O = 15 \text{ wt.}\%$, $T_g = 22^\circ\text{C}$).	148

<u>Plate</u>	<u>Title</u>	<u>Page</u>
10.8	Crust surface showing fracture ($T_g = 20^\circ\text{C}$, $C_o = 54.1 \text{ wt.}\%$, $v = 1.08 \text{ ms}^{-1}$)	151
10.9	Crust surface of a particle dried at $T_g = 20^\circ\text{C}$ ($C_o = 40 \text{ wt.}\%$, $v = 1.0 \text{ ms}^{-1}$).	151
10.10	Crust surface of a particle dried at $T_g = 59.3^\circ\text{C}$ ($C_o = 40 \text{ wt.}\%$, $v = 1.0 \text{ ms}^{-1}$).	159
10.11	Crust surface of a particle dried at $T_g = 78.3^\circ\text{C}$ ($C_o = 40 \text{ wt.}\%$, $v = 1.0 \text{ ms}^{-1}$).	159
10.12	A drop of slurry ($C_o = 40 \text{ wt.}\%$) suspended from the thin film thermocouple, drying at 20°C .	160

CONTENTS

	<u>Page</u>
SUMMARY	i
ACKNOWLEDGEMENTS	ii
LIST OF FIGURES	iii
LIST OF TABLES	viii
LIST OF PLATES	ix
CHAPTER 1 <u>INTRODUCTION</u>	1
CHAPTER 2 <u>MASS TRANSFER ACROSS A PHASE BOUNDARY</u>	5
2.1 Two-Film Theory	7
2.2 Penetration Theory	8
2.3 Film-Penetration Theory	8
2.4 Boundary Layer Theory	9
CHAPTER 3 <u>DROPLET HEAT AND MASS TRANSFER</u>	10
3.1 Evaporation from Single Droplets and Spheres Under Natural Convection	12
3.2 Evaporation from Single Droplets and Spheres Under Forced Convection	16
3.2.1 Mass Transfer	16
3.2.2 Heat Transfer	27
3.3 Evaporation of Single Droplets at Elevated Temperatures	30

CHAPTER 4	<u>DROPS CONTAINING DISSOLVED AND SUSPENDED SOLIDS</u>	39
4.1	Moisture Movement Through Porous Media	41
4.1.1	Diffusion Theory	41
4.1.2	Capillary Flow Theory	42
4.1.3	Evaporation-Condensation Theory	43
4.1.4	Simultaneous Heat and Mass Transfer Models Based on Irreversible Thermodynamics	43
4.2	Evaporation of Single Droplets Containing Dissolved and Suspended Solids.	43
CHAPTER 5	<u>EVAPORATION OF SPRAYS OF DROPLETS</u>	54
5.1	Sprays of Pure Liquids	57
5.2	Sprays Containing Dissolved and Suspended Solids	59
CHAPTER 6	<u>TEMPERATURE OF EVAPORATING DROPLETS</u>	62
CHAPTER 7	<u>MATHEMATICAL MODELS</u>	71
7.1	Pure Liquid Drops	72
7.1.1	Nusselt Number	72
7.1.2	Heat Transferred to a Drop by Radiation	74
7.1.3	Heat Transferred to a Drop Through Suspension Filament	75
7.1.4	Heat Transferred to a Drop Through The Thin Film Glass Filament Thermocouple	79
7.2	Receding Evaporation Interface Model	81
7.2.1	Heat Transfer at Evaporation Interface	82
7.2.2	Mass Transfer at Evaporation Interface	87

		<u>Page</u>
CHAPTER 8	<u>EXPERIMENTAL APPARATUS</u>	92
8.1	Wind Tunnel	94
8.1.1	Air Reservoir	94
8.1.2	Air Drier	97
8.1.3	Rotameter	100
8.1.4	Air Heater	102
8.1.5	The Working Section	102
8.2	Drop Suspension Filament	106
8.2.1	Glass Filament Fabrication	106
8.2.2	Filament Holder and Deflection Measurement	107
8.3	Thin Film Glass Filament Thermocouple	107
8.3.1	Thin Film Thermocouple Fabrication	109
8.3.2	Thin Film Thermocouple Holder	113
8.3.3	Cold Junction	113
8.3.4	Voltage Indicator and Recorder	116
CHAPTER 9	<u>EXPERIMENTAL PROCEDURE</u>	117
9.1	Instrument Calibration	118
9.1.1	Air Flowrate	118
9.1.2	Temperature	119
9.1.3	Drop Weight	119
9.1.4	Drop Temperature	123
9.2	Experiments	126
9.2.1	Water Drops at Ambient Temperature	126
9.2.2	Water Drops at Elevated Temperature	127
9.2.3	Drops of Aqueous Sodium Sulphate Decahydrate	128
9.2.4	Simultaneous Drop Weight and Drop Temperature Experiments	129

		<u>Page</u>
CHAPTER 10	<u>EXPERIMENTAL RESULTS</u>	130
10.1	Water Drops at Ambient Temperature	
10.2	Water Drops at Elevated Temperatures	131
10.3	Drops of Aqueous Sodium Sulphate Decahydrate	140
10.4	Simultaneous Drop Weight and Core Temperature Measurements of Sodium Sulphate Decahydrate Slurry Drops.	152
10.5	Comparison of Experimental Results and Model Predictions.	161
CHAPTER 11	<u>DISCUSSION</u>	169
11.1	Experimental Techniques	171
11.2	Experimental Results	174
11.2.1	Water Drops at Ambient Temperature	175
11.2.2	Water Drops at Elevated Temperatures	176
11.2.3	Drops of Aqueous Sodium Sulphate Decahydrate	178
11.2.4	Simultaneous Drop Weight and Core Temperature Measurements.	182
11.3	Receding Evaporation Interface Model.	184
CHAPTER 12	<u>CONCLUSIONS AND RECOMMENDATIONS</u>	186
12.1	Conclusions	187
12.2	Recommendations	189

	<u>Page</u>
<u>APPENDIX D</u>	254
D.1 VARIABLES USED IN MODEL	255
D.2 COMPUTER PROGRAM LISTINGS Program Filename: REI MODEL	256
D.3 TABULATION OF MODEL PREDICTIONS	261
NOMENCLATURE	266
REFERENCES	273

CHAPTER 1

INTRODUCTION

CHAPTER 1

INTRODUCTION

Drying is one of the most energy intensive unit operations used in the process industries; because it generally involves the evaporation of water, which has a high latent heat of vaporisation. It is also probably the most common unit operation, since it is invariably encountered in most solids manufacturing processes. Thus there is a wide variety of dryer designs, to cater for the specific solid and drying conditions and finished product specification, in all of which energy economy is important.

Spray drying has found applications in the food, pharmaceutical and chemical industries because of its flexibility in meeting product requirements. It is one of the most economical methods of moisture removal and is especially applicable to heat sensitive materials (94).

Spray drying involves the transformation of a feed in the form of a solution, slurry or paste, into a particulate dried product by the removal of moisture in a single operation. The feed is atomised, to provide a large surface area, and the spray is contacted with a drying medium where a simultaneous heat and mass transfer process occurs. The dried product is then recovered in a series of separation stages.

Particle size distribution features as the most important dried product specification. The ideal product would be one comprising individual particles of equal size. However, in practice, a homogeneous product has not been achieved, although the careful selection of atomising and operating variables can narrow the size range considerably.

In the past, the design of spray dryers has been treated empirically, and the success of existing dryers are due largely to a combination of practical experience and some degree of overdesign, generally following pilot plant trials. One of the prerequisites for the optimum design of spray dryers is an understanding of the controlling mechanisms in the heat and mass transfer process during drying. Although a great deal of fundamental research had been carried out on the evaporation of pure liquid drops (11, 14, 15, 22, 32), experimental data on

the drying of drops containing solids has been limited. This can be attributed partly to the complexities in analysing the heat and mass transfer process after a solid crust has formed. Heat is transferred by convection from the drying medium to the outer surface of the crust and by conduction to the interior. Evaporation then occurs and moisture diffuses through the crust and into the surroundings. As the particle dries, the crust increases in thickness resulting in an increase in the resistance to heat and mass transfer. This invariably increases the core temperature causing a reduction in the partial pressure and temperature driving forces. The transfer process is therefore highly complex and difficult to model mathematically. Furthermore, after the formation of a crust, fracture, shrinkage or inflation may occur, adding a further constraint to any attempt at modelling the drying process.

The present study was therefore initiated to further the understanding of the mechanisms involved in the drying of drops containing solids with the objective of improving the design of spray dryers.

CHAPTER 2

MASS TRANSFER ACROSS A PHASE BOUNDARY

- 2.1 Two-Film Theory
- 2.2 Penetration Theory
- 2.3 Film-Penetration Theory
- 2.4 Boundary Layer Theory

CHAPTER 2

MASS TRANSFER ACROSS A PHASE BOUNDARY

When a concentration gradient exists within a fluid or across a phase boundary, mass transfer will occur to reduce this gradient. Fick (1) deduced, by analogy to heat transfer, that the rate of diffusion of a component A in a mixture of A and B, is directly proportional to the concentration gradient.

$$N_A = -D_{AB} \frac{dC_A}{dy} \quad (2.1)$$

Equation 2.1 is often referred to as Fick's law of diffusion.

A number of mechanisms have been proposed to describe mass transfer across a phase boundary. The two-film theory, the film-penetration theory and more recently the boundary layer theory are the most widely accepted models to describe this phenomenon. On the basis of these theories, a mass transfer coefficient K, can be defined as,

$$N_A = K (C_{A1} - C_{A2}) \quad (2.2)$$

where $(C_{A1} - C_{A2})$ is the concentration driving force.

For the special case of the drying of droplets containing solids, there is an additional crust resistance represented by a crust coefficient k_c . The overall mass transfer coefficient is therefore dependent on the crust coefficient and the gas film coefficient, neglecting any resistance at the interface.

$$\frac{1}{K} = \frac{1}{k_c} + \frac{1}{Hk_g} \quad (2.3)$$

where H = Henry's constant.

To increase the drying rate, an attempt is generally made to maximise the interfacial area, achieved by atomising the feed to produce smaller droplets. However, in practice this also results in a dried product with a large amount of fines which have to be removed in a separation stage.

2.1 Two-Film Theory

In 1923, Whitman (2) attempted to describe the mechanism of mass transfer at the interface between two fluids. He assumed the resistance to transfer lies within a thin laminar layer on either side of the phase boundary and suggested that the film resistances were additive. The concentration gradients are therefore linear within these layers and zero outside. Using Fick's law of diffusion, the model predicts that the overall mass transfer coefficient K , is proportional to the diffusivity D_v .

2.2 Penetration Theory

Higbie (3) laid the basis of the penetration theory for unsteady state mass transfer. He assumed that eddies in the bulk fluid bring discrete elements to the interface where they are exposed to the second phase for a finite period of time. Infinitely fast mass transfer occurs and equilibrium is attained instantaneously. An unsteady state molecular diffusion then occurs and the elements are remixed with the bulk fluid. Solving the unsteady state equations, Higbie showed that the mass transfer coefficient is proportional to $D_v^{0.5}$.

Danckwerts (4) modified the penetration theory by supposing that the surface is continually being replaced by fresh fluid in a random fashion. Assuming the rate of production of fresh surface S_s , is independent of the age of the element, he showed that the average mass transfer coefficient is proportional to $(D_v \cdot S_s)^{0.5}$.

2.3 Film-Penetration Theory

Toor and Marchello (5) incorporated both the principles of the two-film theory and the penetration theory in suggesting that mass transfer occurs as an unsteady state process and that resistance to transfer lies within a laminar film at the interface. Surface renewal was assumed to occur

at intervals due to eddy currents in the bulk fluid. Their analysis showed that for short exposure times, the process can be described by the penetration theory while for prolonged periods, when steady state conditions are justified, the two-film theory is applicable.

2.4 Boundary Layer Theory

The boundary layer theory is the most common approach for predicting heat and mass transfer coefficients for spherical drops. The equations of motion, continuity and energy can be solved approximately to obtain the velocity, concentration and temperature profiles in a thin boundary layer at the interface. Outside the respective boundary layers, flat profiles are assumed. Frössling (6) applied this theory to evaporating drops and showed that the mass transfer coefficient is proportional to $D_v^{0.67}$.

CHAPTER 3

DROPLET HEAT AND MASS TRANSFER

- 3.1 Evaporation from Single Droplets
and Spheres Under Natural Convection
- 3.2 Evaporation from Single Droplets
and Spheres Under Forced Convection
 - 3.2.1 Mass Transfer
 - 3.2.2 Heat Transfer
- 3.3 Evaporation of Single Droplets
at Elevated Temperatures

CHAPTER 3

DROPLET HEAT AND MASS TRANSFER

The evaporation of a liquid droplet is essentially a simultaneous heat and mass transfer process. Maxwell (7) was the first person to publish a theory on the evaporation of droplets, motionless relative to an infinite medium. He assumed that the vapour concentration on the droplet surface C_S , is continuously saturated and showed that,

$$- dm/d\theta = 4\pi r \cdot D_V (C_S - C_\infty) \quad (3.1)$$

From equation 3.1, a gas phase mass transfer coefficient can be defined under stagnant conditions as,

$$k_g = \frac{-dm/d\theta}{4\pi r^2(C_S - C_\infty)} = D_V/r \quad (3.2)$$

The Sherwood number can thus be expressed as

$$Sh_O = k_g (2r)/D_V = 2 \quad (3.3)$$

When a finite relative velocity exists between the drop and continuous phase, additional mass transfer takes place by convection. Frössling (6), by consideration of boundary layer theory, deduced that the right

hand side of equation 3.3 should be multiplied by a 'wind factor', i.e.

$$Sh = 2 (1 + \beta Re^{0.5} Sc^{0.33}) \quad (3.4)$$

where $\beta = 0.276$

Numerous authors have since confirmed these equations which are discussed further in the proceeding sections.

3.1 Evaporation from Single Droplets and Spheres Under Natural Convection

Rates of evaporation were first determined by Sreznevskii (8) in 1882. Experiments were conducted on the convex meniscus at the flat tops of vertical cylindrical columns of 1.8 - 3.6 mm diameter. Evaporation rates were determined by following the outline of the drops through a horizontal microscope.

In 1910, Morse (9) studied the evaporation in air of spheres of iodine placed on the pan of a microbalance and found that the rate of evaporation was proportional to the radii of the spheres. Langmuir (10) investigated Morse's results and derived an equation similar to Maxwell's to account for this proportionality.

Experiments were later carried out by Whytlaw-Gray and Patterson (11) in 1934 on drops of water, aniline, quinoline, methysalicylate and p-cresol with radii of 1-2 mm. He found that the surface of the drops decreased linearly with time, although the volume decreased by a factor of almost a hundred.

No further experiments were made on drops placed on a flat surface; instead, the drops were supported on thin filaments. Measurements by this method were first made in 1927 by Topley and Whytlaw-Gray (12) on spheres of iodine fused to a quartz fibre. The spheres were placed in a cylindrical vessel of radius 2 cm. The walls and bottom of the vessel were covered with a thin layer of potassium hydroxide to absorb the iodine. Their results provided the first quantitative support of Maxwell's equation.

Houghton (13) measured the rate of evaporation of water drops suspended from glass fibres using a horizontal microscope. The fibres were coated with a thin layer of paraffin to reduce distortion and to prevent wetting of the fibre. However, no measurements were taken of drop temperatures.

In their thorough investigation, Langstroth et al. (14) measured optically the evaporation rates of drops of

water and of organic liquids of diameter 1.4 mm. The drops were suspended from glass fibres of 100 μ diameter or from copper-constantan thermocouples. The experiments were carried out in a 20 mm diameter spherical vessel. Although radiation effects were accounted for, the heat flux through the glass fibre was ignored.

Ranz and Marshall (15) studied the evaporation of liquid drops suspended from the end of a glass capillary and thermoelement, inside a special sealed dryer. They correlated their data by the expression,

$$\text{Nu}_O = 2 + 0.60 \text{Pr}^{0.33} \text{Gr}^{0.25} \quad (3.5)$$

Mathers et al. (16) were the first to solve the simultaneous heat and mass transfer equations numerically for natural convection. Their experiments were conducted with internally heated brass spheres coated with naphthalene of 12.7 and 25.4 mm diameter. They proposed,

$$\begin{aligned} \text{Nu}_O &= 2 + 0.282 (\text{Gr.Pr})^{0.37} \\ \text{for } \text{Gr.Pr} &< 10^2 \end{aligned} \quad (3.6)$$

and

$$\begin{aligned} \text{Nu}_O &= 2 + 0.5 (\text{Gr.Pr})^{0.25} \\ \text{for } 10^2 &< \text{Gr.Pr} < 10^6 \end{aligned} \quad (3.7)$$

Working with benzoic acid spheres immersed in a Dewar flask, Steinberger and Treybal (17) divided their data according to the boundary layer becoming turbulent, which they characterised by (Gr.Sc) greater or less than 10^8 . Hence,

$$\begin{aligned} Sh_o &= 0.569 (Gr.Sc)^{0.25} \\ \text{for } Gr.Sc < 10^8 & \end{aligned} \quad (3.8)$$

and

$$\begin{aligned} Sh_o &= 0.0254 (Gr.Sc)^{0.33} \\ \text{for } Gr.Sc > 10^8 & \end{aligned} \quad (3.9)$$

Equation 3.9 was however obtained from only three data points.

Yuge (18) studied the heat transfer under natural convection for internally heated carbon-chrome steel and brass spheres. An auxiliary heater was installed in the support of the spheres to eliminate heat conduction. He expressed his results by,

$$\begin{aligned} Nu_o &= 2 + 0.392 Gr^{0.25} \\ \text{for } 1 < Gr < 10^5 & \end{aligned} \quad (3.10)$$

The evaporation of free drops can also be studied by supporting charged droplets in a Millikan's condenser. Notable studies conducted using this principle were by Woodland and Mack (19) on drops of dibutyl tartrate and

dibutyl phthalate, Nestle (20) on drops of mercury and Gudris and Kulikova (21) on drops of water. Generally, the Millikan's condenser gives less accurate results. Nevertheless it enables droplets as small as a few microns to be studied.

3.2 Evaporation from Single Droplets and Spheres Under Forced Convection

Droplets moving relative to a medium under the influence of gravity and/or inertia are of practical importance since this is the situation in spray dryers. Investigations in this area can generally be classified according to either the mass transfer or heat transfer approach and will be discussed accordingly.

3.2.1 Mass Transfer

The first measurements of the rate of evaporation in a gas stream were apparently those of Majama and Togino (22). Drops of water and organic liquids with diameters of 0.2 mm, were suspended on a horizontal glass fibre in an air current up to 18 ms^{-1} . They found that the rate of change of diameter squared is a constant.

Extremely accurate measurements of evaporation rates of suspended drops in an air current were later made by Frössling (6), whose work has served as a model for all subsequent work in this field. The experiments were carried out on drops of water, aniline and nitrobenzene and spheres of naphthalene with drop diameters of 0.2 - 1.8 mm, at 20°C. The drops were suspended from either a glass fibre or a thermocouple with air velocities between the range 0.2 - 7 ms⁻¹. Evaporation rates were determined photographically and correlated by equation 3.4, with a β value of 0.276. An interesting result observed by Frössling was the variation of evaporation rates over the surface of spheres of naphthalene. Evaporation rate was found to be maximum at the front stagnation point, reducing to a minimum just past the equator, to a lower maximum at the rear of the sphere.

Vyrubov (23) studied the rate of freely falling water drops of 2 mm diameter in a 1 m long vertical tube. Hot air between 40 - 100°C was passed down the tube and droplets collected on a weighing pan. He expressed his results by,

$$\text{Sh} = 0.52 \text{ Re}^{0.5} \quad (3.11)$$

Johnstone and Eades (24) measured the rate of evaporation of drops of dibutyl phthalate, 0.4 - 0.7 mm

diameter, suspended on glass fibres and of molten sulphur on filaments of wolframite at 130 - 190°C in a short horizontal tube of 2 cm diameter. They found that the time for complete evaporation was a function of initial drop radius and their results agree favourably with theoretical predictions.

In their experiments with water drops at 0 - 40°C, Kinzer and Gunn (25) used the method of instantaneous photography with side illumination. Smaller droplets were charged and allowed to fall freely through detector rings while drops greater than 1 mm were supported in free flight by a hydrodynamic force. For the range of drop sizes 0.6 - 3.0 mm diameter, they obtained the same relationship as Frössling (equation 3.4) with a β value of 0.23 for $100 < Re < 1600$. Of exceptional interest however, was their finding that at very small Re (less than 0.9) the 'wind factor' is unity, i.e. $\beta = 0$. As Re increases, β increases to a value of 0.46 at $Re = 4$, then gradually falls to 0.23 at $Re = 100$.

The fundamental work of Ranz and Marshall (15) in 1952 was further confirmation of Frössling's results, differing only in the value of β . They found β to be equal to 0.30. They suspended drops of water and benzene from the capillary end of a microburette of

radius 30-50 μ at air temperatures up to 200°C. Liquid was supplied continuously from the burette maintaining a constant drop size. The experimental data was expressed both as Nusselt and Sherwood numbers and the same relationship applies with Sc replacing Pr.

$$\text{Nu} = 2 + 0.6 \text{Re}^{0.5} \text{Pr}^{0.33} \quad (3.12)$$

and

$$\text{Sh} = 2 + 0.6 \text{Re}^{0.5} \text{Sc}^{0.33} \quad (3.13)$$

The Ranz and Marshall equation has since been the most widely quoted for pure liquid droplets.

By using the same method as the previous workers, i.e. keeping the drop diameter constant, Hsu et al. (26) measured the rate of evaporation of drops of heptane with a diameter of 1.8 mm at 37°C and Re between 70 and 300. They were mainly interested in the influence of droplet shape on the rate of evaporation. Because of the larger drop sizes and low surface tension of heptane, the drops were pear shaped on fine capillaries and truncated spheres on wide ones. They expressed their results by,

$$\text{Sh} = 2 (1 + 0.272 \text{Re}^{0.5} \text{Sc}^{0.33}) [1 + 1.147(1-\mu_h)] \\ [1 - 0.0371(1-d_v/d_h)] \quad (3.14)$$

where $\mu_h = 6 v_1/sd_h$

v_1 = volume

s = surface area

d_h = maximum horizontal distance

d_v = height of drop.

The diameter term in Sh was replaced by $6v_1/s$.

Working with cork spheres wetted with organic liquids, Ingebo (27) proposed that,

$$\text{Sh} = 2 + 0.3 (\text{Re} \cdot \text{Sc})^{0.6} k/k_f \quad (3.15)$$

for $1000 < \text{Re} < 1600$

where k and k_f are the thermal conductivities of air and the diffusing vapour respectively.

However, Maisel and Sherwood (28), working with calcium silicate spheres wetted with water or benzene, found that the benzene evaporated so quickly that the surface of the spheres was never really wetted. It should be noted nevertheless, that their experiments were conducted at a Re range between 2,000 and 50,000.

Garner and Grafton (29) measured the dissolution rate of 12.7 mm diameter pressed benzoic acid spheres in water by a photographic technique and correlated their results by,

$$\text{Sh} = 44 + 0.48 \text{Re}^{0.5} \text{Sc}^{0.33} \quad (3.16)$$

for $20 < \text{Re} < 1000$.

They explained that the limiting value of 44 was due to natural convection. However, in a later investigation Garner and Suckling (30), using the same apparatus and technique and a greater range of sphere sizes, correlated their results together with the earlier work above. Using an assumed limiting value of 2, they found that,

$$Sh = 2 + 0.95 Re^{0.5} Sc^{0.33} \quad (3.17)$$

for $100 < Re < 700$.

Following the technique of previous workers (31), Pasternak and Gauvin (32) suspended spheres of celite impregnated with water from a hypodermic needle. The spheres were placed inside a 38.1 mm diameter glass column through which hot air was passed. Using sphere sizes of 5.59 - 11.63 mm diameter, they correlated their results by,

$$Sh = 0.692 Re^{0.514} Sc^{0.33} \quad (3.18)$$

They confirmed this expression in their later work (33) on radioactive celite spheres impregnated with acetone in free fall; the induced radioactivity being a means of measuring the particle velocity.

Fuchs (34) has suggested that internal circulation in a drop may double the heat and mass transfer. This was illustrated by the work of Ward et al (35). Their results from four systems, water in cyclohexane and cyclohexane, isobutanol and o-toluidine in water showed that mass transfer can be enhanced from 4 - 6 fold. Taking this into account, they proposed,

$$Sh = 0.61 \left[\frac{\mu_c}{\mu_d + \mu_c} \right]^{0.5} (Re.Pr)^{0.5} \quad (3.19)$$

Steinberger and Treybal (17) proposed that natural and forced convection to spheres are additive.

Working with cast benzoic acid spheres of 12.7, 19.1 and 25.4 mm in upward flowing streams of water and propylene glycol, they proposed,

$$Sh = Sh_0 + 0.347 (Re.Sc^{0.5})^{0.62} \quad (3.20)$$

where Sh_0 is the natural convection contribution given by equations 3.8 and 3.9.

Using experimental results published by eleven different authors on heat and mass transfer data from gas as well as liquid streams, they showed that the above correlation gave excellent agreement.

Jones and Smith (36) studied the evaporation of naphthalene, camphor and benzoic acid by suspending spheres in an air stream moving at high velocity through rotameter tubes. They observed that although the particles spun erratically, the mass transfer coefficient showed no significant difference when compared to that from stationary particles. This phenomenon was attributed to the fact that one side of a spinning sphere is stationary relative to the gas while the other side meets the flow at twice its linear velocity. A relationship was proposed which takes into account the Reynolds number of the gas, Re_g . For the laminar region,

$$Sh = 2 + 25 (Re.Sc.Re_g^{0.5})^{0.33} \quad (3.21)$$

and for the turbulent region,

$$Sh = 2 + 0.055 (Re.Sc.Re_g^{0.5})^{0.5} \quad (3.22)$$

Kinard et al. (37) suggested that boundary layer theory cannot accurately predict overall transfer since it takes no account of the turbulent wake behind the droplet. They considered separately the forced convection in front of, and behind, the separation zone of the boundary layer. Using data from Ranz and Marshall (15), Garner and Suckling (30) and Steinberger and Treybal (17), they added an additional term to account for transfer in the wake.

$$Sh = 2.0 + Sh_o + 0.45 Re^{0.5} Sc^{0.33} + 0.00484 Re.Sc^{0.33} \quad (3.23)$$

In the analytical approach by Locheil and Calderbank (38), a quartic velocity profile in the boundary layer around a spherical droplet was assumed. The resultant differential equations were solved and they found that the overall transfer rate can be described by,

$$Sh = 0.84 Re^{0.5} Sc^{0.33} \quad (3.24)$$

However, it was also noted that at the front stagnation point, the maximum transfer can have a coefficient as high as 1.34.

More recently workers have concentrated on local mass transfer rates around an evaporating droplet. Hoffman and Ross (39) presented a theoretical model for predicting heat transfer at the front stagnation point of an evaporating droplet. Their model was based on an assumed temperature profile of polynomial form in the boundary layer. Predictions from the model showed good agreement with the experimental data of Frössling (6), Silbulkin (40) and Aksel'rud (41) for $Re = 200$ but not at the lower Re values. It is quite likely that this discrepancy was due to natural convection effects becoming more predominant. They also proposed that mass transfer causes a decrease in the convective heat transfer, an observation made earlier by Ranz (42). They suggested that the relative decrease is a function only of the Spalding number B' , where,

$$B' = C_p \Delta T / (\lambda - \dot{q}/\dot{m}) \quad (3.25)$$

However, this proposal was not conclusively verified and moreover this effect is only known to occur significantly under intensive evaporation rates.

A unique method of drop suspension was used by Audu (43). He suspended hemispherical drops from a rotating nozzle in a horizontal wind tunnel, exposing all sides of the evaporating drop to the impinging air. For ambient conditions, he expressed his results as,

$$Sh = 2.0 + 0.473 Re^{0.5} Sc^{0.33} \quad (3.26)$$

Although the author suggested that the feed was supplied at an 'appropriate' temperature to minimise extra heat input, it is however not clear how this was achieved. It should be noted that the nozzle, being of the same diameter as the hemispherical drop will impose on the flow pattern of air around the drop resulting in profiles that may not be consistent with that of a spherical drop.

Using a quasi-steady vaporisation model developed earlier (44), Frazier and Chang (45) fitted the results of Hoffman and Gauvin (46) for 700 - 1000 μ drops of water, methanol and benzene and cumene at 130 - 560°C. Their model was based on the integrated values of the physical and transport properties over the vapour film length. They proposed that the evaporation rate be expressed as,

$$\dot{m} = \dot{m}_0 \left[(1 + \dot{m}_0' / \dot{m}_0) f(Gr.Pr) \right] \quad (3.27)$$

where $f(Gr.Pr) = A (Gr.Pr)^{1/n}$

$$A = 0.15, \quad n = 2 \quad \text{for} \quad Gr < 4.22/Pr$$

$$\text{and } A = 0.215, \quad n = 4 \quad \text{for} \quad 4.22/Pr \lesssim Gr < 10^5$$

This model was however not fully tested on data from other sources.

Miura et al. (47) studied the rate of heat and mass transfer from floating droplets in an ascending air current. The apparatus was similar to that of Garner and Kendrick (48). Droplets of water were floated by an 'inverted' parabolic velocity profile, i.e. low velocity in the centre, surrounded by an annular region of high velocity. Their technique was however restricted to the study of relatively large drops (2.9 - 3.3 mm) at high air velocities (7.5 - 9 ms⁻¹). It is interesting to note that their data points were well represented by the Ranz and Marshall equation for drops suspended from a fine capillary.

A laser light scattering technique was used by Davis et al. (49) to determine drop sizes of submicron aerosol droplets. Charged droplets (0.5 - 0.9 μ) were suspended in an electric field in a pressure controlled light scattering cell. Using an argon laser, they were able to measure drop sizes during the evaporation of dioctyl phthalate in helium and nitrogen at 37°C. It should be stressed that this technique is relatively new and extremely accurate especially for submicron droplets.

More recently, Sandoval-Robles et al. (50) studied the mass transfer from a sphere in perfect streamline conditions. A suspended sphere was rotated at constant velocity around a circular channel of

stationary liquid, offering the ideal hydrodynamic condition of no turbulence and a perfectly flat velocity profile. Their results showed a significant dependency on the Reynolds number.

$$\text{For } 2 < \text{Re} < 20, \quad \text{Sh} = 1.032 \text{Re}^{0.385} \text{Sc}^{0.33} \quad (3.28)$$

$$20 < \text{Re} < 2000, \quad \text{Sh} = 0.803 \text{Re}^{0.474} \text{Sc}^{0.33} \quad (3.29)$$

$$\text{and } 2000 < \text{Re} < 23000, \quad \text{Sh} = 0.3 \text{Re}^{0.593} \text{Sc}^{0.33} \quad (3.30)$$

3.2.2 Heat Transfer

Heat transfer from solid spheres was initially studied during the nineteen twenties by Swiss and German physicians and meteorologists using a Davos Frigorimeter. This consists of a hollow blackened internally heated copper sphere with a thermostat to maintain a constant surface temperature. Büttner (51) correlated most of the published data of these workers and concluded that,

$$\text{Nu} = 0.70 \text{Re}^{0.52} \quad (3.31)$$

for $10^3 < \text{Re} < 10^5$

Later, in a comprehensive study, Williams (52) collated data from Büttner (51), Vyrubov (53) and Johnstone et al. (54) and proposed,

$$\text{Nu} = 0.33 \text{Re}^{0.6} \quad (3.32)$$

for $20 < \text{Re} < 150,000$

The author however points out that this equation is not valid at low values of Re.

Kramers (55) used steel spheres of 7.1, 7.9 and 12.6 mm diameter, suspended vertically by a pair of fine thermocouple leads in a vertical stream of air, water or oil. This was the first attempt to work with media other than air. He proposed the correlation,

$$\text{Nu} = 2 + 1.3 \text{Pr}^{0.15} + 0.66 \text{Re}^{0.5} \text{Pr}^{0.31} \quad (3.33)$$

$$\text{for } 0.4 \leq \text{Re} \leq 2000 \text{ and } 0.7 < \text{Pr} < 400$$

The second term on the right hand side was necessary to bring into line data for air, water and oil. However, as pointed out by Rowe et al (56), the Pr term may be a result of disturbance by the high frequency field used for heating the sphere. It is also likely that temperature gradients at the surface of the spheres affected the physical properties of the liquids.

Tsubouchi and Sato (57) used an original technique of measuring steady state heat transfer. They suspended thermistor spheres of 0.3 to 2.0 mm diameter in a wind tunnel. A current was supplied to the sphere and a measure of the voltage, current and resistance gave the amount of heat dissipated and the temperature. Their results were correlated by,

$$\text{Nu} = 2.0 + 0.5 \text{Re}^{0.5} \quad (3.34)$$

$$\text{for } 0.1 < \text{Re} < 1000$$

In an extensive study by Yuge (18) on metal spheres in a wind tunnel, he compared the effects of cross, opposed and parallel flows. For metal spheres less than 6 mm, an unsteady state method was used, a preheated sphere being plunged into an air stream. The larger spheres (6 - 60 mm) were heated internally and an auxiliary heater located on the rear facing supporting stem prevented any heat loss. His results were presented as,

$$\text{Nu} = 2 + 0.493 \text{ Re}^{0.5} \quad (3.35)$$

$$\text{for } 10 < \text{Re} < 1.8 \times 10^3$$

and

$$\text{Nu} = 2 + 0.300 \text{ Re}^{0.5664} \quad (3.36)$$

$$\text{for } 1.8 \times 10^3 < \text{Re} < 1.5 \times 10^5$$

It should be noted however, that a standard deviation in Nu of $\pm 0.1\%$ would be needed to justify the index in equation 3.36 to four significant figures.

Rowe et al. (56) published an excellent review paper on heat and mass transfer to spheres. They presented heat transfer data on the cooling of internally heated copper spheres in air and in water. The dissolution of benzoic acid spheres in water and the sublimation of naphthalene in air were also studied. The heat and mass transfer data in air were correlated as,

$$\text{Nu} = 2 + 0.69 \text{Re}^{0.5} \text{Pr}^{0.33} \quad (3.37)$$

and

$$\text{Sh} = 2 + 0.69 \text{Re}^{0.5} \text{Sc}^{0.33} \quad (3.38)$$

However, a coefficient of 0.79 was observed for water. They suggested that the observed higher transfer rates could be due to uncertainties in predicting the diffusion coefficient in water.

A dilatometric method was used by Adams and Pinder (58) together with cinematography to obtain an average heat transfer coefficient for evaporation of isopentane and cyclopentane in a continuous phase of glycerin-water solution. The method involved injecting a small air bubble into a drop and as evaporation occurred, the increase in volume of the vapour bubble was measured by a dilatometric tube. They fitted their data with the expression,

$$\text{Nu} = 7550 \text{Pr}^{-0.75} [\mu_c / (\mu_c + \mu_d)]^{4.3} \text{Bo}^{0.33} \quad (3.39)$$

3.3 Evaporation of Single Droplets at Elevated Temperatures

When a droplet exists in a relatively high temperature atmosphere two forms of heat transfer must be taken into account; heat transfer resulting from mass transfer and by radiation.

The high temperature gradients present will result in some heat transfer inwards by conduction being used to heat up the vapour diffusing outwards. Ranz (42) showed that the heat actually reaching the surface of an evaporating drop may be as little as 25% of the total heat transferred; the rest being absorbed by the cold vapour in its radial flow from the drop.

Marshall (59) developed a differential equation to describe the differential heat balance over a spherical shell and solved this to give an expression for the temperature T as a function of distance x , through the gas film surrounding the drop.

$$\frac{T - T_S}{T_g - T_S} = \frac{\exp(-E/x) - \exp(-E/r_1)}{\exp(-E/R_f) - \exp(-E/r_1)} \quad (3.40)$$

where $E = \dot{m} C_{pf} / 4\pi k_f$

and $R_f =$ outer radius of gas film

and $r_1 =$ radius of evaporating droplet

One obvious simplification was that he neglected any variation in the thermal conductivity and heat capacity of the gas film, caused by temperature and concentration gradients. However, these effects would be small.

On differentiating the above equation at the surface of the drop, the Nusselt number was expressed as,

$$\text{Nu}_A = \frac{2E/r_1}{\exp(E(1/r_1 - 1/R_f)) - 1} \quad (3.41)$$

Ranz (42) derived the same expression but included an additional term for radiation effect in his analysis.

Hoffman and Gauvin (46) observed the evaporation of droplets of water, methanol, cumene, pentane and benzene on a thin glass fibre placed inside an enclosed heated stainless steel sphere containing superheated vapour. Drop diameters ranged from 0.4 to 1.4 mm and temperatures from 100 to 550°C and evaporation rates were recorded photographically. They found that at high temperatures, the rate of heat transfer was not governed by natural convection but dependent on the transfer number B, where $B = C_p \Delta T / \lambda$. Their results were represented by the expression,

$$B' \text{Nu}_A (\text{Pr})^{-0.33} = 3.2 B^{0.97} \quad (3.42)$$

where B' is as defined in equation 3.25.

It should be stressed however that this equation is only valid when the gas and the containing walls of the vessel are at the same temperature, which restricts its usefulness. In a later investigation, Pei and Gauvin (60) extended the study using the same apparatus

as Hoffman and Gauvin (46) for the evaporation of benzene and methanol from porous celite spheres. They found that the heat transfer was dependent on the parameter Gr/Re^2 and proposed the correlation,

$$(Nu_{AM}/Re^{0.5}) (B'/Pr^{0.33}) = 3.32 (Gr/Re^2)^{0.007} \quad (3.43)$$

where

Nu_{AM} = Nusselt number in the absence of mass transfer.

The weak dependence of the Nusselt number on Gr/Re^2 is obvious and suggests that the results could have been correlated omitting this ratio.

Pei et al. (61) modified the stainless steel sphere used by Pei and Gauvin (60) to provide a stream of superheated steam (150 - 750°C) at a Reynolds range of 5.5 to 510. They pointed out that forced and natural convection were non-additive and that the transition is gradual. From their results they concluded that natural convection is negligible when Gr/Re^2 is less than 0.2, and for values greater than 10 forced convection effects has little influence. However, they could not propose a heat transfer equation to account for this dependency.

Using the film theory analysis similar to that of Hoffman and Gauvin (46), Downing (62) derived an equivalent correction factor originally proposed by

Spalding (63) where,

$$\text{Nu}_A/\text{Nu}_{AM} = (1/B') \ln (1+B') \quad (3.44)$$

However, this correction could not account for his experimental observations on the evaporation of water, acetone, benzene and hexane in a jet of dry air passing over the drops in the Reynolds number range of 24 to 325 and a temperature range between 27 to 340°C. Further empirical correction factors were introduced, resulting in,

$$\text{Nu} = \text{MN} \frac{\ln(1+B')}{B'} (2.0 + 0.6 \text{Re}^{0.5} \text{Pr}^{0.33}) \quad (3.45)$$

and

$$\text{Sh} = \text{M} (2.0 + 0.6 \text{Re}^{0.5} \text{Sc}^{0.33}) \quad (3.46)$$

where $M = 1 - 0.4 (1 - T_S/T_g)$

$$N = 1 - 0.4 \left[1 - \frac{\ln(1+B')}{B'} \right]$$

It should be noted that the average physical and transport properties were calculated at an average film temperature T_f , defined as,

$$(T_f - T_S)/(T_g - T_S) = 0.6$$

and therefore should only be used in that context.

Toei et al. (64) investigated the evaporation of water drops into superheated steam and air for Reynolds numbers between 9 and 120 and Prandtl numbers between 0.7 and 1.0. They proposed that,

$$\text{Sh} (p_{\text{bm}}/P_t)^{-0.20} = 2.0 + 0.65 \text{Re}^{0.5} \text{Sc}^{0.33} \quad (3.47)$$

where p_{bm} = average partial pressure in the boundary layer.

This correction ratio is very similar to the equivalent correction for temperature in the vapour film used by Downing (62).

Lee and Ryley (65) suspended drops of water on a fine horizontal glass fibre (50 μ diameter) in a horizontal test section. Air and superheated steam at Reynolds numbers between 64 and 250 were used as the gaseous media and evaporation rates were followed optically. A correlation similar to that of Ranz and Marshall (15) was obtained with a coefficient of 0.74. Like previous investigators, they assumed constant physical properties over the gas film. They found however, that the correction factor proposed by Ranz (42) and Spalding (63) did not deviate very much from unity for steam pressures between 1 to 2 bar. It must be pointed out that radiation effects were ignored in their analysis.

Frazier and Hellier (66) studied the evaporation of Freon 113 in an air stream by injecting a stream of

droplets (440μ) across a high temperature jet of air at 669°C . Changes in drop size were recorded photographically and they concluded that the Ranz and Marshall equation underestimates the mass transfer coefficient by a factor of 4. Their results were however, recalculated by Crosby and Stewart (67) using corrections for the net flow through the interface based on the film theory and a much smaller deviation of 33% was obtained between predicted and experimental values.

Trommelen and Crosby (68) evaporated drops of water in superheated steam and in air at velocities of $1.5 - 2.1 \text{ ms}^{-1}$. The drops were suspended from two 76μ thermocouple leads hung from a fine horizontal glass fibre. This technique enables the simultaneous measurement of drop weight and drop temperature. They found that at equal velocities and temperatures, the evaporation rate was greater in air than in superheated steam. However, at higher temperatures this difference decreased. Their results confirmed the findings of Toei et al. (64) and indicated the applicability of the Ranz and Marshall equation for evaporation in superheated steam. In their thorough analysis, they accounted for heat transferred through the thermocouple wires. However, by using the cross sectional area of the wires for this purpose, they underestimated the area of the bead at the junction by at least a factor of 4.

Matlosz et al. (69) observed the evaporation of droplets of n-hexane in a stagnant environment of nitrogen and argon at 275°C. They were mainly interested in the combustion of fuel vapours at high temperatures and pressures of 6.8 - 102 atm., well above the normal operating pressures of spray dryers.

Audu (43) proposed a temperature correction factor to account for his results at elevated temperatures. For $26.5^{\circ}\text{C} < T_g < 118.5^{\circ}\text{C}$, he correlated his results by,

$$\text{Sh} = 2.0 + 0.44 \left((T_g - T_s) / 293 \right)^{-0.008} \text{Re}^{0.5} \text{Sc}^{0.33} \quad (3.48)$$

However, the magnitude of the Sherwood number would have to be relatively high to justify the index of the temperature correction term.

Recently, Kadota and Hiroyasu (70) derived equations for the change of diameter and temperature with time for an evaporating drop at high temperatures. A quasi-steady model was used, which included the effects of natural convection, non-ideal behaviour and effects of high mass transfer rates on temperature and concentration profiles and boundary layer thickness. Results from an earlier paper (71) on the evaporation of various organic liquids and water at 100 - 500°C were found to be in good agreement with the model.

To summarise, it can be said that almost all heat transfer measurements were made in air whilst the majority of mass transfer experiments were made in water. Different techniques of drop suspension have been employed, covering an extensive temperature and relative velocity range. Whilst the majority of researchers support the Ranz and Marshall equation, information about some aspects of drop behaviour on the heat and mass transfer are scanty.

The effect of turbulence, circulation within a drop and drop oscillation are known to have significant effect on heat and mass transfer rates but have not been thoroughly investigated. Conversely, effects of intense mass transfer at high temperatures have been widely investigated but agreement between experimenters is often lacking.

From the above review it is clear that the problem of the evaporation of pure liquid droplets especially under extreme conditions are by no means fully understood.

CHAPTER 4

DROPS CONTAINING DISSOLVED AND SUSPENDED SOLIDS

- 4.1 Moisture Movement Through Porous Media
 - 4.1.1 Diffusion Theory
 - 4.1.2 Capillary Flow Theory
 - 4.1.3 Evaporation-Condensation Theory
 - 4.1.4 Simultaneous Heat and Mass Transfer
Models Based on Irreversible Thermodynamics
- 4.2 Evaporation of Single Droplets Containing
Dissolved and Suspended Solids.

CHAPTER 4

DROPS CONTAINING DISSOLVED AND SUSPENDED SOLIDS

When a droplet contains dissolved or suspended solids, the vapour pressure at the drop surface is lowered resulting in a reduction in the mass transfer rate. The surface temperature of the evaporating droplet will consequently increase above the thermodynamic wet bulb temperature. The drying characteristics are then related to the formation of a solid phase on the surface of the droplet, providing an additional resistance to moisture transfer into the surrounding media.

In the case of droplets containing dissolved solids, experimentation has shown that evaporation commences at a constant rate (15, 68, 72), termed the initial drying period. When the droplet moisture content falls below a critical value, a solid crust commences from a preferential site, usually the point of maximum mass transfer, and spreads around the droplet. As the crust thickens, the crust resistance becomes predominant and the evaporation rate decreases. This is classified as the falling rate drying period.

For drops containing suspended solids, vapour pressure lowering effects are generally negligible. Evaporation may commence with an initial constant period, but this may be very short depending on the solids content. Once a solid crust is formed, the falling rate period follows.

The drying rate after crust formation however, can vary for different materials, and in certain cases for drops of the same material. The characteristics of the crust determines whether fracture, rupture, inflation, shrinkage or shrivelling occur. The degree of these phenomena can also vary between one drop and another of similar size under apparently identical conditions making it extremely difficult to predict the exact drying rate.

4.1 Moisture Movement Through Porous Media

Three generally accepted theories have been proposed for the migration of moisture in porous media; the diffusion theory, the capillary flow theory and the evaporation-condensation theory. Recently, the concepts of irreversible thermodynamics are becoming more widely used to describe this phenomenon.

4.1.1 Diffusion Theory

The migration of moisture by diffusion through the pores was originally proposed by Lewis (73). This is

expressed mathematically as,

$$\frac{\partial C}{\partial \theta} = \frac{\partial(D_{\text{eff}} \cdot \frac{\partial C}{\partial r})}{\partial r} \quad (4.1)$$

where the effective diffusivity D_{eff} , may vary with the moisture concentration.

Based on this diffusion theory, Sherwood (74) suggested that moisture can either be transferred as liquid water through the pores followed by evaporation on the solid surface, or by vaporisation of the liquid below the solid surface followed by vapour diffusion through the pores. The limitation of this theory lies in the difficulty in solving the diffusion equation for cases of variable diffusivities and when shrinkage occurs.

4.1.2. Capillary Flow Theory

The classical picture of capillary flow theory applied to porous media was first laid down by Buckingham (75) who introduced the concept of 'capillary potential'. This theory was later supported by Ceaglske and Hougen (76) with their work on the movement of moisture in sand. They showed that water may actually move towards a region of high concentration provided the high concentration region possesses a fine pore structure. Nevertheless, in the presence of an adequate temperature gradient, the resulting vapour pressure gradient may overcome the capillary potential.

4.1.3 Evaporation-Condensation Theory

The evaporation-condensation theory assumes that moisture is present in the pendular state. The liquid water is held in rings at the waists of the pores and moisture migration occurs entirely in the vapour phase by vaporisation and subsequent condensation. Gurr et al. (77) and others (78, 79) have proved this assumption valid for systems subjected to a temperature gradient. Harmathy (80) developed a model based on this theory to successfully predict the drying rates of clay bricks.

4.1.4 Simultaneous Heat and Mass Transfer Models Based on Irreversible Thermodynamics.

This theory is based on the application of the principles of irreversible thermodynamics, proposed initially by Lykov (81). This approach has the intrinsic advantage of not requiring the assumption of any controlling mechanism of internal moisture diffusion. However, the resulting set of differential equations require the use of a moisture diffusivity and thermogradient coefficient, both of which have to be obtained experimentally.

4.2 Evaporation of Single Droplets Containing Dissolved and Suspended Solids

In addition to studies of pure liquids, Ranz and Marshall (15) also presented data on the evaporation of

solutions of ammonium nitrate and sodium chloride, a suspension of green dye and reconstituted dried whole milk. For the evaporation of dissolved solids, they made the simplifying assumption that during the period before crust formation evaporation will proceed as though the drop surface was saturated regardless of the average concentration within the drop. Although results from ammonium nitrate solutions confirmed this assumption it was later challenged by Charlesworth and Marshall (72). Ranz and Marshall's results were basically qualitative because of the complications of heats of solution and crystallisation, and changes in the density and shrinkage during drying.

Duffie and Marshall (82) carried out a qualitative study on a wide range of products in a 6.1 m high cocurrent drier. They were mainly interested in the effects of feed temperature, feed concentration and air temperature on the bulk density of the dried products. From their observation of dried particle characteristics, they were able to postulate four factors contributing to the formation of hollow particles.

- 1) Hollow particles may result by the rapid formation of a vapour-impervious film on the droplet surface causing 'puffing' when the vaporising moisture within cannot readily escape.

- 2) If the rate of evaporation exceeds the rate of diffusion of solids back into the drop, internal voids may be created.
- 3) If a rigid porous shell is formed initially, capillary suction draws liquid and solids to the surface creating subatmospheric pressures and internal voids. The particle may eventually collapse.
- 4) Entrained gases in the feed may also result in hollow particles.

They were able to classify materials according to their particle structures i.e. film forming and crystalline materials, but observed that the mechanism of hollow particle formation may be different within each classification.

Charlesworth and Marshall (72) carried out an extensive study on the drying of fifteen different aqueous systems. The drops were suspended from a vertical glass filament of 340μ diameter which was itself attached to another horizontal glass filament, the deflection of which determined the weight of the drop. An equation was proposed for the time of complete formation of a solid crust assuming spherical symmetry. However, the scatter of the data points indicated that the simplifying assumptions were not valid. Localised variations in mass

transfer may have resulted in a time interval between the initial appearance of a crust and when it completely covered the drop. They also presented a generalised description of the behaviour of a drying droplet, shown in Figures 4.1 and 4.2. Up to the point of crust formation, the characteristics were similar irrespective of the solute concentration and drying conditions. After crust formation however, the behaviour of the droplet was entirely controlled by the nature of the crust and whether the drying temperature was above or below the boiling point of the droplet. Evidently, because of the variation from particle to particle even under identical conditions, a quantitative analysis was not possible. The drying curves for sodium sulphate drops presented in Figure 4.3 show this variation.

Trommelen and Crosby (68) compared the drying rate curves of four food products and various inorganic salts drying in air and superheated steam. They found that with the exception of skimmed milk and sodium sulphate droplets, all materials dried faster in air than in steam at about 150°C; rates were however comparable at a higher temperature of about 400°C. Drop temperatures were also measured but the nature of the temperature-time curves showed no consistent trend between different materials. The resistance to heat and mass transfer was found to alter significantly if inflation or rupture occurred, generating more surface area. This lead to the conclusion that drying rates and the structures of dried materials are product specific.



Aston University

Illustration has been removed for copyright restrictions

Figure 4.1 Characteristics of drying droplets at air temperatures below the boiling point (72).



Aston University

Illustration has been removed for copyright restrictions

Figure 4.2 Characteristics of drying droplets at air temperatures above the boiling point (72).

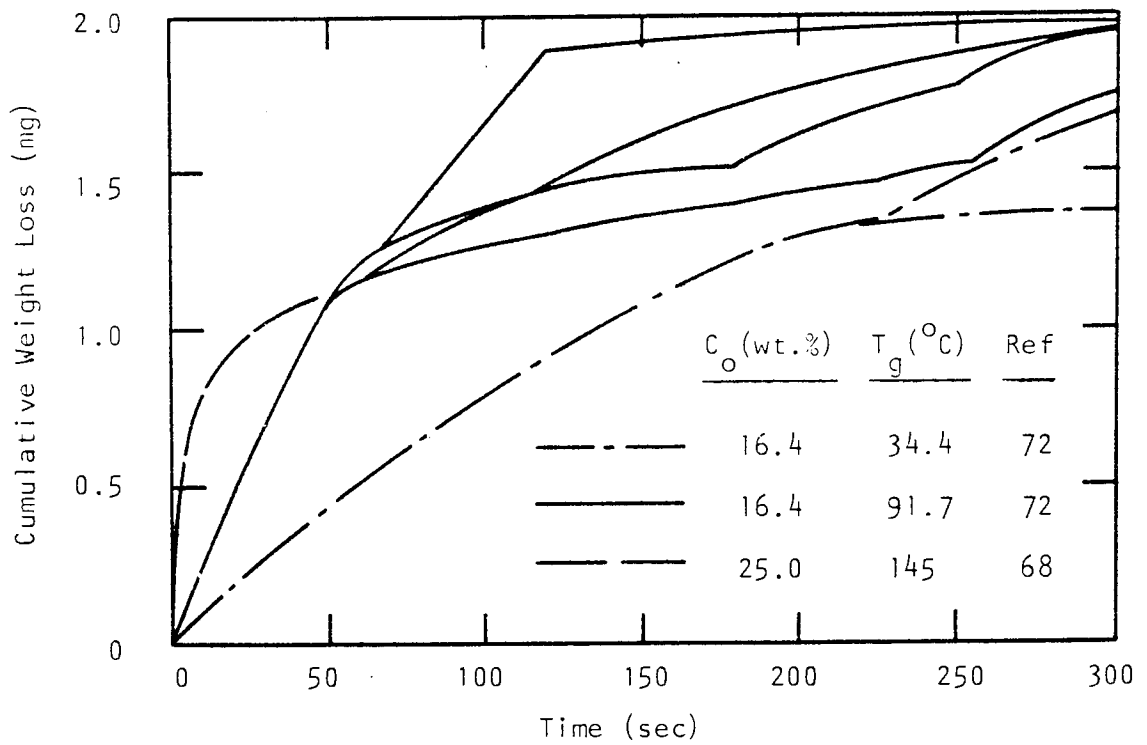


Figure 4.3 Drying curves for aqueous sodium sulphate drops.


 Aston University

Illustration has been removed for copyright restrictions

Figure 4.4 Drying rate curves for aqueous sodium sulphate drops with an initial moisture content of 9.6 kg water/kg solute (83).

Miura et al. (83) used the same technique as Charlesworth and Marshall (72) to study the drying of drops of sodium sulphate, skimmed milk and a suspension of bentonite. The equation for time of appearance of a crust proposed by Charlesworth and Marshall was found to be reasonably accurate although it was consistently lower than the experimental values. They observed that at an air temperature of 150°C, a droplet of sodium sulphate initially dried at a constant rate followed by a sudden fall after completion of crust formation. The crust was subsequently burst open due to boiling, and drying at another constant rate followed before gradually falling off again to total dryness. At the lower temperature of 99°C, the drying rate curve was similar but no bursting occurred, although fractures were evident. The drying rate curves are shown in Figure 4.4. Skimmed milk droplets showed very distinct constant and falling rate periods with inflation after skin formation. Drying rate curves for bentonite were identical to those of pure water droplets at all temperatures and moisture contents. They proposed an equation to predict crust thickness based on a mass balance of solids in a droplet.

$$(Y - 1) = \frac{1 - Z^3}{3GZ^2 - 3G^2Z + G^3} \quad (4.2)$$

$$\text{where } Z = r/r_0$$

$$Y = C/C_0$$

$$G = \psi/r_0$$

The equation was derived on the basis of a similar density for the crust and core, which is a gross over simplification.

The drying of sodium sulphate and detergent drops were studied by Audu and Jeffreys (84) in a wind tunnel. They proposed a crust mass transfer coefficient k_c , expressed as,

$$k_c = \frac{D_v \varepsilon^{1.5}}{\psi} \quad (4.3)$$

The concept of a crust coefficient is based on the assumption that the transfer path for heat and mass will be different once a crust is formed, effectively uncoupling the equations. They found experimentally that the crust resistance can account for as much as 64.2% of the total resistance. However, no allowance was made for heat transferred by conduction from the nozzle on which the drops were suspended. A crust thickness model was proposed, based on a mass balance of moisture in the surrounding air. The model however, predicted values as much as 20% higher than experimental results.

The evaporation history of saline drops of sodium chloride and calcium carbonate have been studied by both Joffre et al. (85) and El Golli et al. (86). They found

that the change of surface area was a linear function of time. The latter also proposed an equation to predict evaporation times for saline drops based on the concept of water activity in the electrolyte solution.

Wijlhuizen et al. (87) presented a 'solid sphere' and 'hollow sphere' model for an evaporating droplet. They were mainly interested in the inactivation of phosphatase during the drying of skimmed milk. The model was essentially based on the work of Van der Lijn (88) who introduced a concentration and temperature dependent diffusion coefficient. The 'hollow sphere' model assumes an initial gas bubble of known size in a droplet and a uniform concentration profile. The resulting diffusion equations were solved with the necessary boundary conditions to predict moisture concentrations and droplet temperatures during drying. However, by not allowing for the formation of a crust, the model has limited applications especially in the falling rate period.

A simultaneous heat and mass transfer model based on vapour diffusion and liquid moisture movement by capillary suction was proposed by Haertling (89) for porous hygroscopic materials. The model overestimates the drying curves for burned clay and clay brick with low porosities, suggesting that liquid moisture migration by capillary suction is less significant in low porosity materials.

Esubiyi (90) developed a momentum-heat transfer model based on an assumed vapour velocity through the pores of a solid crust described by the Kozeny equation (91). He expressed the crust coefficient as,

$$k_c = \frac{\epsilon^3}{5 (1 - \epsilon)^2 \mu_c S^2} \left[\frac{\rho_c}{\psi} \right] \quad (4.4)$$

Experimental results for the drying of Portland cement slurries, using essentially the same measuring technique as Audu (43), confirmed the validity of this model. The equation however requires the porosity ϵ , and specific surface area S , to be determined experimentally. This is often difficult with spray dried particles which are small (less than 200μ) and usually fragile.

More recently Sano and Keey (92) presented a more realistic model for the drying of droplets containing colloidal material into solid hollow spheres. The mechanism for the formation of hollow spheres was based on the assumption that once the equilibrium vapour pressure of the moisture inside the droplet exceeds the pressure of the ambient air, the particle inflates instantaneously and ruptures. After inflation, two limiting ways of deformation were proposed;

- 1) the maximum radius remains constant but void radius increases due to moisture loss,
- or 2) the void radius remains constant but the outer radius shrinks.

Using techniques similar to Charlesworth and Marshall (72), they dried droplets of skimmed milk at temperatures between 100 and 150°C and showed that the second proposal, i.e. a shrinking outer radius, gave the best approximation to their results. The computation however requires an experimentally determined inflation ratio, which is the ratio of the maximum radius after inflation to the initial radius. Although their results were computed with an inflation ratio of 0.88, they found that a ratio of 1.1 was required to fit the data of Trommelen and Crosby (68) for the same material and temperature. The basis of this model was also used by Sano and Yamamoto (93) to predict the drying rates of drops of polyacrylonitrile in dimethyl formamide assuming a receding interface and a constant concentration distribution. A modified diffusion coefficient, derived empirically, had to be used to fit their data.

CHAPTER 5

EVAPORATION OF SPRAYS OF DROPLETS

- 5.1 Sprays of Pure Liquids
- 5.2 Sprays Containing Dissolved and Suspended Solids

CHAPTER 5

EVAPORATION OF SPRAYS OF DROPLETS

The analysis of the evaporation characteristics of droplets within a spray presents a far more complex problem. Although the fundamental concepts still apply, there are the added difficulties in defining a representative droplet diameter, relative velocity and droplet trajectory. During the evaporation of a spray of pure liquid, the mean droplet size may decrease but can also increase during some parts of the evaporation process when the smaller droplets disappear. Hence, it is highly unlikely that the use of a mean droplet size will adequately characterize the evaporation process of a non-uniform spray. A droplet size distribution function is the best representation of droplets during the evaporation of a spray. The more common distribution functions for sprays are presented in Table 5.1 and have been discussed extensively by Masters (94).

In the vicinity of the atomiser, the high concentration of droplets and high relative velocities give rise to rapid evaporation. This causes a corresponding rapid reduction in the surrounding air temperature and consequently the temperature and concentration driving forces.

TABLE 5.1 Droplet Size Distribution Functions

<u>Distribution</u>	<u>Equation</u>
Normal	$\frac{d(N)}{d(d_p)} = \frac{1}{S_N \sqrt{2\pi}} \cdot \exp - \left[\frac{(\bar{d}_p - d_p)^2}{2S_N^2} \right]$
Log-Normal	$\frac{d(N)}{d(d_p)} = \frac{1}{d_p S_G \sqrt{2\pi}} \cdot \exp - \left[\frac{(\log d_p - \log d_{gm})^2}{2S_G^2} \right]$
Square Root Normal	$\frac{d(N)}{d(d_p)} = \frac{1}{2 \sqrt{2\pi} d_p S_G} \cdot \exp - \left[\frac{(\sqrt{d_p} - \sqrt{d_{gm}})^2}{2S_G^2} \right]$
Upper Limit	$\frac{d(N)}{d(d_p)} = \frac{1}{d_p S_G \sqrt{2\pi}} \cdot \exp - \left[\frac{\log((d_{max} - d_p)/d_{gm})^2}{2S_G^2} \right]$
Nukiyama-Tanasawa	$\frac{d(N)}{d(d_p)} = a_n d_p^2 \cdot \exp(-b_n d_p^q)$
Rosin-Rammler	$V_p = 100^{-[(d_p/d_R)^2]}$

where $d(N)$ = number of droplets in size increment

V_p = volume percent oversize

d_p = droplet size

\bar{d}_p = mean droplet size

d_{gm} = geometric mean size

d_{max} = maximum droplet size

d_R = Rosin-Rammler mean size

S_N = number standard deviation

S_G = geometric standard deviation

a_n, b_n = constants

q = dispersion coefficient

5.1 Sprays of Pure Liquids

An attempt was made by Probert (95) to represent the drop size distribution of a fuel spray by the Rosin-Rammler equation (96). Assuming no relative velocity, he predicted that a spray with a narrow size distribution will evaporate completely in less time than one with a wide distribution if the mean diameters are the same. This early attempt however, ignored any change in the temperature driving force during evaporation. This study was extended by Fledderman and Hanson (97) for conditions of relative velocity but assuming a Nukiyama-Tanasawa type distribution (98). Their equation was too complex to be of practical value.

Marshall (59) presented a comprehensive stepwise method for the evaluation of spray evaporation. Dividing the size distribution into small size groups, the change of the average droplet diameter in each selected group can be calculated over short time intervals. Although the method was only set out for pure liquid droplets at no relative velocity, the results were useful in illustrating the relative effects of the drying air temperature. He showed that 90% of the evaporation in the majority of spray drying operations is completed during the first 1.5 seconds, with the air temperature falling to within 17°C of the outlet air temperature during this period.

Manning and Gauvin (99) developed useful measuring techniques in their study of heat and mass transfer of water sprays in cocurrent and crosscurrent air flows. Spray evaporation was measured by a colourimetric method using a red dye and the droplet size distribution was determined using an immersion cell containing Varsol. Their results however, showed a considerable scatter of data points. This may be in part attributed to the uncertainty in predicting relative velocities and droplet sizes in the vicinity of the atomising nozzle.

Bose and Pei (100) studied the evaporation of water sprays from a 152.4 mm I.D. cocurrent drier. They concluded that the relative velocity between spray and air caused a significant increase in the heat and mass transfer rates, contrary to the findings of Dlouhy and Gauvin (101). Their results were well represented by the Ranz and Marshall equation which takes account of relative velocities.

Dickinson and Marshall (102) presented a computational study of the evaporation of sprays of pure liquid droplets under conditions of both negligible and significant relative velocities. Although the analysis took account of non-uniform size distributions, the assumption of idealised conditions of constant droplet temperature and ideal flow limits its use.

Miura et al. (47) investigated the effects of drop to drop interaction on the rate of drop to fluid heat and mass transfer. By suspending glass beads in series to water drops, they proposed that,

$$\text{for } b/d_{j-1} \leq 2, \text{ Nu/Nu}_R = 0.71 (b/d_{j-1})^{0.25} (d_j/d_{j-1})^{0.167} + 0.07 \quad (5.1)$$

$$\text{for } b/d_{j-1} > 2, \text{ Nu/Nu}_R = 0.42 (b/d_{j-1})^{0.125} + 0.41 \quad (5.2)$$

where b = distance between adjacent droplet surfaces and d_j, d_{j-1} = droplet diameter in 'j' and the adjacent 'j-1' group.

Although Miura and Ohtani (103) later proposed a model based on these equations and confirmed its validity with results from water sprays emitting from a pneumatic nozzle, the evaluation of $b, d_j,$ and d_{j-1} , values was tedious and relied on probability theory.

5.2 Sprays Containing Dissolved and Suspended Solids

When solids are present in a spray, the extent of vapour pressure lowering and resistances to moisture transfer will vary throughout the size distribution. As evaporation proceeds, the concentration of solids in the smaller droplets will increase much faster than the larger ones, resulting in a wide variation in the concentration driving force. This phenomenon also results in the solid phase not appearing simultaneously throughout the size distribution. The analysis is therefore highly complex and investigations in this field are limited.

Dlouhy and Gauvin (101) studied the evaporation of solutions of calcium lignosulphonate using experimental methods similar to Manning and Gauvin (99). Using the step-wise method proposed by Marshall (59) and a Nusselt number of 2, they were able to predict the drying rate curves, which were in good agreement with experimental results. Their method requires a knowledge of the drop size distribution which must be determined experimentally.

Baltas and Gauvin (104) attempted to account for radial gradients of humidity, spray mass velocity and air velocity in the same drier as Dlouhy and Gauvin (101). Although they were successful in predicting radial humidity and mass flow profiles, the predicted evaporation rates for a sodium nitrate spray were 3.5 times greater than the observed rates. It should be noted that their model is only applicable to the free fall zone.

Katta and Gauvin (105) proposed equations to predict the three dimensional motion of droplets in a spray drier based on assumed size distributions and ideal flow patterns. Their model predicts droplet trajectories and evaporation rates for sodium lignosulphonate sprays but lack experimental verification. An interesting conclusion was that an optimum nozzle depth and air temperature exist for maximum efficiency and capacity.

More recently Miura et al. (106) reported on the drying of water, sodium chloride and skimmed milk solutions, atomised from a two fluid pneumatic nozzle and a hollow cone nozzle. Assuming a Nukiyama-Tanasawa distribution, they showed that the previously derived equations for evaporation in a spray cloud (5.1 and 5.2), predicted their results more accurately than the Ranz and Marshall equation.

CHAPTER 6

TEMPERATURE OF EVAPORATING DROPLETS

CHAPTER 6

TEMPERATURE OF EVAPORATING DROPLETS

To predict the evaporation rate, it is necessary to be able to specify or estimate the droplet surface temperature in order to evaluate the temperature driving force. For the case of a pure liquid droplet, if a dynamic equilibrium is established between heat and mass transfer, and if all the heat transferred is consumed for evaporation, the surface temperature T_s , can be expressed as,

$$\frac{T_g - T_s}{p_s - p_g} = \frac{k_g A_m \lambda}{h_g A_h} \quad (6.1)$$

When an evaporating droplet contains dissolved solids, the saturated vapour pressure is lowered and the droplet temperature will be higher than for a drop of pure liquid under similar conditions. When suspended solids are present, the surface temperature will initially approximate that for a pure liquid droplet. However, in both cases once a solid crust is formed, the additional resistance to moisture diffusion will result in the core temperature rising above the saturated wet bulb temperature

(15). A typical core temperature profile demonstrating this phenomenon is shown in Figure 6.1 for a drop containing reconstituted dried whole milk.

Williams and Schmitt (107) have shown that the heat of crystallisation should be taken into account when drying salt solutions. For ammonium nitrate solutions for example, the heat of crystallisation amounts to 20% of the latent heat of vaporisation. Assuming $A_h = A_m$, equation 6.1 becomes,

$$\frac{T_g - T_s}{p_s - p_g} = \frac{k_g (\lambda - C_c)}{h_g} \quad (6.2)$$

where C_c is the heat evolved by crystallisation per unit mass of water evaporated.

Ranz and Marshall (15) embedded a 12.7μ manganin-constantan thermocouple inside a suspended drop to measure drop temperatures during evaporation. However, simultaneous measurements of evaporation rates and drop temperatures were not possible since there was interference of the gas flow patterns due to the thermocouple leads. They found that drops of ammonium nitrate and sodium chloride solutions evaporated with a surface temperature corresponding to that of the saturated solution even though the initial concentration was less than saturation. With drops containing 3.0×10^{-4} gm of ammonium nitrate, drop temperatures increased initially



Aston University

Illustration has been removed for copyright restrictions

Figure 6.1 Drop temperature history for reconstituted dried whole milk (15).



Aston University

Illustration has been removed for copyright restrictions

Figure 6.2 Drop Temperature histories for aqueous sodium sulphate (68, 72).

due to the heat of solution followed by a very sharp rise when crystallisation occurred. Although sensible heat transferred from the feed solution was accounted for, no correction was included for conduction along the thermocouple wires.

Charlesworth and Marshall (72) used the same type of thermocouple leads as the previous authors (15) and presented temperature histories for sodium sulphate, potassium sulphate, ammonium nitrate, calcium chloride, sodium acetate and coffee extract. For a concentration of 8.2 wt.% sodium sulphate, the temperature history was very similar to that observed by Ranz and Marshall (15). However, at a higher concentration of 16.4 wt.%, crust fracture had a significant effect on the temperature history (Figure 6.2). Again however, no account was taken of heat conduction along the leads.

Fuchs (34) found that for typical experimental conditions, i.e. drop diameters of 1 mm and wire diameters of 25μ , the ratio of heat flux through the wire to that through the gaseous medium may have values of 0.8 for copper-constantan thermocouples, and 0.04 for quartz and glass fibres. Clearly therefore, it is erroneous to ignore the additional heat flux especially through thermocouples.

Downing (62) measured drop temperatures using thermocouple leads of increasing diameter and extrapolated the measurements to zero diameter to estimate the heat conducted along the wire. However, he observed that organic liquid drops climbed up the wires and different wet bulb temperatures were indicated depending on the position of the thermocouple junction in the drop.

Trommelen and Crosby (68) were the first to measure simultaneously the weight and temperature of an evaporating drop by suspending drops from a chromel-constantan thermocouple fixed to the end of a glass filament which acted as a torsion balance. An expression was derived from a heat balance along the thermocouple wires and solved for the heat transferred to a suspended drop. The cross sectional area of the wires were however, used as the heat transfer area whereas the drops were in contact with a spherical bead at the junction. Their experimental results showed that food products in general exhibit no constant temperature period, unlike clay slurry and inorganic salts. The temperature histories however, can be interrupted by fracture, inflation or collapse after which it can vary from one drop to another as shown in Figure 6.2.

Miura et al. (83) suspended drops of inorganic salts, skimmed milk and bentonite from a quartz filament



of 0.3 mm diameter and measured the drop temperatures by inserting a 40μ manganin-constantan thermocouple in the centre of each drop. Their result of temperature history for an aqueous sodium sulphate drop at an air temperature of 99°C was generally consistent with those of the previous authors (72). For the case of high air temperature (149°C), illustrated in Figure 6.3, they found that the drop temperature rose initially and after completion of crust formation, 'boiling' within the drop occurred. This fractured the crust resulting in another constant temperature period before rising again to the air temperature.

Van der Lijn (88) used a continuum model, assuming heat and mass transfer occurs over an arbitrary control volume in the continuous phase, to predict drop temperatures and confirmed it with temperature histories of drops of maltose-water solution, measured with a 45μ chromel-constantan thermocouple. Heat conduction through the thermocouple was found to increase the heat flux by 2%. The continuum model however, does not account for the effect of the presence of other droplets on the heat and mass transfer.

Recently, Sano and Keey (92) proposed a hollow sphere model (described in Section 4.2) and derived equations to predict the temperature of an evaporating drop containing colloidal material. The temperature history was measured

Illustration has been removed for copyright restrictions

Figure 6.3 Drop temperature histories for aqueous sodium sulphate at initial moisture content of 9.6 kg water/kg solute. (83).

Illustration has been removed for copyright restrictions

Figure 6.4 Comparison between experimental and calculated drop temperature for a drop containing skimmed milk. (83).

by suspending a drop at the junction of a manganin
-copper thermocouple, with wire diameters of 30μ .
The model was found to slightly underestimate the drop
temperature especially at high air temperatures (150°C),
as shown in Figure 6.4. This was probably due to the
omission of a correction term for high mass flux (59)
and conduction along the thermocouples.

CHAPTER 7

MATHEMATICAL MODELS

- 7.1 Pure Liquid Drops
 - 7.1.1 Nusselt Number
 - 7.1.2 Heat Transferred to a Drop by Radiation
 - 7.1.3 Heat Transferred to a Drop Through the Suspension Filament
 - 7.1.4 Heat Transferred to a Drop Through the Thin Film Glass Filament Thermocouple
- 7.2 Receding Evaporation Interface Model
 - 7.2.1 Heat Transfer at Evaporation Interface
 - 7.2.2 Mass Transfer at Evaporation Interface

CHAPTER 7

MATHEMATICAL MODELS

Two models will be discussed in the following sections. For pure liquid drops, an expression for the experimental Nusselt number has been derived and heat transfer by radiation and by conduction along the filament have been accounted for. For slurry drops, a Receding Evaporation Interface model has been proposed to predict the evaporation rate, core temperature and crust thickness of an evaporating drop.

7.1 Pure Liquid Drops

This section will be discussed with reference to water drops.

7.1.1 Nusselt Number

To determine the experimental value of the Nusselt number, the following assumptions were made:

- 1) The drop is spherical with a constant density;
- 2) The temperature at the surface of the drop is equal to the wet bulb temperature;

- 3) The temperature driving force remains constant;
- 4) The latent heat of vaporisation and thermal conductivity are evaluated at the mean temperature between the air and the drop.

The rate of mass transfer to a spherical drop can be expressed as:

$$-\frac{dW}{d\theta} = \frac{dQ/d\theta}{\lambda} \quad (7.1)$$

The heat transferred can be determined from,

$$dQ/d\theta = h_g A \Delta T \quad (7.2)$$

Substituting equation 7.2 into 7.1 gives,

$$-\frac{dW}{d\theta} = \frac{h_g A \Delta T}{\lambda} \quad (7.3)$$

Since $W = (\pi d_p^3 \rho_d)/6$, equation 7.3 becomes,

$$h_g = - \frac{\rho_d \lambda}{6 \Delta T} \cdot \frac{1}{d_p} \cdot \frac{d(d_p^3)}{d\theta} \quad (7.4)$$

The Nusselt number Nu , is defined as,

$$Nu = \frac{h_g d_p}{k}$$

Substituting equation 7.4 into the above expression,

$$Nu = - \frac{\rho_d \lambda}{6k\Delta T} \cdot \frac{1}{d_p} \cdot \frac{d(d_p^3)}{d\theta} \quad (7.5)$$

Since $\frac{d(d_p^3)}{d\theta} = \frac{3d_p^2}{2} \cdot \frac{d(d_p^2)}{d\theta}$

Therefore,

$$Nu = - \frac{\rho_d \lambda}{4k\Delta T} \cdot \frac{d(d_p^2)}{d\theta} \quad (7.6)$$

Under conditions of relative velocity, the derivative of d_p^2 with respect to time varies with the instantaneous drop size.

7.1.2 Heat Transferred to a Drop by Radiation

Apart from forced convective heat transfer, radiation effects have been taken into account. Using the same assumptions as in the preceding section, the radiative heat transfer rate q_e , was expressed as,

$$q_e = \sigma A F_a e (T_g'^4 - T_s'^4) \quad (7.7)$$

where T_g' and T_s' are expressed in degrees Kelvin and σ = Stefan-Boltzmann constant.

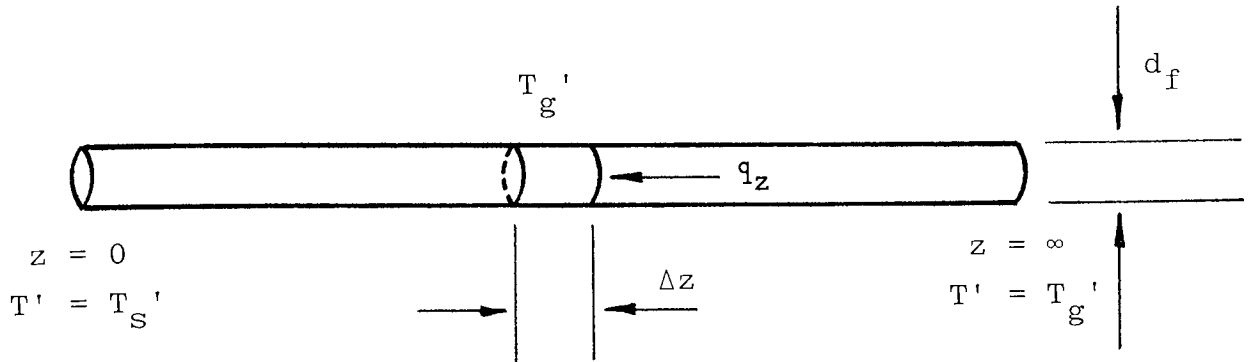
The geometry factor F_a , was assumed to be unity since the drop was for all practical purposes surrounded by the drying chamber. The emissivity e , was taken to be that of the drop since it was so much smaller than the drying chamber.

7.1.3 Heat Transferred to a Drop through the Suspension Filament

Heat was transferred to the drop through the suspension filament which was itself exposed to the hot drying air. The following assumptions were made in deriving an expression for this additional heat input.

- 1) Heat is transferred to the filament from the surroundings by radiation and convection.
- 2) The physical properties of the filament are constant.
- 3) The temperature around the filament is constant and equal to the temperature of the air.
- 4) The heat transfer coefficient on the surface of the filament is constant.
- 5) There is no radial temperature gradient.
- 6) The length of the filament is very much larger than the diameter, i.e. infinite length.
- 7) The geometry factor is assumed to be unity.

Consider a cylinder of infinite length,



where q_z = heat flux in the z direction.

For an element Δz ,

Heat in by conduction	$= q_z \pi d_f^2 / 4$
Heat in by radiation	$= \sigma (\pi d_f \Delta z) e_g (T_g'^4 - T'^4)$
Heat in by convection	$= h_f (\pi d_f \Delta z) (T_g' - T')$
Heat out by conduction	$= q_{z+\Delta z} \pi d_f^2 / 4$

A heat balance over the element Δz gives,

$$q_{z+\Delta z} \pi d_f^2 / 4 = q_z \pi d_f^2 / 4 + \sigma (\pi d_f \Delta z) e_g (T_g'^4 - T'^4) + h_f (\pi d_f \Delta z) (T_g' - T') \quad (7.8)$$

Rearranging equation 7.8 and dividing by Δz ,

$$\frac{q_{z+\Delta z} - q_z}{\Delta z} = \frac{4\sigma e_g}{d_f} (T_g'^4 - T'^4) + \frac{4h_f}{d_f} (T_g' - T') \quad (7.9)$$

In the limit as Δz approaches zero,

$$\frac{dq}{dz} = \frac{4\sigma e_g}{d_f} (T_g'^4 - T'^4) + \frac{4h_f}{d_f} (T_g' - T') \quad (7.10)$$

According to Fourier's law,

$$q = -k_t \frac{dT'}{dz}$$

Substituting into equation 7.10,

$$\frac{d^2T'}{dz^2} = - \frac{4}{k_t d_f} \left[\sigma e_g (T_g'^4 - T'^4) + h_f (T_g' - T') \right] \quad (7.11)$$

$$\text{Let } P = \frac{dT'}{dz}, \text{ hence } \frac{d^2T'}{dz^2} = P \frac{dP}{dT'}$$

Substituting into equation 7.11,

$$P \frac{dP}{dT'} = - \frac{4}{k_t d_f} \left[\sigma e_g (T_g'^4 - T'^4) + h_f (T_g' - T') \right] \quad (7.12)$$

Integrating equation 7.12,

$$\frac{p^2}{2} = - \frac{4}{k_t d_f} \left[\sigma e_g T_g'^4 T' - \frac{\sigma e_g T'^5}{5} + h_f T_g' T' - \frac{h_f T'^2}{2} + C_1 \right] \quad (7.13)$$

where C_1 = Integrating constant.

Using the following boundary conditions,

at $z = 0$, $T' = T_s'$

and at $z = \infty$, $T' = T_g'$ and $\frac{dT'}{dz} = 0$

$$C_1 = \left[\frac{\sigma e_g T_g'^5}{5} - \sigma e_g T_g'^5 + \frac{h_f T_g'^2}{2} - (h_f T_g'^2) \right] \quad (7.14)$$

Substituting equation 7.14 into 7.13,

$$\left[\frac{dT'}{dz} \right]^2 = \frac{8}{k_t d_f} \left[\frac{\sigma e_g}{5} (T'^5 - T_g'^5) - \sigma e_g T_g'^4 (T' - T_g') + \frac{h_f}{2} (T'^2 - T_g'^2) - h_f T_g' (T' - T_g') \right] \quad (7.15)$$

Taking square roots and rearranging,

$$\frac{dT'}{dz} = \pm \left[\frac{4}{5k_t d_f} \left(2 \sigma e_g (T'^5 - T_g'^5) - 10 \sigma e_g T_g'^4 (T' - T_g') + 5h_f (T' - T_g')^2 \right) \right]^{0.5} \quad (7.16)$$

The rate of heat transfer to a drop q_f , can be expressed as,

$$q_f = - \frac{\pi d_f^2}{4} k_t \cdot \left. \frac{dT'}{dz} \right|_{z=0} \quad (7.17)$$

where $\frac{\pi d_f^2}{4}$ = Area of filament in contact with the suspended drop.

Substituting $\frac{dT'}{dz}$ at $z = 0$ from equation 7.16 into 7.17,

the final expression for the heat transferred through the filament is,

$$q_f = \frac{\pi}{2} \left[\frac{k_t d_f^3}{5} \left(2 \sigma e_g (T_s')^5 - T_g'^5 \right) - 10 \sigma e_g T_g'^4 (T_s' - T_g') + 5 h_f (T_s' - T_g')^2 \right]^{0.5} \quad (7.18)$$

7.1.4 Heat Transferred to a Drop Through The Thin Film Glass Filament Thermocouple

When a drop is suspended from the thin film thermocouple, additional heat will be transferred through the nickel wire which extends into the drop. Ignoring convection

effects since the nickel wire was enclosed in the glass filament, and using the same analysis as the previous section, the temperature gradient at the tip of the nickel wire is,

$$\frac{dT_w'}{dz} = \frac{+}{-} \left[\frac{8\sigma e_w}{k_w d_w} \left(\frac{(T_s'^5 - T_g'^5)}{5} - T_g'^4 (T_s' - T_g') \right) \right]^{0.5} \quad (7.19)$$

The rate of heat transfer to a drop through the nickel wire q_w , can be expressed as,

$$q_w = - \pi d_w (W_i + d_w/4) k_w \cdot \left. \frac{dT_w'}{dz} \right|_{z=0} \quad (7.20)$$

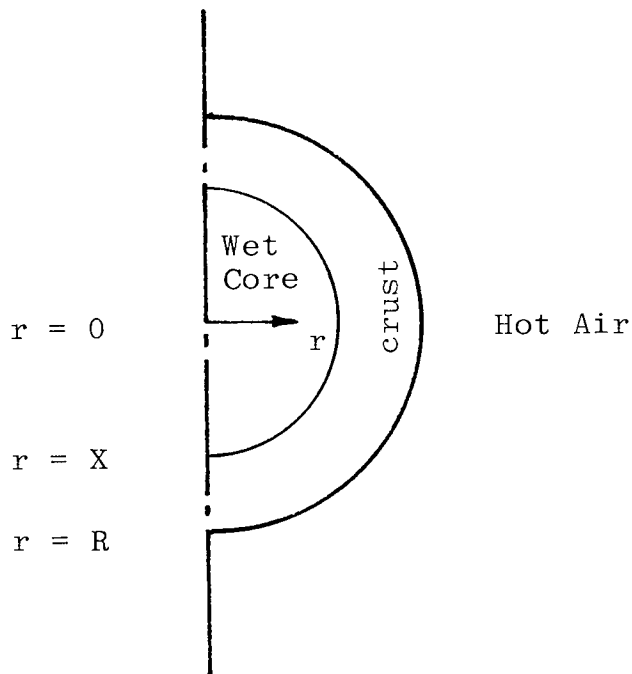
where $\pi d_w (W_i + d_w/4)$ is the total surface area of the wire in contact with the drop.

Substituting equation 7.19 into 7.20 gives,

$$q_w = 2\pi (W_i + d_w/4) \left[2 \sigma e_w d_w k_w \left(\frac{(T_s'^5 - T_g'^5)}{5} - T_g'^4 (T_s' - T_g') \right) \right]^{0.5} \quad (7.21)$$

7.2 Receding Evaporation Interface Model

Consider a slurry droplet after a crust has been formed. Let the outer radius of the crust be $r = R$ and the evaporation interface be $r = X$.



The following assumptions are made.

- 1) Evaporation only occurs at the evaporation interface, which is the interface between the wet core and dry crust.

- 2) The evaporation interface $r = X$, recedes into the wet core as evaporation proceeds.
- 3) The crust once formed, does not shrink or inflate i.e. R remains constant. It is also assumed that no fracture occurs.
- 4) the core temperature T_c , is uniform throughout the core.
- 5) Heat is transferred from the drying air to the crust solely by convection.
- 6) Heat is transferred through the crust by conduction.
- 7) The moisture is transferred from the evaporation interface by vapour diffusion through the pores, represented by an effective diffusivity D_{eff} .
- 8) The core density remains constant during the evaporation process, i.e. as water evaporates at the interface, it precipitates an equivalent amount of solid as crust.
- 9) The energy and water vapour storage within the crust is negligible.

7.2.1 Heat Transfer at Evaporation Interface

An energy balance over the evaporation interface $r = X$, can be expressed as,

Rate of energy from crust = Rate of energy for evaporation
 + Rate of energy into core

In mathematical form,

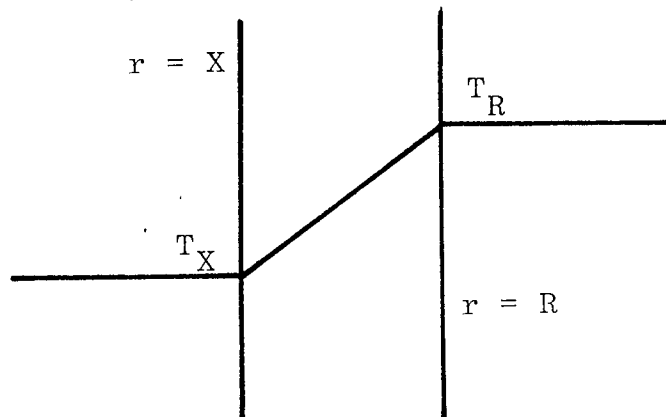
$$4\pi X^2 k_{tc} \left[\frac{\delta T}{\delta r} \right]_X = - 4\pi X^2 \rho_{co} x_w (\lambda - C_c) \left[\frac{dX}{d\theta} \right] + \frac{4}{3} \pi X^3 C_{pc} \rho_{co} \left[\frac{dT_c}{d\theta} \right] \quad (7.22)$$

x_w = mass fraction of water in core
 C_c = heat evolved by crystallisation per unit mass of water evaporated.

This reduces to,

$$- \frac{dX}{d\theta} = \frac{k_{tc}}{\rho_{co} x_w (\lambda - C_c)} \left[\frac{\partial T}{\partial r} \right]_X - \frac{C_{pc} X}{3x_w (\lambda - C_c)} \left[\frac{dT_c}{d\theta} \right] \quad (7.23)$$

Assumption 9 implies that a linear temperature gradient exists in the crust,



Hence the rate of heat transfer can be expressed as,

$$Q_r = 4\pi r^2 k_{tc} \left[\frac{\partial T}{\partial r} \right] = \text{Constant} \quad (7.24)$$

Integrating equation 7.24 between the limits $r = R$ and $r = X$, gives,

$$Q_r = 4\pi k_{tc} (T_R - T_X) \left[\frac{RX}{R-X} \right] \quad (7.25)$$

At $r = R$,

$$Q_R = 4\pi k_{tc} R^2 \left[\frac{\partial T}{\partial r} \right]_R \quad (7.26)$$

and at $r = X$,

$$Q_X = 4\pi k_{tc} X^2 \left[\frac{\partial T}{\partial r} \right]_X \quad (7.27)$$

Since, $Q_r = Q_R = Q_X$,

$$\left[\frac{\partial T}{\partial r} \right]_R = (T_R - T_X) \left[\frac{X}{R(R - X)} \right] \quad (7.28)$$

$$\text{and} \quad \left[\frac{\partial T}{\partial r} \right]_X = \frac{R^2}{X^2} \left[\frac{\partial T}{\partial r} \right]_R \quad (7.29)$$

If it is further assumed that $T_X = T_c$, equation 7.28 becomes,

$$\left[\frac{\partial T}{\partial r} \right]_R = (T_R - T_C) \left[\frac{X}{R(R - X)} \right] \quad (7.30)$$

Also at $r = R$,

$$4 \pi R^2 k_{tc} \left[\frac{\partial T}{\partial r} \right]_R = 4 \pi R^2 h_g (T_g - T_R) \quad (7.31)$$

where $h_g =$ gas film heat transfer coefficient.

Substituting equation 7.30 into 7.31,

$$(T_R - T_C) = \left[\frac{R(R - X)h_g}{k_{tc} X} \right] (T_g - T_R) \quad (7.32)$$

$$\text{Let } a_0 = \frac{R(R - X)h_g}{k_{tc} X}$$

Hence equation 7.32 becomes,

$$(T_R - T_C) = a_0 (T_g - T_R)$$

and rearranging,

$$(T_R - T_C) = \left[\frac{a_0}{1 + a_0} \right] (T_g - T_C) \quad (7.33)$$

Substituting equation 7.33 into 7.30,

$$\left[\frac{\partial T}{\partial r} \right]_R = \left[\frac{a_0}{1 + a_0} \right] \left[\frac{X}{R(R - X)} \right] (T_g - T_C) \quad (7.34)$$

A further substitution of this expression into equation 7.29 gives,

$$\left[\frac{\partial T}{\partial r} \right]_X = \left[\frac{a_0}{1 + a_0} \right] \left[\frac{R}{X(R - X)} \right] (T_g - T_c) \quad (7.35)$$

Substituting equation 7.35 and the value of a_0 into the energy balance equation 7.23 results in,

$$- \frac{dX}{d\theta} = \frac{R^2 h_g k_{tc}}{\rho_{CO} x_w (\lambda - C_c)} \left[\frac{1}{(k_{tc} - Rh_g)X^2 + R^2 h_g X} \right] (T_g - T_g)$$

$$- \frac{C_{pc} X}{3x_w (\lambda - C_c)} \left[\frac{dT_c}{d\theta} \right] \quad (7.36)$$

$$\text{Let } a_1 = \frac{R^2 h_g k_{tc}}{\rho_{CO} x_w (\lambda - C_c)}$$

$$a_2 = k_{tc} - Rh_g$$

$$a_3 = R^2 h_g$$

$$a_4 = \frac{C_{pc}}{3x_w (\lambda - C_c)}$$

Hence, equation 7.36 becomes,

$$- \frac{dX}{d\theta} = \left[\frac{a_1}{a_2 X^2 + a_3 X} \right] (T_g - T_c) - a_4 X \left[\frac{dT_c}{d\theta} \right] \quad (7.37)$$

The application of equation 7.37 is discussed in the following section.

7.2.2 Mass Transfer at Evaporation Interface

A mass balance over the evaporation interface can be expressed as,

Rate of mass transfer = Rate of vapour diffusion from interface

In mathematical form,

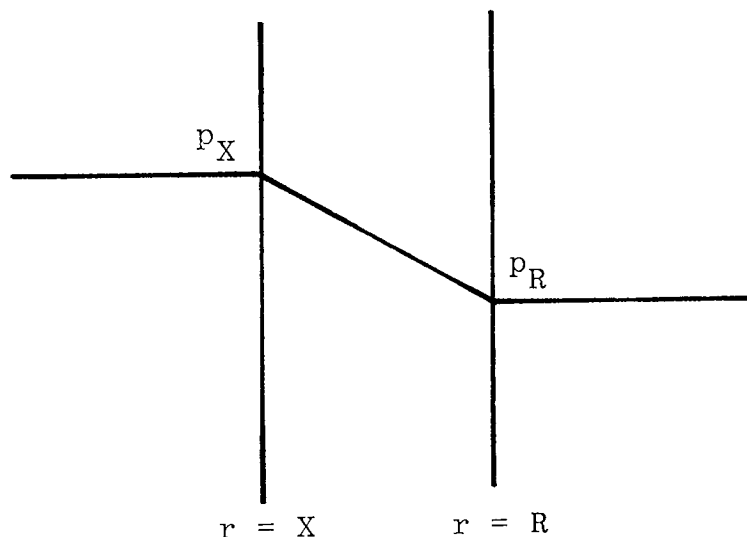
$$- 4\pi X^2 \rho_{CO} x_w \cdot \frac{dX}{d\theta} = - 4\pi X^2 D_{eff} \left[\frac{M_w}{R_c T_c} \right] \left[\frac{\partial p}{\partial r} \right]_X \quad (7.38)$$

where p = moisture concentration expressed as partial pressure and R_c = Universal gas constant

This reduces to,

$$\frac{dX}{d\theta} = \left[\frac{D_{eff}}{\rho_{CO} x_w} \right] \left[\frac{M_w}{R_c T_c} \right] \left[\frac{\partial p}{\partial r} \right]_X \quad (7.39)$$

As in the case of heat transfer, a linear concentration gradient can be assumed.



The rate of mass transfer can be expressed as,

$$J_r = - 4 \pi r^2 D_{\text{eff}} \left[\frac{\partial p}{\partial r} \right] = \text{constant} \quad (7.40)$$

Following the same analysis as in the case of heat transfer, the following equations can be derived,

$$\left[\frac{\partial p}{\partial r} \right]_R = (p_R - p_X) \left[\frac{X}{R(R - X)} \right] \quad (7.41)$$

and
$$\left[\frac{\partial p}{\partial r} \right]_X = \frac{R^2}{X^2} \left[\frac{\partial p}{\partial r} \right]_R \quad (7.42)$$

At the evaporation interface, if it is assumed that,

$p_X = p_C$, equation 7.41 becomes,

$$\left[\frac{\partial p}{\partial r} \right]_R = (p_R - p_C) \left[\frac{X}{R(R - X)} \right] \quad (7.43)$$

Also at $r = R$,

$$- 4 \pi R^2 D_{\text{eff}} \left[\frac{\partial p}{\partial r} \right]_R = - 4 \pi R^2 k_g (p_g - p_R) \quad (7.44)$$

where k_g = gas film mass transfer coefficient.

Substituting equation 7.43 into 7.44,

$$(p_R - p_C) = \left[\frac{R(R - X)k_g}{D_{\text{eff}} X} \right] (p_g - p_R) \quad (7.45)$$

$$\text{Let } b_0 = \frac{R(R - X)k_g}{D_{\text{eff}} X}$$

Hence,

$$(p_R - p_c) = \left[\frac{b_0}{1 + b_0} \right] (p_g - p_c) \quad (7.46)$$

Substituting equation 7.46 into 7.43,

$$\left[\frac{\partial p}{\partial r} \right]_R = \left[\frac{b_0}{1 + b_0} \right] \left[\frac{X}{R(R - X)} \right] (p_g - p_c) \quad (7.47)$$

A further substitution of this expression into equation 7.42 gives

$$\left[\frac{\partial p}{\partial r} \right]_X = \left[\frac{b_0}{1 + b_0} \right] \left[\frac{R}{X(R - X)} \right] (p_g - p_c) \quad (7.48)$$

Substituting equation 7.48 and the value of b_0 into the mass balance equation 7.39 results in,

$$\frac{dX}{d\theta} = \frac{R^2 D_{\text{eff}} M_w k_g}{\rho_{CO} x_w R_c} \left[\frac{1}{(D_{\text{eff}} - Rk_g) X^2 + R^2 k_g X} \right] \frac{(p_g - p_c)}{T_c} \quad (7.49)$$

$$\text{Let } b_1 = \frac{R^2 D_{\text{eff}} M_w k_g}{\rho_{CO} x_w R_c}$$

$$b_2 = D_{\text{eff}} - Rk_g$$

$$b_3 = R^2 k_g$$

Equation 7.49 reduces to,

$$\frac{dX}{d\theta} = \left[\frac{b_1}{b_2 X^2 + b_3 X} \right] \frac{(p_g - p_c)}{T_c} \quad (7.50)$$

Equations 7.50 and 7.37 have to be solved simultaneously since they are coupled heat and mass transfer equations.

Equating 7.50 and 7.37 gives,

$$\frac{dT_c}{d\theta} = \left[\frac{a_1/a_4}{a_2 X^2 + a_3 X} \right] \frac{(T_g - T_c)}{X} + \left[\frac{b_1/a_4}{b_2 X^2 + b_3 X} \right] \frac{(p_g - p_c)}{T_c X} \quad (7.51)$$

From equation 7.38, the rate of mass transfer can be expressed as,

$$- \frac{dW}{d\theta} = - 4\pi X^2 \rho_{CO} x_w \left[\frac{dX}{d\theta} \right] \quad (7.52)$$

Substituting for $\frac{dX}{d\theta}$ from equation 7.50,

$$- \frac{dW}{d\theta} = - 4\pi X^2 \rho_{CO} x_w \left[\frac{b_1}{b_2 X^2 + b_3 X} \right] \frac{(p_g - p_c)}{T_c} \quad (7.53)$$

Equations 7.50, 7.51 and 7.53 can be solved simultaneously by a Runge-Kutta 4th order method to give the crust thickness, core temperature and weight of

the drop as a function of time. The solution requires an expression for the vapour pressure p_c , at the evaporation interface, which is a function only of the core temperature.

$$p_c = f(T_c)$$

A computer program (filename: REI MODEL) was developed to solve the differential equations above on a Commodore PET 32K microcomputer. A listing of the program is included in Appendix D.2.

CHAPTER 8

EXPERIMENTAL APPARATUS

- 8.1 Wind Tunnel
 - 8.1.1 Air Reservoir
 - 8.1.2 Air Drier
 - 8.1.3 Rotameter
 - 8.1.4 Air Heater
 - 8.1.5 The Working Section
- 8.2 Drop Suspension Filament
 - 8.2.1 Glass Filament Fabrication
 - 8.2.2 Filament Holder and Deflection Measurement
- 8.3 Thin Film Glass Filament Thermocouple
 - 8.3.1 Thin Film Thermocouple Fabrication
 - 8.3.2 Thin Film Thermocouple Holder
 - 8.3.3 Cold Junction
 - 8.3.4 Voltage Indicator and Recorder

CHAPTER 8

EXPERIMENTAL APPARATUS

The experimental apparatus comprised a wind tunnel which supplied drying air to the working section in which drops were suspended. The suspension device incorporated a fine glass filament, between 0.176 - 0.2 mm diameter and 150 mm long.

The suspension technique was previously used for the drying of droplets by Frössling (6), Trommelen and Crosby (68) and Charlesworth and Marshall (72) at temperatures ranging from 18 to 400°C. However, for this study a unique thermocouple was developed for the simultaneous measurement of evaporation rate and drop temperature during drying. A fine nickel wire (50 μ diameter) was inserted through a hollow glass filament (0.18-0.2 mm O.D.) and a thin film of copper was deposited onto the outside of the filament under high vacuum. A junction was therefore created at the tip of the filament where about 0.5 mm of nickel wire was exposed.

8.1 The Wind Tunnel

The wind tunnel was designed to supply hot dry air, at a constant humidity and temperature to the working section. A schematic diagram of the tunnel is shown in Figure 8.1 and Plate 8.1.

Compressed air, from the mains supply at 6.53 bar, was piped into a reservoir to dampen any fluctuations. The pressure was then reduced to 1.43 bar and dried by passage through a packed column of silica-gel and aluminate-silicate molecular sieve in a horizontal QVF pipe section. The air flowrate was controlled with a needle valve and measured with a 14F G.E.C. rotameter. The air was heated by two 1 kW electric bar heaters fitted inside an 80 mm O.D. copper tube.

The working section was fabricated from standard 28 mm O.D. copper tube with two windows located midway up the section.

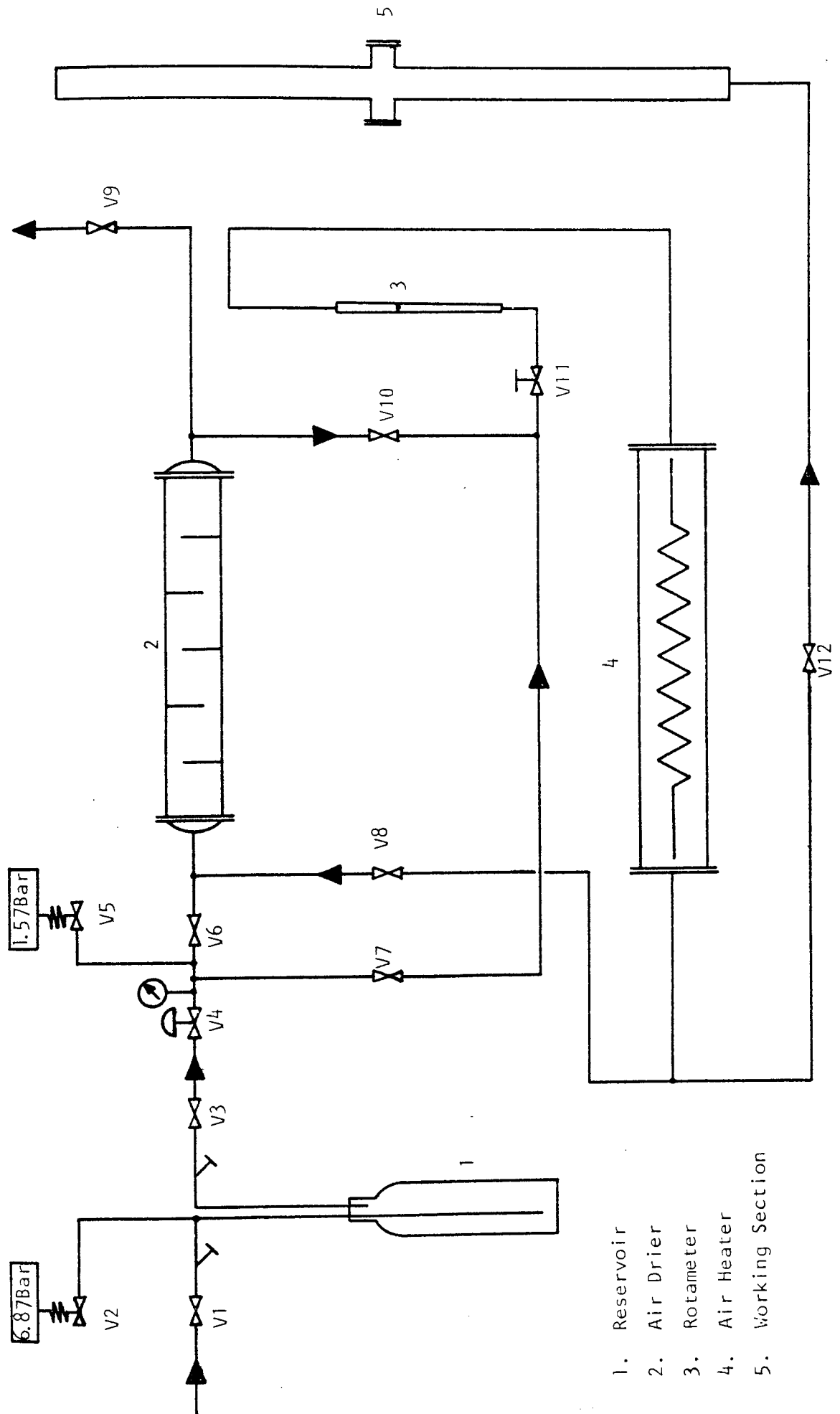
The pipework was designed such that hot air could be redirected over the air drier for regeneration of the desiccants in situ.

8.1.1 Air Reservoir

The air reservoir was fabricated from a standard pressurised gas cylinder with a maximum working pressure



Plate 8.1 Layout of the Wind Tunnel



1. Reservoir
2. Air Drier
3. Rotameter
4. Air Heater
5. Working Section

Figure 8.1 Schematic Diagram of Wind Tunnel.

of 21.70 bar. The schematic diagram and details of the pipework are presented in Figures 8.2 and 8.3.

A 12.7 mm Saunders diaphragm valve (V1) was provided on the inlet side with a 12.7 mm Spirax Sarco strainer. A 12.7 mm pressure relief valve (V2) set at 6.87 bar was also connected to the inlet to the reservoir. The inlet pipe terminated inside the cylinder at a depth of 700 mm from the top. The outlet pipe left at the top of the cylinder and passed through another 12.7 mm Spirax Sarco strainer and a 12.7 mm Hartesley globe valve (V3). The pressure was then reduced to 1.43 bar through a 12.7 mm Spirax Sarco pressure reducing valve (V4). A pressure indicator and a 15 mm Hartesley 5 -15 lbs pressure relief valve (V5), set at 1.57 bar were fitted downstream of the pressure reducing valve.

8.1.2 Air Drier

The air was dried by passage through a packed column of self-indicating silica-gel (6 mesh) and a column of self-indicating aluminate-silicate molecular sieve (type 4A, 1.59 mm pellets). Figure 8.4 illustrates the detailed dimensions of the drier.

The silica-gel and molecular sieve were packed into a 447 mm long horizontal glass pipe section of 87 mm O.D. Five 'three-quarter' baffle plates were located evenly along the column to aid redistribution of the air.

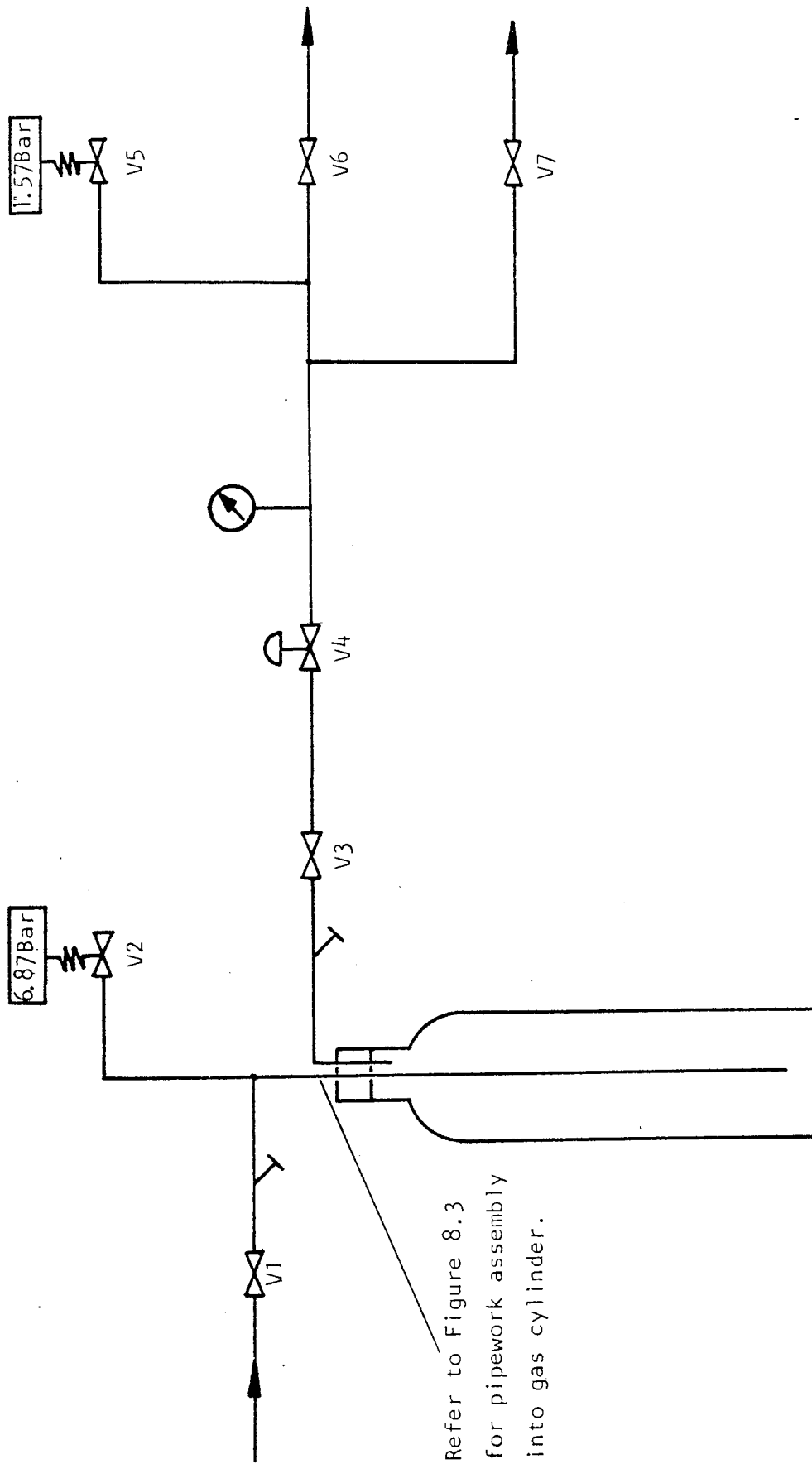
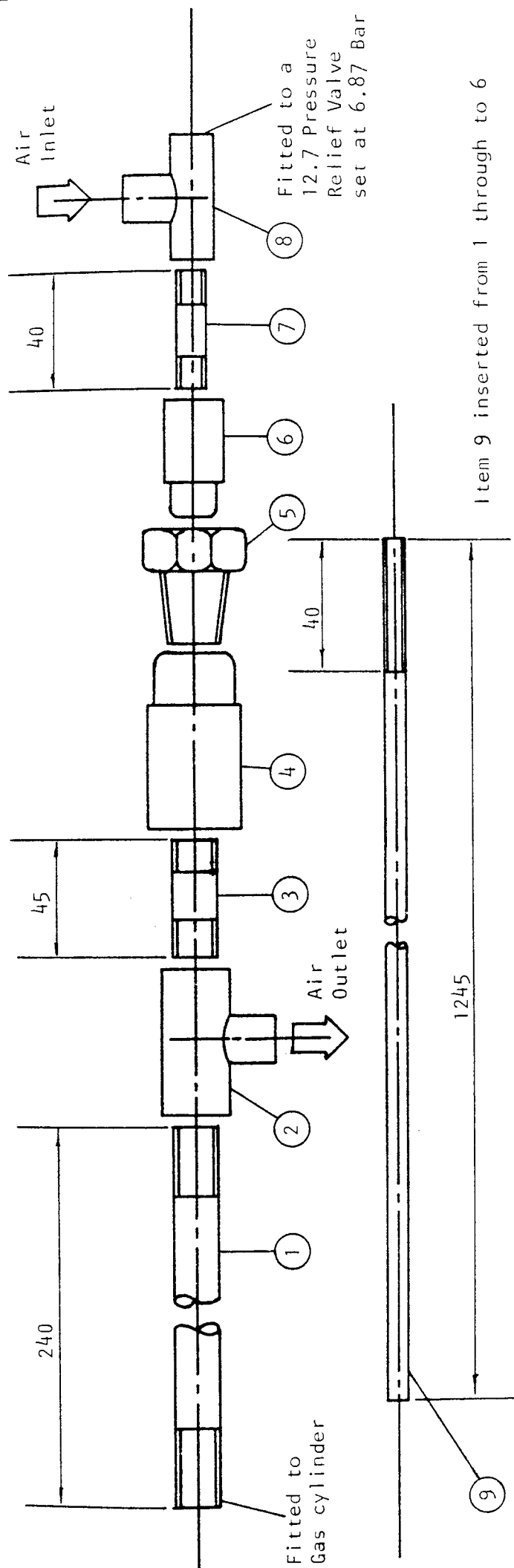


Figure 8.2 Air Reservoir - Schematic Diagram of Pipework.



Item No.	Description	Material
1	19.05 N.B. Tube	Mild Steel
2	19.05 N.B. Unequal T-piece	Mild Steel
3	19.05 N.B. Tube	Mild Steel
4	19.05 to 12.7 BSP Reducer	Mild Steel
5	12.7 BSP Taper Nut	Mild Steel
6	9.53 to 12.7 BSP Reducer	Mild Steel
7	12.7 N.B. Tube	Mild Steel
8	12.7 Equal T-piece	Mild Steel
9	9.53 N.B. Tube	Mild Steel

All Dimensions in mm.

Item 9 inserted from 1 through to 6

Figure 8.3 Pipework Assembly into Gas Cylinder

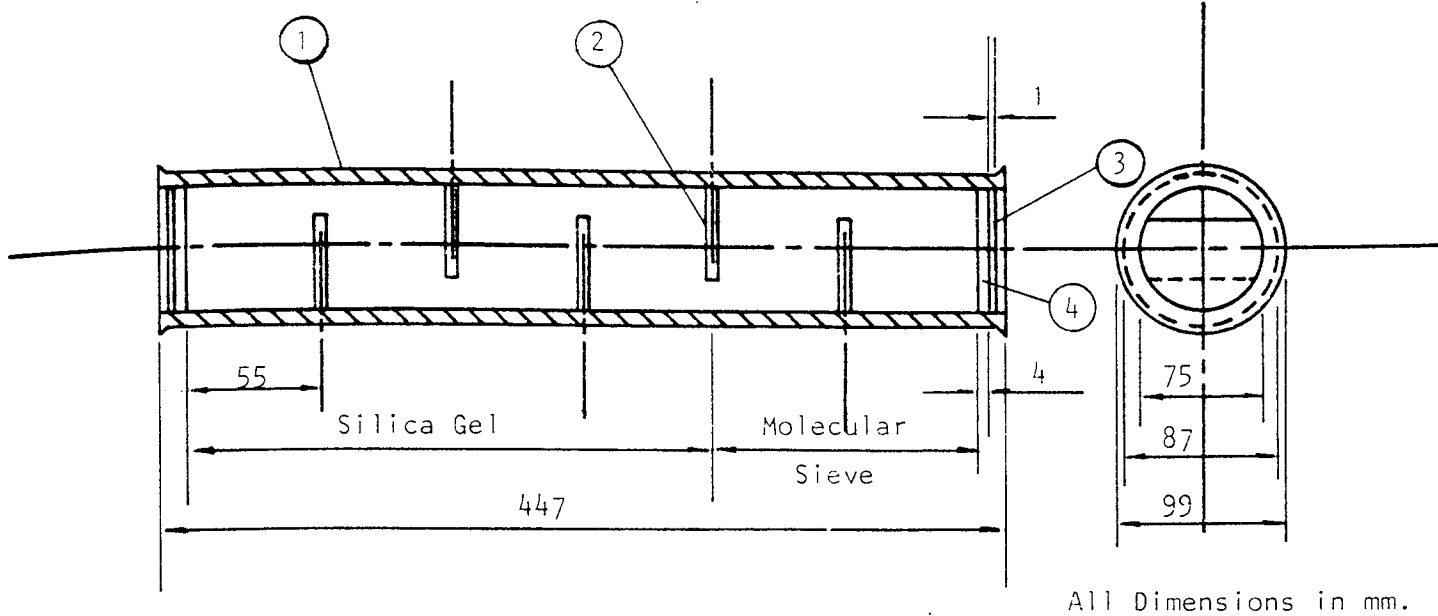
The inlet and outlet moisture content of the air was measured during commissioning using a wet and dry bulb hygrometer. At ambient temperature, the outlet air was found to have a humidity of 0.1 g/kg. This value did not deviate by more than 1.0%, provided at least 25 mm of the molecular sieve packing remained unsaturated, as indicated by the absence of colour change. Therefore, experiments were always conducted with at least this minimum amount of unsaturated desiccant.

Two layers of 100 mesh, 41 gauge stainless steel wire mesh were fitted after the drier to prevent any fine particles from being carried downstream.

The pipework was designed such that regeneration of the desiccants could be carried out in situ. This operation was performed by opening valve V7, closing V6 and V10, opening V9 and V8 and finally closing V12 in that sequence.

8.1.3 Rotameter

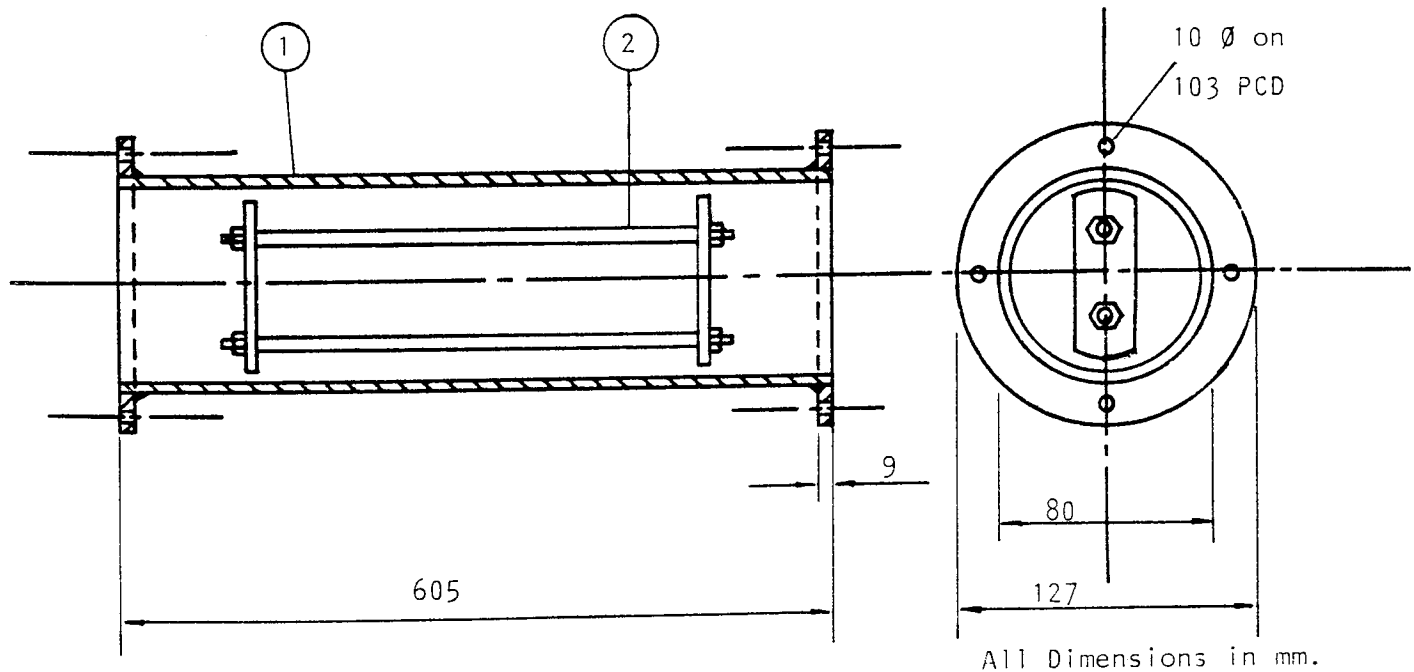
The air flowrate was controlled with a 12.7 mm Crane needle valve (V6) and measured by means of a 14F G.E.C. Elliot rotameter with a Duralumin float. The pipe fittings were also designed to accommodate a size 7F rotameter for better accuracy at low air velocities.



All Dimensions in mm.

Item No.	Description	Material
1	QVF Pipe Section	Glass
2	Baffle Plates	Copper
3	Wire Mesh	Stainless Steel
4	Knit Mesh	Stainless Steel

Figure 8.4 Air Drier Assembly



All Dimensions in mm.

Item No.	Description	Material
1	Heater Pipe	Copper
2	Heater Elements	Tungsten

Figure 8.5 Air Heater Assembly

8.1.4 Air Heater

The air was heated by two 1 kW electric bar heaters placed inside a 605 mm long standard 80 mm O.D. copper tube, mounted horizontally. The air temperature was controlled with a Rotary Regavolt voltage regulator connected to the electrical supply of the heaters, giving a temperature range from ambient to about 300°C. When the system had stabilised, the temperature of the air supplied to the working section did not deviate by more than 0.5°C.

Three layers of stainless steel wire mesh (30 mesh, 32 gauge), spaced 2 mm apart were placed inside the 22 mm O.D. copper tube immediately after the heater to ensure a uniform and stable air temperature.

The heater and all subsequent pipework downstream were insulated with 25.4 mm thick glass fibre insulation.

The detailed dimensions of the heater are shown in Figure 8.5.

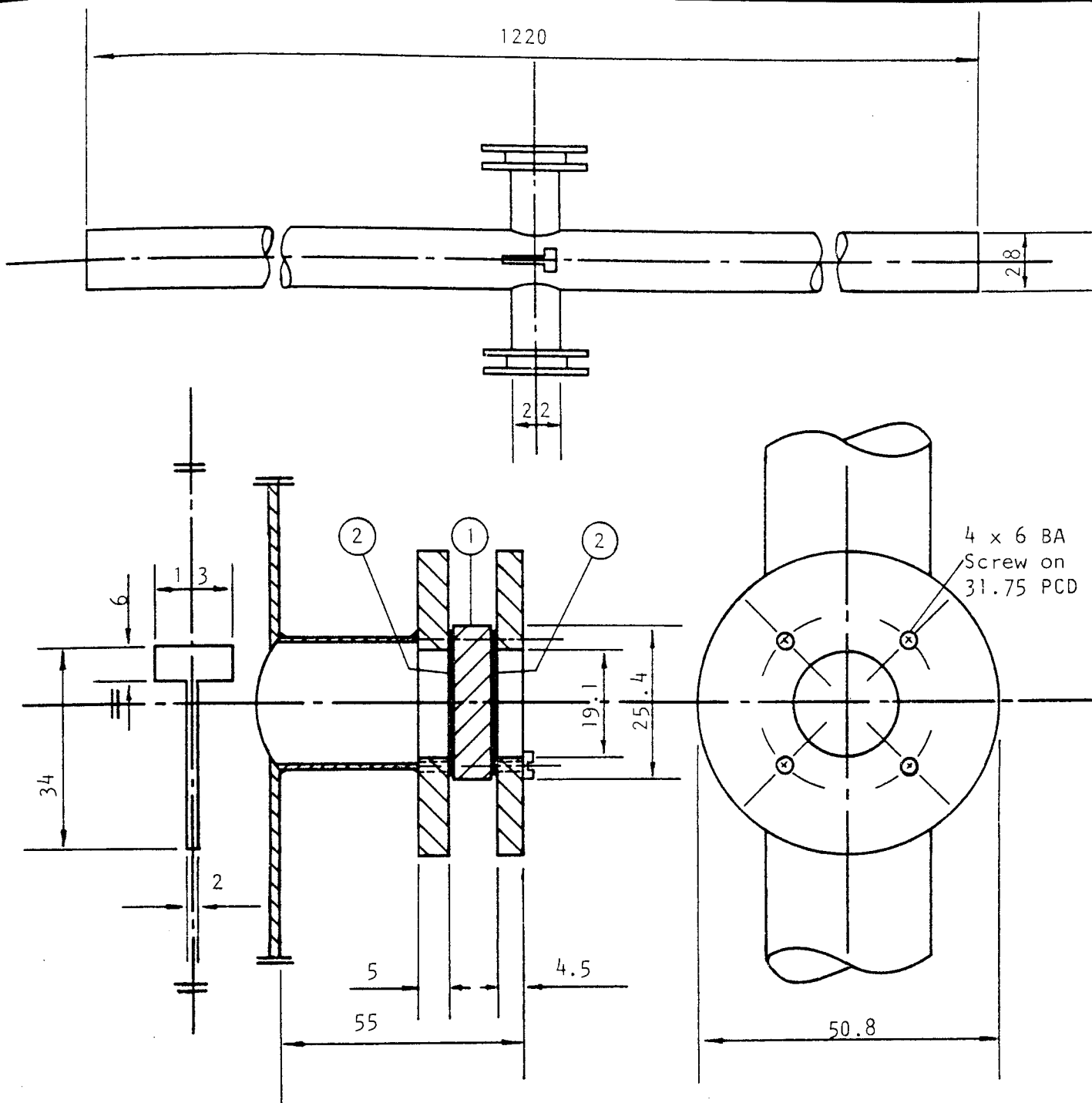
8.1.5 The Working Section

The working section of the wind tunnel was fabricated from a standard copper tube, 28 mm O.D. and 1220 mm long, mounted vertically. Two windows were located opposite each other midway up the tube. The windows were flanged

to take an optically flat glass, 6.35 mm thick and 25.4 mm diameter, through which the suspended drop could be photographed, with the required back lighting. An access slit, 34 mm long was provided at right angles to the window, through which the glass filament and suspended drop could be inserted into the tunnel.

Detailed drawings of the working section are presented in Figure 8.6.

The inlet to the working section was coupled to the rest of the pipework by a 28 mm copper to copper right angle elbow. The inside of this elbow was packed with steel wool between two layers of 5 mm thick knit mesh (0.15 mm wire diameter, 4 stitches per cm), held together by two pieces of 30 mesh, 32 gauge wire mesh. To further ensure that a flat velocity profile would be presented to the suspended drop, three layers of fine stainless steel wire mesh (100 mesh, 41 gauge), spaced 1 mm apart, were placed about 6 pipe diameters upstream from the point of drop suspension. The velocity profile was recorded during commissioning with a pitot static tube and a Furness electronic micromanometer, with its output connected to a Tarkan chart recorder. The profile across the section where the drop was suspended, is shown in Figure 8.7.



All Dimensions in mm.

Item No.	Description	Material
1	6.35 mm Thick Optical Flat	Glass
2	1 mm Thick Gaskets	Asbestos Fibre

Figure 8.6 Working Section and Viewing Window Assembly.

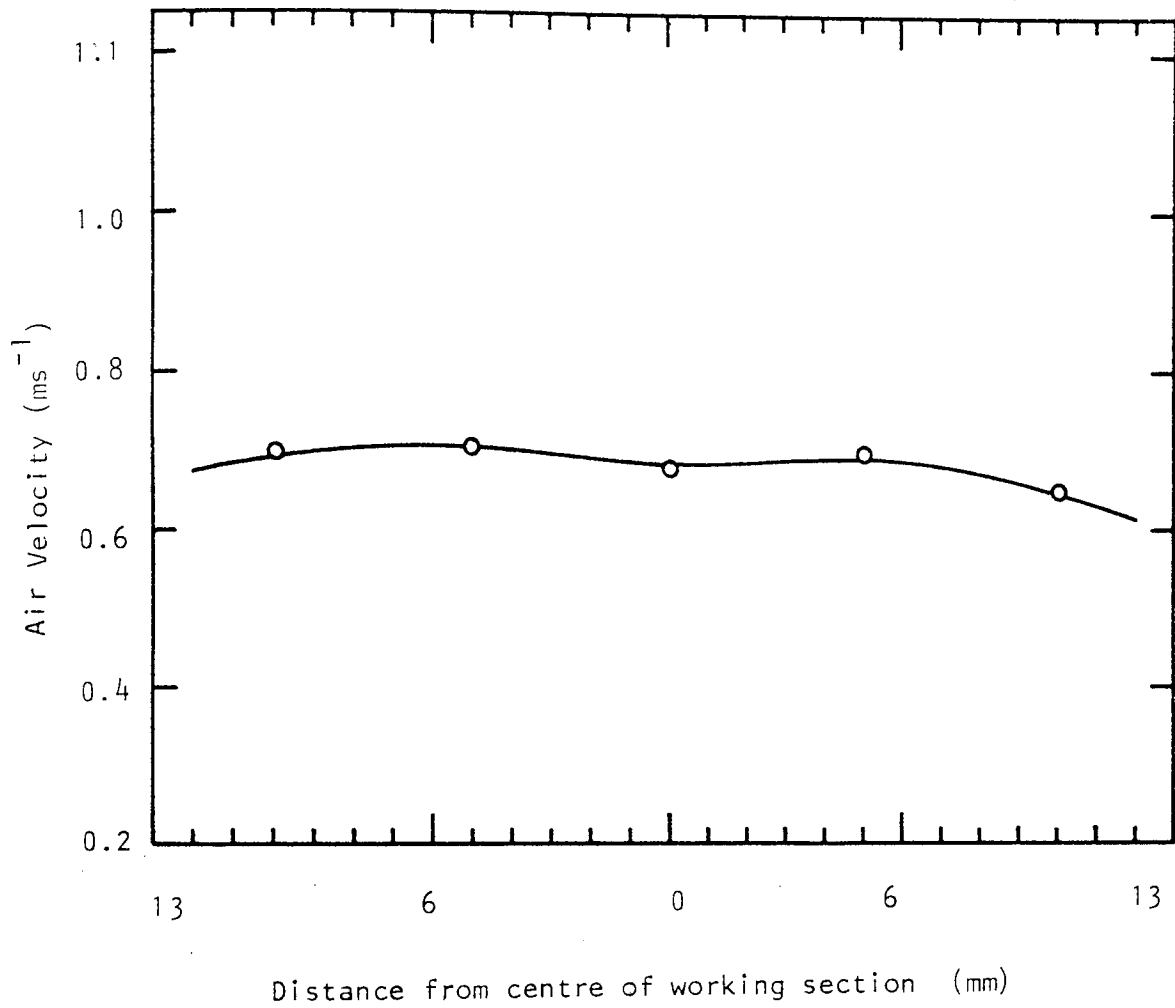


Figure 8.7 Typical velocity profile across the working section.

The entire length of the working section was covered with 25.4 mm thick fibre glass insulation to prevent heat loss.

8.2 Drop Suspension Filament

Drops were suspended at the free end of a fine glass filament of 0.176 - 0.2 mm diameter and 150 mm long. The fixed end of the filament was held in a stainless steel clamp and the measured angular deflection provided a continuous weight measurement.

8.2.1 Glass Filament Fabrication

The glass filament was drawn from a 9.525 mm diameter soda-lime glass rod. A length of about 100 mm was heated in the middle until the glass was almost 'flowing'. The two ends were then rapidly drawn apart; the stretching and rapid cooling resulted in a fine flexible filament at the heated section.

After cutting off the required length, one end of the filament was heated very gently to give a smooth 45° bend and the tip was touched off in the flame to give a knob.

8.2.2 Filament Holder and Deflection Measurement

The fixed end of the filament was held horizontally in a clamp mounted on a block of polypropylene, which slid on a retort stand. Figure 8.8 shows the details of the filament holder.

The angular deflection was measured with a perspex protractor mounted on the side of the polypropylene block. Measurements were taken at a distance of 25 mm from the free end of the filament to give the largest deflection to weight ratio.

8.3 Thin Film Glass Filament Thermocouple

The thin film glass filament thermocouple was fabricated from a 250 mm long hollow glass filament of 0.18-0.2 mm diameter with a bore of 0.07 - 0.10 mm. A 50 μ nickle wire (99% purity) was threaded through the filament and copper was deposited onto the outer surface of the filament using a vacuum coating technique.

The thin film thermocouple holder was designed to serve as a cold junction reference for voltage measurements.

8.3.1 Thin Film Thermocouple Fabrication

The hollow filament was drawn from a piece of 100 mm long soda-lime glass tube of 12.7 mm O.D. and 11.113 mm I.D. After one end of the tube had been sealed, the centre section was heated gently and 'blown' from the open end to give a thin walled 'bulb'.

The expanded section was again heated gently until the 'bulb' just began to 'flow'. The two ends were then rapidly stretched apart, giving a hollow filament of between 0.18 - 0.2 mm O.D. A length of about 250 mm was then broken off.

The procedure for insertion of the nickle wire was as follows:-

- 1) A length of glass capillary, 40 mm long and with a bore slightly larger than the O.D. of the filament was used as a 'guide sleeve'. The 'sleeve' was inserted over the end of the filament and the end of the nickle wire was carefully inserted into the filament to a depth of about 10 mm. (Step 1, Figure 8.9).
- 2) The 'sleeve' was gently held down and the filament pulled through taking the nickle wire with it until only 5 mm of the filament remained 'sleeved'. (Step 2, Figure 8.9).

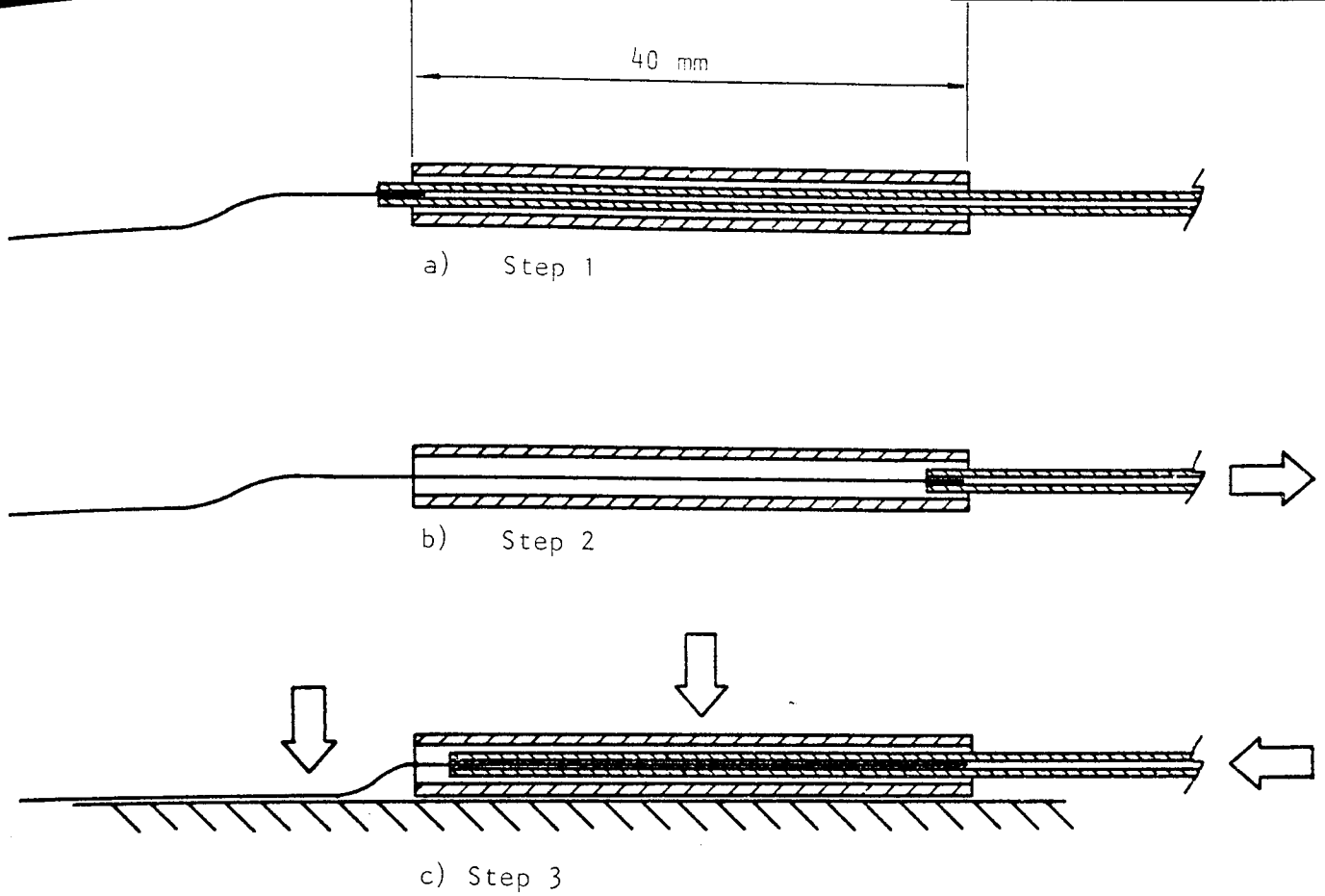
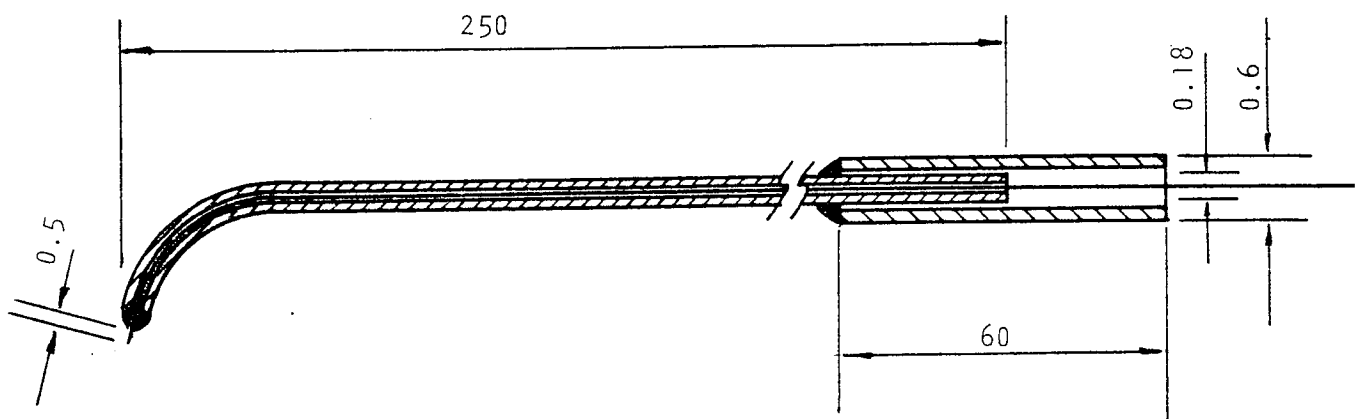


Figure 8.9 Procedure for Insertion of Nickel Wire into the Hollow Filament.



All Dimensions in mm.

Figure 8.10 Threaded Filament Ready for Coating.

3) The free end of the nickle wire and the 'sleeve' were gently pressed onto an adhesive tape and the filament was carefully pushed back through the sleeve. (Step 3, Figure 8.9).

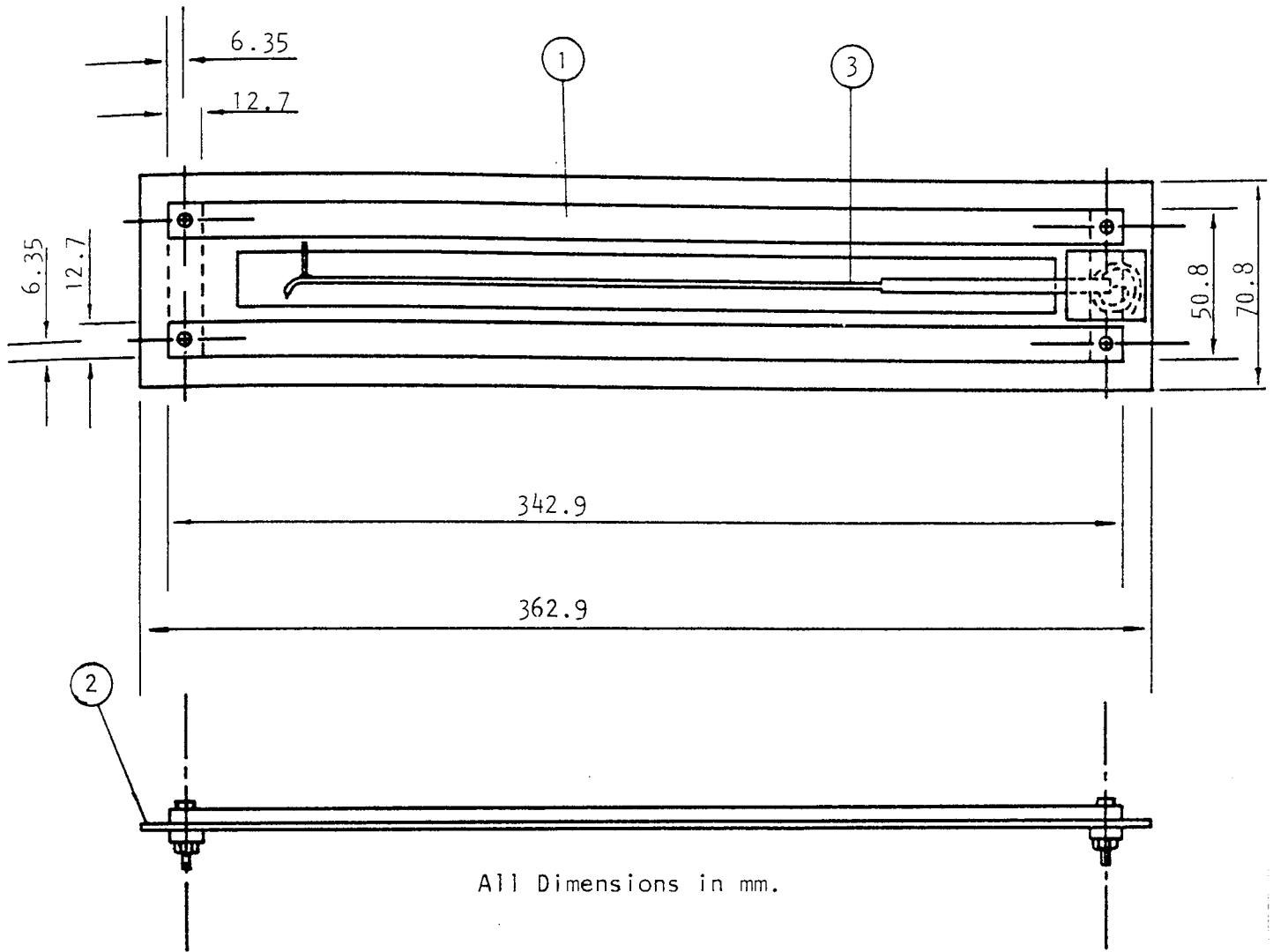
The procedure was repeated between Steps 2 and 3, until the wire emerged from the other end of the filament.

The free end of the filament was heated gently to give a smooth 45° bend and the end sealed with a quick setting epoxy resin, Araldite Rapid.

A glass capillary of 0.6 mm O.D. was 'sleeved' and sealed over the fixed end of the filament to strengthen it for insertion into the cold junction pocket.

To obtain a durable and adhesive coating, the glass surface had to be thoroughly cleaned to remove any contaminants. Initial cleaning was carried out by immersion in a dilute solution of a detergent (Decon 90). After rinsing with distilled water, final cleaning was achieved with a cotton bud soaked in iso-propanol. Figure 8.10 shows the threaded filament ready for vacuum coating.

The threaded filament was mounted on a mild steel frame, the dimensions of which are shown in Figure 8.11, and copper was evaporated from a platinum boat onto the top and underside of the filament. This process was carried out



Item No.	Description
1	Mild Steel Frame
2	1.5 mm Thick Cardboard
3	Glass Filament Thermocouple

Figure 8.11 Mild Steel Frame.

in a vacuum chamber at a pressure between 10^{-4} - 10^{-5} Torr giving a copper film of between 50-100⁰A thick. Further details of the vacuum coating equipment and technique can be found in the handbook by Holland (108).

8.3.2 Thin Film Thermocouple Holder

The thin film thermocouple was held in a specially designed holder which also served as a cold junction pocket. The holder consisted of two basic components, the retort clamp and the ice container. The retort clamp was fabricated from a block of clear perspex (40 X 50 X 50 mm) with a 13.1 mm hole to fit the retort stand.

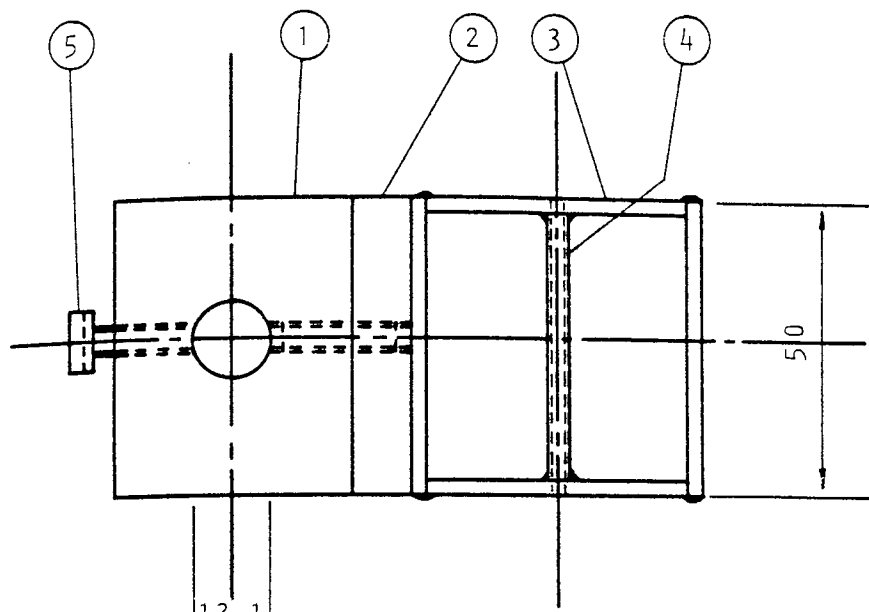
The ice container was fabricated from 2.5 mm thick clear perspex, fitted together with Araldite. A stainless steel needle tube was fitted through the container, acting as the cold junction pocket.

The ice container was fitted to a nylon angle adjustment plate which was connected to the retort clamp via a 20 mm long O BA threaded rod.

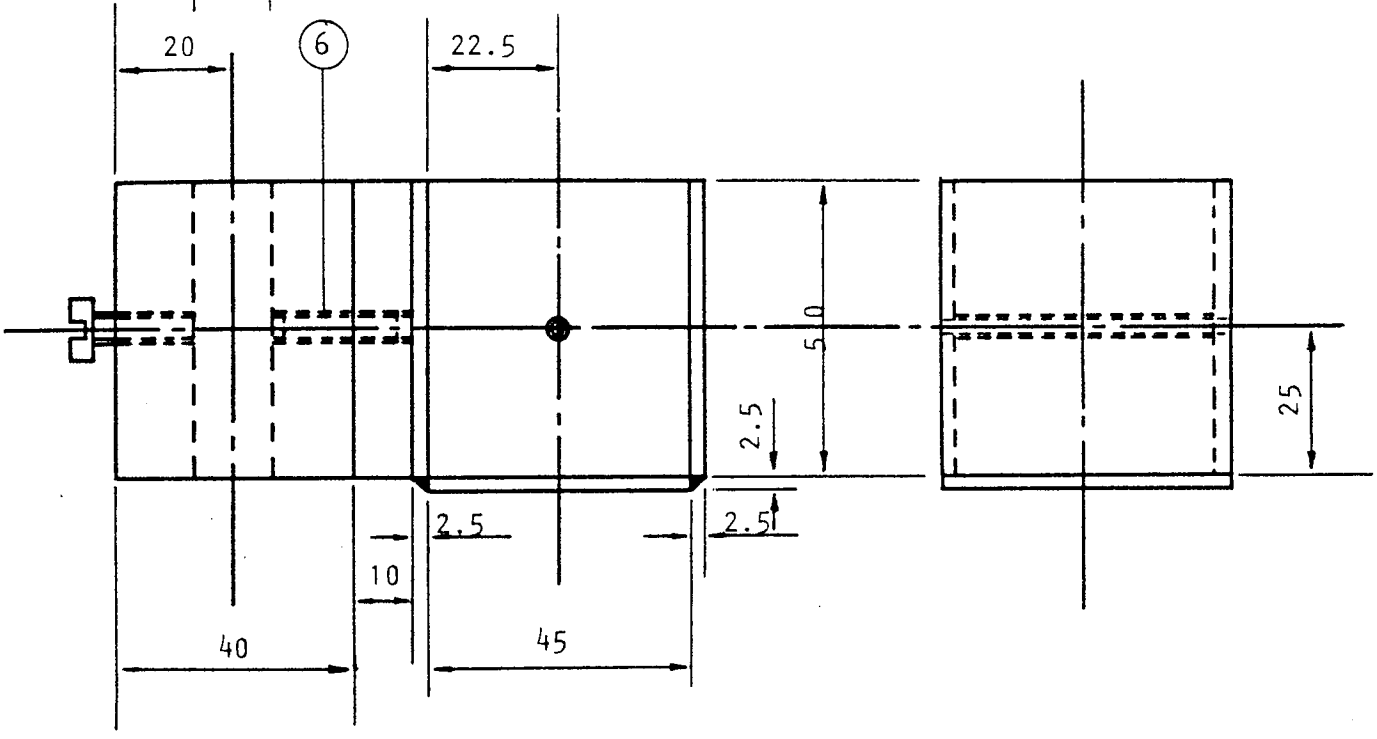
Details of the assembly are shown in Figure 8.12.

8.3.3 Cold Junction

The cold junction of the thermocouple was made by winding a piece of 50 μ diameter nickle wire round the

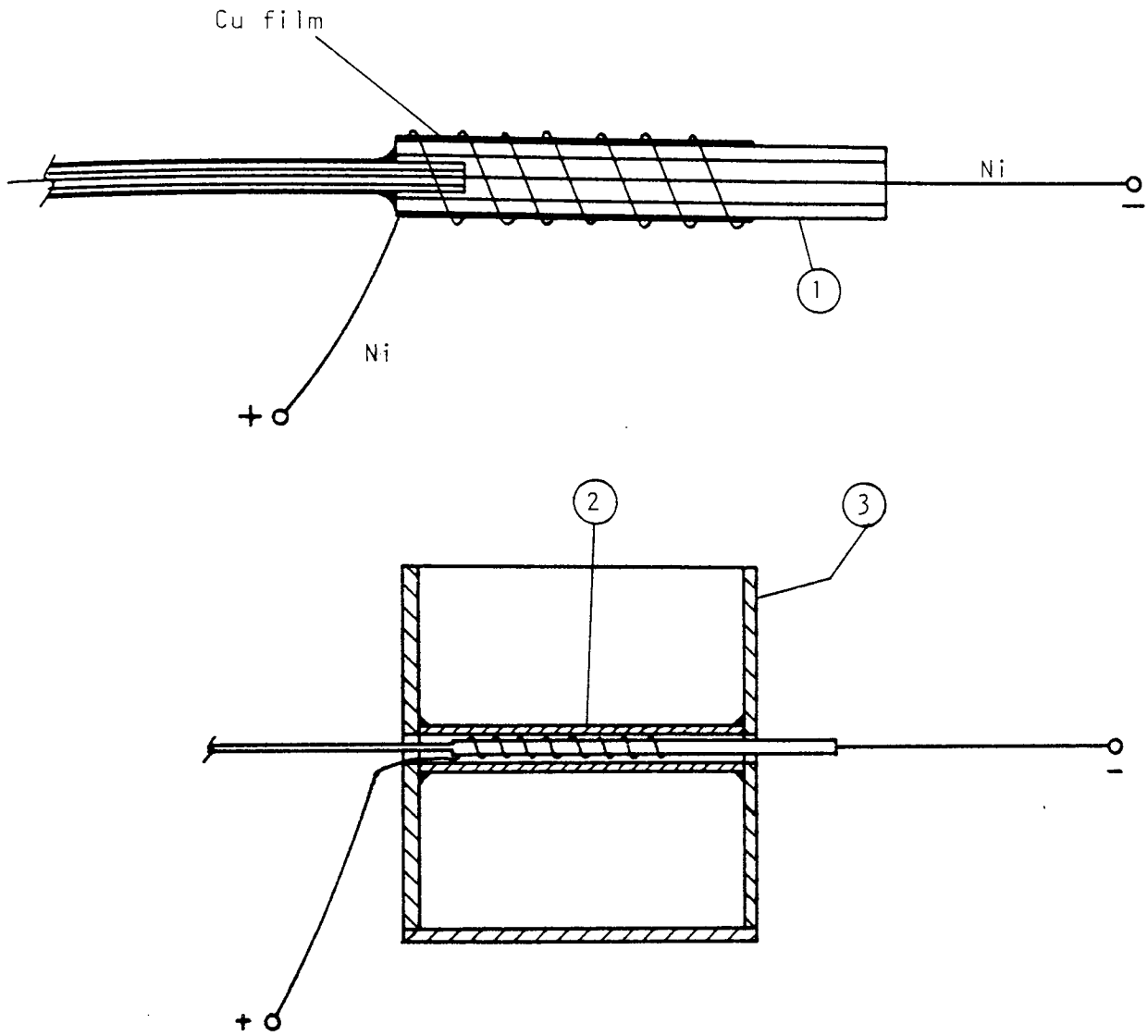


All Dimensions in mm.



Item No.	Description	Material
1	Retort Clamp	Clear Perspex
2	Angle Adjustment Plate	Nylon
3	Ice Container	Clear Perspex
4	Cold Junction Pocket	2 mm O.D. S.Steel Needle Tube
5	Locking Screw	OBA - Brass
6	Connecting Rod	OBA - Brass

Figure 8.12 Thin Film Thermocouple Holder Assembly.



Item No.	Description
1	Glass Capillary
2	Cold Junction Pocket
3	Ice Container

Figure 8.13 The Cold Junction and its location in the Ice Container.

glass capillary at the fixed end of the thin film thermocouple. The glass capillary was then inserted into the cold junction pocket in the ice container. Figure 8.13 shows the details of the cold junction and its location in the ice container.

8.3.4 Voltage Indicator and Recorder

The voltage from the thermocouple was measured with a Comark D.C. Microvoltmeter (Type 1221) on a 0 - 10 mV full scale deflection. The output of the microvoltmeter was connected to a Tarkan chart recorder. Setting the chart speed of the recorder, enabled a simultaneous time and voltage reading to be recorded.

CHAPTER 9

EXPERIMENTAL PROCEDURE

- 9.1 Instrument Calibration
 - 9.1.1 Air Flowrate
 - 9.1.2 Temperature
 - 9.1.3 Drop Weight
 - 9.1.4 Drop Temperature
- 9.2 Experiments
 - 9.2.1 Water Drops at Ambient Temperature
 - 9.2.2 Water Drops at Elevated Temperature
 - 9.2.3 Drops of Aqueous Sodium Sulphate Decahydrate
 - 9.2.4 Simultaneous Drop Weight and Drop Temperature Experiments

CHAPTER 9

EXPERIMENTAL PROCEDURE

9.1 Instrument Calibration

In each experiment, air velocity, air temperature and drop weight were measured. Drop weight and drop temperature were also measured simultaneously in a series of experiments using the thin film thermocouple. The calibration of instruments used for these measurements is discussed below.

9.1.1 Air Flowrate

The air flowrate was measured by means of a 14F G.E.C. rotameter with a Duralumin float. The float position in the rotameter was calibrated against the flowrate of dry gas, at ambient temperature, measured with a Parkinson gas meter. Air velocity in the working section of the wind tunnel was then calculated for different temperatures using the appropriate air densities.

9.1.2 Temperature

The air temperature at the entry to the air drier and in the working section, and the wall temperature of the air heater were measured with Ni-Cr/Ni-Al thermocouples. The voltages from the thermocouples were measured with a Comark Digital Thermometer (Type 3501) via a Comark 20 way Manual Selector Unit (Type 1694). The digital thermometer was factory calibrated with automatic cold junction compensation and had a resolution of 0.5°C. The calibration was further checked with a standard Ni-Cr/Ni-Al thermocouple and a millivoltmeter using a uniform temperature water bath.

9.1.3 Drop Weight

The weight of an evaporating drop was measured by the deflection of the glass filament. The glass filament was calibrated using different lengths of cotton threads as standard weights. A trace of vaseline was smeared onto the tip of the filament so that the cotton thread could be suspended from it.

A typical calibration curve for drop weight against deflection is shown in Figure 9.1. However, the measured deflections during a run had to be corrected for the drag force caused by the upward flowing air.

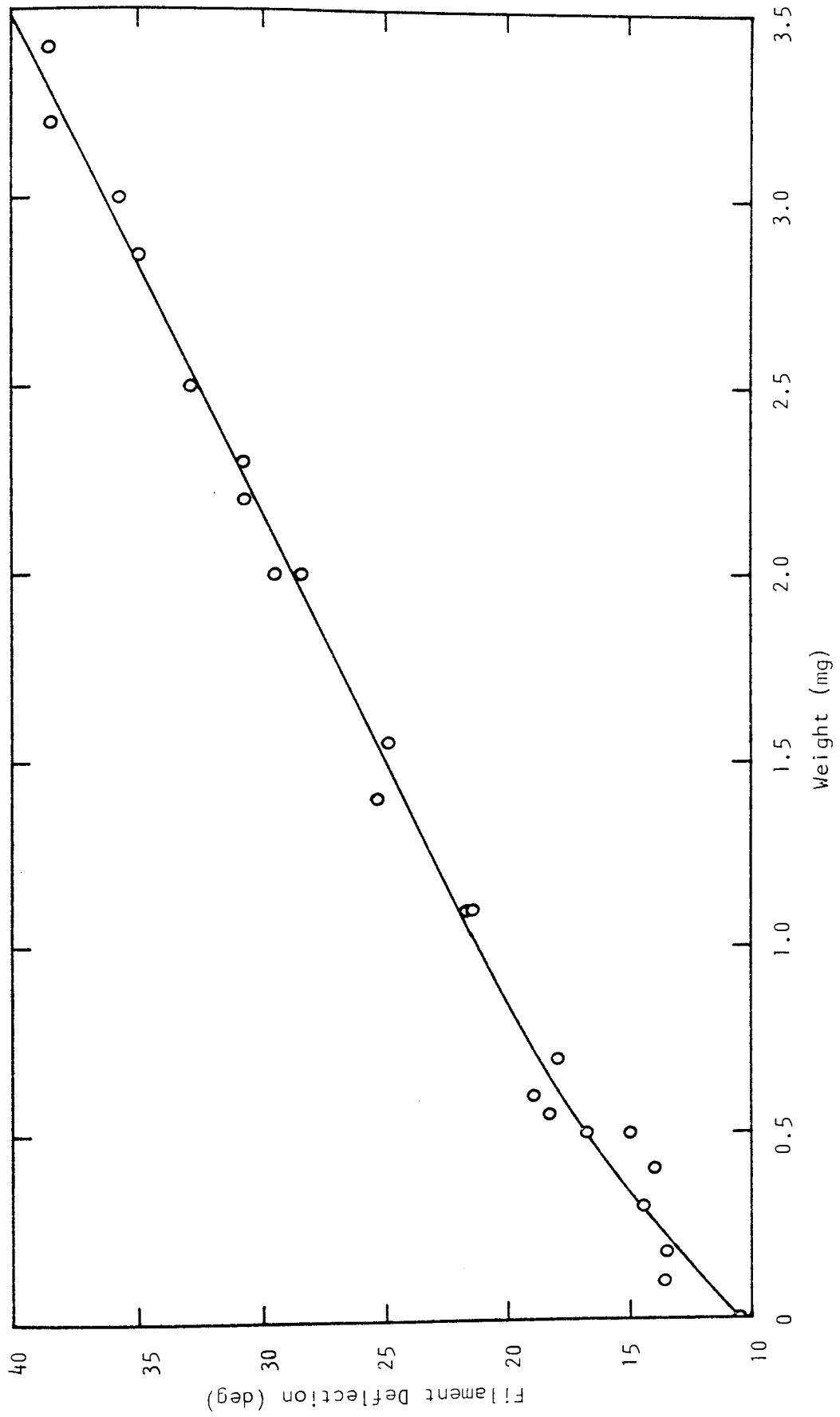


Figure 9.1 Glass Filament Calibration Curve (C4, 5, 6).

The total drag force F_t , on the drop and the section of the filament inside the tunnel can be expressed as,

$$F_t = F_d + F_f \quad (9.1)$$

where F_d = drag force on spherical drop

F_f = drag force on filament

For the drop,

$$F_d = C_d A_p \rho v^2/2 \quad (9.2)$$

and for the filament,

$$F_f = C_f A_f \rho v^2/2 \quad (9.3)$$

where C_d, C_f = drag coefficients for a sphere and cylinder respectively.

A_p, A_f = projected areas for a sphere and cylinder respectively.

For a typical experimental condition,

$$v = 0.316 \text{ ms}^{-1}$$

$$d_p = 1.069 \times 10^{-3} \text{ m}$$

$$d_f = 1.764 \times 10^{-4} \text{ m}$$

$$\mu = 1.8 \times 10^{-5} \text{ kg ms}^{-1}$$

$$\rho = 1.205 \text{ kgm}^{-3}$$

Length of filament inside tunnel = $12 \times 10^{-3} \text{ m}$

Hence, for the filament,

$$\begin{aligned} \text{Re}_f &= 0.316 (1.764 \times 10^{-4})(1.205)/1.8 \times 10^{-5} \\ &= 3.73 \end{aligned}$$

The drag coefficient for a horizontal cylinder at a Reynolds number of 3.73 is 5 (109).

Therefore,

$$\begin{aligned} F_f &= 5 (1.764 \times 10^{-4})(13 \times 10^{-3})(1.205)(0.316)^2/2 \\ &= 6.898 \times 10^{-7} \text{ N} \end{aligned}$$

Similarly for the drop,

$$\begin{aligned} \text{Re} &= 0.316(1.069 \times 10^{-3})(1.205)/1.8 \times 10^{-5} \\ &= 22.61 \end{aligned}$$

The drag coefficient for a sphere at a Reynolds number of 22.61 is 3 (109).

Therefore,

$$\begin{aligned} F_d &= 3 (\pi/4)(1.069 \times 10^{-3})^2(1.205)(0.316)^2/2 \\ &= 1.620 \times 10^{-7} \text{ N} \end{aligned}$$

The total drag force caused by the upward flowing air,

$$\begin{aligned} F_t &= (6.898 + 1.620) \times 10^{-7} \text{ N} \\ &= 8.518 \times 10^{-7} \end{aligned}$$

The actual weight of a suspended drop was therefore the measured weight (from the deflection) plus (F_t/g).

9.1.4 Drop Temperature

Drop temperatures were measured with the thin film glass filament thermocouple. The voltage output was measured with a Comark D.C. Microvoltmeter (Type 1221) and recorded with a Tarkan chart recorder.

Dry air in the working section of the wind tunnel, at a velocity of 2.0 ms^{-1} , was used as the uniform temperature source for calibration. The thin film thermocouple was calibrated against a standard Ni-Cr/Ni-Al thermocouple over a temperature range of 8.75°C to 110.25°C .

For the purposes of calibration, a glass helical coil immersed in an ice bath was located between the air heater and the working section. The air temperature was cooled to 8.75°C by the addition of sodium chloride to the ice bath (25 wt.%); air was heated by the air heater together with the addition of warm water to the bath.

The calibration curves for the thin film thermocouple are presented in Figures 9.2 and 9.3. The curve can be accurately approximated by two linear sections and therefore a linear regression analysis was used. The resulting variation between voltage output and temperature was found to be,

$$T_S = 43.27 V + 3.02 \text{ for } V \leq 1.1 \text{ mV} \quad (9.4)$$

and $T_S = 37.95 V + 9.90 \text{ for } 1.1 \text{ mV} < V < 2.65 \text{ mV} \quad (9.5)$

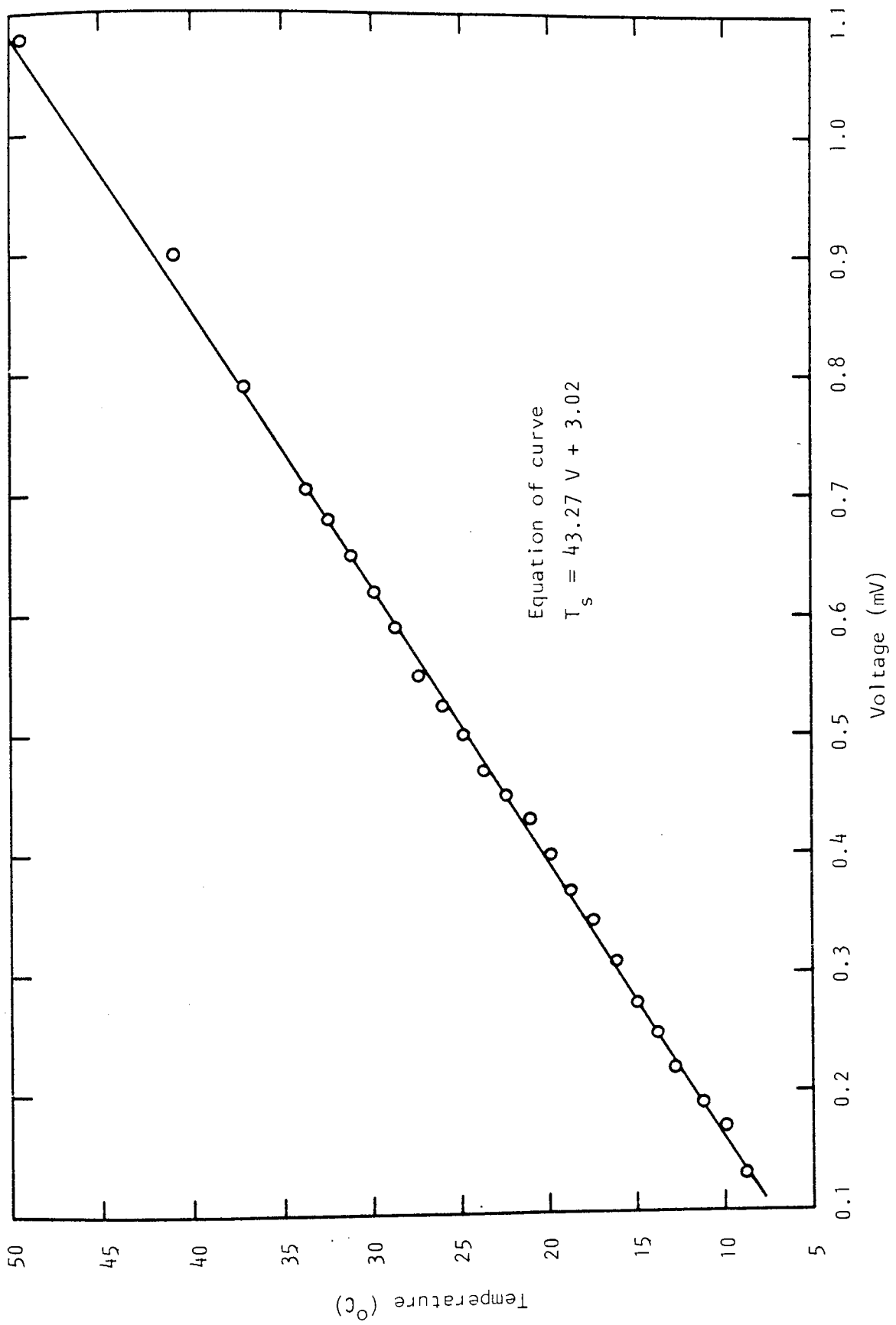


Figure 9.2 Thin Film Glass Filament Thermocouple Calibration Curve for $V \leq 1.1$ mV.

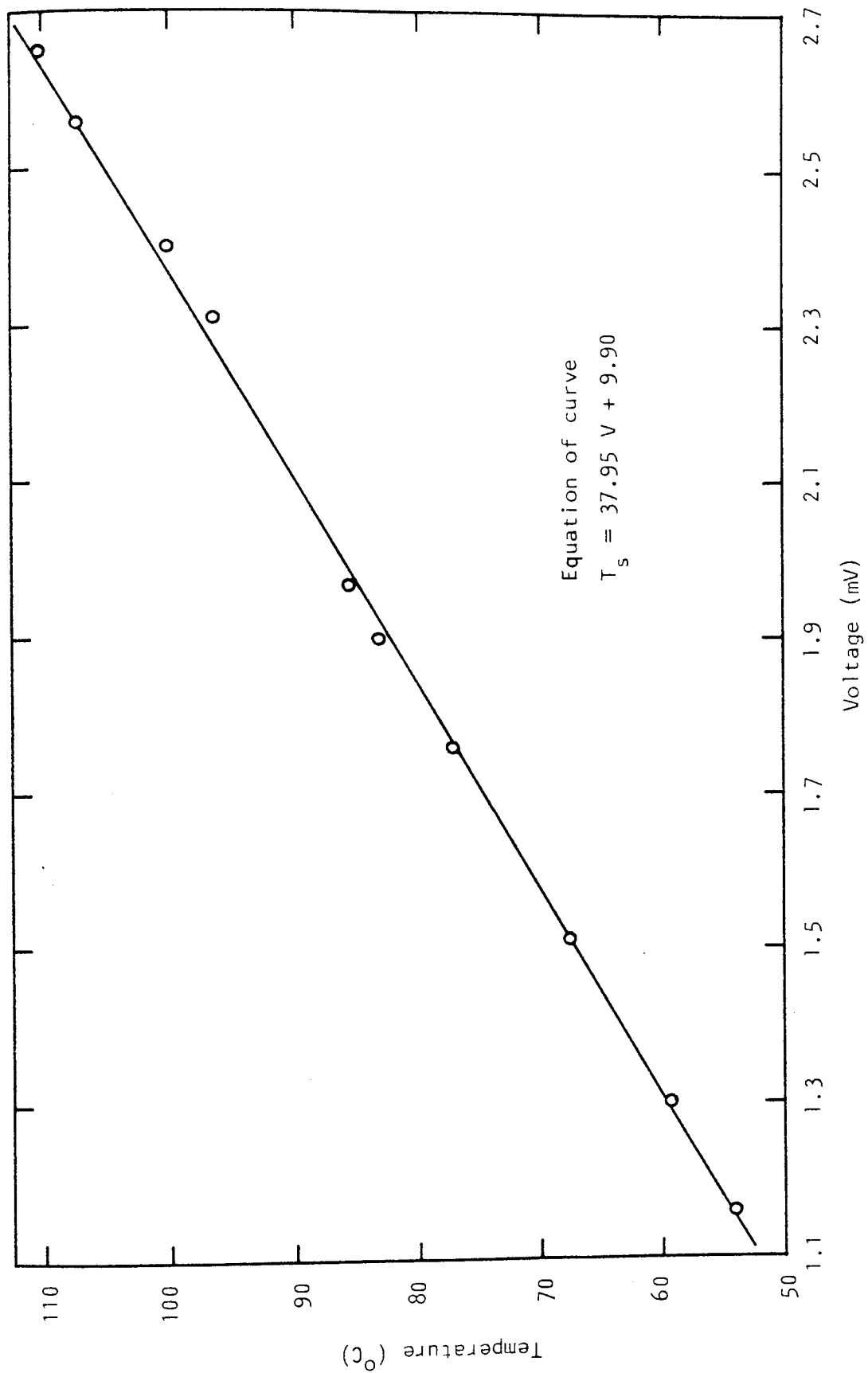


Figure 9.3 Thin Film Glass Filament Thermocouple Calibration Curve for
 1.1 mV < V < 2.65 mV.

9.2 Experiments

The experiments were divided into the following categories,

- 1) The evaporation of water drops at ambient temperature
- 2) The evaporation of water drops at elevated temperatures.
- 3) The evaporation of drops of aqueous sodium sulphate decahydrate at varying air velocities and air temperatures.
- 4) The simultaneous measurement of evaporation rates and drop temperatures of drops of aqueous sodium sulphate decahydrate using the thin film thermocouple.

9.2.1 Water Drops at Ambient Temperature

A drop of distilled water was formed at the end of the needle (0.5 mm diameter) of a hypodermic syringe and transferred to the tip of the glass filament. The filament was depressed slightly during the transfer so that when the drop attached itself, the filament would not oscillate under the sudden weight.

The initial deflection of the filament outside the working section was noted so that the buoyancy forces caused by the upward flowing air in the working section could be accounted for. The deflection of the filament was subsequently recorded at varying time intervals, until the drop became so small (less than about 0.3 mm diameter), that its shape was distorted by the suspension filament. The sphericity of the drop during each experiment was checked by photography using a Chinon 35 mm camera with a telephoto extension lens and backlighting.

The required velocity in the working section was controlled by adjusting the needle valve V11, for the corresponding volume flowrate of air. The air velocity was varied between 0.026 - 0.772 ms⁻¹ for a range of drop Reynolds number between 1.85 - 58.15.

The wet bulb temperature was measured by means of a Ni-Cr/Ni-Al thermocouple with the thermojunction covered with a thin paper tissue saturated with distilled water.

9.2.2 Water Drops at Elevated Temperature

The evaporation of water drops was studied for air temperatures of 34, 46.5, 63 and 79°C at a constant air velocity of about 0.77 ms⁻¹.

The procedure for evaporation rate and drop temperature measurements was similar to that for water drops at ambient temperature, as discussed in section 9.2.1

9.2.3 Drops of Aqueous Sodium Sulphate Decahydrate

Solutions of sodium sulphate decahydrate were made up by the addition of the calculated amount of Analar quality salt (supplied by Fisons Scientific Apparatus Limited), to a fixed volume of distilled water. Four concentrations were used in this series of experiments, 5, 15, 30.3 and 54.1 wt.% solids.

The drops were transferred to the glass filament by means of a hypodermic syringe. At the higher concentrations the slurry and the hypodermic needle had to be warmed slightly to dissolve the solids before being transferred to the glass filament. This was done to prevent any premature crystallisation and hence blockage occurring in the hypodermic needle.

The air temperature was varied between 20 - 110°C. The air velocity was varied between 0.50 - 3.0 ms⁻¹, corresponding to a range of drop Reynolds number between 33 and 125.

At the end of each run, the solid particle remaining at the end of the filament was gently removed with a needle and glued onto an aluminium stud. The stud was then placed in a vacuum chamber and a thin film of gold-palladium was deposited onto the particle by a sputtering technique. The coated specimen was then introduced into the specimen chamber of a Scanning Electron Microscope (S.E.M.) where it was scanned by a fine electron beam. A three-dimensional image of the specimen, up to a magnification of 5,000 was displayed on the Visual Display Unit (V.D.U.) and selected areas of the specimen could be photographed with a 35 mm camera attached to the S.E.M.

9.2.4 Simultaneous Drop Weight and Drop Temperature Experiments

This series of experiments were conducted with the thin film thermocouple. Drops of aqueous sodium sulphate decahydrate at a concentration of 40 wt% solids were evaporated at air velocities between 1.0 - 1.523 ms⁻¹. Air temperatures were between 20 - 80°C, corresponding to a drop Reynolds number between 65 and 75.

The thermal e.m.f. from the thin film thermocouple was recorded on a Tarkan chart recorder at a chart speed of 5 cm.min⁻¹.

CHAPTER 10

EXPERIMENTAL RESULTS

- 10.1 Water Drops at Ambient Temperature
- 10.2 Water Drops at Elevated Temperatures
- 10.3 Drops of Aqueous Sodium Sulphate
Decahydrate
- 10.4 Simultaneous Drop Weight and Core
Temperature Measurements of Sodium
Sulphate Decahydrate Slurry Drops
- 10.5 Comparison of Experimental Results
and Model Predictions

CHAPTER 10

EXPERIMENTAL RESULTS

10.1 Water Drops at Ambient Temperature

The experimental results for water drops at ambient temperature are presented as Nusselt numbers calculated from equation 7.6. The results of these experiments, covering a velocity range of 0.026 - 0.772 ms⁻¹, are presented in Appendix A.4.1 and summarised in Table 10.1. A plot of Nu against Re^{0.5} Pr^{0.33} is presented in Figure 10.1.

A computer program (File name:- EVAPORATION) written in Commodore Basic on a Commodore PET 32K Microcomputer was used to analyse the data. A listing of the program is presented in Appendix A.3.1.

A least squares correlation technique, described in Appendix A.2.1, was used to correlate the results according to the equation,

$$\text{Nu} = 2 + \phi \text{ Re}^{0.5} \text{ Pr}^{0.33} \quad (10.1)$$

The value of ϕ was found to be 0.66 with a correlation coefficient of 0.98.

TABLE 10.1 EVAPORATION OF WATER DROPS AT AMBIENT TEMPERATURE

UNITS

MEAN DIAMETER = mm
 AIR VELOCITY = m/s
 AIR AND DROP TEMP. = C
 NUSSELT EQUATION = $2 + .662 RE^{.5} PR^{.33}$
 CORRELATION COEFF. = .981

EXP NO.	MEAN DIA.	AIR VEL	REY NO.	AIR TEMP	DROP TEMP	NU (EXP)	NU	RE ^{.5} PR ^{.33}
27	1.088	.715	51.62	22.5	8.0	7.015	6.233	6.410
28	1.059	.699	49.15	22.5	8.0	6.827	6.039	6.254
29	.880	.620	36.21	22.5	8.0	6.505	5.652	5.368
30	.955	.620	39.30	22.5	8.0	7.027	6.212	5.592
31	1.023	.525	35.67	22.5	8.0	6.817	6.047	5.328
32	1.010	.525	35.22	22.5	8.0	6.519	5.745	5.294
33	1.007	.427	28.54	22.5	8.0	5.635	4.881	4.766
34	1.157	.427	32.79	22.5	8.0	6.223	5.509	5.109
35	1.092	.326	23.65	22.5	8.0	5.775	5.069	4.338
36	.833	.326	18.04	22.5	8.0	5.537	4.735	3.789
37	1.079	.301	21.64	21.5	7.5	5.475	4.773	4.150
38	1.057	.301	21.20	21.5	7.5	5.322	4.614	4.108
39	.948	.259	16.36	21.5	7.5	5.014	4.285	3.608
40	1.129	.259	19.47	21.5	7.5	5.330	4.650	3.937
41	1.025	.211	14.41	21.5	7.5	5.019	4.330	3.386
42	1.025	.211	14.41	21.5	7.5	5.034	4.345	3.386
43	1.025	.166	11.33	21.5	7.5	4.551	3.880	3.003
44	1.155	.253	19.62	19.5	8.0	5.360	4.686	3.952
45	1.204	.253	20.45	19.5	8.0	5.795	5.130	4.035
46	1.105	.253	18.77	19.5	8.0	5.204	4.521	3.866
47	1.155	.253	19.62	19.5	8.0	4.968	4.295	3.952
48	1.155	.332	25.71	19.5	8.0	5.758	5.065	4.523
49	1.155	.332	25.71	19.5	8.0	5.685	4.993	4.523
50	1.078	.184	13.26	20.0	8.5	4.589	3.923	3.249
51	1.083	.184	13.32	20.0	8.5	4.620	3.955	3.256
52	1.083	.124	8.97	20.0	8.5	4.333	3.695	2.673
53	1.083	.124	8.97	20.0	8.5	4.278	3.640	2.673
54	1.080	.085	6.11	20.0	8.5	3.999	3.386	2.205
55	1.083	.085	6.13	20.0	8.5	3.973	3.360	2.208
56	1.083	.045	3.28	20.0	8.5	3.726	3.150	1.615
57	1.083	.045	3.28	20.0	8.5	3.736	3.160	1.615
58	1.080	.026	1.85	20.0	8.5	3.459	2.913	1.214
59	1.080	.026	1.85	19.6	8.0	3.402	2.857	1.214
70	1.139	.765	57.91	22.0	8.0	6.708	5.935	6.789
71	1.139	.772	58.15	23.5	8.0	6.456	5.681	6.803

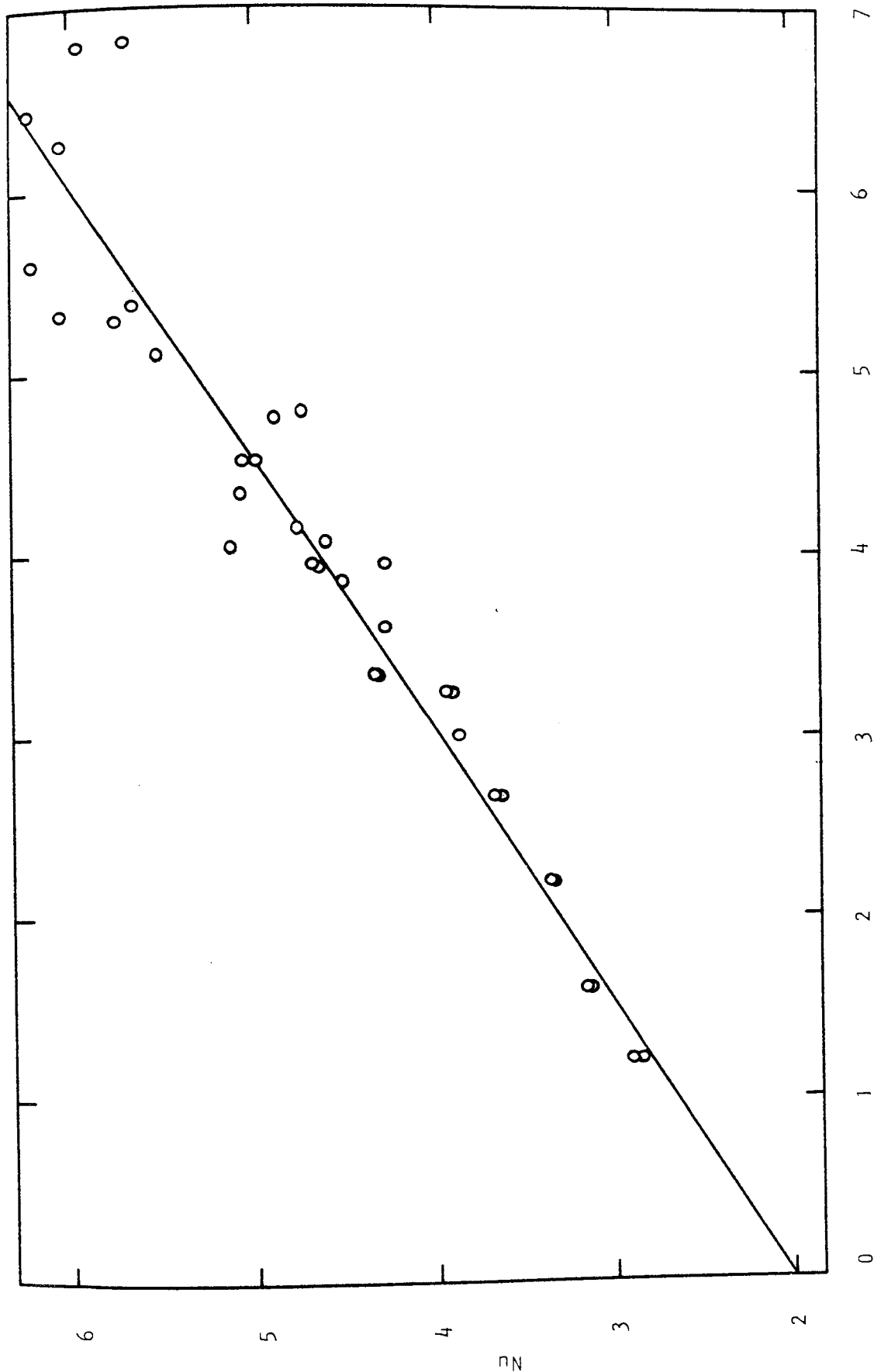
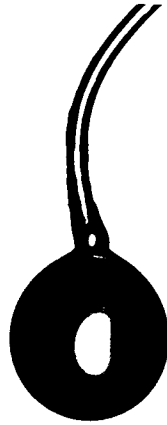
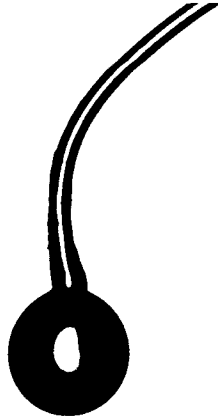


Figure 10.1 Plot of Nu Against $Re^{0.5} Pr^{0.33}$ at Ambient Temperature (21°C)



$\theta = 0$ secs, $d_p = 1.46$ mm



$\theta = 316$ secs, $d_p = 0.91$ mm

Plate 10.1 Decrease in drop diameter of a suspended drop of water at ambient temperature and an air velocity of 0.5 ms^{-1} .

It should be noted that the Nusselt numbers obtained from the results have been corrected for heat transferred by radiation and heat conduction through the filament. Both these additional heat input terms have been described in sections 7.1.2 and 7.1.3.

Plate 10.1 shows the decrease in drop size under typical experimental conditions.

10.2 Water Drops at Elevated Temperatures

The results for the evaporation of water drops at the temperatures of 34, 46.25, 63 and 79°C are summarised in Tables A36 - A39 in Appendix A.4.2 and Figures 10.2 to 10.5.

The experimental Nusselt number was calculated for each drop size during a run by equation 7.6. The instantaneous value of $d(d_p^2)/d\theta$ at each drop size, obtained from a plot of d_p^2 against time, was used instead of a mean value for the run.

As in the case at ambient temperature, a least squares fitting technique, was used to determine the value of ϕ in equation 10.1 for the four temperatures. The values of ϕ are presented in Table 10.2.

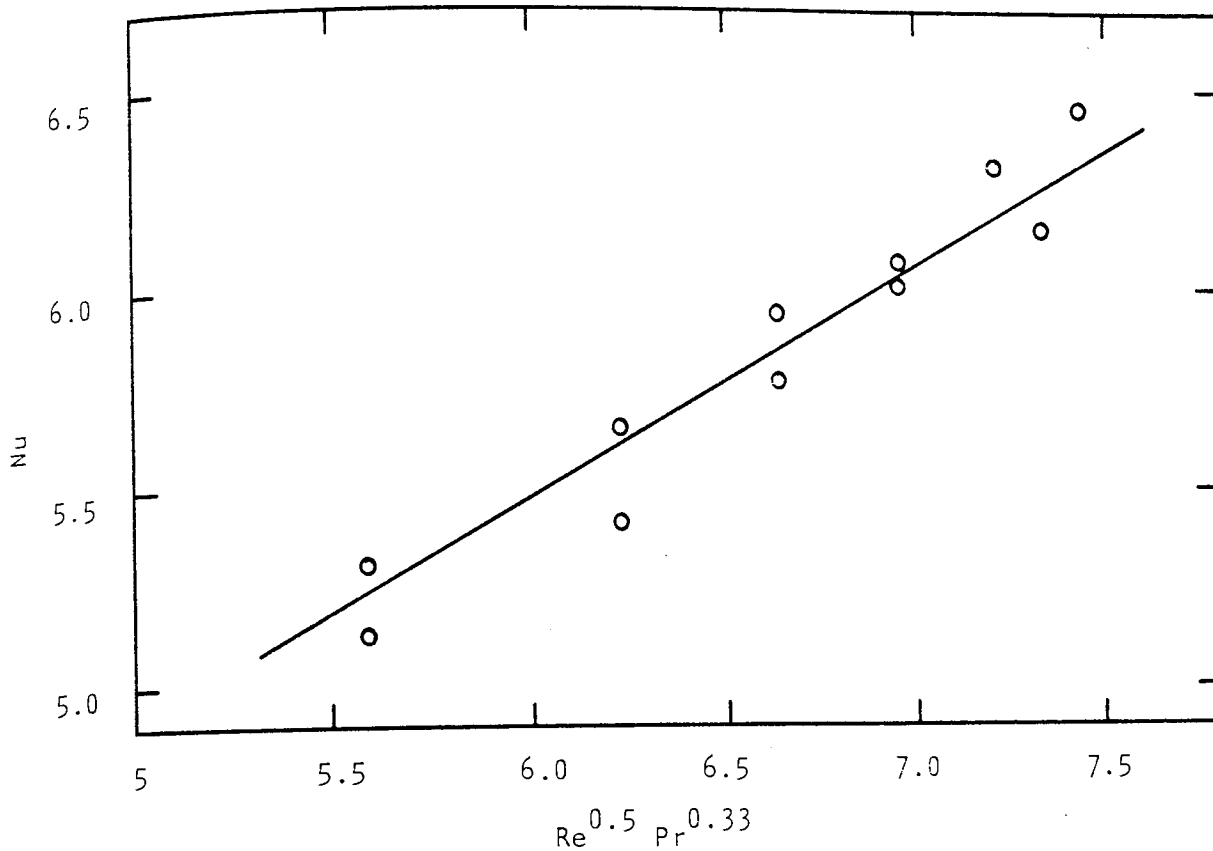


Figure 10.2 Plot of Nu Against $Re^{0.5} Pr^{0.33}$ for T_g at 33.5 and 34°C.

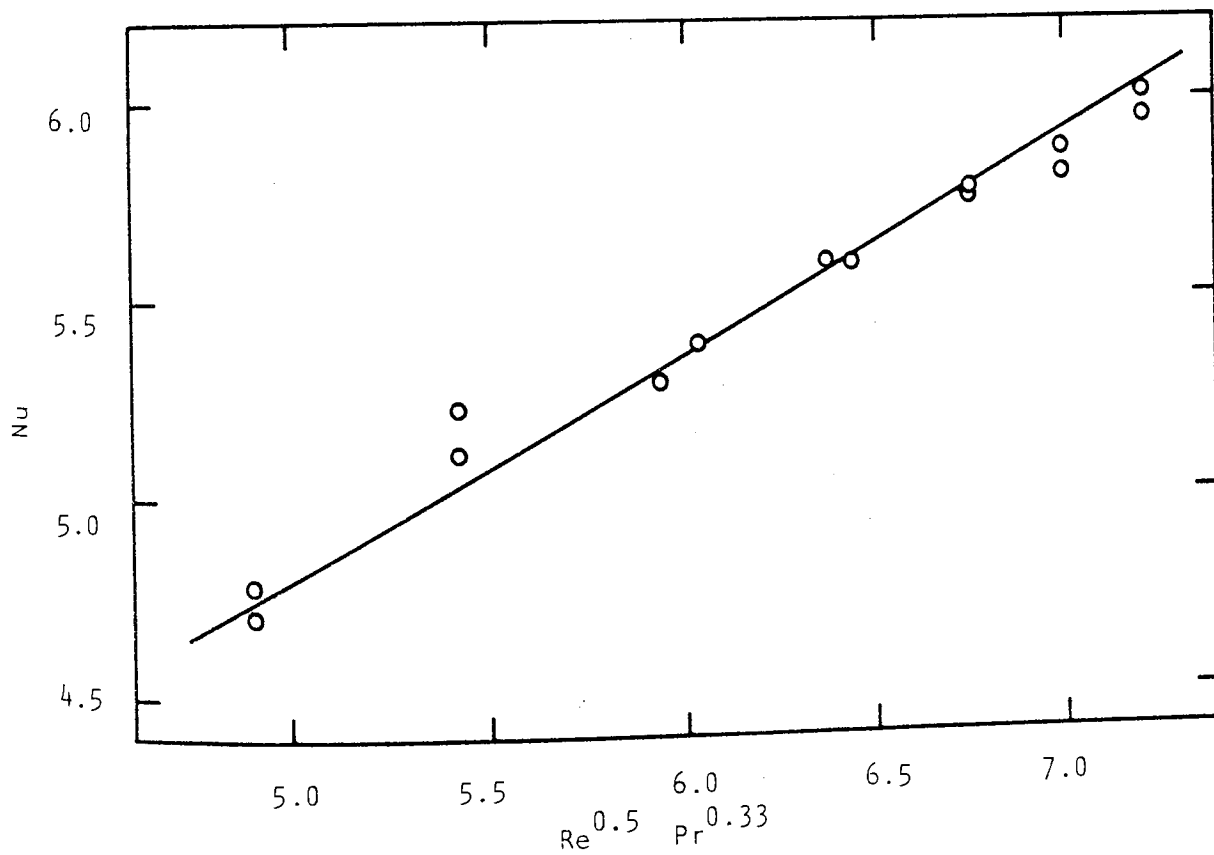


Figure 10.3 Plot of Nu Against $Re^{0.5} Pr^{0.33}$ for T_g at 46.25°C

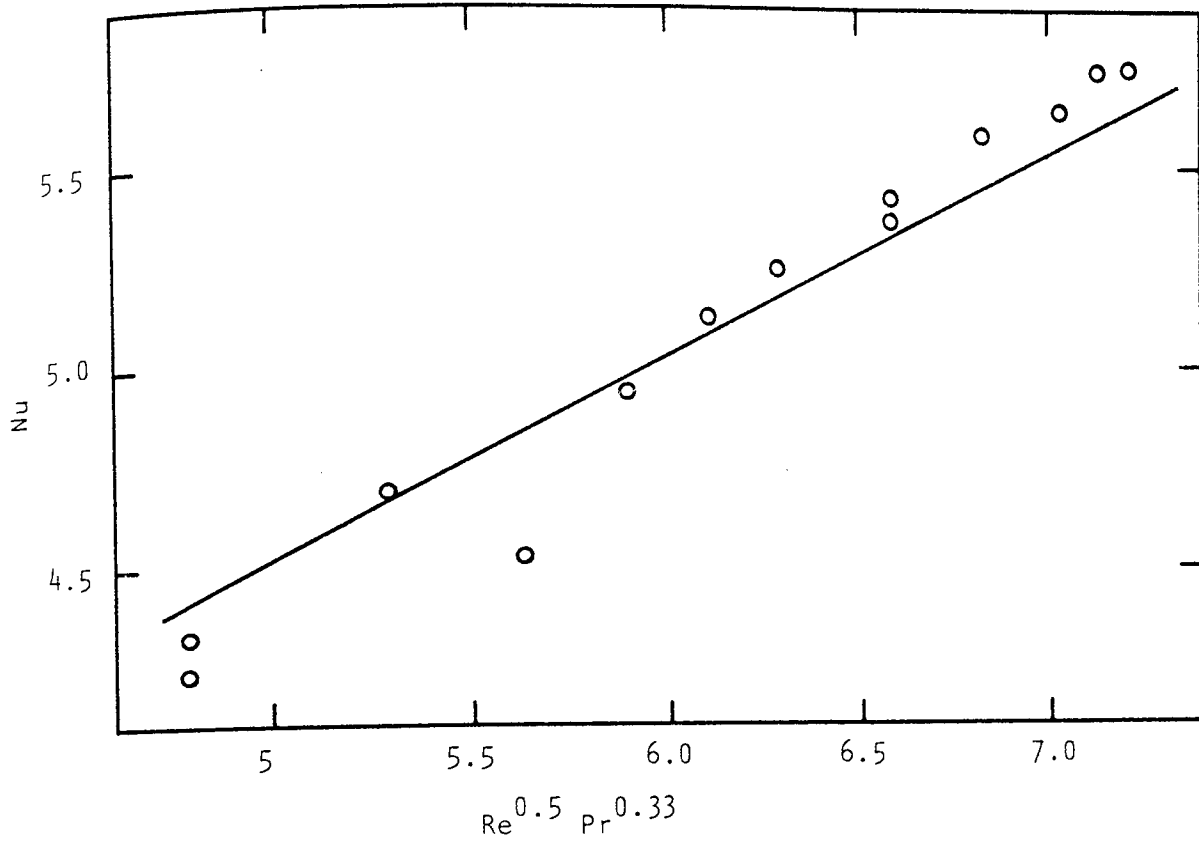


Figure 10.4 Plot of Nu Against $Re^{0.5} Pr^{0.33}$ for T_g at $63^\circ C$

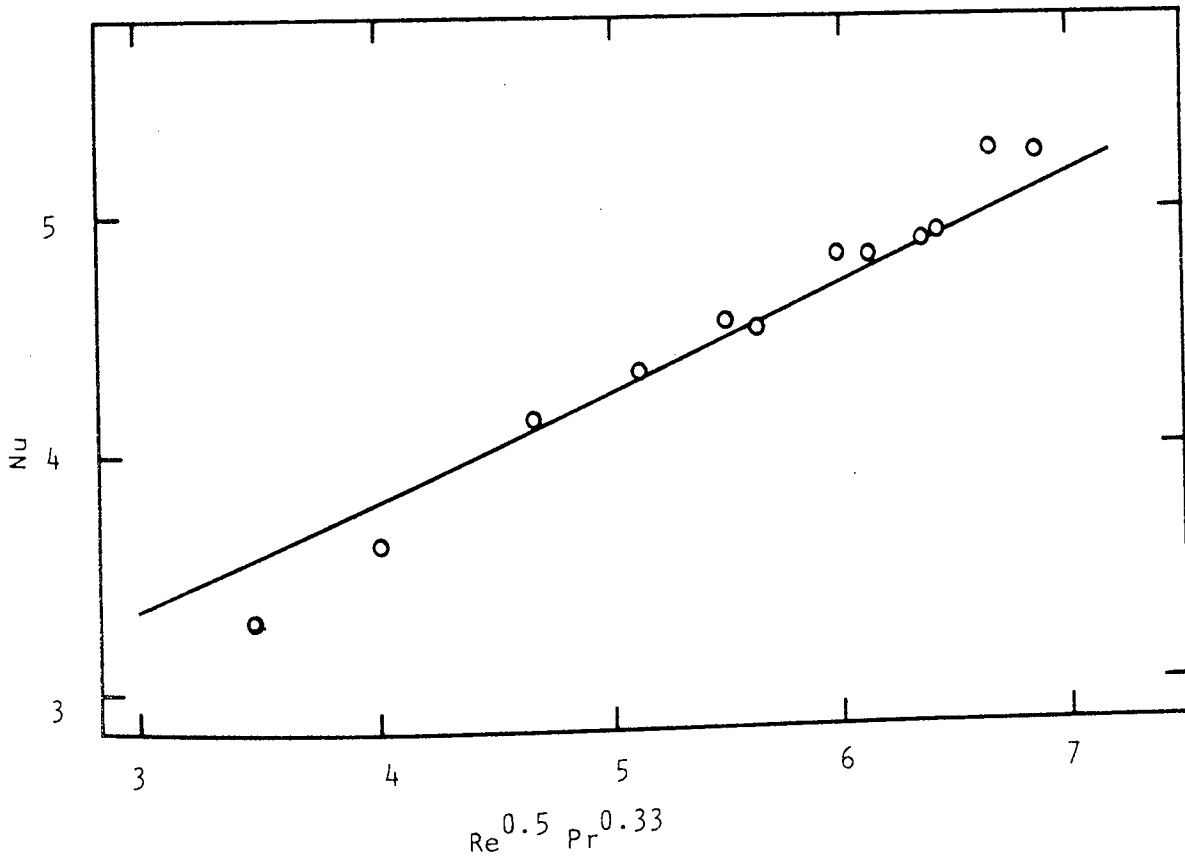


Figure 10.5 Plot of Nu Against $Re^{0.5} Pr^{0.33}$ for T_g at $79^\circ C$

Table 10.2 Values of ϕ at Elevated Temperatures

Temp (°C)	ϕ	Correlation Coefficient
34.0	0.58	0.97
46.25	0.56	0.98
63.0	0.50	0.96
79	0.45	0.96

It is apparent from the table that a single value of ϕ would not adequately correlate the data over the temperature range. The experimental results were thus correlated by the introduction of the Transfer number B, where $B = C_p \Delta T / \lambda$ and a modified Nusselt equation was proposed.

$$Nu = 2 + \phi (1/B)^n Re^{0.5} Pr^{0.33} \quad (10.2)$$

A least squares correlation technique, described in Appendix A.2.2, was used to correlate the data according to the above equation.

The resulting correlation was found to be,

$$Nu = 2 + 0.19 (1/B)^{0.24} Re^{0.5} Pr^{0.33} \quad (10.3)$$

with a correlation coefficient of 0.98.

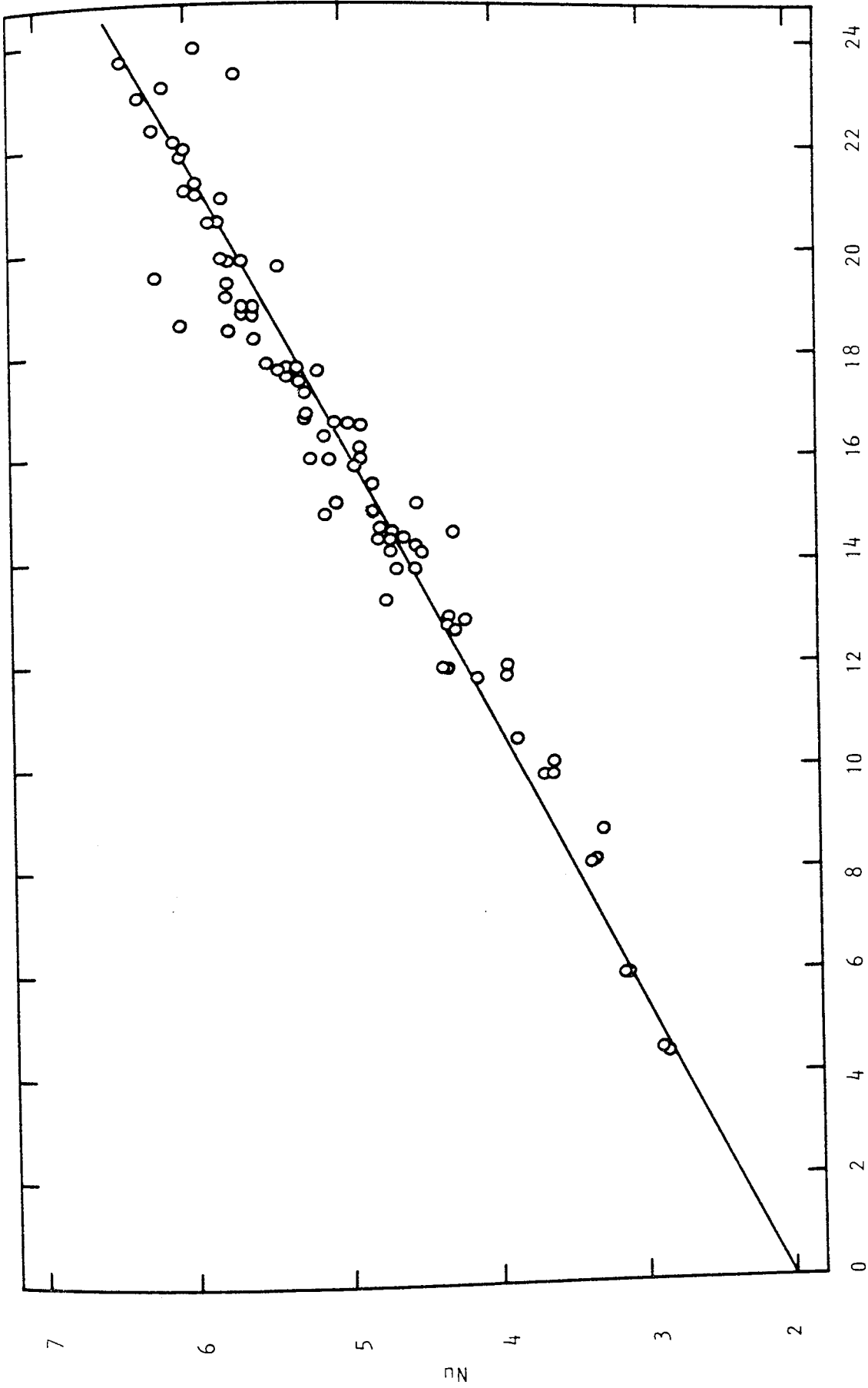


Figure 10.6 Plot of Nu Against $(1/B)^{0.24} Re^{0.5} Pr^{0.33}$ for T_g Between $19.5 - 79^\circ C$

Figure 10.6 shows a plot of Nu against $(l/B)^{0.24} Re^{0.5} Pr^{0.33}$, for T_g between 19.5 - 79°C.

10.3 Drops of Aqueous Sodium Sulphate Decahydrate

Four concentrations of aqueous sodium sulphate decahydrate were used in this series of experiments; 5, 15, 30.3 and 54.1 wt.% solids at varying air velocities and temperatures.

The measured weights of the evaporating drops were corrected for radiation and heat conduction along the suspension filament. The weight correction W_c , was expressed as,

$$W_c = (Q_f + Q_e)/(\lambda - C_c) \quad (10.4)$$

where Q_f and Q_e are the total amount of heat transferred through the filament and by radiation respectively.

For a finite change in time $\Delta\theta$, mean drop temperatures and diameters are justified.

Hence,

$$Q_f = \frac{\Delta\theta\pi}{2} \left[\frac{k_t d_f^3}{5} \left(2\sigma e_s (T_{sm}'^5 - T_g'^5) - 10\sigma e_s T_g'^4 (T_{sm}' - T_g') + 5 h_t (T_{sm}' - T_g')^2 \right) \right]^{0.5} \quad (10.5)$$

$$\text{and } Q_e = \sigma e_s \pi d_{pm}^2 (T_g^4 - T_{sm}^4)$$

where T_{sm} and d_{pm} are the mean drop temperature and diameter respectively in Δt .

The weight correction calculated from equation 10.4 was added to the measured weight at the end of each time interval to give the corrected weight. Tables 10.1 - 10.3 summarise the results in this section.

Figure 10.7 shows three drying curves at air velocities 0.50, 1.53 and 2.92 ms^{-1} for a constant concentration of 5 wt.% solids at ambient temperature. The curves show an initial linear period, consistent with evaporation from liquid drops, followed by a gradual decrease to complete dryness. At the highest velocity, the slope of the curve changes much earlier and more abruptly than those at the lower velocities. The electron micrographs of the dried particles at air velocities 0.50 and 2.92 ms^{-1} are shown in Plates 10.2 and 10.3. The crusts were relatively smooth, showing no pores of any significant size. At the higher velocity, the crust showed distinct parallel 'furrows' on the surface.

Figure 10.8 illustrates four curves at air temperatures 20, 40, 66.5 and 110°C for a concentration of 5 wt.% solids and a velocity of 1.09 ms^{-1} . The trend of the curves are similar to the previous case. It is interesting

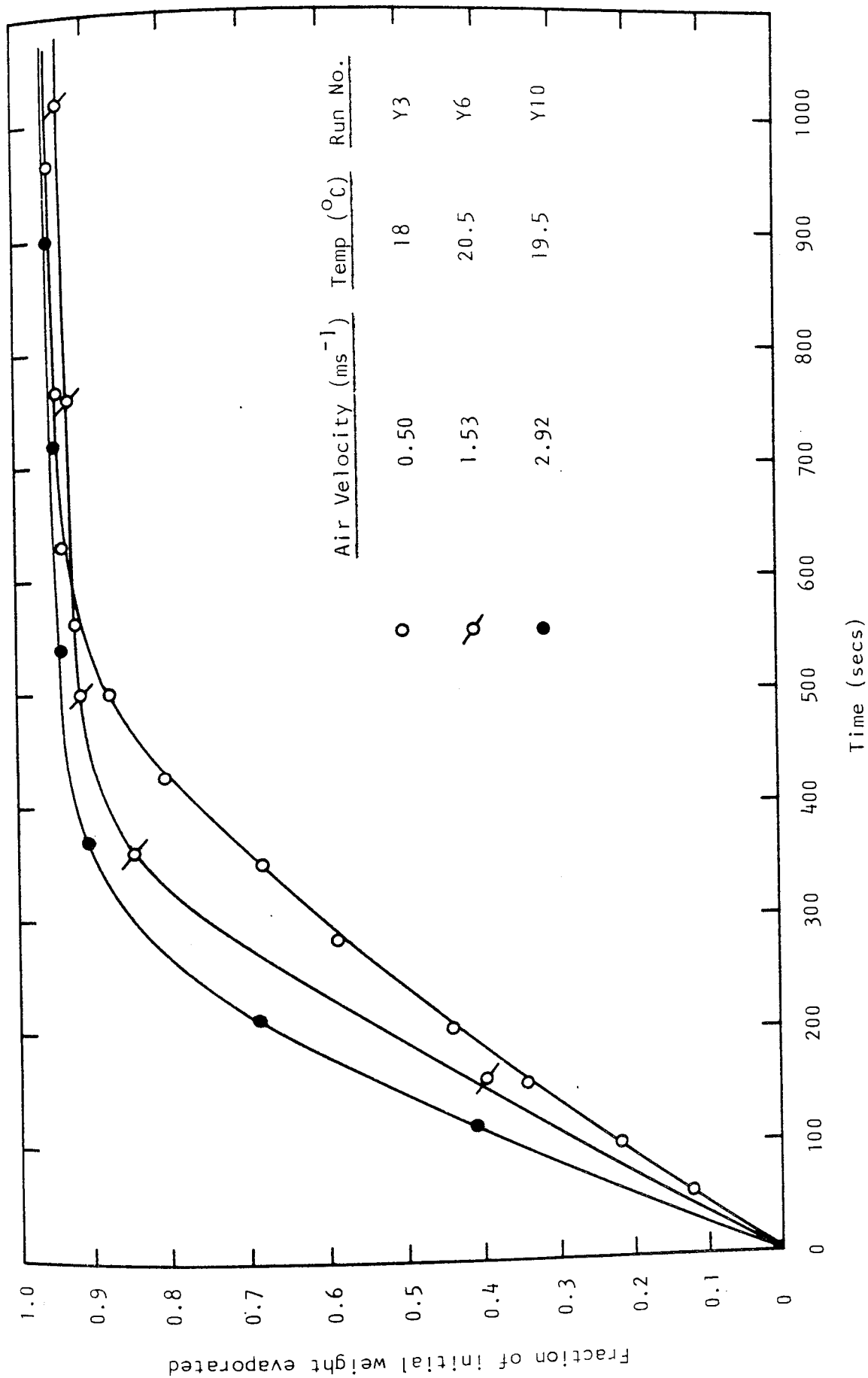


Figure 10.7 Drying of drops of aqueous sodium sulphate decahydrate (5 wt.%) at varying velocities.

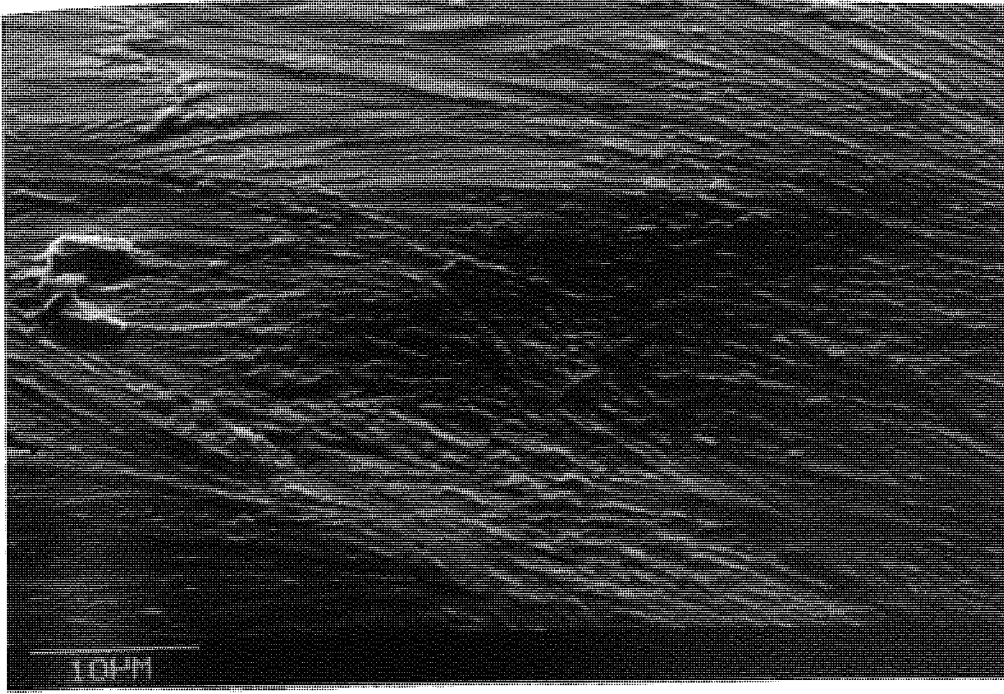


Plate 10.2 Crust surface of a particle dried with an air velocity of 0.50 ms^{-1} ($C_o = 5 \text{ wt.}\%$, $T_g = 18^\circ\text{C}$)

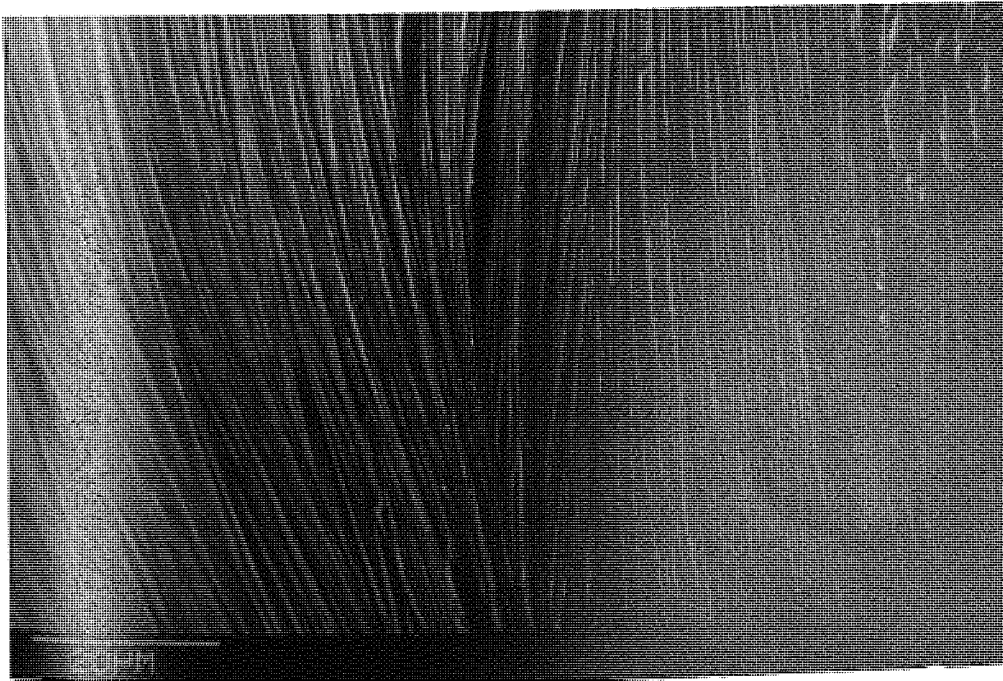


Plate 10.3 Crust surface of a particle dried with an air velocity of 2.92 ms^{-1} ($C_o = 5 \text{ wt.}\%$, $T_g = 19.5^\circ\text{C}$)

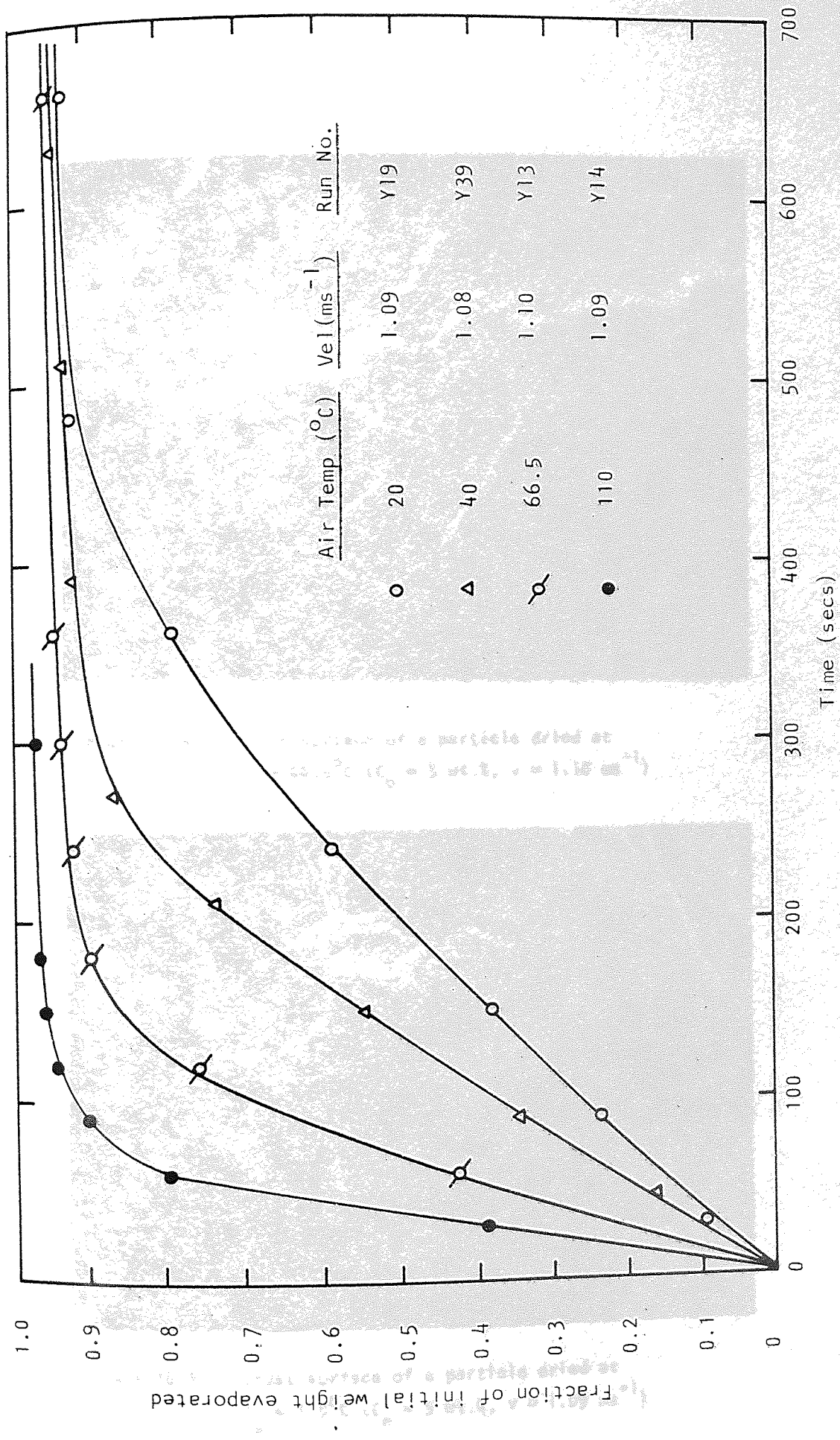


Figure 10.8 Drying of drops of aqueous sodium sulphate decahydrate (5 wt.%) at high temperatures.

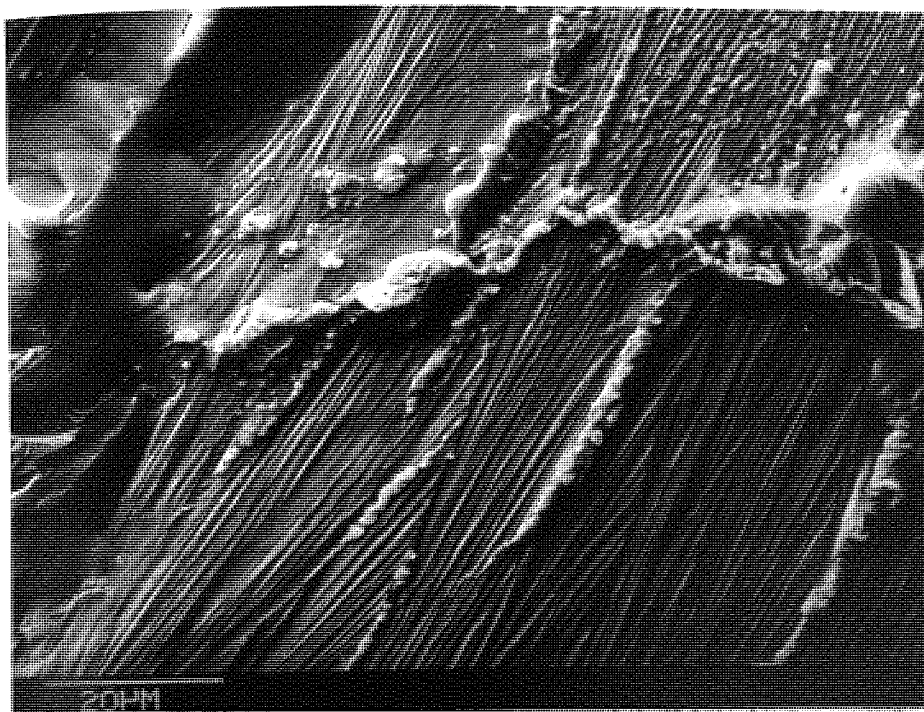


Plate 10.4 Crust surface of a particle dried at
 $T_g = 66.5^\circ\text{C}$ ($C_o = 5 \text{ wt.}\%$, $v = 1.10 \text{ ms}^{-1}$)

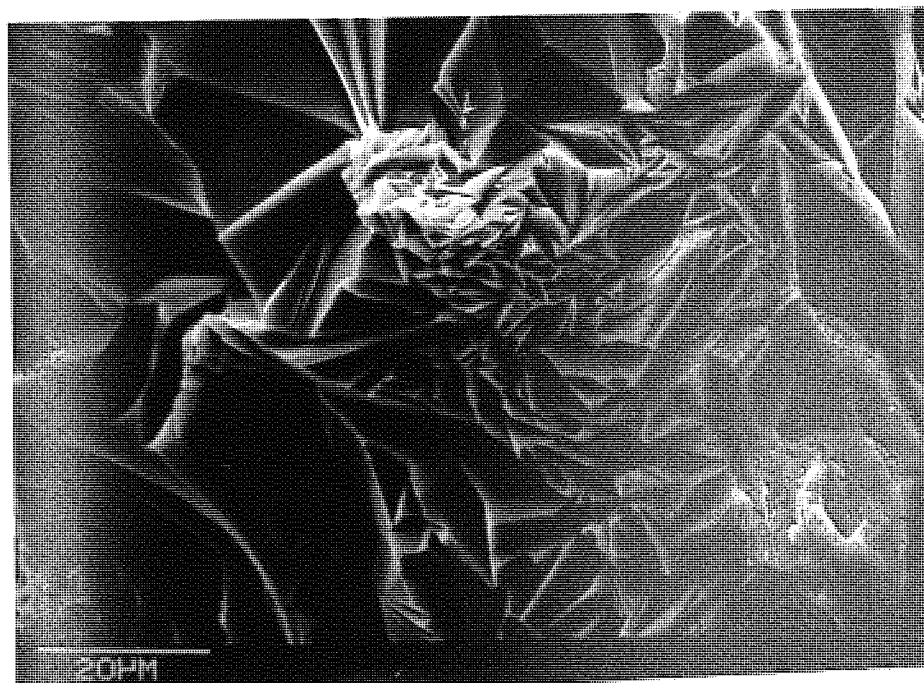


Plate 10.5 Crust surface of a particle dried at
 $T_g = 110^\circ\text{C}$ ($C_o = 5 \text{ wt.}\%$, $v = 1.09 \text{ ms}^{-1}$)

to note that a 5 fold increase in air temperature had a greater effect on the evaporation rate than a corresponding increase in velocity. The electron micrographs at 66.5 and 110°C are presented in Plates 10.4 and 10.5. At 66.5°C the crust was still relatively smooth but with larger and rougher crystals present on the surface. At 110°C, the crust surface was very rough with large crystals clearly evident.

At a concentration of 15 wt.% solids, the evaporation rates were correspondingly lower as expected. The drying curves at air velocities 0.502, 1.08 and 3.0 ms⁻¹ at ambient temperature are presented in Figure 10.9. At the higher velocities, identical experiments had resulted in significantly different curves after crust formation. This was a direct result of the crust fracturing, causing a sudden increase in the evaporation rate. On occasions, pieces of the crust on fracturing fell away, indicated by a very sudden weight loss. The electron micrographs supports this inference. The surfaces were very rough with pores clearly visible (Plate 10.6). A 'blow-hole' in the crust is clearly evident from Plate 10.7.

The above trend was also evident at the higher temperatures of 40, 60 and 90°C, except that fracturing and distortion of the original shape occurred more frequently. The slopes of the curves after crust formation

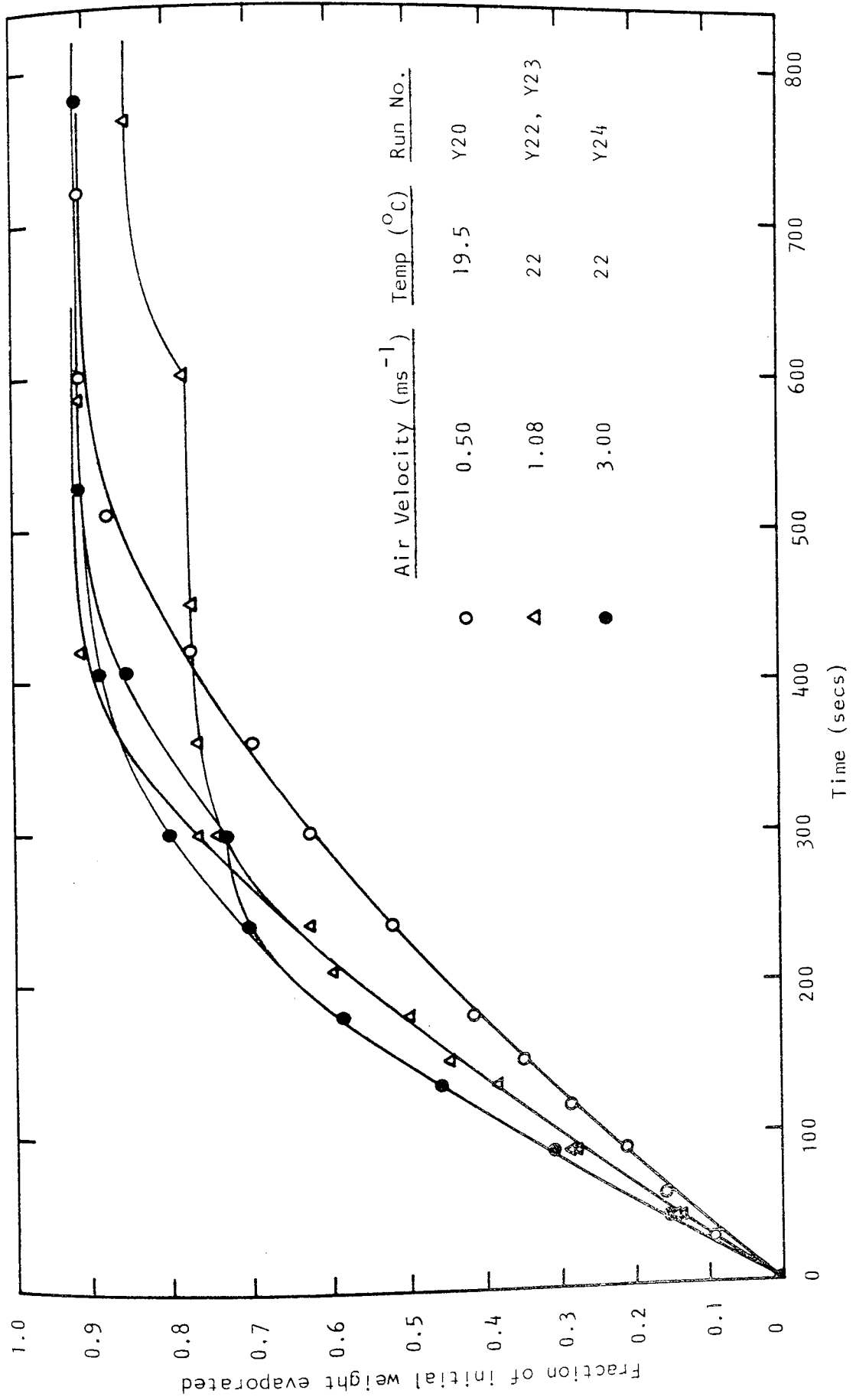


Figure 10.9 Drying drops of aqueous sodium sulphate decahydrate (15 wt.%) at varying velocities.



Plate 10.6 Crust surface of a particle dried at an air velocity of 3.0 ms^{-1} ($C_o = 15 \text{ wt.}\%$, $T_g = 22^\circ\text{C}$)

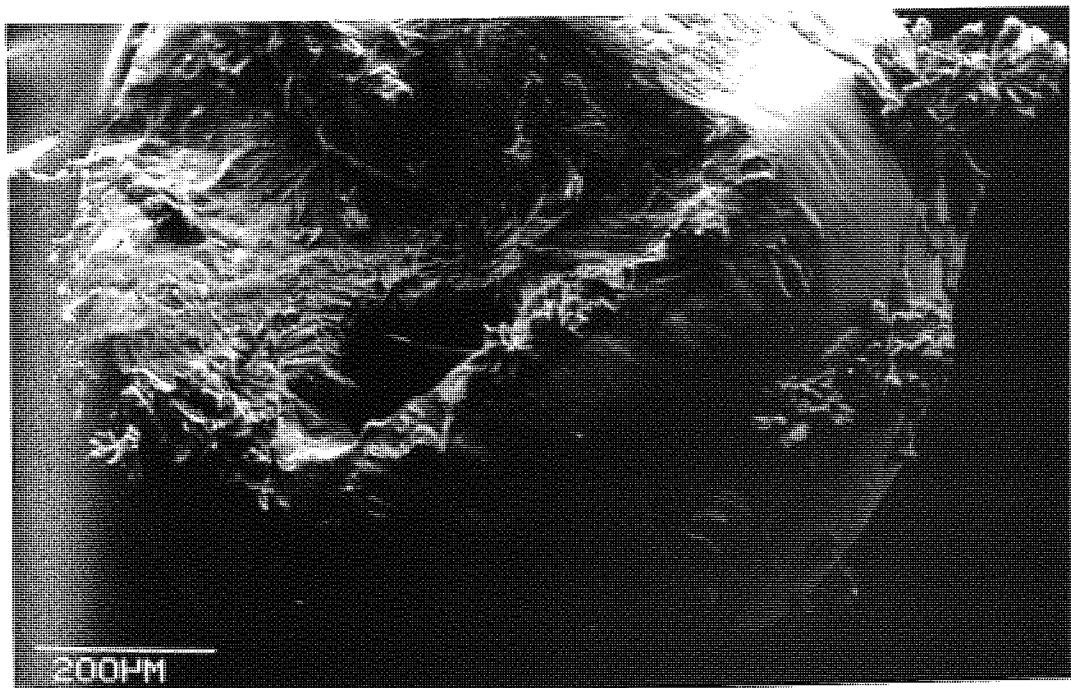


Plate 10.7 Crust surface showing a 'blow hole' at an air velocity of 3.0 ms^{-1} ($C_o = 15 \text{ wt.}\%$, $T_g = 22^\circ\text{C}$)

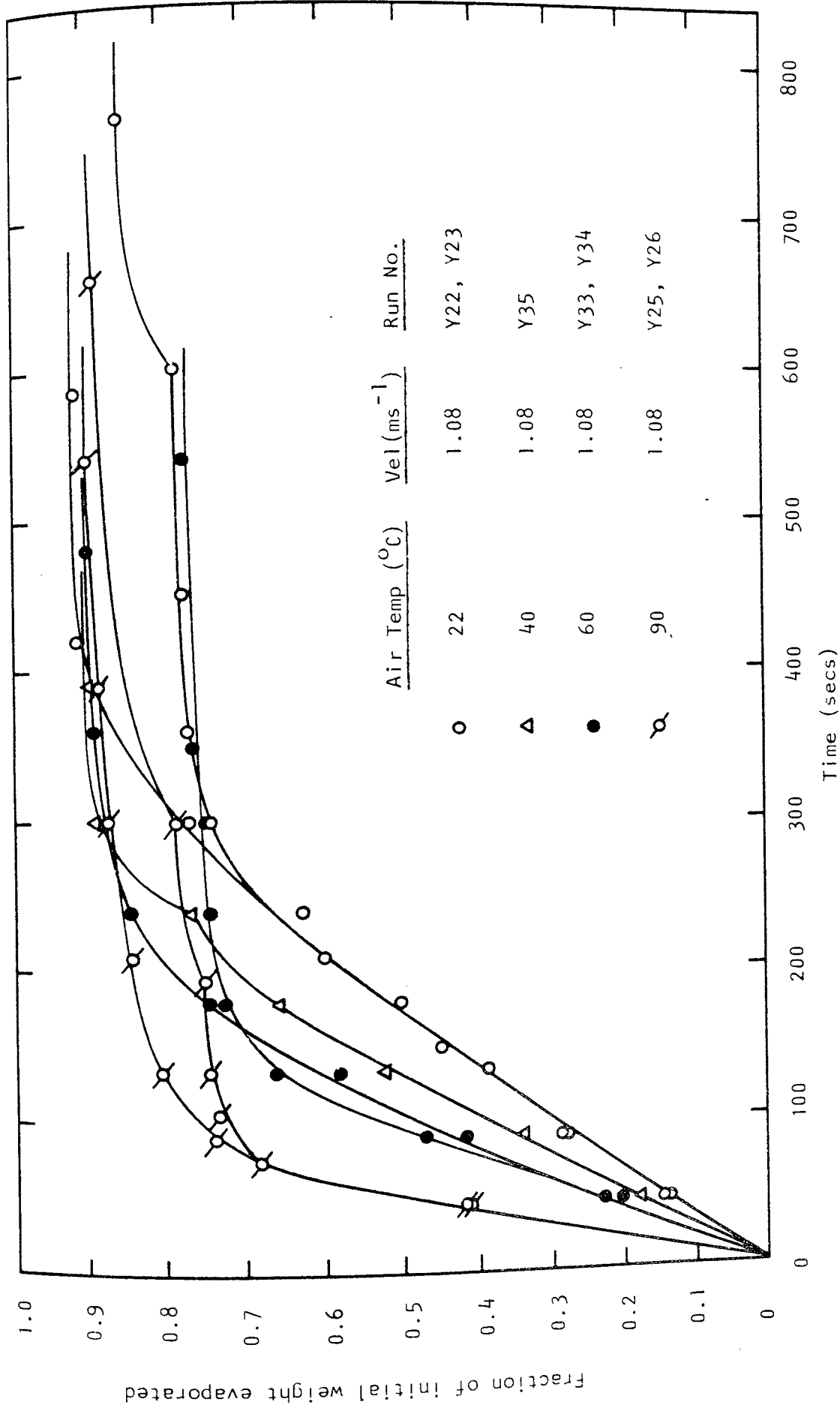


Figure 10.10 Drying of drops of aqueous sodium sulphate decahydrate (15 wt.%) at high temperatures.

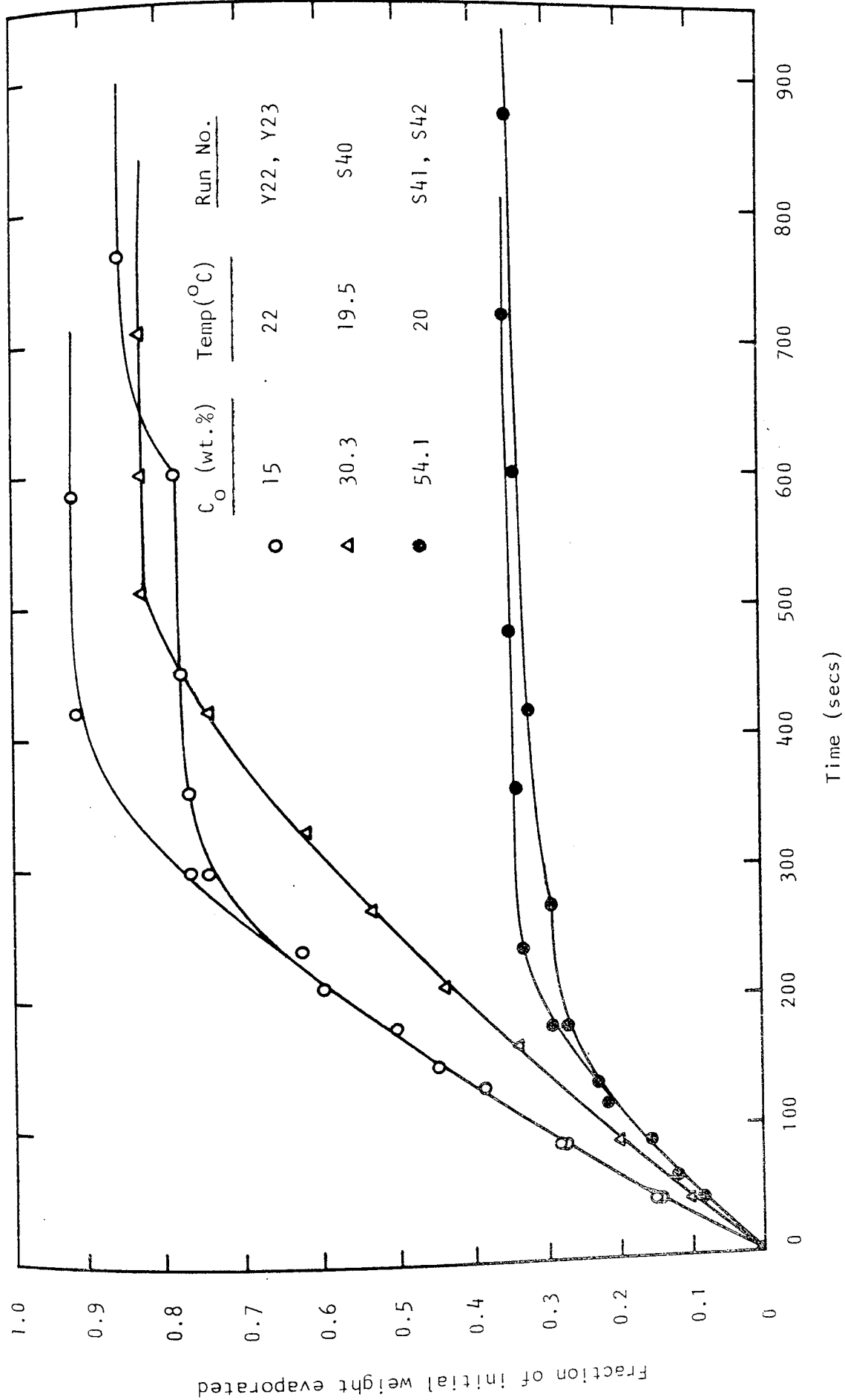


Figure 10.11 Drying of drops of aqueous sodium sulphate decahydrate with varying initial concentrations ($v = 1.08 \text{ ms}^{-1}$).

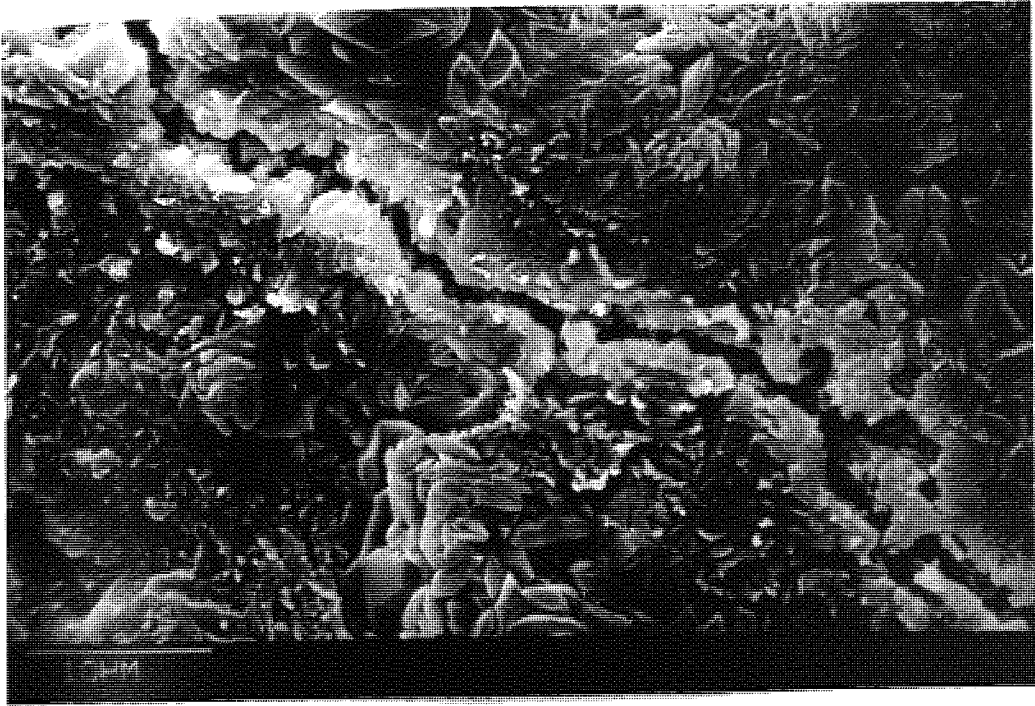


Plate 10.8 Crust surface showing fracture
 $T_g = 20^\circ\text{C}$, $C_o = 54.1 \text{ wt.}\%$, $v = 1.08 \text{ ms}^{-1}$)

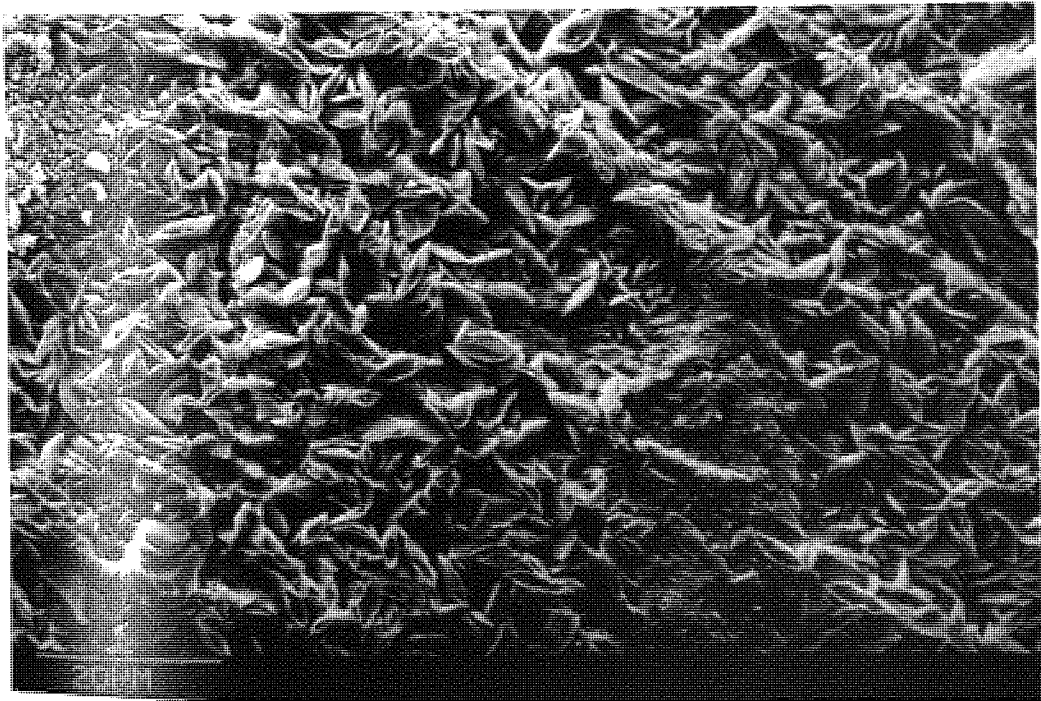


Plate 10.9 Crust surface of a particle dried at
 $T_g = 20^\circ\text{C}$ ($C_o = 40 \text{ wt.}\%$, $v = 1.0 \text{ ms}^{-1}$)

seemed to change randomly depending on the exact moment when a fracture or 'blow hole' occurred as evident from Figure 10.10.

Figure 10.11 shows the drying curves at high concentrations, 30.3 and 54.1 wt.% solids compared to one at 15 wt.%. At 54.1 wt.% solids, the crust was formed instantly, after which the evaporation rate decreased very rapidly. Consequently it took a considerable time before total dryness was achieved. The resultant crust was rough and large pores were present. Fractures on the surface were also clearly evident, as shown in Plate 10.8.

10.4 Simultaneous Drop Weight and Core Temperature Measurements of Sodium Sulphate Decahydrate Slurry Drops.

Drops of aqueous sodium sulphate decahydrate at a concentration of 40 wt.% were dried at 20, 40.7, 59.3 and 78.3°C. The measured weights were corrected for radiation and conduction along the thin film thermocouple according to equations 7.21 and 10.4. The results of the drying rates and core temperatures are tabulated in Tables C1 - C8 in Appendix C.1.

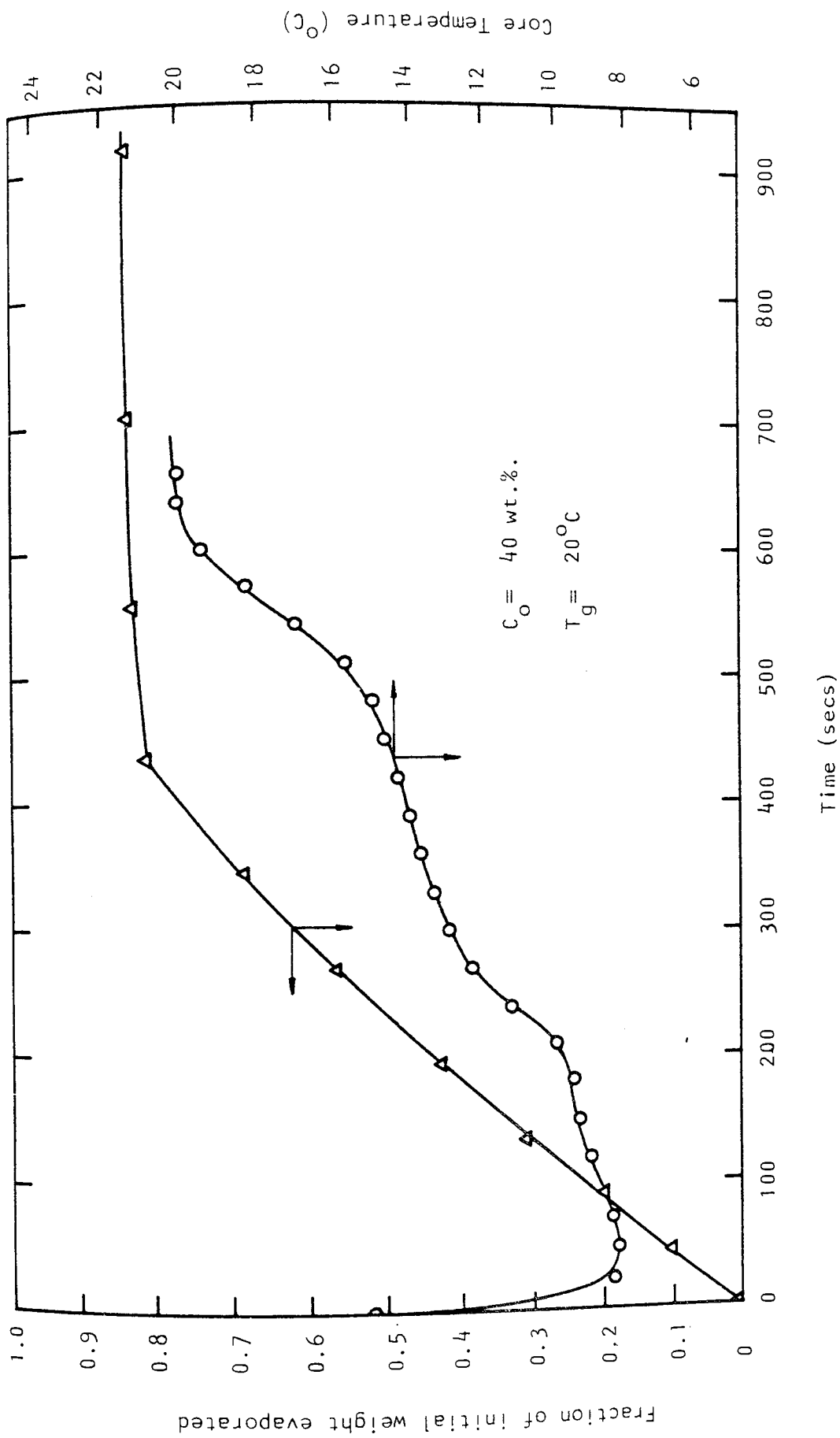


Figure 10.12 Simultaneous Drop Weight and Core Temperature Measurements at $T_g = 20^\circ\text{C}$.

Figure 10.12 shows the drying curve and the core temperature history measured simultaneously by the thin film thermocouple at an air temperature of 20°C. There was an initial transient period in the core temperature history curve before equilibrium was established and the core temperature reduced to the wet bulb temperature. The core temperature then rose steadily as the resistance to heat and mass transfer increased with the crust thickness. After about 540 seconds, the measured core temperature rose very sharply and reached the air temperature within 70 seconds. This sudden rise in temperature was caused by the evaporation interface receding away from the thermojunction, resulting in the dry crust temperature being measured.

The drying curves and core temperature histories at air temperatures of 40.7, 59.3 and 78.3°C are presented in Figures 10.13, 10.14 and 10.15 respectively. The trend of the core temperature curves for these higher air temperatures were quite unique. After the initial transient, the core temperatures rose gradually until it reached about 33°C when they showed a very sudden fall before increasing again very steeply to the respective air temperatures. This phenomenon was caused by the fact that decahydrate crystals melt at about 33°C, absorbing heat in the process; the latent heat of fusion being +239 kJ. kg⁻¹ (110). However, as soon as the temperature fell below the

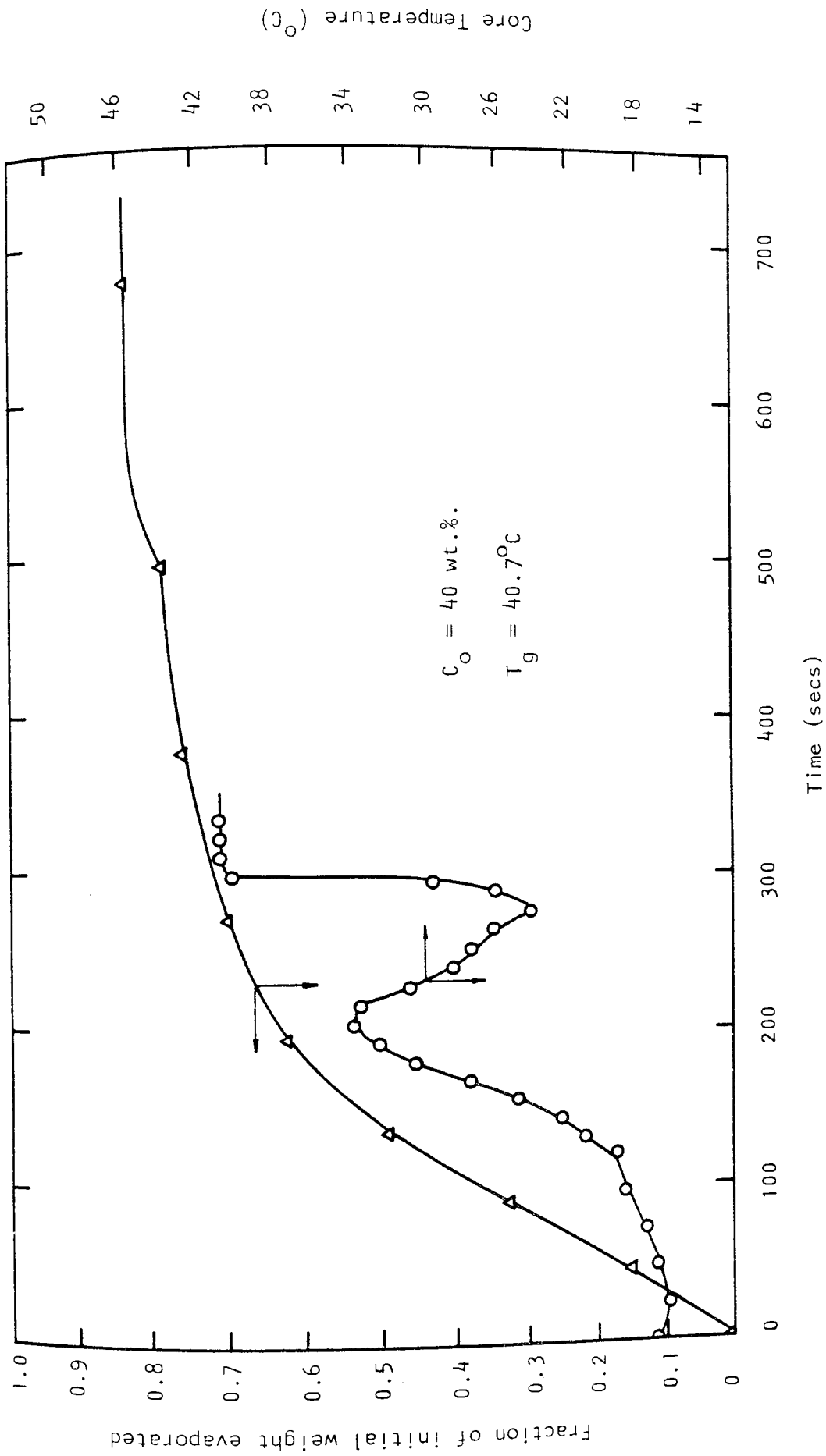


Figure 10.13 Simultaneous Drop Weight and Core Temperature Measurements at $T_g = 40.7^\circ\text{C}$.

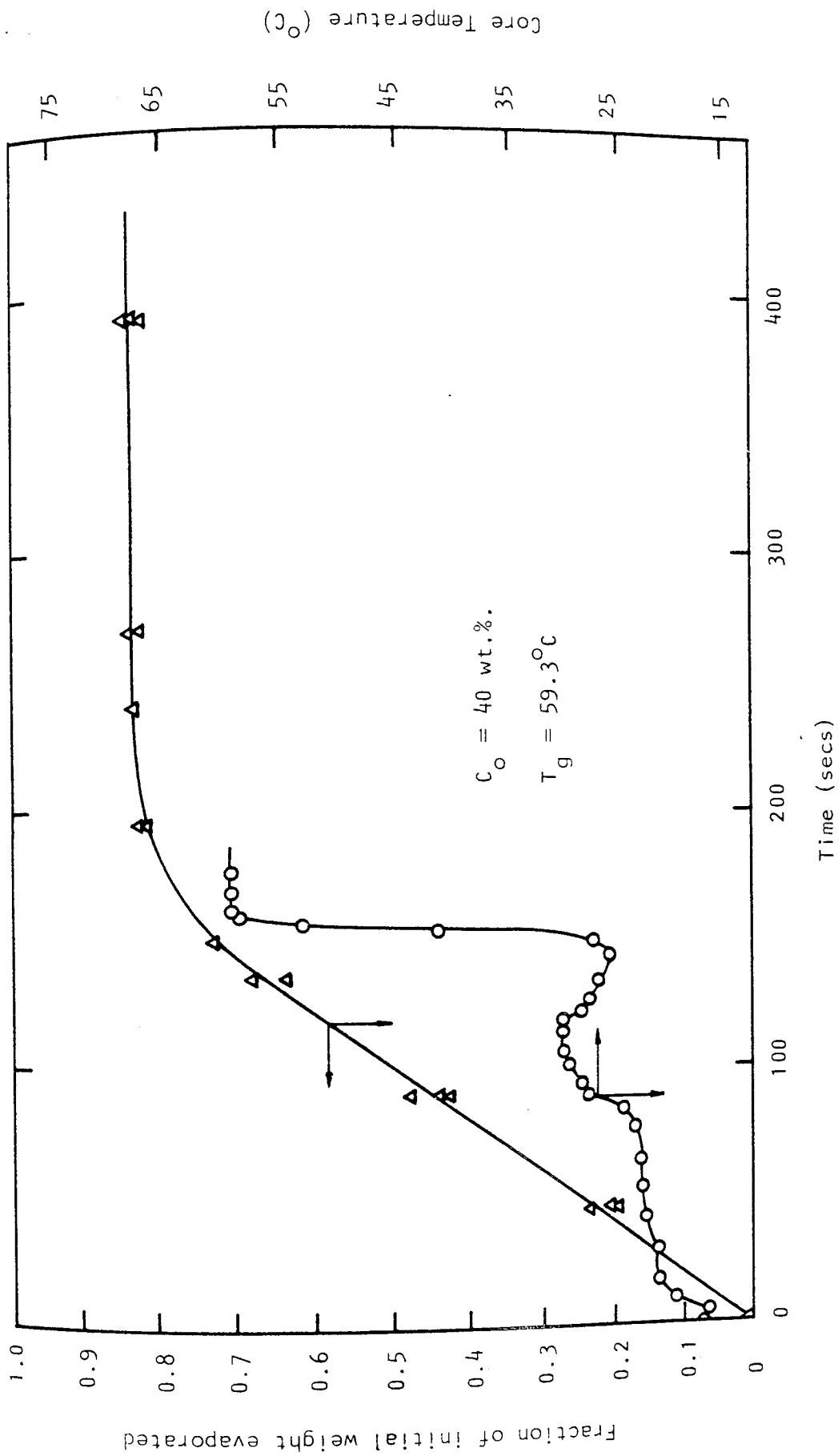


Figure 10.14 Simultaneous Drop Weight and Core Temperature Measurements at $T_g = 59.3^\circ\text{C}$.

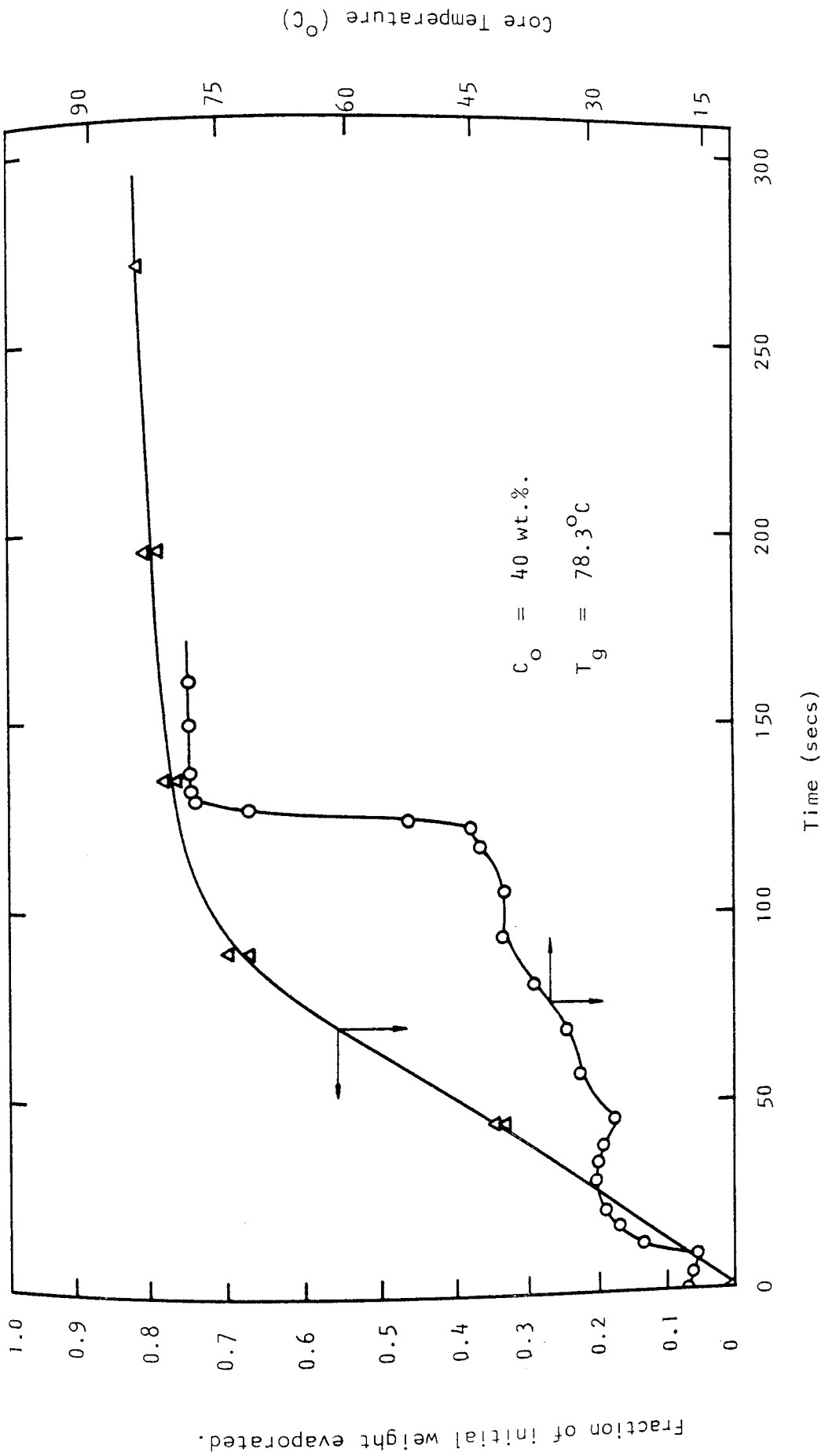


Figure 10.15 Simultaneous Drop Weight and Core Temperature Measurements at $T_g = 78.3^\circ\text{C}$

melting point, the melting process was temporarily halted and the core temperature consequently rose again. Nevertheless, this melting and recrystallisation occurred very rapidly resulting in a relatively smooth core temperature curve showing a gradual fall. After this fall, the core temperature rose very sharply, partly due to the reason mentioned earlier but mainly because of the negative solubility of the anhydrous sulphate.

The drying curves at all the temperatures investigated show a similar trend to those reported in the previous section. As expected, the evaporation rates were much higher at higher temperatures but as soon as a substantial crust was formed, the rates reduced significantly.

The electron micrograph in Plate 10.9 show the relative small crystals at the low drying temperature of 20°C while the larger crystals and more porous surface at higher drying temperatures are illustrated in Plates 10.10 and 10.11.

Plate 10.12 shows a drop of slurry suspended from the thin film thermocouple at the moment of introduction into the wind tunnel and after 350 seconds.

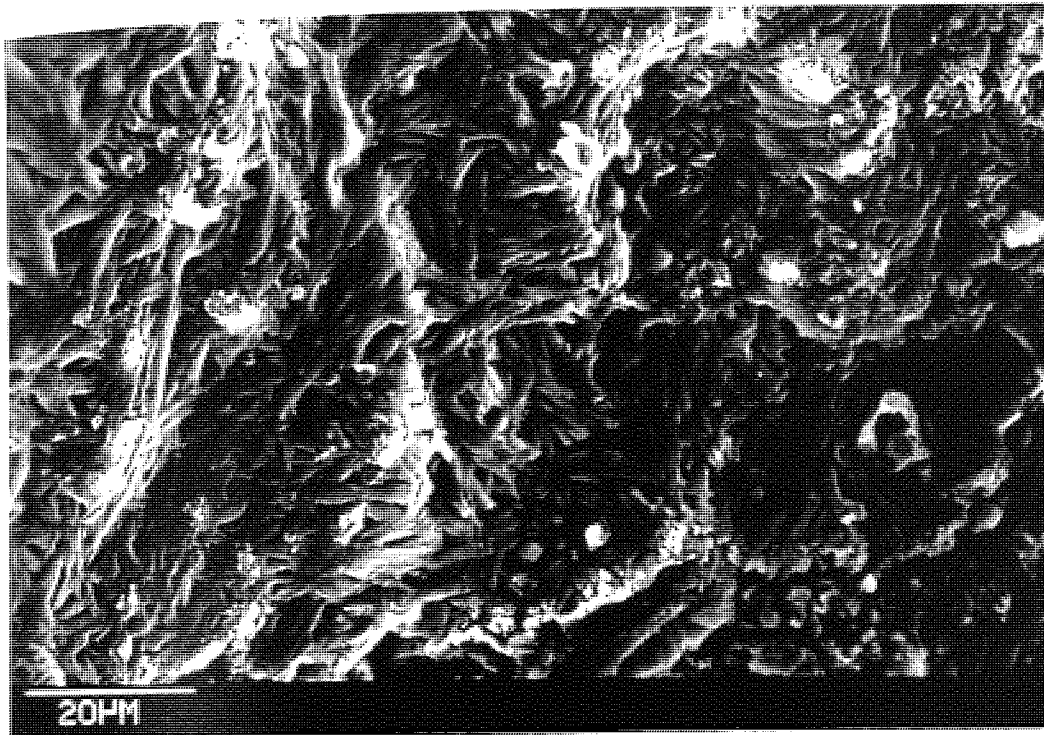


Plate 10.10 Crust surface of a particle dried at
 $T_g = 59.3^\circ\text{C}$ ($C_o = 40$ wt.%, $v = 1.0$ ms⁻¹)

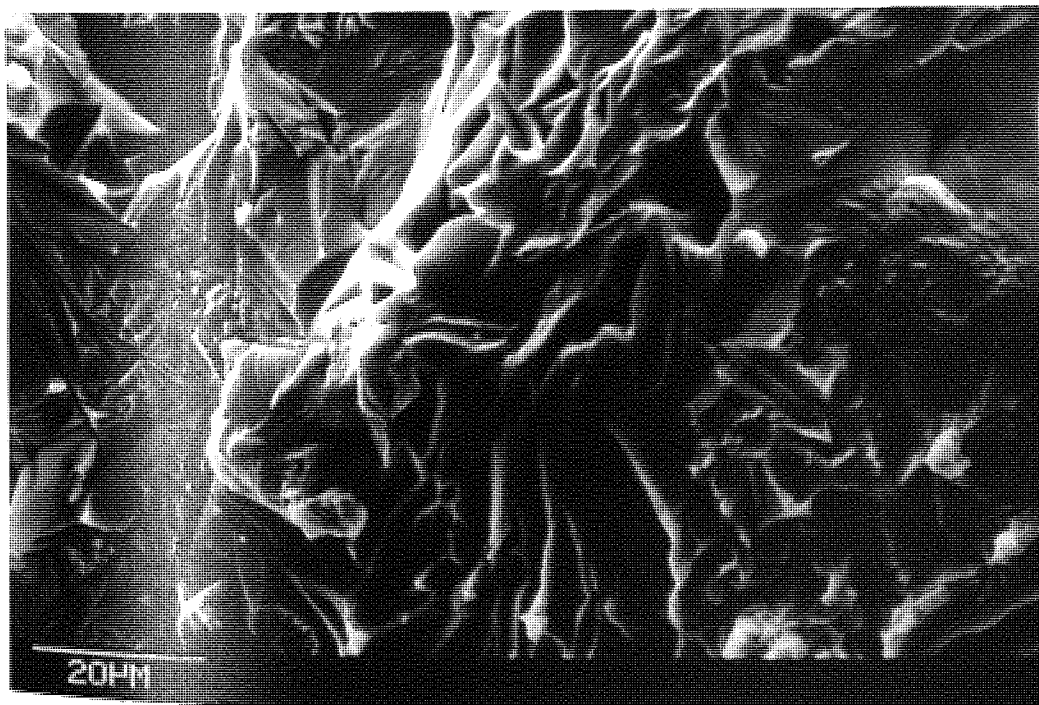
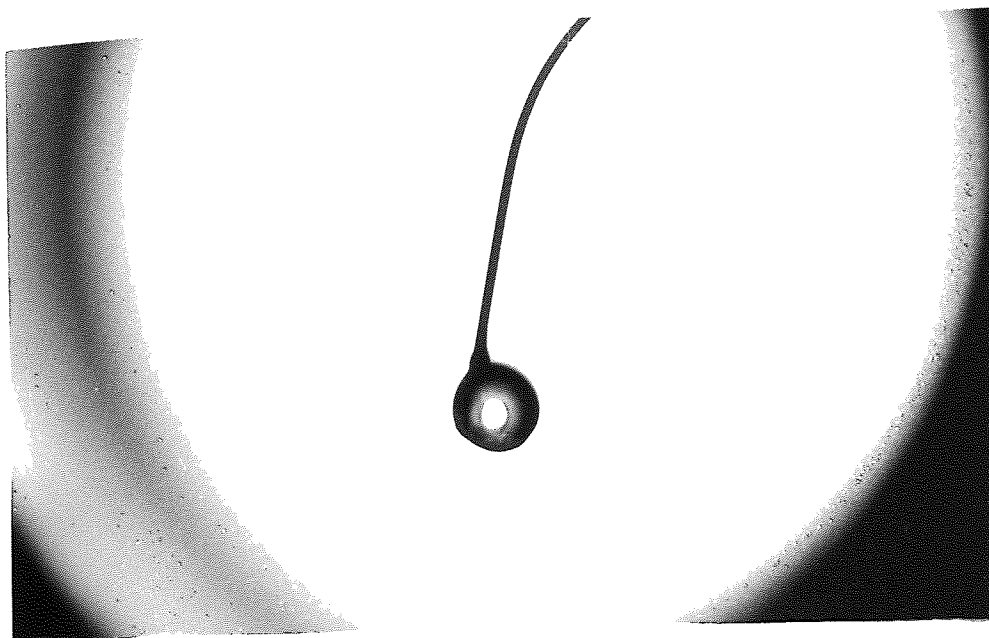


Plate 10.11 Crust surface of a particle dried at
 $T_g = 78.3^\circ\text{C}$ ($C_o = 40$ wt.%, $v = 1.0$ ms⁻¹)



$\theta = 0$ secs.



$\theta = 350$ secs.

Plate 10.12 A drop of slurry ($C_0 = 40$ wt.%) suspended from the thin film thermocouple, drying at 20°C .

10.5 Comparisons of Experimental Results and Model Predictions

The Receding Evaporation Interface model as discussed in section 7.2 was used to model the drying of aqueous sodium sulphate decahydrate and compared to the results presented in section 10.4.

The modelling was carried out on a Commodore PET 32K microcomputer and a listing of the program is presented in Appendix D.2. The program uses a Runge-Kutta 4th order technique to integrate simultaneously for the variation of core temperature, crust thickness and drop weight with time. The change of vapour pressure with temperature and other variables required in the modelling are given in Appendix D.1.

For experiments with air temperatures above 33°C, the model had to be modified to include an additional heat absorption term because of the unusual behaviour of the decahydrate crystals.

$$\Delta H = \frac{4}{3} \pi R^3 \rho_{CO} (1 - x_w) \lambda_f \quad (10.7)$$

where λ_f = Latent heat of fusion.

Hence, the fall in drop temperature ΔT_S , can be expressed as,

$$\Delta T_S = \frac{\Delta H}{W C_{pc}} \quad (10.8)$$

The experimental core temperature history at an air temperature of 20°C was compared to that predicted by the model in Figure 10.16. The agreement was excellent up to about 540 seconds when the measured temperature rose sharply unlike the gradual increase predicted by the model. The reason for this discrepancy had been discussed in section 10.4. The measured temperature after this period was that of the crust while the model predicted the actual core temperature. This discrepancy at the final stages of the drying process was also evident at the higher air temperatures.

Figure 10.17, 10.18 and 10.19 compare the model predictions with the experimental core temperatures at air temperatures of 40.7, 59.3 and 78.3°C respectively. The modification included to account for the latent heat of fusion at 33°C had correctly predicted a fall in temperature, comparable to that of the experimental data. The trend of the curves were in good agreement with the experimental data points; although admittedly the agreement was not as good as that at 20°C.

The predicted crust thickness curves under the same experimental conditions are shown in Figure 10.20. No crust thickness measurements were taken except of the final dried particles because of the difficulty in obtaining measurements from partially dried particles.

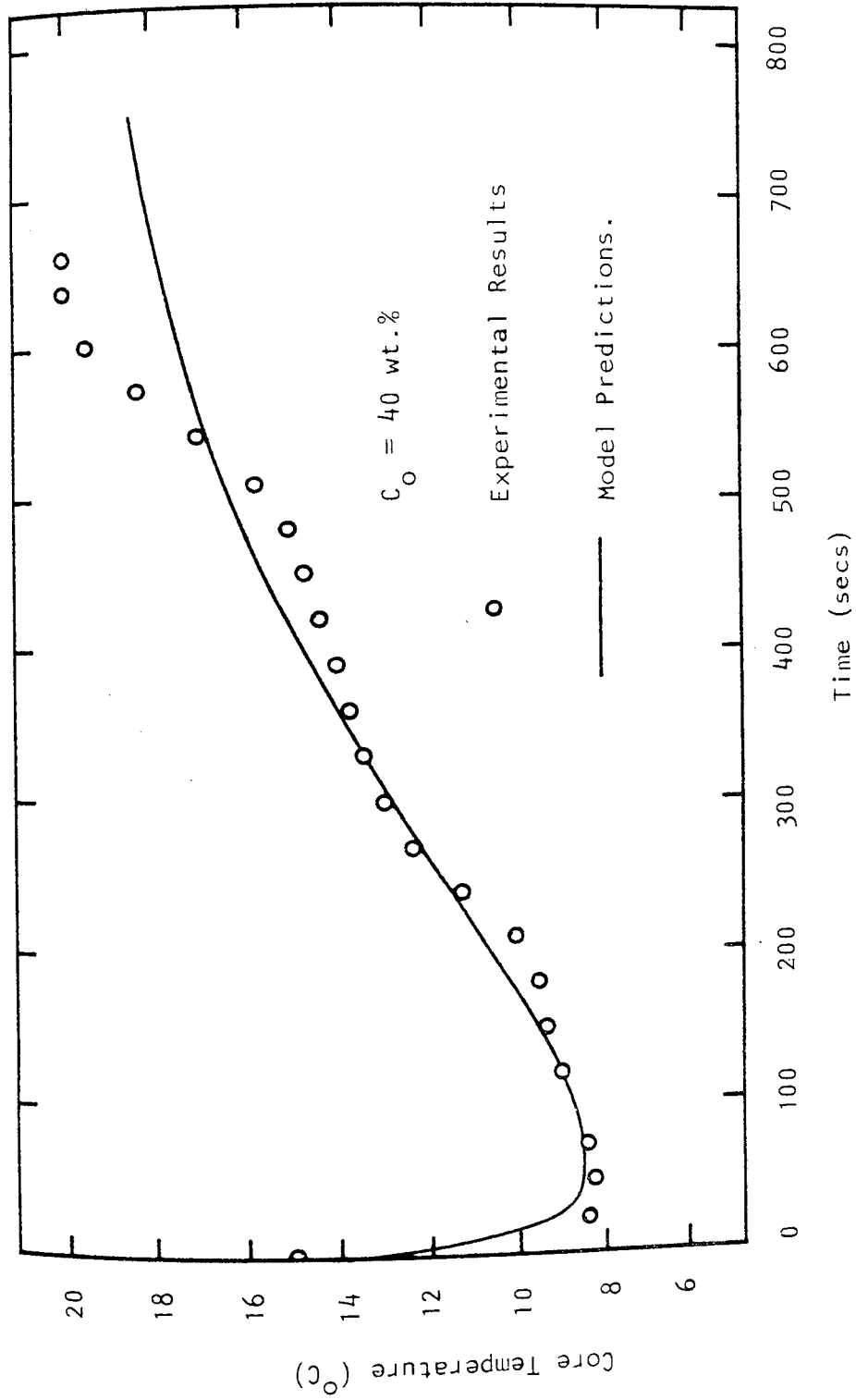


Figure 10.16 Comparison of Experimental Core Temperatures with Model Predictions at $T_g = 20^\circ\text{C}$

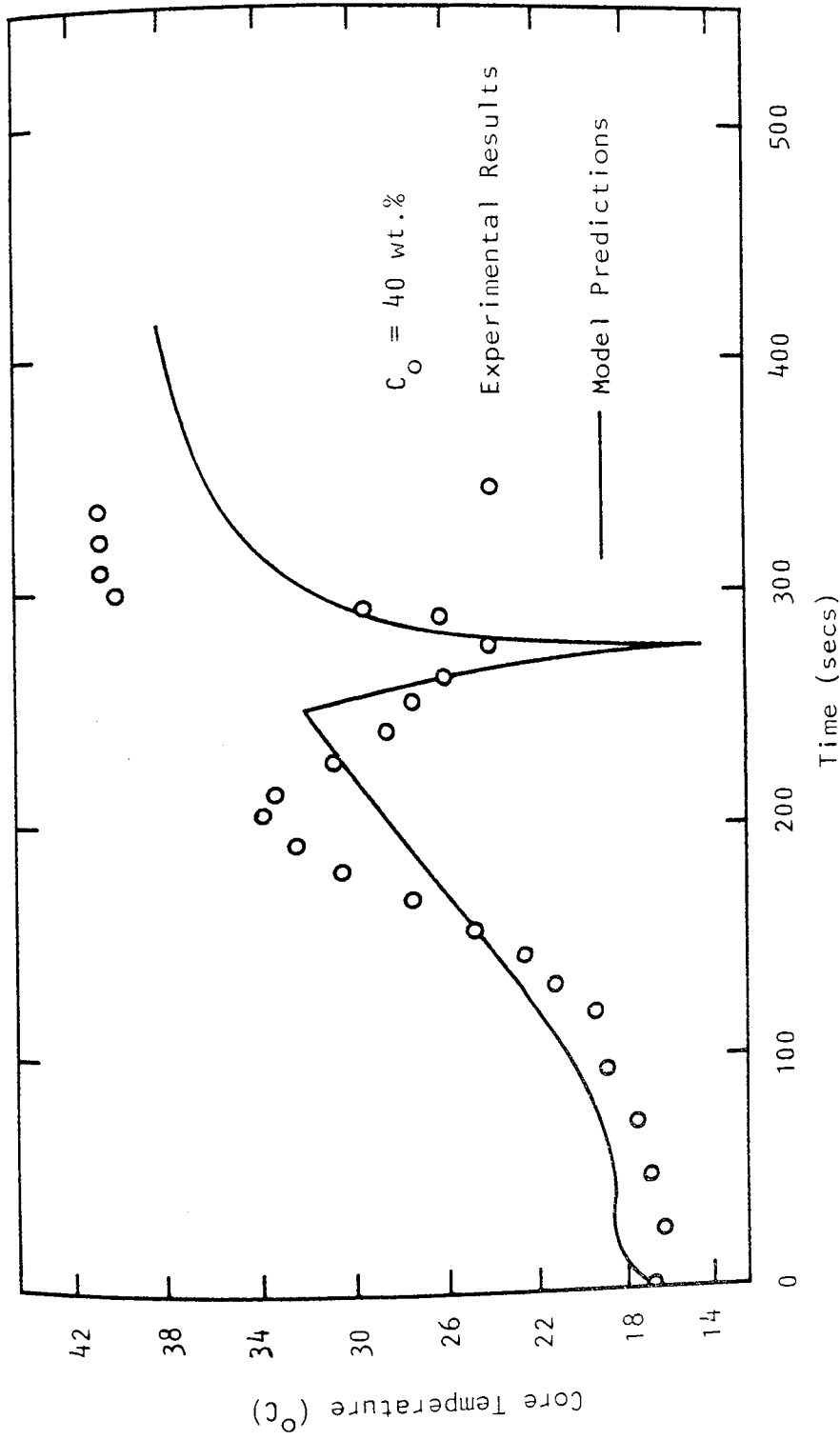


Figure 10.17 Comparison of Experimental Core Temperature with Model Predictions at $T_g = 40.7^\circ\text{C}$.

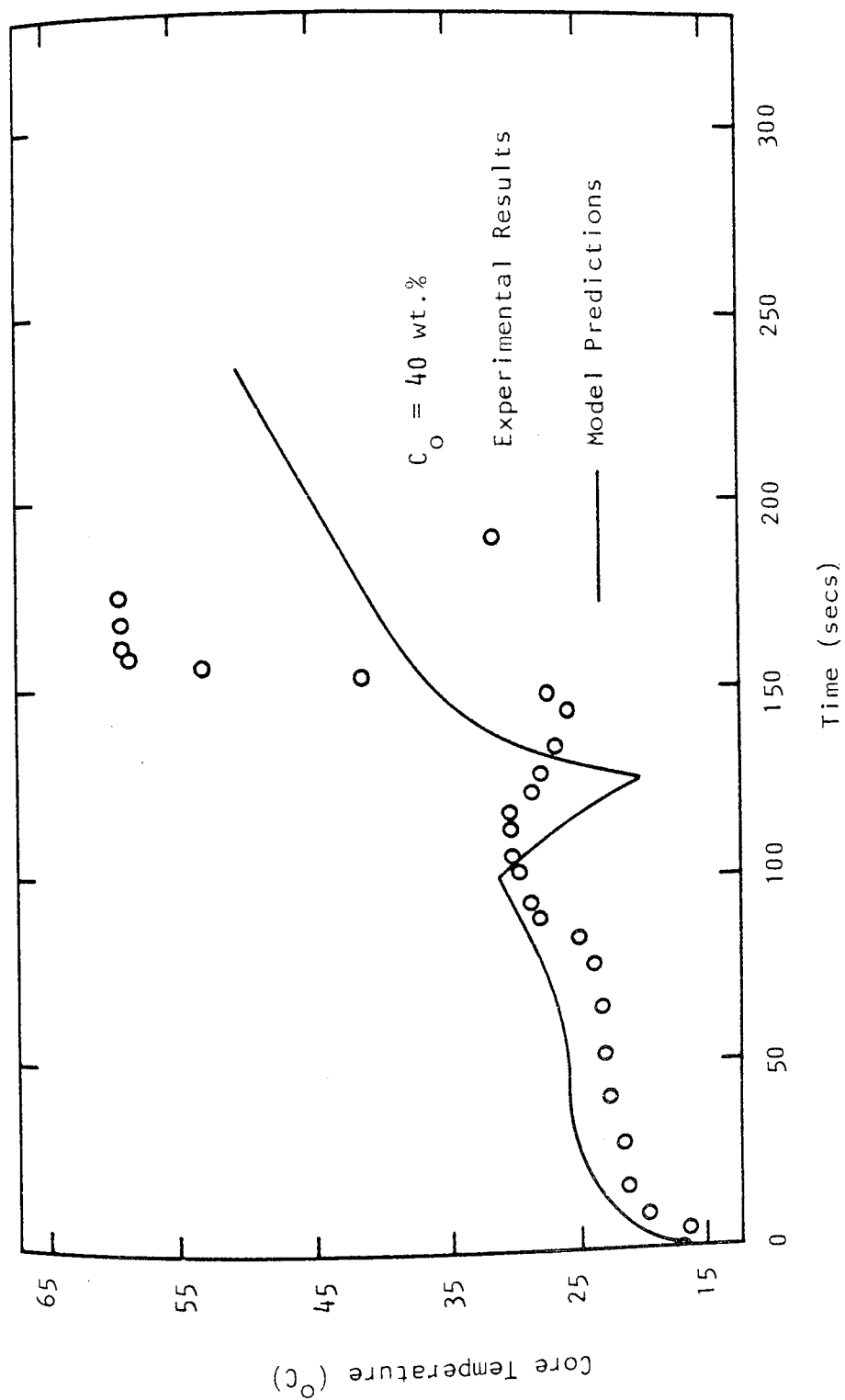


Figure 10.18 Comparison of Experimental Core Temperatures with Model Predictions at $T_g = 59.3^\circ\text{C}$.

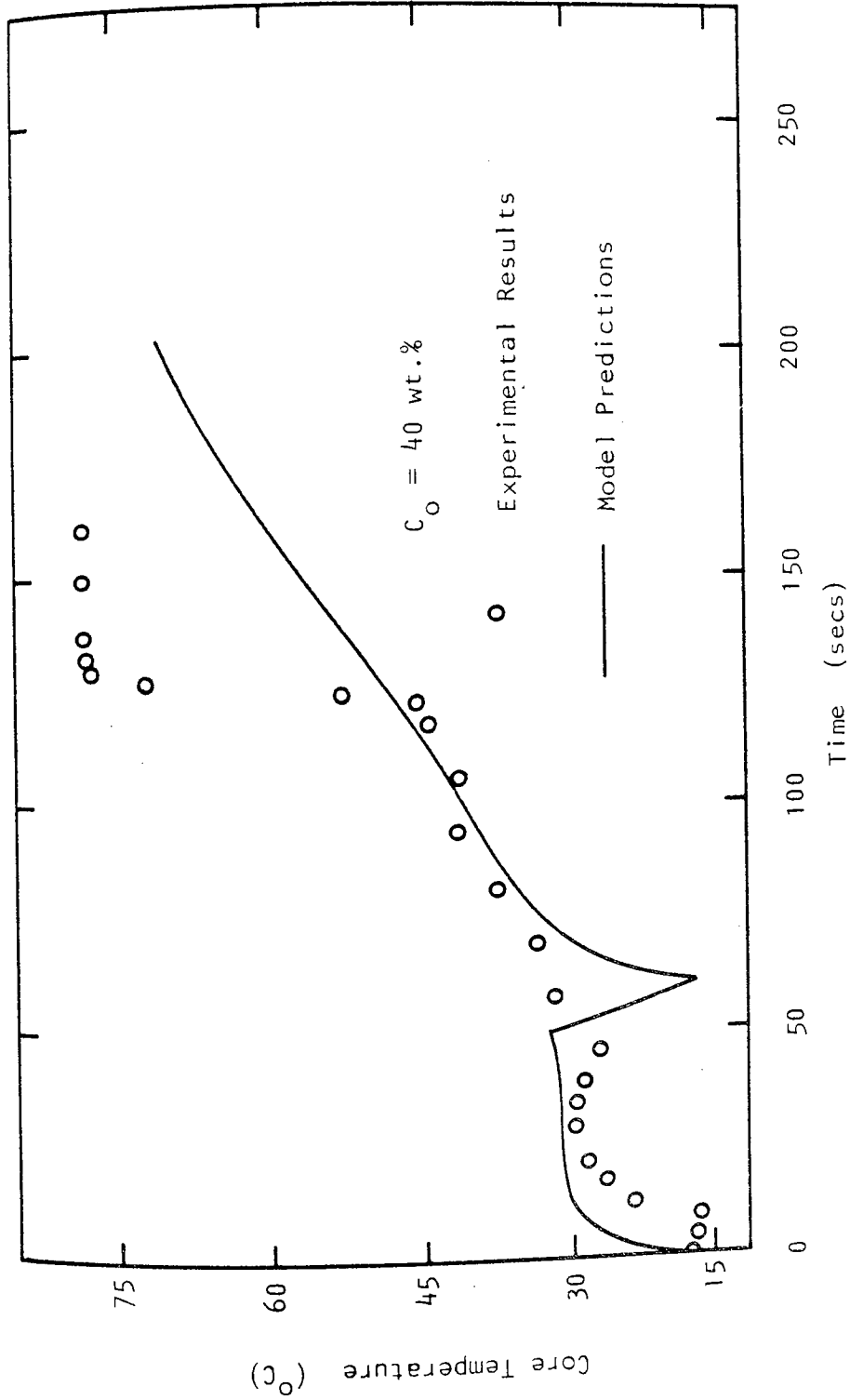


Figure 10.19 Comparison of Experimental Core Temperatures with Model Predictions at $T_g = 78.3^\circ\text{C}$

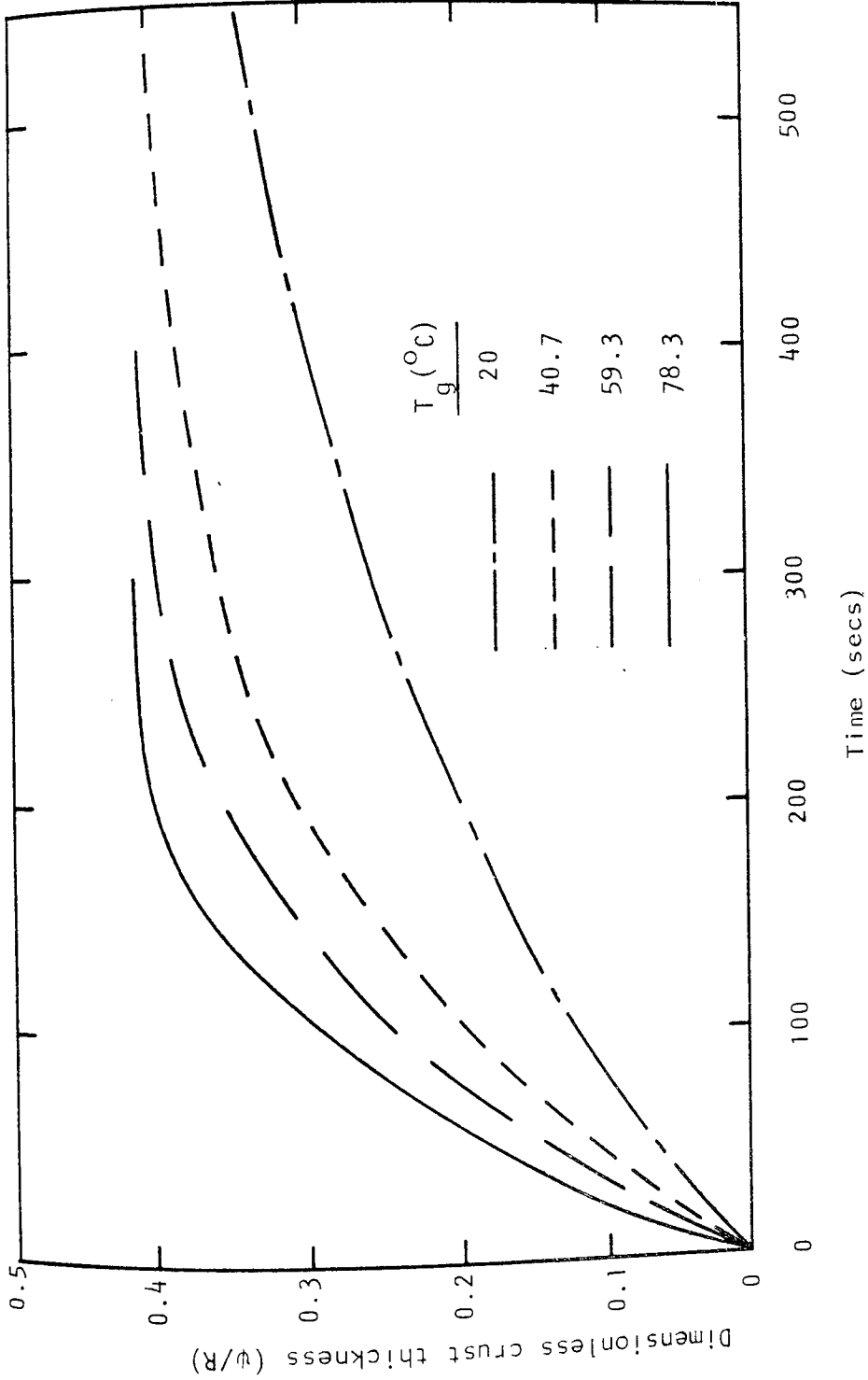


Figure 10.20 Model predictions of crust thickness as a function of time for $C_0 = 40$ wt.%.
 for $C_0 = 40$ wt.%.

When a partially dried particle was removed from the wind tunnel the sudden cooling caused rapid crystallisation which gave an erroneous crust thickness measurement.

The drying curves predicted from the model agree reasonably well during the first drying period. However, the curves overestimated the weight of the drop during the second period after a substantial crust had formed. It is likely that bits of the dried crust on fracturing may have fallen away giving a low weight measurement.

CHAPTER 11

DISCUSSION

- 11.1 Experimental Techniques
- 11.2 Experimental Results
 - 11.2.1 Water Drops at Ambient Temperature
 - 11.2.2 Water Drops at Elevated Temperatures
 - 11.2.3 Drops of Aqueous Sodium Sulphate Decahydrate
 - 11.2.4 Simultaneous Drop Weight and Core Temperature Measurements
- 11.3 Receding Evaporation Interface Model

CHAPTER 11

DISCUSSION

Different designs of wind tunnel and different evaporation rate measurement techniques (15, 25, 43, 49, 50) have been used by various investigators. The wind tunnel is generally designed to supply drying air, at a constant velocity and temperature, to simulate as closely as possible conditions in a spray dryer or other equipment involving the evaporation of a spray. Ideally, droplets covering a size range similar to the distribution encountered in sprays should be studied. However, as is evident from Chapter 3, this presents practical difficulties in droplet suspension and evaporation rate measurement. Furthermore, the progressive change of structure of crust forming particles would be impossible to observe without highly sophisticated equipment. As a compromise, the smallest practicable drop size has therefore to be studied, giving measurable weight loss and changes in structure that are visible through a telephoto lens.

The present design of the wind tunnel and the drop suspension technique will be discussed in the following

sections. In particular the advantages and novelty of the thin film thermocouple will be highlighted.

Numerous equations have been proposed by different investigators to predict Nusselt and Sherwood numbers. However, agreement between different sources are often lacking, especially at elevated temperatures. The present correlations will be discussed and compared with other published equations.

The evaporation rate curves for sodium sulphate decahydrate slurries will be discussed in relation to the applicability of the Receding Evaporation Interface model derived in section 7.2 and compared to previously published drying curves for the same material. In particular, the importance of crust structure under different drying conditions and the effect of fractures on the evaporation rate will be highlighted.

11.1 Experimental Techniques

Previous investigators have used different methods of supplying a drying medium to an evaporating drop. Ranz and Marshall (15) and Charlesworth and Marshall (72) used a vertical nozzle to provide a stream of hot air, Audu (43) used a horizontal wind tunnel while Sandoval-Robles et al. (50) suspended spheres in a circular channel of stationary liquid.

In a horizontal wind tunnel, the suspended drop tends to be displaced slightly in the direction of the flow and the suspension filament, nozzle or capillary inevitably disturbs the flow pattern around the drop to some extent. In addition free convection currents caused by differences in densities, which would normally flow vertically upwards, would be dragged towards the wake of the drop. Conversely, with upward flowing air in a vertical tunnel, the suspension device resides in the wake of the drop, where it is least likely to disturb the flow. Convection currents also tend to move symmetrically around the drop with the flow, simulating more closely a drop in free flight. Consequently, a vertical wind tunnel with upward flowing air was designed and adapted for the present investigation.

Nozzles, capillaries and glass filaments have been used for drop suspension by various researchers. The nozzles used by Audu (43) had the disadvantage of having a similar diameter to the drop itself, resulting in a significant disturbance to the flow pattern of air around the drop. Heat conduction through the nozzles was also substantial because of the large surface area in contact with the drop. Conversely, glass filaments can be fabricated to very small diameters (0.17 mm) and therefore, much smaller and more spherical drops can be studied. In the present study, the surface area of the drop in contact with the suspension filament was extremely small, less than 0.8%, and therefore heat conduction was minimal.

Drop temperatures have mainly been measured by previous investigators with fine thermocouples by suspending drops from thermojunctions. However, a number of researchers ignored the heat conduction through the thermocouple leads which would invariably have raised the temperature at the junction. Furthermore, if any part of the junction is not completely immersed in the drop, an average temperature between the exposed and immersed part of the junction is recorded. The problem becomes more complex when crust formation occurs. Since a temperature gradient exists between the wet core and the outside surface of the crust, the measured temperature is very dependent on the precise location of the thermojunction in the particle.

The thin film thermocouple, developed in the present investigation, was a novel drop temperature measuring device incorporating provision for simultaneous drop weight measurement, which in the past has been measured separately on supposedly identical drops. The thin film thermocouple, as described in section 8.3, consisted of a hollow glass filament threaded with a 50 μ diameter nickel wire and coated with a thin film of copper. Nickel and copper were chosen as the conducting elements because of their large thermal electromotive force (e.m.f.) change per degree change in temperature. Copper has a thermal e.m.f. of +760 mV relative to platinum at 100°C while nickel has a corresponding value of -1480 mV (111). The difference and hence sensitivity is therefore comparable to the more

commonly used thermocouples. Although both nickel and copper films adhere readily to glass, the latter is more easily evaporated, having a melting point of 1200°C at a pressure of 10^{-2} Torr. Furthermore, nickel melt would rapidly dissolve the tungsten filament heater, resulting in an open circuit.

The surface area of the thermojunction of the thin film thermocouple was comparable to that of a conventional argon welded junction, but being a single length of coated nickel wire (0.5 mm long), it was totally immersed and extended into the core of the particle. It therefore measured the core temperature. This was the first time that such a thermocouple, using effectively a single fine wire, had been used to measure drop temperatures. The thermocouple had the added advantage of enabling accurate measurements to be made of temperature profiles in the crust of drops containing solids by using different lengths of exposed wire at the tip of the thermocouple.

11.2 Experimental Results

Evaporation of pure liquids has been studied extensively, partly because pure liquid systems are less complex since there is no crust formation. Commercially, the evaporation of pure liquids, e.g. in fuel atomisation, crop spraying, humidification operations etc., poses less problems than the drying of sprays containing solids.

In the latter, after crust formation has occurred, evaporation rates are controlled predominantly by the resistance to moisture diffusion in the crust. However, the structure, and in particular the porosity of the crust have been mainly ignored in the past due to the difficulty in quantifying these parameters. The process becomes even more complex when fractures, shrinkage or inflation occur.

11.2.1 Water Drops at Ambient Temperature

At ambient temperature, the value of ϕ in equation 10.1 was found to be 0.66, which is in good agreement with the value of 0.69 reported by Rowe et al. (56), 0.625 by Miura et al. (83) and 0.60 by Ranz and Marshall (15). This agreement therefore served to confirm the reliability of the present design of wind tunnel and drop suspension technique.

The experimental Nusselt numbers were calculated from equation 7.6 using a constant value of $d(d_p^2)/d\theta$ for each set of results. This is justified at ambient temperature because the diameter squared against time curves would be almost linear, as evident from the results in Appendix A.4.1. It should be noted that the experimental Nusselt numbers have been corrected for heat conduction along the filament and heat transferred by radiation, as described in sections 7.1.2 and 7.1.3. Ranz and Marshall (15) and a number of other investigators (72, 92) ignored these

corrections assuming them to be insignificant. Whilst this is probably justified for results obtained at low temperatures, as will be shown later, at elevated temperatures these heat correction terms can be quite substantial.

In the absence of natural convection, the limiting Nusselt number at $Re = 0$ is 2. If the present results are fitted by a linear regression without assuming a constant value of 2, the Nusselt equation would be,

$$Nu = 2.10 + 0.64 Re^{0.5} Pr^{0.33} \quad (11.1)$$

The constant is therefore not significantly different from the assumed value of 2 which has a theoretical basis.

The present results could have been presented as Sherwood numbers, but as is widely accepted, thermal properties of air can be predicted very accurately whereas molecular diffusivities are quoted with less confidence.

11.2.2 Water Drops at Elevated Temperatures

At elevated temperatures, the values of ϕ varied from 0.58 to 0.45 for T_g between 33.5 and 79°C. This is not unexpected since at higher heat and mass transfer rates, some of the heat transferred from the drying medium is taken up by the outward diffusing vapour.

Downing (62) has proposed, from a theoretical derivation, that at elevated temperatures,

$$\text{Nu} = \frac{1}{B} \ln(1+B) [2 + 0.60 \text{Re}^{0.5} \text{Pr}^{0.33}] \quad (11.2)$$

However, his experimental results could not be adequately predicted using this equation. It is interesting to note that up to about 100°C, the value of $\frac{1}{B} \ln(1+B)$ is almost unity, having little effect as a correction term.

Audu (43) proposed a temperature correction term $(T_g - T_s)/293$, to fit his results. However, an index of -0.008 was used which suggests that the results could have been correlated omitting this term.

Both the above empirical correlations were applied to the present results but could not predict the Nusselt number with any accuracy. It has been shown by Spalding (63) that heat transferred to the outward diffusing vapour at high temperatures could be accounted for by the dimensionless Transfer number B. The Transfer number would also account, to a first approximation, for the inaccuracy of assuming constant film properties since it includes the temperature driving force and heat capacity. Consequently, the Transfer number was included in equation 10.1 to correlate the results at elevated temperatures, resulting in the modified Nusselt equation,

$$\text{Nu} = 2 + 0.19 (1/B)^{0.24} \text{Re}^{0.5} \text{Pr}^{0.33} \quad (10.3)$$

with a correlation coefficient of 0.98.

Although the introduction of the Transfer number was semi-empirical, it nevertheless gave an excellent correlation coefficient and there is no evidence that any more complicated or theoretical approach would give a better result (62).

As in the case at ambient temperature, the experimental Nusselt numbers were corrected for heat conduction along the filament and heat transferred by radiation. These corrections for the additional heat flux were found to be quite substantial especially at the maximum temperature investigated. At $T_g = 79^\circ\text{C}$ for example, for a drop diameter of 0.532 mm, the extra heat input accounted for 24.65% of the total heat transferred. This supports the earlier statement by Fuchs (34) that this additional heat input should not be ignored.

11.2.3 Drops of Aqueous Sodium Sulphate Decahydrate

The drying curves for drops of aqueous sodium sulphate decahydrate were presented in Figures 10.7 - 10.15 as fraction of initial weight evaporated against time for the concentrations, air velocities and temperatures investigated. The results were presented in this manner to smooth out any slight variations in the initial weight of the drops and to be consistent with those published

by Charlesworth and Marshall (72) and Trommelen and Crosby (68) for comparison purposes.

The measured weights were corrected for heat conduction along the suspension filament and radiation by equation 10.4. In theory, the weight correction varies with drop temperature and diameter and an integration over the time interval would be necessary. However, using a mean drop temperature and mean drop diameter over the interval should be a good approximation and was therefore used instead in the present analysis.

The drying curves show reasonably good agreement with those published by Charlesworth and Marshall. However, the present investigation also included higher concentrations; up to 54.1 wt.% solids. Clearly, such high concentrations tend to create problems in transferring a drop onto a suspension filament because of premature crystallisation in the hypodermic needle, which partly explains the lack of published data to date. Commercially, there are numerous advantages in having a feed to a spray dryer of high solids concentrations, the most obvious of which are to obtain a higher solids throughput and the more economical use of thermal energy.

During the first period of drying, the rate of heat transfer was controlled by the vapour film resistance, described mathematically by equation 7.2. This period was

characterised by the evaporation from a free liquid surface and the drying curves approximated those of pure liquid drops. The solids concentration would be expected to rise from the initial concentration towards a saturation value commonly termed the critical moisture content. This critical value is often only dependent on the drop temperature, irrespective of the initial solids concentration. However, for slurry drops where the initial solids concentrations were much higher than that at the critical value, crust formation occurred almost instantaneously and a first drying period was not evident.

Drying rates in the second drying period i.e. after crust formation, showed a great deal of variation even under identical drying conditions, as is evident from Figures 10.9 and 10.10. This was a phenomenon experienced by both Charlesworth and Marshall, and Trommelen and Crosby. During this period, the resistance of the crust to moisture diffusion became predominant and the structure of the crust, and in particular the porosity, had a significant effect on the subsequent evaporation rate. The porosity of the crust was governed largely by the initial concentration of the drop; a higher initial solids content giving rise to a more porous crust. However, the high solids content also resulted in a thicker crust which in turn increased the resistance to moisture diffusion. The electron micrographs in Plates 10.3, 10.6 and 10.8 show this effect clearly.

At a concentration of 5 wt.% solids and low air temperatures, pores were hardly evident even at a magnification of 5000 and the crusts appeared relatively smooth, as evident from Plate 10.2. At high velocities, parallel 'furrows' were evident (Plate 10.3), seemingly caused by a 'shearing' effect at the boundary layer. At higher solids concentrations (15 wt. % and above) and/or higher air temperatures, larger crystals and pores were visible, as evident from Plates 10.6 and 10.11. It appeared therefore that a critical state existed whereby a crust, from a relatively smooth and non-porous structure reverted to a rough and jagged surface with significantly large pores. The factors that controlled this critical state appeared to be the initial concentration and the air temperature. As will be discussed in the next section, at higher temperatures (above 33°C), anhydrous sulphate would be deposited which has a different crystal structure to the monoclinic decahydrate.

Crusts formed from drops of high solids concentrations were more prone to fractures and 'blow holes'. When a fracture occurred, the resistance to moisture diffusion suddenly diminished and evaporation proceeded at a high rate. However, the fractures were quickly filled in by further deposition of crust and the process repeated itself. This resulted in dried particles that were distorted in shape with fractures and occasionally large 'blow holes'. The repeated fractures and 'blow-holes'

may also result in pieces of crust falling away, as is evident from the sudden drastic loss in weight shown in Figures 10.9 and 10.10. This may presumably be one of the causes of fine dust in spray dried products. If such is the case, measures to minimise such dust, which in commercial practice must either be recycled or agglomerated in a subsequent stage, could include a lower solids concentration or a less intense drying temperature. Clearly therefore, an optimum operating condition would be required for a maximum throughput with the minimum of fines for a particular product.

11.2.4 Simultaneous Drop Weight and Core

Temperature Measurements

These experiments were the first attempt at a simultaneous drop weight and core temperature measurement using the novel thin film thermocouple developed for this purpose.

The behaviour of sodium sulphate during drying at temperatures above about 33°C is unusual in that it forms different hydrates with incongruent melting points (112). Below the transition temperature of 32.4°C, the monoclinic decahydrate crystals are in equilibrium with the liquid phase. At the transition point, the rhombic crystals of anhydrous sulphate commence to separate and exist in equilibrium with the decahydrate and the saturated solution.

From the transition point up to about 125°C, the solubility of the anhydrous sulphate actually decreases with increasing temperature.

The shape of the core temperature curves show this behaviour clearly at air temperatures above 33°C, by the sudden fall at about the transition point. The fall in temperature resulted in a sudden increase in the temperature driving force and consequently the heat and mass transfer rate. This invariably caused rapid evaporation and an increase in the crust growth rate which resulted in the core temperature rising immediately. As the temperature increased, the crust growth rate was further enhanced by the negative solubility of the anhydrous sulphate. This in turn increased the core temperature even higher.

The depression of the core temperature curves at about the transition point appeared to be less drastic at the higher air temperatures as evident from Figures 10.13 and 10.15. This was a result of the higher heat transfer rates at the higher air temperatures, tending to very rapidly re-establish the equilibrium.

It should be noted that the unusual behaviour of sodium sulphate was not evident from the drying curves alone, discussed in section 11.2.3. This clearly highlighted the advantage of the thin film thermocouple as an investigative tool especially when salts, electrolytes etc. are present.

11.3 Receding Evaporation Interface Model

As evident from the previous section, the modelling of the drying of sodium sulphate decahydrate slurry drops would be complicated by the formation of hydrates and the negative solubility of the anhydrous sulphate.

The modelling was initially carried out using a constant crust porosity without much success. It appeared therefore that this assumption used in the model was not valid as the crust thickness increased. Experimental determination of crust porosity by the usual methods on such a small and brittle crust was not possible. An empirical expression was therefore formulated for the porosity as a function of the crust thickness where,

$$\epsilon = 1 - 2.4 (\psi/R) \quad (11.3)$$

The remarkable accuracy of the model predictions at 20°C served to confirm the validity of this expression.

The model predictions at the higher air temperatures were fairly good although not as accurate as that at 20°C. The modification included to account for the latent heat of fusion at 33°C, accurately predicted the fall and rise of the core temperature at the transition point. After the transition point, the model underestimated the core temperature because no modification was

included for the negative solubility of the anhydrous sulphate. To model this particular section of the curve would be extremely difficult and probably do not justify the computer time and effort.

The model predicted the first period of the drying curve reasonably well but overestimated the second period because of the formation of the anhydrous instead of the decahydrate salt at high temperature. Fractures and 'blow holes' could also have resulted in pieces of the crust falling away. The occurrence of fracture, shrinkage or inflation are dependent on the particular material being dried, the initial solids concentration and the drying air temperature. Even under identical conditions and concentrations, different drops are known to behave quite differently depending on the exact moment a fracture occurs. This uncertainty would of course be impossible to model without a further understanding of the precise mechanisms that control these phenomena.

In spite of the complications with sodium sulphate decahydrate slurries, the model had proved to be reasonably accurate and would be expected to perform much better with other slurry materials.

CHAPTER 12

CONCLUSIONS AND RECOMMENDATIONS

12.1 Conclusions

12.2 Recommendations

CHAPTER 12

CONCLUSIONS AND RECOMMENDATIONS

12.1 Conclusions

The major conclusions from this study are,

- 1) The literature review showed that some disagreement exists as to the form of the Nusselt equation for heat transfer to drops. Furthermore, the majority of previous investigators who measured evaporation rates from suspended drops, ignored heat conduction along the drop suspension filament and thus incurred significant experimental errors.

- 2) None of the previously published correlations could adequately predict the Nusselt numbers obtained from the experimentation. Therefore, a modified Nusselt equation (equation 10.3), which included the Transfer number was proposed and agreement with the experimental results were excellent; a correlation coefficient of 0.98 was obtained. The contribution to heat transfer by conduction along the drop suspension filament was taken into account and analysis of the results showed that at $T_g = 79^{\circ}\text{C}$, as much as 21.7% of the total heat transferred to a suspended drop could be attributed to this source.

- 3) The drying of drops (1 - 1.5 mm diameter) of aqueous sodium sulphate decahydrate at temperatures between 18 - 110°C, was characterised by two distinct drying periods; an initial constant period and a falling period as soon as a crust was formed. After crust formation, fractures occurred randomly but was more frequent at higher concentrations and temperatures.
- 4) This research involved the first attempt at a simultaneous drop weight and core temperature measurement using a novel thin film thermocouple, developed specially for this purpose. The heat conduction along the drop suspension device was reduced because of the unique design of this thermocouple, using essentially a single 50 μ diameter nickel wire.
- 5) The Receding Evaporation Interface model which was developed for slurry drops, was found to be applicable to drops of sodium sulphate decahydrate slurries with an initial concentration of 40 wt.%. The model predicted core temperatures accurately for drying temperatures between 20 to 78.3°C. However, the model could not account for the occurrence of fractures, which were observed to take place randomly.

12.2 Recommendations

- 1) The thin film thermocouple was developed for the simultaneous drop weight and core temperature measurement. The thermocouple could be modified to measure the temperature profile within the crust of a suspended particle. This could be achieved by using different lengths of exposed nickel wire at the thermojunction of the thermocouple.

- 2) The drying of sodium sulphate decahydrate slurries has been studied extensively and the mathematical model was found to be applicable. This model should be further applied to other materials under more extreme drying conditions to test its validity.

- 3) The occurrence of fractures in individual particles could not be predicted by the model. A more detailed study should be undertaken to obtain a further understanding of this phenomenon with the objective of improving the existing model.

APPENDICES

APPENDIX A

- A.1 PHYSICAL PROPERTIES USED IN ANALYSIS OF WATER DROPS
 - A.1.1 Air
 - A.1.2 Water
 - A.1.3 Glass Filament
- A.2 LEAST SQUARES METHOD FOR DATA CORRELATION
 - A.2.1 Constant Air Temperature
 - A.2.2 Variable Air Temperature
- A.3 COMPUTER PROGRAM LISTINGS
 - A.3.1 Program Filename: EVAPORATION
 - A.3.2 Program Filename: CORR TEMP
- A.4 TABULATION OF RESULTS
 - A.4.1 Water Drops at Ambient Temperature
Tables A1 to A35.
 - A.4.2 Water Drops at Elevated Temperatures
Tables A36 to A39.

APPENDIX A

A.1 PHYSICAL PROPERTIES USED IN ANALYSIS OF WATER DROPS

A.1.1 Air

Density, $\rho = 1.2929(273.15/(273.15+T_g))$ kg m⁻³

Thermal Conductivity, $k = (4.296 \times 10^{-5}(T_g+T_s)/2 + 0.014) \times 1.731$
W m⁻¹ K⁻¹

Viscosity, $\mu = 4.568 \times 10^{-8}(T_g+T_s)/2 + 1.720 \times 10^{-5}$ kg m⁻¹ s⁻¹

<u>Air Temperature (°C)</u>	<u>Heat Capacity (J kg⁻¹ K⁻¹)</u>
22	1025.77
34	1031.00
46	1036.23
63	1041.47
79	1046.70

A.1.2 Water

Latent Heat of Vaporisation, $\lambda = 2.326 (1075.95 - 1.025 T_S)$
kJ kg⁻¹

Diffusivity of Vapour in Air,

$$D_v = 0.22 \left[\frac{(T_g' + T_s')/2}{273.15} \right]^{1.75} \times 10^{-4}$$

m² s⁻¹

Emissivity of Drop, $e = 0.955$

Stefan-Boltzmann Constant, $\sigma = 5.6697 \times 10^{-8}$ W m⁻² K⁻⁴

Drop Temperature (°C)

Density (kgm⁻³)

8.0	1000.1
13.0	999.4
17.5	998.7
21.5	998.0
25	997.0

A.1.3 Glass Filament

Diameter of Filament, $d_f = 0.1764 \times 10^{-3}$ m

Thermal Conductivity, $k_t = 0.6404$

W m⁻¹ K⁻¹

Emissivity of Filament, $e_g = 0.94$

Heat Transfer Coefficient of Filament, $h_f = Cr Re_f^m Pr^{0.33} k/d_f$
W m⁻² K⁻¹

where $Cr = 0.989$ and $m = 0.33$ for $Re_f < 4$

$Cr = 0.911$ and $m = 0.385$ for $4 \leq Re_f < 40$

$Cr = 0.683$ and $m = 0.466$ for $Re_f \geq 40$

A.2 LEAST SQUARES METHOD FOR DATA CORRELATION

A.2.1 Constant Air Temperature

From Equation 10.1,

$$Nu = 2 + \phi Re^{0.5} Pr^{0.33}$$

Rearranging and taking logarithms to the base e ,

$$\log_e (Nu-2) = \log_e \phi + \log_e (Re^{0.5} Pr^{0.33}) \quad (A.1)$$

Let $Y1 = \log_e (Nu-2)$

$$Y2 = \log_e (Re^{0.5} Pr^{0.33})$$

$$Y3 = \log \phi$$

At $Y2_i$, the error between the data and the approximating function can be expressed by,

$$\delta (Y1_i) = Y1_i - Y2_i - Y3 \quad (A.2)$$

The objective function is to minimise the sum of the errors squared, expressed as,

$$\delta (Y1_i)^2 = \sum_{i=1}^n (Y1_i - Y2_i - Y3)^2 \quad (A.3)$$

Differentiating $\delta(Y1_i)^2$ with respect to $Y3$ and setting the resultant differential equation to zero,

$$\frac{d(\delta(Y1_i)^2)}{d(Y3)} = -2 \sum_{i=1}^n (Y1_i - Y2_i - Y3) = 0 \quad (A.4)$$

Hence,

$$Y3 = (\sum Y1_i - \sum Y2_i)/n \quad (A.5)$$

The value of ϕ can then be evaluated by taking the exponential of Y3,

$$\phi = \exp (Y3) \quad (A.6)$$

The multiple correlation coefficient R1 can be evaluated by the expression,

$$R1 = \left[1 - \frac{\text{Residual sum of squares}}{\text{Total sum of squares}} \right]^{0.5} \quad (A.7)$$

In the present notation,

$$R1 = \left[1 - \frac{\sum (Y1_i - Y2_i - Y3)^2}{\sum (Y1_i - \bar{Y}1)^2} \right]^{0.5} \quad (A.8)$$

where $\bar{Y}1 = (\sum Y1_i)/n$

Equations A.5, A.6, and A.8 are included in the computer program "EVAPORATION", listed in Appendix A.3.1. for data analysis at constant temperature.

A.2.2 Variable Air Temperature

From the proposed equation 10.2,

$$Nu = 2 + \phi (1/B)^{\eta} Re^{0.5} Pr^{0.33}$$

Rerranging and taking logarithms to the base e,

$$\log_e (Nu-2) = \log_e \phi + \eta \log_e (1/B) + \log_e (Re^{0.5} Pr^{0.33}) \quad (A.9)$$

As in the previous section,

$$\text{Let, } Y1 = \log_e (Nu-2)$$

$$Y2 = \log_e (Re^{0.5} Pr^{0.33})$$

$$Y3 = \log_e \phi$$

$$Y4 = \log_e (1/B)$$

The errors squared $\delta(Y1_i)^2$, is thus expressed as,

$$\delta(Y1_i)^2 = \sum_{i=1}^n (Y1_i - Y2_i - Y3 - \eta Y4_i)^2 \quad (A.10)$$

The objective function is to select values of Y3 and η to minimise $\delta(Y1_i)^2$.

Differentiating $\delta(Y1_i)^2$ with respect to Y3 and η respectively, and equating both expression to zero,

$$\frac{\partial(\delta(Y1_i)^2)}{\partial(Y3)} = -2 \sum_{i=1}^n (Y1_i - Y2_i - Y3 - \eta Y4_i) = 0 \quad (A.11)$$

and

$$\frac{\partial(\delta(Y1_i)^2)}{\partial \eta} = -2 \sum_{i=1}^n Y4_i (Y1_i - Y2_i - Y3 - \eta Y4_i) = 0 \quad (A.12)$$

Expanding Equation A.11,

$$\sum Y1_i - \sum Y2_i - nY3 - \eta \sum Y4_i = 0$$

and hence,

$$Y3 = (\sum Y1_i - \sum Y2_i - \eta \sum Y4_i) / n \quad (A.13)$$

Similarly expanding equation A.12,

$$\sum (Y4_i \cdot Y1_i) - \sum (Y4_i \cdot Y2_i) - Y3 \sum Y4_i - \eta \sum (Y4_i)^2 = 0 \quad (A.14)$$

Substituting Equation A.13 into A.14 and rearranging,

$$\eta = \frac{n \sum (Y4_i \cdot Y1_i) - n \sum (Y4_i \cdot Y2_i) - (\sum Y4_i)(\sum Y1_i) + (\sum Y4_i)(\sum Y2_i)}{n \sum (Y4_i)^2 - (\sum Y4_i)^2} \quad (A.15)$$

The value of η can then be used in equation A.13 to evaluate Y3.

The correlation coefficient for the approximating function is expressed as,

$$R1 = \left[1 - \frac{\sum (Y1_i - Y2_i - Y3 - \eta Y4_i)^2}{\sum (Y1_i - \bar{Y1})^2} \right]^{0.5} \quad (A.16)$$

A computer program 'CORR TEMP', listed in Appendix A.3.2. was used to correlate the results at variable air temperatures according to equations A.13, A.15 and A.16.

A.3 COMPUTER PROGRAM LISTINGS

A.3.1 Program Filename: EVAPORATION

```

10 REM EVALUATION OF NUSSELT NOS. FOR
11 REM WATER DROPS AT CONSTANT TEMP.
12 REM
13 REM SYMBOLS
14 REM RO(J) = FLOWRATE
15 REM VA = VISCOSITY OF AIR
16 REM PR = PRANDTL NO. OF AIR
17 REM ED = EMISIVITY OF DROP
18 REM EG = EMISIVITY OF FILAMENT
19 REM TA(J) = AIR TEMP.
20 REM TD(J) = DROP TEMP.
21 REM DN = DROP DENSITY
22 REM DF = DIA. OF FILAMENT
23 REM KT = THERM COND OF FILAMENT
24 REM PI = PIE (3.14159)
25 REM S = STEFAN-BOLTZMAN CONST.
26 REM DA(J) = AIR DENSITY
27 REM K(J) = THERM COND OF AIR
28 REM LA(J) = LATENT HEAT OF EVAP.
29 REM M = SLOPE OF REGRESS LINE
30 REM C = CONST OF REGRESS LINE
31 REM R = CORR COEFF OF REGRESS
32 REM DD(I) = DROP DIA
33 REM V(J) = AIR VELOCITY
34 REM MD(J) = MEAN DIA
35 REM RE(J) = DROP REYNOLDS NO
36 REM RG = REYNOLDS NO OF FILAMENT
37 REM HT = H.T.C. OF FILAMENT
38 REM QR = HEAT RADIATED
39 REM QF = HEAT THRU FILAMENT
40 REM NE(J) = EXP. NUSSELT NO
41 REM NC = NUSSELT CORRECTION
42 REM NU(J) = CORRECTED NUSSELT NO
43 REM DE(I) = DEFLECTION OF FILAMENT
44 REM WS = COEFF OF RE↑.5*PR↑.33 IN NU EQN.
45 REM W9 = CORR COEFF IN NU EQN.
115 DIM N2(50),X(50),Y(50),DE(50),DD(50),K(50),LA(50)
116 DIM V(50),MD(50),RE(50),TA(50),TD(50),DN(50)
117 DIM RO(50),NU(50),F1(50),NE(50),DA(50),WW(50)
118 DIM W1(50),W2(50)
119 REM
120 REM INPUT EXPERIMENTAL CONDITIONS
125 REM INPUT THE NUMBER OF SETS OF DATA
126 READ N1
130 REM INPUT THE EXPT. NOS.
135 FORJ=1TON1
137 READWW(J)
139 NEXT
140 REM INPUT NO OF READINGS IN EACH SET
142 FORJ=1TON1:READN2(J)

```

```

145 NEXT
146 REM INPUT FLOWRATE IN EACH SET
148 FORJ=1TON1:READ RO(J)
149 NEXT
150 PRINT"INPUT VISC. OF AIR (KG/M/SEC)":INPUTVA
160 PRINT"INPUT PR. OF DRYING MEDIUM":INPUTPR
170 PRINT"INPUT EMISIVITY OF DROP":INPUTED
172 PRINT"INPUT EMISIVITY OF FILAMENT":INPUTEG
175 REM INPUT AIR TEMP FOR EACH SET
180 FOR J=1TON1
181 READ TA(J)
182 NEXT
201 REM INPUT DROP TEMP FOR EACH SET
205 FORJ=1TON1
206 READTD(J)
207 NEXT
223 REM INPUT DENSITY OF DROP
230 READ DN
235 REM
237 PRINT"INPUT DIAMETER OF FILAMENT (M)":INPUTDF
238 PRINT"INPUT THERMAL CONDOC. OF FILAMENT (W/M/K)":INPUTKT
239 REM
240 REM SET VALUE OF CONSTANTS
242 PI=22/7:S=5.6697E-8
250 REM
260 REM EVALUATE PHYSICAL PROPS.
265 FORJ=1TON1
270 DA(J)=1.2929*273.15/(273.15+TA(J)):NEXT
280 FORJ=1TON1:K(J)=(4.2956E-5*(TA(J)+TD(J))/2+.014)*1.7307
282 NEXT
290 FORJ=1TON1:LA(J)=(1075.95-1.0246*TD(J))*2.326:NEXT
300 REM
310 REM CONVERT TEMP. TO K
320 FORJ=1TON1:TA(J)=TA(J)+273.15:TD(J)=TD(J)+273.15:NEXT
350 REM
352 REM CALIBRATION CURVE FOR FILAMENT
355 M1=5.1646E-4:C1=-5.4991E-3
430 REM
440 REM DATA ANALYSIS
445 REM DEFLECTION / TIME DATA INPUT
450 FORJ=1TON1
460 FORI=1TON2(J):READX(I)
466 NEXT
480 FORI=1TON2(J):READ DE(I)
486 NEXT
487 REM
488 REM CALCULATE DROP DIA. AND RATE OF CHANGE OF D12
490 FORI=1TON2(J)
491 DD(I)=((6*(M1*DE(I)+C1))/PI/DN)^(1/3)*10
492 Y(I)=DD(I)^2

```

```

493 NEXT
495 NN=N2(J)
500 GOSUB10000
510 SA=M:C2=C:R2=R
515 REM TEST FOR LINEARITY
517 IF(1-R)>.015THEN 519
518 GOTO520
519 PRINT"3 SLOPE OF D↑2 VS TIME NOT LINEAR":END
520 REM
530 REM REYNOLDS NUMBER
540 V(J)=RO(J)/60*1.2047/DA(J)/PI/((26E-3)↑2)*4/1000
550 FORI=1TON2(J):MD=DD(I)+MD:NEXT
551 MD=MD/N2(J)
555 MD(J)=MD:MD=MD/1000
560 RE(J)=V(J)*MD*DA(J)/VA
570 F1(J)=RE(J)↑.5*PR↑(1/3)
580 REM
600 REM RADIATION CALC.
610 QR=S*PI*MD↑2*EI*(TA(J)↑4-TD(J)↑4)
620 REM
630 REM HEAT THRU FILAMENT
640 RG=V(J)*DF*DA(J)/VA
650 IFRG>40THENCR=.683:G=.466
660 IFRG<40THENCR=.911:G=.385
670 IFRG<4THENCR=.989:G=.33
680 HT=CR*RG↑G*PR↑(1/3)*K(J)/DF
685 QF=2*S*EG*(TD(J)↑5-TA(J)↑5)
690 QF=QF-(10*S*EG*TA(J)↑4*(TD(J)-TA(J)))
695 QF=QF+(5*HT*(TD(J)-TA(J))↑2)
700 QF=(QF*KT*DF↑3/5)↑.5
710 QF=QF*PI/2
720 REM
730 REM HEAT CORRECTION FACTOR
740 NC=(QR+QF)/MD/PI/(TA(J)-TD(J))/K(J)
770 REM
780 REM NUSSOLT CALCU.
795 NE(J)=-((LA(J)*DN/4/(TA(J)-TD(J))/K(J)*SA)
797 NU(J)=NE(J)-NC
820 REM
825 REM RETURN TO EVALUATE NEXT SET OF RESULTS
900 NEXTJ
906 REM CALCULATE COEFF FOR RE↑.5*PR↑.33
907 GOSUB20000
908 REM
909 REM NUMBERS ARE ROUNDED OFF
910 FORJ=1TON1
911 MD(J)=INT(MD(J)*1E3+.5)/1E3:V(J)=INT(V(J)*1E3+.5)/1E3
912 RE(J)=INT(RE(J)*1E2+.5)/1E2:TA(J)=TA(J)-273.15
913 TD(J)=TD(J)-273.15:NU(J)=INT(NU(J)*1E3+.5)/1E3
914 F1(J)=INT(F1(J)*1E3+.5)/1E3:NE(J)=INT(NE(J)*1E3+.5)/1E3

```

```

915 NEXT
918 W5=INT(W5*1E3+.5)/1E3;W9=INT(W9*1E3+.5)/1E3
919 REM
920 REM PRINTING RESULTS
930 OPEN 1,4:OPEN2,4,1:OPEN3,4,2
940 A$="EVAPORATION OF WATER DROPS AT AMBIENT TEMPERATURE"
990 PRINT#1,:PRINT#1,TAB(6);"TABLE 10.1 ";A$
995 PRINT#1,TAB(6);"-----";
996 PRINT#1,"-----"
1000 PRINT#1:PRINT#1
1010 PRINT#1,TAB(6);"  UNITS"
1020 PRINT#1,TAB(6);"-----"
1030 PRINT#1,TAB(6);"MEAN DIAMETER           = 0.1MM"
1040 PRINT#1,TAB(6);"AIR VELOCITY             = 0.17/0.57"
1050 PRINT#1,TAB(6);"AIR AND DROP TEMP.       = C"
1052 PRINT#1
1053 PRINT#1,TAB(6);"NUSSELT EQUATION         = 2 +";W5;"RE↑.5*PR↑.33"
1054 PRINT#1,TAB(6);"CORRELATION COEFF.      =";W9
1060 PRINT#1:PRINT#1
1070 PRINT#1,TAB(6);"EXP  MEAN  AIR    REY  AIR  DROP";
1080 PRINT#1,"  NU"
1090 PRINT#1,TAB(6);"NO.  DIA.  VEL    NO.  TEMP  TEMP";
1100 PRINT#1,"  (EXP)  NU    RE↑.5*PR↑.33"
1110 PRINT#1,TAB(5);"-----";
1120 PRINT#1,"-----"
1130 F$="      99    9.999  9.999  99.99  99.9  99.9  "
1135 B$="  9.999  9.999      9.999"
1140 PRINT#3,F$+B$
1145 FORJ=1TON1
1150 PRINT#2,WWW(J),MD(J),V(J),RE(J),TA(J),TD(J);
1160 PRINT#2,NE(J),NU(J),F1(J)
1165 NEXT
1170 END
10000 REM
10003 REM SUBROUTINE FOR LINEAR REGRESS
10005 S1=0:S2=0:S3=0:B2=0:B3=0:S4=0:S5=0:S6=0:S7=0:M=0:C=0:R=0
10010 FORA=1TONN
10020 S1=S1+X(A)*Y(A)
10030 S2=S2+X(A)
10040 S3=S3+Y(A)
10050 NEXT
10060 B2=S2/NN:B3=S3/NN
10070 FORA=1TONN:S4=S4+((X(A)-B2)↑2):S5=S5+((Y(A)-B3)↑2):NEXT
10080 S6=S4/NN:S7=S5/NN
10090 M=((S1/NN)-(B2*B3))/S6:C=B3-M*B2:R=(M↑2*S6/S7)↑.5
10100 RETURN
20000 REM
20010 REM SUBROUTINE FOR LEAST SQUARES FITTING
20020 FORJ=1TON1
20030 W1(J)=LOG(NU(J)-2)

```

```

20040 W2(J)=LOG(F1(J))
20050 NEXT
20060 W3=0:W4=0:W5=0:W6=0:W7=0:W8=0:W9=0
20070 FORJ=1TON1
20080 W3=W3+W1(J)
20090 W4=W4+W2(J)
20100 NEXT
20110 W5=(W3-W4)/N1:W6=W3/N1
20120 FORJ=1TON1
20130 W7=W7+(W1(J)-W5-W2(J))*2
20140 W8=W8+(W1(J)-W6)*2
20150 NEXT
20160 W9=(1-(W7/W8))*1.5
20165 W5=EXP(W5)
20170 RETURN

```

A.3.2 Program Filename: CORR TEMP

```

50 REM CORRELATION OF RESULTS AT ELEVATED TEMPS.
51 REM
60 REM
61 REM TA(I)= AIR TEMP (C)
62 REM TD(I)= DROP TEMP (C)
63 REM CP(I) = HEAT CAPACITY (J/KG/K)
64 REM LA(I)= LATENT HEAT OF EVAP. (KJ/KG)
65 REM B(I) = TRANSFER NO.
66 REM NU(I)= NUSSELT NO.
67 REM F1(I)= RE↑.5*PR↑.33
68 REM
90 DIM TA(16),TD(16),CP(16),LA(16),B(16),F2(16),N2(16)
95 DIM W1(16,10),W2(16,10),Y3(16,10),NU(16,10),F1(16,10)
100 N=15
105 FOR I=1 TO N
107 READ N2(I):NEXT
110 FOR I=1 TO N
120 READ TA(I)
130 NEXT
140 FOR I=1 TO N:READ TD(I):NEXT
150 FOR I=1 TO 5
160 READ C(I)
165 C(I)=C(I)/1000
170 NEXT
180 FOR I=1 TO 5
190 IF I<8 THEN CP(I)=C(1):GOTO 240
200 IF I<11 THEN CP(I)=C(2):GOTO 240
210 IF I<13 THEN CP(I)=C(3):GOTO 240
220 IF I<15 THEN CP(I)=C(4):GOTO 240
230 IF I<17 THEN CP(I)=C(5)
240 NEXT
245 REM
246 REM PHYSICAL PROPS
250 FOR I=1 TO N
260 LA(I)=(1075.95-1.0246*TD(I))*2.326
270 B(I)=CP(I)*(TA(I)-TD(I))/LA(I)
290 NEXT
295 REM
296 REM INPUT NU AND RE↑.5*PR↑.33
300 FOR I=1 TO N
310 FOR J=1 TO N2(I)
320 READ NU(I,J)
330 NEXT
340 FOR J=1 TO N2(I)
350 READ F1(I,J)
360 NEXT
370 NEXT
400 FOR I=1 TO N

```



```

410 FORJ=1TON2(I)
420 W1(I,J)=LOG(NU(I,J)-2)
430 W2(I,J)=LOG(F1(I,J))
435 Y3(I,J)=LOG(1/B(I))
440 NEXTJ
450 NEXTI
460 W3=0:W4=0:W5=0:W6=0:W7=0:W8=0:W9=0:N3=0
470 FORI=1TON
480 FORJ=1TON2(I)
490 W3=W3+W1(I,J)
500 W4=W4+W2(I,J)
501 Y1=Y1+(Y3(I,J)*W1(I,J))
502 Y2=Y2+(Y3(I,J)*W2(I,J))
503 Y4=Y4+(Y3(I,J)2)
504 Y5=Y5+Y3(I,J)
505 N3=N3+1
510 NEXTJ
520 NEXTI
525 B1=(N3*Y1-N3*Y2+W4*Y5-Y5*W3)/(N3*Y4-Y52)
527 B2=(W3-B1*Y5-W4)/N3
530 W6=W3/N3
540 FORI=1TON
550 FORJ=1TON2(I)
570 W8=W8+(W1(I,J)-W6)2
575 Y6=Y6+(W1(I,J)-B2-B1*Y3(I,J)-W2(I,J))2
580 NEXTJ
590 NEXTI
595 Y7=(1-Y6/W8)1.5
597 REM NUMBERS ARE ROUNDED OFF
600 B1=INT(B1*1E3+.5)/1E3
605 B2=EXP(B2):B2=INT(B2*1E3+.5)/1E3
610 Y7=INT(Y7*1E3+.5)/1E3
620 REM PRINTING RESULTS
630 PRINT"COEFF COEFF OF NU EQN.      ="B2
640 PRINT"INDEX INDEX FOR (1/B)      ="B1
650 PRINT"CORRELATION CORRELATION COEFF.  ="Y7
660 END

```

A.4 TABULATION OF RESULTS

A.4.1 Water Drops at Ambient Temperature

Tables A1 to A35

TABLE A 1

EXPT. NO. = 27
AIR TEMP. (C) = 22.5
DROP TEMP. (C) = 8
MEAN DROP DIA. (mm) = 1.088
AIR VELOCITY (m/s) = .715
REYNOLDS NO. = 51.62
NUSSOLT NO. (EXP) = 7.015
NUSSOLT NO. (CORRECTED) = 6.233
RE↑.5*PR↑.33 = 6.41

<u>TIME(sec)</u>	<u>DEFLECTION(DEG)</u>	<u>WEIGHT(mg)</u>
.0	13.00	1.2149
36.0	12.60	1.0083
110.0	12.10	.7501
168.0	11.60	.4918
281.0	11.10	.2336

TABLE A 2

EXPT. NO. = 28
AIR TEMP. (C) = 22.5
DROP TEMP. (C) = 8
MEAN DROP DIA. (mm) = 1.059
AIR VELOCITY (m/s) = .699
REYNOLDS NO. = 49.15
NUSSOLT NO. (EXP) = 6.827
NUSSOLT NO. (CORRECTED) = 6.039
RE↑.5*PR↑.33 = 6.254

<u>TIME(sec)</u>	<u>DEFLECTION(DEG)</u>	<u>WEIGHT(mg)</u>
.0	13.60	1.5248
57.0	13.10	1.2665
123.0	12.50	.9567
176.0	12.10	.7501
276.0	11.50	.4402
355.0	11.10	.2336
419.0	10.85	.1045

TABLE A 3

EXPT. NO. = 29
AIR TEMP. (C) = 22.5
DROP TEMP. (C) = 8
MEAN DROP DIA. (mm) = .88
AIR VELOCITY (m/s) = .62
REYNOLDS NO. = 36.21
NUSSELT NO. (EXP) = 6.505
NUSSELT NO. (CORRECTED) = 5.652
RE↑.5*PR↑.33 = 5.368

<u>TIME(sec)</u>	<u>DEFLECTION(DEG)</u>	<u>WEIGHT(mg)</u>
.0	12.50	.9567
63.0	12.00	.6984
164.0	11.40	.3885
260.0	11.00	.1820
325.0	10.75	.0528

TABLE A 4

EXPT. NO. = 30
AIR TEMP. (C) = 22.5
DROP TEMP. (C) = 8
MEAN DROP DIA. (mm) = .955
AIR VELOCITY (m/s) = .62
REYNOLDS NO. = 39.3
NUSSELT NO. (EXP) = 7.027
NUSSELT NO. (CORRECTED) = 6.212
RE↑.5*PR↑.33 = 5.592

<u>TIME(sec)</u>	<u>DEFLECTION(DEG)</u>	<u>WEIGHT(mg)</u>
.0	13.10	1.2665
91.0	12.40	.9050
154.0	11.90	.6468
211.0	11.50	.4402
295.0	11.00	.1820
393.0	10.75	.0528

TABLE A 5

EXPT. NO. = 31
 AIR TEMP. (C) = 22.5
 DROP TEMP. (C) = 8
 MEAN DROP DIA. (mm) = 1.023
 AIR VELOCITY (m/s) = .525
 REYNOLDS NO. = 35.67
 NUSSELT NO. (EXP) = 6.817
 NUSSELT NO. (CORRECTED) = 6.047
 RE↑.5*PR↑.33 = 5.328

<u>TIME(sec)</u>	<u>DEFLECTION(DEG)</u>	<u>WEIGHT(mg)</u>
.0	14.40	1.9379
100.0	13.40	1.4215
155.0	12.90	1.1632
221.0	12.40	.9050
284.0	11.90	.6468
365.0	11.40	.3885
501.0	10.90	.1303
576.0	10.65	.0012

TABLE A 6

EXPT. NO. = 32
 AIR TEMP. (C) = 22.5
 DROP TEMP. (C) = 8
 MEAN DROP DIA. (mm) = 1.01
 AIR VELOCITY (m/s) = .525
 REYNOLDS NO. = 35.22
 NUSSELT NO. (EXP) = 6.519
 NUSSELT NO. (CORRECTED) = 5.745
 RE↑.5*PR↑.33 = 5.294

<u>TIME(sec)</u>	<u>DEFLECTION(DEG)</u>	<u>WEIGHT(mg)</u>
.0	13.80	1.6280
60.0	13.30	1.3698
94.0	12.90	1.1632
156.0	12.40	.9050
235.0	11.90	.6468
316.0	11.40	.3885
450.0	10.90	.1303
540.0	10.65	.0012

TABLE A 7

EXPT. NO. = 33
 AIR TEMP. (C) = 22.5
 DROP TEMP. (C) = 8
 MEAN DROP DIA. (mm) = 1.007
 AIR VELOCITY (m/s) = .427
 REYNOLDS NO. = 28.54
 NUSSELT NO. (EXP) = 5.635
 NUSSELT NO. (CORRECTED) = 4.881
 RE↑.5*PR↑.33 = 4.766

<u>TIME(sec)</u>	<u>DEFLECTION(DEG)</u>	<u>WEIGHT(mg)</u>
.0	13.55	1.4989
50.0	13.20	1.3182
85.0	12.80	1.1116
156.0	12.30	.8534
246.0	11.80	.5951
340.0	11.30	.3369
495.0	10.80	.0787
573.0	10.70	.0270

TABLE A 8

EXPT. NO. = 34
 AIR TEMP. (C) = 22.5
 DROP TEMP. (C) = 8
 MEAN DROP DIA. (mm) = 1.157
 AIR VELOCITY (m/s) = .427
 REYNOLDS NO. = 32.79
 NUSSELT NO. (EXP) = 6.223
 NUSSELT NO. (CORRECTED) = 5.509
 RE↑.5*PR↑.33 = 5.109

<u>TIME(sec)</u>	<u>DEFLECTION(DEG)</u>	<u>WEIGHT(mg)</u>
.0	14.30	1.8863
52.0	13.80	1.6280
129.0	13.20	1.3182
185.0	12.80	1.1116
254.0	12.30	.8534
334.0	11.80	.5951
436.0	11.30	.3369
555.0	10.80	.0787

TABLE A 9

EXPT. NO. = 35
 AIR TEMP. (C) = 22.5
 DROP TEMP. (C) = 8
 MEAN DROP DIA. (mm) = 1.092
 AIR VELOCITY (m/s) = .326
 REYNOLDS NO. = 23.65
 NUSSELT NO. (EXP) = 5.775
 NUSSELT NO. (CORRECTED) = 5.069
 RE↑.5*PR↑.33 = 4.338

<u>TIME(sec)</u>	<u>DEFLECTION(DEG)</u>	<u>WEIGHT(mg)</u>
.0	14.10	1.7830
64.0	13.60	1.5248
139.0	13.10	1.2665
209.0	12.60	1.0083
300.0	12.00	.6984
380.0	11.60	.4918
485.0	11.10	.2336
626.0	10.70	.0270

TABLE A 10

EXPT. NO. = 36
 AIR TEMP. (C) = 22.5
 DROP TEMP. (C) = 8
 MEAN DROP DIA. (mm) = .833
 AIR VELOCITY (m/s) = .326
 REYNOLDS NO. = 18.04
 NUSSELT NO. (EXP) = 5.537
 NUSSELT NO. (CORRECTED) = 4.735
 RE↑.5*PR↑.33 = 3.789

<u>TIME(sec)</u>	<u>DEFLECTION(DEG)</u>	<u>WEIGHT(mg)</u>
.0	12.50	.9567
53.0	12.10	.7501
136.0	11.60	.4918
265.0	11.10	.2336
365.0	10.80	.0787
400.0	10.70	.0270

TABLE A 11

EXPT. NO. = 37
AIR TEMP. (C) = 21.5
DROP TEMP. (C) = 7.5
MEAN DROP DIA. (mm) = 1.079
AIR VELOCITY (m/s) = .301
REYNOLDS NO. = 21.64
NUSSELT NO. (EXP) = 5.475
NUSSELT NO. (CORRECTED) = 4.773
RE↑.5*PR↑.33 = 4.15

<u>TIME(sec)</u>	<u>DEFLECTION(DEG)</u>	<u>WEIGHT(mg)</u>
.0	13.85	1.6539
69.0	13.35	1.3956
168.0	12.60	1.0083
274.0	12.10	.7501
370.0	11.60	.4918
489.0	11.10	.2336
580.0	10.85	.1045

TABLE A 12

EXPT. NO. = 38
AIR TEMP. (C) = 21.5
DROP TEMP. (C) = 7.5
MEAN DROP DIA. (mm) = 1.057
AIR VELOCITY (m/s) = .301
REYNOLDS NO. = 21.2
NUSSELT NO. (EXP) = 5.322
NUSSELT NO. (CORRECTED) = 4.614
RE↑.5*PR↑.33 = 4.106

<u>TIME(sec)</u>	<u>DEFLECTION(DEG)</u>	<u>WEIGHT(mg)</u>
.0	13.60	1.5248
85.0	13.10	1.2665
165.0	12.60	1.0083
361.0	11.60	.4918
462.0	11.10	.2336
574.0	10.85	.1045

TABLE A 13

EXPT. NO. = 39
AIR TEMP. (C) = 21.5
DROP TEMP. (C) = 7.5
MEAN DROP DIA. (mm) = .948
AIR VELOCITY (m/s) = .259
REYNOLDS NO. = 16.36
NUSSELT NO. (EXP) = 5.014
NUSSELT NO. (CORRECTED) = 4.285
RE↑.5*PR↑.33 = 3.608

<u>TIME(sec)</u>	<u>DEFLECTION(DEG)</u>	<u>WEIGHT(mg)</u>
.0	12.80	1.1116
128.0	12.10	.7501
227.0	11.60	.4918
344.0	11.10	.2336
469.0	10.85	.1045

TABLE A 14

EXPT. NO. = 40
AIR TEMP. (C) = 21.5
DROP TEMP. (C) = 7.5
MEAN DROP DIA. (mm) = 1.129
AIR VELOCITY (m/s) = .259
REYNOLDS NO. = 19.47
NUSSELT NO. (EXP) = 5.33
NUSSELT NO. (CORRECTED) = 4.65
RE↑.5*PR↑.33 = 3.937

<u>TIME(sec)</u>	<u>DEFLECTION(DEG)</u>	<u>WEIGHT(mg)</u>
.0	14.50	1.9896
120.0	13.60	1.5248
208.0	13.10	1.2665
302.0	12.60	1.0083
389.0	12.10	.7501
483.0	11.60	.4918
605.0	11.10	.2336
686.0	10.85	.1045

TABLE A 15

EXPT. NO. = 41
 AIR TEMP. (C) = 21.5
 DROP TEMP. (C) = 7.5
 MEAN DROP DIA. (mm) = 1.025
 AIR VELOCITY (m/s) = .211
 REYNOLDS NO. = 14.41
 NUSSELT NO. (EXP) = 5.019
 NUSSELT NO. (CORRECTED) = 4.33
 RE↑.5*PR↑.33 = 3.386

<u>TIME(sec)</u>	<u>DEFLECTION(DEG)</u>	<u>WEIGHT(mg)</u>
.0	13.50	1.4731
78.0	13.00	1.2149
155.0	12.50	.9567
261.0	12.00	.6984
370.0	11.50	.4402
502.0	11.00	.1820
626.0	10.75	.0528

TABLE A 16

EXPT. NO. = 42
 AIR TEMP. (C) = 21.5
 DROP TEMP. (C) = 7.5
 MEAN DROP DIA. (mm) = 1.025
 AIR VELOCITY (m/s) = .211
 REYNOLDS NO. = 14.41
 NUSSELT NO. (EXP) = 5.034
 NUSSELT NO. (CORRECTED) = 4.345
 RE↑.5*PR↑.33 = 3.386

<u>TIME(sec)</u>	<u>DEFLECTION(DEG)</u>	<u>WEIGHT(mg)</u>
.0	13.50	1.4731
82.0	13.00	1.2149
165.0	12.50	.9567
265.0	12.00	.6984
375.0	11.50	.4402
503.0	11.00	.1820
628.0	10.75	.0528

TABLE A 17

EXPT. NO. = 43
 AIR TEMP. (C) = 21.5
 DROP TEMP. (C) = 7.5
 MEAN DROP DIA. (mm) = 1.025
 AIR VELOCITY (m/s) = .165
 REYNOLDS NO. = 11.33
 NUSSELT NO. (EXP) = 4.551
 NUSSELT NO. (CORRECTED) = 3.88
 RE↑.5*PR↑.33 = 3.003

<u>TIME(sec)</u>	<u>DEFLECTION(DEG)</u>	<u>WEIGHT(mg)</u>
.0	13.50	1.4731
104.0	13.00	1.2149
197.0	12.50	.9567
307.0	12.00	.6984
425.0	11.50	.4402
576.0	11.00	.1820
694.0	10.75	.0528

TABLE A 18

EXPT. NO. = 44
 AIR TEMP. (C) = 19.5
 DROP TEMP. (C) = 8
 MEAN DROP DIA. (mm) = 1.155
 AIR VELOCITY (m/s) = .253
 REYNOLDS NO. = 19.62
 NUSSELT NO. (EXP) = 5.36
 NUSSELT NO. (CORRECTED) = 4.686
 RE↑.5*PR↑.33 = 3.952

<u>TIME(sec)</u>	<u>DEFLECTION(DEG)</u>	<u>WEIGHT(mg)</u>
.0	14.20	1.8346
89.0	13.70	1.5764
181.0	13.20	1.3182
280.0	12.70	1.0599
375.0	12.20	.8017
499.0	11.70	.5435
635.0	11.20	.2853
760.0	10.95	.1561

TABLE A 19

EXPT. NO. = 45
 AIR TEMP. (C) = 19.5
 DROP TEMP. (C) = 8
 MEAN DROP DIA. (mm) = 1.204
 AIR VELOCITY (m/s) = .253
 REYNOLDS NO. = 28.45
 NUSSELT NO. (EXP) = 5.795
 NUSSELT NO. (CORRECTED) = 5.13
 RE↑.5*PR↑.33 = 4.835

<u>TIME(sec)</u>	<u>DEFLECTION(DEG)</u>	<u>WEIGHT(mg)</u>
.0	14.90	2.1962
140.0	14.20	1.8346
231.0	13.60	1.5248
305.0	13.20	1.3182
413.0	12.70	1.0599
483.0	12.20	.8017
605.0	11.70	.5435
739.0	11.20	.2853
800.0	10.95	.1561

TABLE A 20

EXPT. NO. = 46
 AIR TEMP. (C) = 19.5
 DROP TEMP. (C) = 8
 MEAN DROP DIA. (mm) = 1.105
 AIR VELOCITY (m/s) = .253
 REYNOLDS NO. = 18.77
 NUSSELT NO. (EXP) = 5.204
 NUSSELT NO. (CORRECTED) = 4.521
 RE↑.5*PR↑.33 = 3.866

<u>TIME(sec)</u>	<u>DEFLECTION(DEG)</u>	<u>WEIGHT(mg)</u>
.0	13.80	1.6280
120.0	13.20	1.3182
221.0	12.70	1.0599
330.0	12.20	.8017
460.0	11.70	.5435
600.0	11.20	.2853
695.0	10.95	.1561

TABLE A 21

EXPT. NO. = 47
 AIR TEMP. (C) = 19.5
 DROP TEMP. (C) = 8
 MEAN DROP DIA. (mm) = 1.155
 AIR VELOCITY (m/s) = .253
 REYNOLDS NO. = 19.62
 NUSSELT NO. (EXP) = 4.968
 NUSSELT NO. (CORRECTED) = 4.295
 RE↑.5*PR↑.33 = 3.952

<u>TIME(sec)</u>	<u>DEFLECTION(DEG)</u>	<u>WEIGHT(mg)</u>
.0	14.20	1.8346
165.0	13.70	1.5764
194.0	13.20	1.3182
300.0	12.70	1.0599
420.0	12.20	.8017
535.0	11.70	.5435
720.0	11.20	.2853
830.0	10.95	.1561

TABLE A 22

EXPT. NO. = 48
 AIR TEMP. (C) = 19.5
 DROP TEMP. (C) = 8
 MEAN DROP DIA. (mm) = 1.155
 AIR VELOCITY (m/s) = .332
 REYNOLDS NO. = 25.71
 NUSSELT NO. (EXP) = 5.758
 NUSSELT NO. (CORRECTED) = 5.065
 RE↑.5*PR↑.33 = 4.523

<u>TIME(sec)</u>	<u>DEFLECTION(DEG)</u>	<u>WEIGHT(mg)</u>
.0	14.20	1.8346
81.0	13.70	1.5764
177.0	13.20	1.3182
266.0	12.70	1.0599
375.0	12.20	.8017
485.0	11.70	.5435
607.0	11.20	.2853
690.0	10.95	.1561

TABLE A 23

EXPT. NO. = 49
AIR TEMP. (C) = 19.5
DROP TEMP. (C) = 8
MEAN DROP DIA. (mm) = 1.155
AIR VELOCITY (m/s) = .332
REYNOLDS NO. = 25.71
NUSSELT NO. (EXP) = 5.685
NUSSELT NO. (CORRECTED) = 4.993
RE↑.5*PR↑.33 = 4.523

<u>TIME(sec)</u>	<u>DEFLECTION(DEG)</u>	<u>WEIGHT(mg)</u>
.0	14.20	1.8346
90.0	13.70	1.5764
180.0	13.20	1.3182
270.0	12.70	1.0599
380.0	12.20	.8017
495.0	11.70	.5435
615.0	11.20	.2853
703.0	10.95	.1561

TABLE A 24

EXPT. NO. = 50
AIR TEMP. (C) = 20
DROP TEMP. (C) = 8.5
MEAN DROP DIA. (mm) = 1.078
AIR VELOCITY (m/s) = .184
REYNOLDS NO. = 13.26
NUSSELT NO. (EXP) = 4.589
NUSSELT NO. (CORRECTED) = 3.923
RE↑.5*PR↑.33 = 3.249

<u>TIME(sec)</u>	<u>DEFLECTION(DEG)</u>	<u>WEIGHT(mg)</u>
.0	14.00	1.7313
85.0	13.50	1.4731
225.0	13.00	1.2149
335.0	12.50	.9567
470.0	12.00	.6984
670.0	11.40	.3885
795.0	11.00	.1820
915.0	10.75	.0528

TABLE A 25

EXPT. NO. = 51
 AIR TEMP. (C) = 20
 DROP TEMP. (C) = 8.5
 MEAN DROP DIA. (mm) = 1.083
 AIR VELOCITY (m/s) = .184
 REYNOLDS NO. = 13.32
 NUSSELT NO. (EXP) = 4.62
 NUSSELT NO. (CORRECTED) = 3.955
 RE↑.5*PR↑.33 = 3.256

<u>TIME(sec)</u>	<u>DEFLECTION(DEG)</u>	<u>WEIGHT(mg)</u>
.0	14.00	1.7313
95.0	13.50	1.4731
225.0	13.00	1.2149
330.0	12.50	.9567
470.0	12.00	.6984
629.0	11.50	.4402
792.0	11.00	.1820
918.0	10.75	.0528

TABLE A 26

EXPT. NO. = 52
 AIR TEMP. (C) = 20
 DROP TEMP. (C) = 8.5
 MEAN DROP DIA. (mm) = 1.083
 AIR VELOCITY (m/s) = .124
 REYNOLDS NO. = 8.97
 NUSSELT NO. (EXP) = 4.333
 NUSSELT NO. (CORRECTED) = 3.695
 RE↑.5*PR↑.33 = 2.673

<u>TIME(sec)</u>	<u>DEFLECTION(DEG)</u>	<u>WEIGHT(mg)</u>
.0	14.00	1.7313
103.0	13.50	1.4731
220.0	13.00	1.2149
355.0	12.50	.9567
500.0	12.00	.6984
665.0	11.50	.4402
855.0	11.00	.1820
965.0	10.75	.0528

TABLE A 27

EXPT. NO. = 53
 AIR TEMP. (C) = 20
 DROP TEMP. (C) = 0.5
 MEAN DROP DIA. (mm) = 1.083
 AIR VELOCITY (m/s) = .124
 REYNOLDS NO. = 8.97
 NUSSELT NO. (EXP) = 4.278
 NUSSELT NO. (CORRECTED) = 3.64
 RE↑.5*PR↑.33 = 2.673

<u>TIME(sec)</u>	<u>DEFLECTION(DEG)</u>	<u>WEIGHT(mg)</u>
.0	14.00	1.7313
120.0	13.50	1.4731
253.0	13.00	1.2149
396.0	12.50	.9567
540.0	12.00	.6984
695.0	11.50	.4402
876.0	11.00	.1820
989.0	10.75	.0528

TABLE A 28

EXPT. NO. = 54
 AIR TEMP. (C) = 20
 DROP TEMP. (C) = 0.5
 MEAN DROP DIA. (mm) = 1.08
 AIR VELOCITY (m/s) = .085
 REYNOLDS NO. = 6.11
 NUSSELT NO. (EXP) = 3.999
 NUSSELT NO. (CORRECTED) = 3.386
 RE↑.5*PR↑.33 = 2.205

<u>TIME(sec)</u>	<u>DEFLECTION(DEG)</u>	<u>WEIGHT(mg)</u>
.0	14.00	1.7313
125.0	13.50	1.4731
280.0	13.00	1.2149
445.0	12.40	.9050
583.0	12.00	.6984
725.0	11.50	.4402
943.0	11.00	.1820
1060.0	10.75	.0528

TABLE A 29

EXPT. NO. = 55
 AIR TEMP. (C) = 20
 DROP TEMP. (C) = 8.5
 MEAN DROP DIA. (mm) = 1.083
 AIR VELOCITY (m/s) = .085
 REYNOLDS NO. = 6.13
 NUSSELT NO. (EXP) = 3.973
 NUSSELT NO. (CORRECTED) = 3.36
 RE↑.5*PR↑.33 = 2.208

<u>TIME(sec)</u>	<u>DEFLECTION(DEG)</u>	<u>WEIGHT(mg)</u>
.0	14.00	1.7313
130.0	13.50	1.4731
250.0	13.00	1.2149
407.0	12.50	.9567
585.0	12.00	.6984
736.0	11.50	.4402
950.0	11.00	.1820
1050.0	10.75	.0528

TABLE A 30

EXPT. NO. = 56
 AIR TEMP. (C) = 20
 DROP TEMP. (C) = 8.5
 MEAN DROP DIA. (mm) = 1.083
 AIR VELOCITY (m/s) = .045
 REYNOLDS NO. = 3.28
 NUSSELT NO. (EXP) = 3.726
 NUSSELT NO. (CORRECTED) = 3.15
 RE↑.5*PR↑.33 = 1.615

<u>TIME(sec)</u>	<u>DEFLECTION(DEG)</u>	<u>WEIGHT(mg)</u>
.0	14.00	1.7313
150.0	13.50	1.4731
304.0	13.00	1.2149
450.0	12.50	.9567
645.0	12.00	.6984
813.0	11.50	.4402
1010.0	11.00	.1820
1135.0	10.75	.0528

TABLE A 31

EXPT. NO. = 57
 AIR TEMP. (C) = 20
 DROP TEMP. (C) = 8.5
 MEAN DROP DIA. (mm) = 1.083
 AIR VELOCITY (m/s) = .045
 REYNOLDS NO. = 3.28
 NUSSELT NO. (EXP) = 3.736
 NUSSELT NO. (CORRECTED) = 3.16
 RE↑.5*PR↑.33 = 1.615

<u>TIME(sec)</u>	<u>DEFLECTION(DEG)</u>	<u>WEIGHT(mg)</u>
.0	14.00	1.7313
153.0	13.50	1.4731
300.0	13.00	1.2149
446.0	12.50	.9567
650.0	12.00	.6984
800.0	11.50	.4402
1015.0	11.00	.1820
1130.0	10.75	.0528

TABLE A 32

EXPT. NO. = 58
 AIR TEMP. (C) = 20
 DROP TEMP. (C) = 8.5
 MEAN DROP DIA. (mm) = 1.08
 AIR VELOCITY (m/s) = .026
 REYNOLDS NO. = 1.85
 NUSSELT NO. (EXP) = 3.459
 NUSSELT NO. (CORRECTED) = 2.913
 RE↑.5*PR↑.33 = 1.214

<u>TIME(sec)</u>	<u>DEFLECTION(DEG)</u>	<u>WEIGHT(mg)</u>
.0	14.00	1.7313
140.0	13.50	1.4731
360.0	12.90	1.1632
480.0	12.50	.9567
660.0	12.00	.6984
854.0	11.50	.4402
1077.0	11.00	.1820
1230.0	10.75	.0528

TABLE A 33

EXPT. NO. = 59
 AIR TEMP. (C) = 19.6
 DROP TEMP. (C) = 8
 MEAN DROP DIA. (mm) = 1.08
 AIR VELOCITY (m/s) = .026
 REYNOLDS NO. = 1.85
 NUSSELT NO. (EXP) = 3.402
 NUSSELT NO. (CORRECTED) = 2.857
 RE↑.5*PR↑.33 = 1.214

<u>TIME(sec)</u>	<u>DEFLECTION(DEG)</u>	<u>WEIGHT(mg)</u>
.0	14.00	1.7313
145.0	13.50	1.4731
380.0	12.90	1.1632
495.0	12.50	.9567
680.0	12.00	.6984
870.0	11.50	.4402
1090.0	11.00	.1820
1245.0	10.75	.0528

TABLE A 34

EXPT. NO. = 70
 AIR TEMP. (C) = 22
 DROP TEMP. (C) = 8
 MEAN DROP DIA. (mm) = 1.139
 AIR VELOCITY (m/s) = .765
 REYNOLDS NO. = 57.91
 NUSSELT NO. (EXP) = 6.708
 NUSSELT NO. (CORRECTED) = 5.935
 RE↑.5*PR↑.33 = 6.789

<u>TIME(sec)</u>	<u>DEFLECTION(DEG)</u>	<u>WEIGHT(mg)</u>
.0	13.95	1.7055
50.0	13.45	1.4473
110.0	12.95	1.1891
150.0	12.70	1.0599
205.0	12.20	.8017
275.0	11.70	.5435
390.0	11.20	.2853
460.0	10.95	.1561

TABLE A 35

EXPT. NO. = 71
AIR TEMP. (C) = 23.5
DROP TEMP. (C) = 8
MEAN DROP DIA. (mm) = 1.139
AIR VELOCITY (m/s) = .772
REYNOLDS NO. = 58.15
NUSSELT NO. (EXP) = 6.456
NUSSELT NO. (CORRECTED) = 5.681
RE↑.5*PR↑.33 = 6.883

<u>TIME(sec)</u>	<u>DEFLECTION(DEG)</u>	<u>WEIGHT(mg)</u>
.0	13.95	1.7055
49.0	13.45	1.4473
95.0	12.95	1.1891
140.0	12.70	1.0599
180.0	12.20	.8017
255.0	11.70	.5435
360.0	11.20	.2853
432.0	10.95	.1561

A.4.2 Water Drops at Elevated Temperatures

Tables A36 to A39

TABLE A 36

UNITS

TIME = s
 DIAMETER = mm
 AIR VELOCITY = m/s
 AIR AND DROP TEMP. = C
 NUSSELT EQUATION = $2 + .58 RE^{.5} PR^{.33}$
 CORRELATION COEFF. = .968

EXPT NO. 72 AIR TEMP. 34 DROP TEMP. 13

TIME	DIA.	AIR VEL.	REY NO.	NU (EXP)	NU	RE ^{.5} PR ^{.33}
.0	1.444	.769	69.05	7.166	6.435	7.430
35.0	1.360	.769	65.05	7.053	6.314	7.212
75.0	1.265	.769	60.49	6.826	6.075	6.955
122.0	1.153	.769	55.11	6.713	5.940	6.638
165.0	1.013	.769	48.42	6.471	5.656	6.222
240.0	.817	.769	39.05	6.226	5.311	5.588

EXPT NO. 73 AIR TEMP. 33.5 DROP TEMP. 12

TIME	DIA.	AIR VEL.	REY NO.	NU (EXP)	NU	RE ^{.5} PR ^{.33}
.0	1.404	.768	67.11	6.878	6.145	7.325
60.0	1.265	.768	60.49	6.768	6.017	6.955
104.0	1.153	.768	55.11	6.546	5.773	6.638
155.0	1.013	.768	48.42	6.227	5.413	6.222
235.0	.817	.768	39.05	6.083	5.168	5.588

UNITS

TIME = s
 DIAMETER = mm
 AIR VELOCITY = m/s
 AIR AND DROP TEMP. = C
 NUSSELT EQUATION = $2 + .56 RE^{.5} PR^{.33}$
 CORRELATION COEFF. = .983

EXPT NO. 68 AIR TEMP. 46.25 DROP TEMP. 17.5

TIME	DIA.	AIR VEL.	REY NO.	NU (EXP)	NU	RE ^{.5} PR ^{.33}
.0	1.444	.769	64.66	6.694	5.953	7.207
25.0	1.361	.769	60.92	6.550	5.802	6.995
56.0	1.265	.769	56.65	6.534	5.776	6.746
89.0	1.128	.769	50.48	6.373	5.590	6.368
128.0	.980	.769	43.86	6.121	5.293	5.935
185.0	.817	.769	36.57	6.028	5.119	5.420
215.0	.668	.769	29.92	5.741	4.706	4.902

EXPT NO. 69 AIR TEMP. 46.25 DROP TEMP. 17.5

TIME	DIA.	AIR VEL.	REY NO.	NU (EXP)	NU	RE ^{.5} PR ^{.33}
.0	1.444	.769	64.66	6.751	6.009	7.207
26.0	1.361	.769	60.92	6.614	5.867	6.995
58.0	1.265	.769	56.65	6.510	5.752	6.746
85.0	1.153	.769	51.61	6.373	5.596	6.439
126.0	1.013	.769	45.34	6.201	5.386	6.035
180.0	.817	.769	36.57	6.141	5.231	5.420
210.0	.668	.769	29.92	5.829	4.794	4.902

TABLE A 38

UNITS

TIME = s
 DIAMETER = mm
 AIR VELOCITY = m/s
 AIR AND DROP TEMP. = C
 NUSSELT EQUATION = $2 + .504 RE^{.5} PR^{.33}$
 CORRELATION COEFF. = .963

EXPT NO. 77		AIR TEMP. 63		DROP TEMP. 21.5		
TIME	DIA.	AIR VEL.	REY NO.	NU (EXP)	NU	RE ^{.5} PR ^{.33}
.0	1.520	.787	64.44	6.515	5.757	7.212
23.0	1.445	.787	61.27	6.487	5.649	7.032
50.0	1.266	.787	53.67	6.192	5.421	6.582
90.0	1.088	.787	46.12	5.922	5.122	6.101
125.0	.925	.787	39.25	5.375	4.522	5.628
180.0	.668	.787	28.35	5.257	4.229	4.783

EXPT NO. 78		AIR TEMP. 63		DROP TEMP. 21.5		
TIME	DIA.	AIR VEL.	REY NO.	NU (EXP)	NU	RE ^{.5} PR ^{.33}
.0	1.483	.787	62.90	6.515	5.757	7.125
26.0	1.361	.787	57.72	6.353	5.591	6.825
45.0	1.266	.787	53.67	6.138	5.368	6.582
73.0	1.153	.787	48.90	6.030	5.244	6.282
95.0	1.013	.787	42.96	5.761	4.940	5.888
125.0	.817	.787	34.65	5.599	4.691	5.288
160.0	.668	.787	28.35	5.362	4.334	4.783

TABLE A 39

UNITS

TIME = s
 DIAMETER = mm
 AIR VELOCITY = m/s
 AIR AND DROP TEMP. = C

 NUSSELT EQUATION = $2 + .45 RE^{.5} PR^{.33}$
 CORRELATION COEFF. = .964

EXPT NO. 64 AIR TEMP. 79 DROP TEMP. 25.5

TIME	DIA.	AIR VEL.	REY NO.	NU (EXP)	NU	RE ^{.5} *PR ^{.33}
.0	1.461	.744	54.53	6.020	5.250	6.649
25.0	1.334	.744	49.81	5.664	4.891	6.355
45.0	1.178	.744	43.97	5.616	4.829	5.971
70.0	1.045	.744	38.99	5.320	4.509	5.622
95.0	.864	.744	32.26	5.211	4.337	5.114
140.0	.532	.744	19.86	4.815	3.628	4.013

EXPT NO. 66 AIR TEMP. 78 DROP TEMP. 25

TIME	DIA.	AIR VEL.	REY NO.	NU (EXP)	NU	RE ^{.5} *PR ^{.33}
.0	1.445	.799	58.05	6.019	5.244	6.860
30.0	1.266	.799	50.85	5.691	4.909	6.421
55.0	1.154	.799	46.33	5.609	4.814	6.129
83.0	.926	.799	37.18	5.404	4.549	5.491
110.0	.669	.799	26.86	5.159	4.138	4.666
140.0	.373	.799	14.97	4.913	3.300	3.483

APPENDIX B

B.1 TABULATION OF RESULTS FOR THE DRYING
 OF DROPS OF AQUEOUS SODIUM SULPHATE
 DECAHYDRATE

APPENDIX B

B.1 TABULATION OF RESULTS FOR THE DRYING OF
DROPS OF AQUEOUS SODIUM SULPHATE DECAHYDRATE

<u>Tables</u>	<u>Initial Conc. (wt.%)</u>	<u>Air Temp (°C)</u>
B1-B4	5	18 - 20.5
B 5	5	40
B 6	5	66.5
B 7	5	110
B8-B11	15	19.5 - 22
B12	15	40
B13, B14	15	60
B15, B16	15	90
B17	30.3	19.5
B18	54.1	20
B19	54.1	20

TABLE B 1

EXPERIMENT NUMBER = Y3
 AQ. SOD. SULPH. DECAHYD. (WT %) = 5
 AIR TEMPERATURE (C) = 18
 AIR VELOCITY (m/s) = .5

<u>TIME(sec)</u>	<u>ACTUAL WT. (mg)</u>	<u>CORRECTED WT. (mg)</u>	<u>FRACT. OF INITIAL WT. EVAPORATED</u>
.0	1.859	1.859	.000
55.0	1.623	1.631	.123
100.0	1.446	1.452	.213
155.0	1.210	1.218	.345
205.0	1.033	1.040	.441
283.0	.756	.766	.588
350.0	.580	.588	.684
425.0	.360	.369	.802
500.0	.228	.235	.874
560.0	.150	.155	.917
630.0	.114	.119	.936
765.0	.100	.105	.943
964.0	.090	.092	.950

TABLE B 2

EXPERIMENT NUMBER = Y6
 AQ. SOD. SULPH. DECAHYD. (WT %) = 5
 AIR TEMPERATURE (C) = 20.5
 AIR VELOCITY (m/s) = 1.53

<u>TIME(sec)</u>	<u>ACTUAL WT. (mg)</u>	<u>CORRECTED WT. (mg)</u>	<u>FRACT. OF INITIAL WT. EVAPORATED</u>
.0	2.125	2.125	.000
160.0	1.251	1.280	.398
360.0	.300	.331	.844
500.0	.170	.188	.912
760.0	.136	.162	.924
1020.0	.120	.139	.934

TABLE B 3

EXPERIMENT NUMBER = Y10
 AQ. SOD. SULPH. DECAHYD. (WT %) = 5
 AIR TEMPERATURE (C) = 19.5
 AIR VELOCITY (m/s) = 2.92

<u>TIME(sec)</u>	<u>ACTUAL WT. (mg)</u>	<u>CORRECTED WT. (mg)</u>	<u>FRACT. OF INITIAL WT. EVAPORATED</u>
.0	2.202	2.202	.000
120.0	1.281	1.304	.408
215.0	.676	.693	.685
370.0	.192	.212	.904
540.0	.128	.142	.936
720.0	.114	.121	.945
900.0	.104	.107	.951

TABLE B 4

EXPERIMENT NUMBER = Y19
 AQ. SOD. SULPH. DECAHYD. (WT %) = 5
 AIR TEMPERATURE (C) = 20
 AIR VELOCITY (m/s) = 1.085

<u>TIME(sec)</u>	<u>ACTUAL WT. (mg)</u>	<u>CORRECTED WT. (mg)</u>	<u>FRACT. OF INITIAL WT. EVAPORATED</u>
.0	2.880	2.880	.000
30.0	2.597	2.603	.096
90.0	2.184	2.195	.238
150.0	1.771	1.782	.381
240.0	1.181	1.196	.585
360.0	.600	.619	.785
480.0	.228	.243	.916
660.0	.200	.214	.926
840.0	.170	.178	.938
1080.0	.127	.130	.955

TABLE B 5

EXPERIMENT NUMBER = Y39
 AQ. SOD. SULPH. DECAHYD. (WT %) = 5
 AIR TEMPERATURE (C) = 40
 AIR VELOCITY (m/s) = 1.08

<u>TIME(sec)</u>	<u>ACTUAL WT. (mg)</u>	<u>CORRECTED WT. (mg)</u>	<u>FRACT. OF INITIAL WT. EVAPORATED</u>
.0	3.211	3.211	.000
45.0	2.656	2.677	.166
90.0	2.078	2.098	.347
150.0	1.428	1.454	.547
210.0	.826	.849	.735
270.0	.420	.441	.863
330.0	.240	.266	.917
510.0	.216	.229	.929
630.0	.170	.173	.946

TABLE B 6

EXPERIMENT NUMBER = Y13
 AQ. SOD. SULPH. DECAHYD. (WT %) = 5
 AIR TEMPERATURE (C) = 66.5
 AIR VELOCITY (m/s) = 1.098

<u>TIME(sec)</u>	<u>ACTUAL WT. (mg)</u>	<u>CORRECTED WT. (mg)</u>	<u>FRACT. OF INITIAL WT. EVAPORATED</u>
.0	2.361	2.361	.000
60.0	1.299	1.353	.427
120.0	.520	.566	.760
180.0	.208	.248	.895
240.0	.170	.198	.916
300.0	.136	.156	.934
360.0	.120	.132	.944
660.0	.120	.120	.949

TABLE B 7

EXPERIMENT NUMBER = Y14
 AQ. SOD. SULPH. DECAHYD. (WT %) = 5
 AIR TEMPERATURE (C) = 110
 AIR VELOCITY (m/s) = 1.087

<u>TIME(sec)</u>	<u>ACTUAL WT. (mg)</u>	<u>CORRECTED WT. (mg)</u>	<u>FRACT. OF INITIAL WT. EVAPORATED</u>
.0	2.892	2.892	.000
30.0	1.712	1.770	.388
60.0	.542	.589	.796
90.0	.252	.290	.900
120.0	.144	.169	.941
150.0	.110	.123	.957
180.0	.097	.102	.965
300.0	.092	.092	.968

TABLE B 8

EXPERIMENT NUMBER = Y20
 AQ. SOD. SULPH. DECAHYD. (WT %) = 15
 AIR TEMPERATURE (C) = 19.5
 AIR VELOCITY (m/s) = .502

<u>TIME(sec)</u>	<u>ACTUAL WT. (mg)</u>	<u>CORRECTED WT. (mg)</u>	<u>FRACT. OF INITIAL WT. EVAPORATED</u>
.0	2.739	2.739	.000
30.0	2.479	2.484	.093
60.0	2.302	2.307	.158
90.0	2.148	2.153	.214
120.0	1.948	1.952	.287
150.0	1.771	1.775	.352
180.0	1.594	1.598	.416
240.0	1.299	1.307	.523
300.0	1.015	1.023	.626
360.0	.816	.824	.699
420.0	.622	.628	.771
510.0	.336	.338	.876
600.0	.252	.252	.908
720.0	.252	.252	.908

TABLE B 9

EXPERIMENT NUMBER = Y22
 AQ. SOD. SULPH. DECAHYD. (WT %) = 15
 AIR TEMPERATURE (C) = 22
 AIR VELOCITY (m/s) = 1.08

<u>TIME(sec)</u>	<u>ACTUAL WT. (mg)</u>	<u>CORRECTED WT. (mg)</u>	<u>FRACT. OF INITIAL WT. EVAPORATED</u>
.0	3.116	3.116	.000
45.0	2.656	2.667	.144
90.0	2.243	2.253	.277
135.0	1.901	1.911	.387
180.0	1.535	1.544	.504
240.0	1.157	1.169	.625
300.0	.784	.794	.745
360.0	.712	.719	.769
450.0	.700	.708	.773
600.0	.680	.682	.781
765.0	.468	.468	.850

TABLE B 10

EXPERIMENT NUMBER = Y23
 AQ. SOD. SULPH. DECAHYD. (WT %) = 15
 AIR TEMPERATURE (C) = 22
 AIR VELOCITY (m/s) = 1.08

<u>TIME(sec)</u>	<u>ACTUAL WT. (mg)</u>	<u>CORRECTED WT. (mg)</u>	<u>FRACT. OF INITIAL WT. EVAPORATED</u>
.0	2.597	2.597	.000
45.0	2.219	2.230	.141
90.0	1.859	1.869	.280
150.0	1.417	1.429	.450
210.0	1.027	1.039	.600
300.0	.602	.613	.764
420.0	.232	.239	.908
585.0	.232	.232	.911

TABLE B 11

EXPERIMENT NUMBER = Y24
AQ. SOD. SULPH. DECAHYD. (WT %) = 15
AIR TEMPERATURE (C) = 22
AIR VELOCITY (m/s) = 3

<u>TIME(sec)</u>	<u>ACTUAL WT. (mg)</u>	<u>CORRECTED WT. (mg)</u>	<u>FRACT. OF INITIAL WT. EVAPORATED</u>
.0	3.211	3.211	.000
45.0	2.715	2.727	.151
90.0	2.196	2.207	.312
135.0	1.724	1.735	.460
180.0	1.322	1.333	.585
240.0	.945	.956	.702
300.0	.820	.827	.743
405.0	.468	.476	.852
525.0	.288	.290	.910
780.0	.288	.288	.910

TABLE B 12

EXPERIMENT NUMBER = Y35
AQ. SOD. SULPH. DECAHYD. (WT %) = 15
AIR TEMPERATURE (C) = 40
AIR VELOCITY (m/s) = 1.08

<u>TIME(sec)</u>	<u>ACTUAL WT. (mg)</u>	<u>CORRECTED WT. (mg)</u>	<u>FRACT. OF INITIAL WT. EVAPORATED</u>
.0	3.069	3.069	.000
45.0	2.508	2.526	.177
90.0	2.007	2.023	.341
135.0	1.446	1.462	.524
180.0	1.033	1.044	.660
240.0	.704	.712	.768
300.0	.340	.342	.889
390.0	.318	.318	.896

TABLE B 13

EXPERIMENT NUMBER = 433
 AQ. SOD. SULPH. DECAHYD. (WT %) = 15
 AIR TEMPERATURE (C) = 60
 AIR VELOCITY (m/s) = 1.08

<u>TIME(sec)</u>	<u>ACTUAL WT. (mg)</u>	<u>CORRECTED WT. (mg)</u>	<u>FRACT. OF INITIAL WT. EVAPORATED</u>
.0	3.600	3.600	.000
45.0	2.833	2.870	.203
90.0	2.066	2.100	.417
135.0	1.476	1.507	.581
180.0	.897	.918	.745
240.0	.542	.561	.844
360.0	.388	.408	.887
480.0	.370	.370	.897

TABLE B 14

EXPERIMENT NUMBER = 434
 AQ. SOD. SULPH. DECAHYD. (WT %) = 15
 AIR TEMPERATURE (C) = 60
 AIR VELOCITY (m/s) = 1.08

<u>TIME(sec)</u>	<u>ACTUAL WT. (mg)</u>	<u>CORRECTED WT. (mg)</u>	<u>FRACT. OF INITIAL WT. EVAPORATED</u>
.0	3.305	3.305	.000
45.0	2.508	2.544	.230
90.0	1.712	1.745	.472
135.0	1.074	1.104	.666
180.0	.886	.905	.726
240.0	.826	.846	.744
300.0	.816	.829	.749
350.0	.784	.789	.761
540.0	.760	.760	.770

TABLE B 15

EXPERIMENT NUMBER = Y25
AQ. SOD. SULPH. DECAHYD. (WT %) = 15
AIR TEMPERATURE (C) = 90
AIR VELOCITY (m/s) = 1.08

<u>TIME(sec)</u>	<u>ACTUAL WT. (mg)</u>	<u>CORRECTED WT. (mg)</u>	<u>FRACT. OF INITIAL WT. EVAPORATED</u>
.0	2.833	2.833	.000
45.0	1.594	1.653	.416
90.0	.704	.743	.738
135.0	.528	.556	.804
210.0	.420	.452	.840
300.0	.336	.358	.874
390.0	.300	.309	.891
540.0	.300	.300	.894

TABLE B 16

EXPERIMENT NUMBER = Y26
AQ. SOD. SULPH. DECAHYD. (WT %) = 15
AIR TEMPERATURE (C) = 90
AIR VELOCITY (m/s) = 1.08

<u>TIME(sec)</u>	<u>ACTUAL WT. (mg)</u>	<u>CORRECTED WT. (mg)</u>	<u>FRACT. OF INITIAL WT. EVAPORATED</u>
.0	2.916	2.916	.000
45.0	1.653	1.713	.413
75.0	.897	.924	.683
105.0	.756	.776	.734
135.0	.728	.742	.746
195.0	.712	.728	.750
300.0	.622	.634	.783
560.0	.336	.336	.885

TABLE B 17

EXPERIMENT NUMBER = 840
 AQ. SOD. SULPH. DECAHYD. (WT %) = 30.3
 AIR TEMPERATURE (C) = 19.5
 AIR VELOCITY (m/s) = 1.08

<u>TIME(sec)</u>	<u>ACTUAL WT. (mg)</u>	<u>CORRECTED WT. (mg)</u>	<u>FRACT. OF INITIAL WT. EVAPORATED</u>
.0	2.762	2.762	.000
45.0	2.479	2.483	.101
90.0	2.190	2.194	.206
165.0	1.800	1.807	.346
210.0	1.546	1.550	.439
270.0	1.275	1.280	.537
330.0	1.039	1.043	.622
420.0	.704	.707	.744
510.0	.484	.485	.824
600.0	.478	.479	.827
705.0	.478	.478	.827

TABLE B 18

EXPERIMENT NUMBER = 841
 AQ. SOD. SULPH. DECAHYD. (WT %) = 54.1
 AIR TEMPERATURE (C) = 20
 AIR VELOCITY (m/s) = 1.08

<u>TIME(sec)</u>	<u>ACTUAL WT. (mg)</u>	<u>CORRECTED WT. (mg)</u>	<u>FRACT. OF INITIAL WT. EVAPORATED</u>
.0	3.376	3.376	.000
45.0	3.081	3.085	.086
90.0	2.845	2.848	.156
135.0	2.591	2.595	.231
180.0	2.444	2.447	.275
270.0	2.361	2.366	.299
420.0	2.266	2.272	.327
600.0	2.207	2.211	.345
870.0	2.184	2.184	.353
1080.0	2.154	2.154	.362

TABLE B 19

EXPERIMENT NUMBER = S42
AQ. SOD. SULPH. DECAHYD. (WT %) = 54.1
AIR TEMPERATURE (C) = 20
AIR VELOCITY (m/s) = 1.08

<u>TIME(sec)</u>	<u>ACTUAL WT. (mg)</u>	<u>CORRECTED WT. (mg)</u>	<u>FRACT. OF INITIAL WT. EVAPORATED</u>
.0	2.833	2.833	.000
60.0	2.479	2.484	.123
120.0	2.213	2.218	.217
180.0	1.983	1.988	.298
240.0	1.889	1.893	.332
360.0	1.853	1.858	.344
480.0	1.836	1.838	.351
720.0	1.830	1.830	.354
1080.0	1.830	1.830	.354

APPENDIX C

- C.1 TABULATION OF RESULTS FOR THE DRYING OF
DROPS OF SODIUM SULPHATE DECAHYDRATE WITH
AN INITIAL CONCENTRATION OF 40 wt.%
- C.2 TABULATION OF EXPERIMENTAL CORE TEMPERATURE
MEASUREMENTS

APPENDIX C

C.1 TABULATION OF RESULTS FOR THE DRYING OF DROPS
OF SODIUM SULPHATE DECAHYDRATE WITH AN INITIAL
CONCENTRATION OF 40 wt.%.
CONCENTRATION OF 40 wt.%.

<u>Tables</u>	<u>Air Temp (°C)</u>
C1	20
C2	40.7
C3-C5	59.3
C6, C7	78.3

TABLE C 1

EXPERIMENT NUMBER = S47
 AQ. SOD. SULPH. DECAHYD. (WT %) = 40
 AIR TEMPERATURE (C) = 20
 AIR VELOCITY (m/s) = 1

<u>TIME(sec)</u>	<u>ACTUAL WT. (mg)</u>	<u>CORRECTED WT. (mg)</u>	<u>FRACT. OF INITIAL WT. EVAPORATED</u>
.0	3.391	3.391	.000
45.0	2.991	3.025	.108
90.0	2.665	2.698	.204
135.0	2.292	2.323	.315
195.0	1.892	1.930	.431
270.0	1.426	1.463	.569
345.0	1.035	1.066	.685
435.0	.595	.627	.815
555.0	.555	.569	.832
705.0	.555	.555	.836
915.0	.555	.555	.836

TABLE C 2

EXPERIMENT NUMBER = S43
 AQ. SOD. SULPH. DECAHYD. (WT %) = 40
 AIR TEMPERATURE (C) = 40.7
 AIR VELOCITY (m/s) = 1

<u>TIME(sec)</u>	<u>ACTUAL WT. (mg)</u>	<u>CORRECTED WT. (mg)</u>	<u>FRACT. OF INITIAL WT. EVAPORATED</u>
.0	2.958	2.958	.000
45.0	2.425	2.500	.155
90.0	1.919	1.989	.328
135.0	1.439	1.501	.492
195.0	1.070	1.106	.626
270.0	.880	.907	.694
375.0	.685	.699	.764
495.0	.610	.621	.790
675.0	.485	.485	.836

TABLE C 3

EXPERIMENT NUMBER = 844
 AQ. SOD. SULPH. DECAHYD. (WT %) = 40
 AIR TEMPERATURE (C) = 59.3
 AIR VELOCITY (m/s) = 1

<u>TIME(sec)</u>	<u>ACTUAL WT. (mg)</u>	<u>CORRECTED WT. (mg)</u>	<u>FRACT. OF INITIAL WT. EVAPORATED</u>
.0	3.357	3.357	.000
45.0	2.425	2.546	.242
90.0	1.626	1.742	.481
150.0	.762	.901	.732
240.0	.555	.565	.832
390.0	.555	.555	.835

TABLE C 4

EXPERIMENT NUMBER = 845
 AQ. SOD. SULPH. DECAHYD. (WT %) = 40
 AIR TEMPERATURE (C) = 59.3
 AIR VELOCITY (m/s) = 1

<u>TIME(sec)</u>	<u>ACTUAL WT. (mg)</u>	<u>CORRECTED WT. (mg)</u>	<u>FRACT. OF INITIAL WT. EVAPORATED</u>
.0	3.011	3.011	.000
45.0	2.265	2.386	.207
90.0	1.572	1.684	.441
135.0	1.093	1.094	.637
195.0	.565	.566	.812
270.0	.535	.536	.822
390.0	.535	.535	.822

TABLE C 5

EXPERIMENT NUMBER = S46
 AQ. SOD. SULPH. DECAHYD. (WT %) = 40
 AIR TEMPERATURE (C) = 59.3
 AIR VELOCITY (m/s) = 1

<u>TIME(sec)</u>	<u>ACTUAL WT. (mg)</u>	<u>CORRECTED WT. (mg)</u>	<u>FRACT. OF INITIAL WT. EVAPORATED</u>
.0	3.184	3.184	.000
45.0	2.398	2.519	.209
90.0	1.706	1.818	.429
135.0	1.005	1.006	.684
195.0	.560	.561	.824
270.0	.510	.511	.840
390.0	.510	.510	.840

TABLE C 6

EXPERIMENT NUMBER = S48
 AQ. SOD. SULPH. DECAHYD. (WT %) = 40
 AIR TEMPERATURE (C) = 78.3
 AIR VELOCITY (m/s) = 1

<u>TIME(sec)</u>	<u>ACTUAL WT. (mg)</u>	<u>CORRECTED WT. (mg)</u>	<u>FRACT. OF INITIAL WT. EVAPORATED</u>
.0	3.150	3.150	.000
45.0	1.860	2.048	.350
90.0	.770	.944	.700
135.0	.600	.692	.780
195.0	.599	.603	.808
270.0	.598	.598	.810

TABLE C 7

EXPERIMENT NUMBER = S49
 AQ. SOD. SULPH. DECAHYD. (WT %) = 40
 AIR TEMPERATURE (C) = 78.3
 AIR VELOCITY (m/s) = 1

<u>TIME(sec)</u>	<u>ACTUAL WT. (mg)</u>	<u>CORRECTED WT. (mg)</u>	<u>FRACT. OF INITIAL WT. EVAPORATED</u>
.0	3.150	3.150	.000
45.0	1.900	2.088	.337
90.0	.860	1.034	.672
135.0	.660	.752	.761
195.0	.659	.663	.789
270.0	.598	.598	.810

C.2 TABULATION OF EXPERIMENTAL CORE
TEMPERATURE MEASUREMENTS

<u>Tables</u>	<u>Air Temp (°C)</u>
C8	20
C9	40.7
C10	59.3
C11	78.3

TABLE C 8

EXPERIMENTAL CORE TEMPERATURE MEASUREMENTS

EXPERIMENT NUMBER = S47/T49
AQ. SOD. SULPH. DECAHYD. (WT %) = 40
AIR TEMPERATURE (°C) = 20
AIR VELOCITY (m/s) = 1

<u>TIME(sec)</u>	<u>VOLTAGE(mV)</u>	<u>TEMP (°C)</u>
.00	.2769	15.00
12.00	.1292	8.61
24.00	.1231	8.35
36.00	.1215	8.28
48.00	.1218	8.29
60.00	.1238	8.38
72.00	.1246	8.41
96.00	.1269	8.51
120.00	.1385	9.01
150.00	.1462	9.35
180.00	.1508	9.55
210.00	.1631	10.08
240.00	.1908	11.28
270.00	.2154	12.34
300.00	.2308	13.01
330.00	.2400	13.40
360.00	.2477	13.74
390.00	.2538	14.00
420.00	.2615	14.34
450.00	.2692	14.67
480.00	.2777	15.04
510.00	.2938	15.73
540.00	.3231	17.00
570.00	.3538	18.33
600.00	.3800	19.46
612.00	.3924	20.00
636.00	.3924	20.00
660.00	.3924	20.00

TABLE C 9

EXPERIMENTAL CORE TEMPERATURE MEASUREMENTS

EXPERIMENT NUMBER = S43/T53
AQ. SOD. SULPH. DECAHYD. (WT %) = 40
AIR TEMPERATURE (°C) = 40.7
AIR VELOCITY (m/s) = 1

<u>TIME(sec)</u>	<u>VOLTAGE(mV)</u>	<u>TEMP (°C)</u>
.00	.3195	16.84
2.40	.3105	16.46
4.80	.3075	16.33
12.00	.3120	16.52
24.00	.3060	16.26
36.00	.3150	16.65
48.00	.3195	16.84
60.00	.3255	17.10
72.00	.3345	17.49
84.00	.3495	18.14
96.00	.3615	18.66
108.00	.3705	19.05
120.00	.3765	19.31
132.00	.4170	21.06
144.00	.4500	22.49
156.00	.5070	24.96
168.00	.5685	27.62
180.00	.6375	30.60
192.00	.6825	32.55
204.00	.7140	33.91
216.00	.7020	33.40
228.00	.6435	30.86
240.00	.5895	28.53
252.00	.5625	27.36
264.00	.5355	26.19
276.00	.4920	24.31
288.00	.5355	26.19
292.80	.6150	29.63
297.60	.8565	40.08
309.60	.8700	40.66
321.60	.8700	40.66
333.60	.8700	40.66

TABLE C 10

EXPERIMENTAL CORE TEMPERATURE MEASUREMENTS

EXPERIMENT NUMBER = S46/T63
 AQ. SOD. SULPH. DECAHYD. (WT %) = 40
 AIR TEMPERATURE (°C) = 59.3
 AIR VELOCITY (m./s) = 1

<u>TIME(sec)</u>	<u>VOLTAGE(mV)</u>	<u>TEMP (°C)</u>
.00	.3252	17.09
4.80	.3127	16.55
9.60	.3811	19.51
16.80	.4199	21.19
28.80	.4239	21.36
40.80	.4495	22.47
52.80	.4574	22.81
64.80	.4652	23.15
76.80	.4791	23.75
84.00	.4978	24.56
88.80	.5754	27.92
93.60	.5912	28.60
100.80	.6159	29.67
105.60	.6270	30.15
112.80	.6330	30.41
117.60	.6330	30.41
122.40	.5951	28.77
127.20	.5754	27.92
134.40	.5570	27.12
144.00	.5327	26.07
148.80	.5694	27.66
153.60	.8867	41.39
156.00	1.1354	52.99
158.00	1.2833	58.60
160.80	1.2988	59.19
168.00	1.3017	59.30
175.20	1.3017	59.30

TABLE C 11

EXPERIMENTAL CORE TEMPERATURE MEASUREMENTS

EXPERIMENT NUMBER = S48/T72
 AQ. SOD. SULPH. DECAHYD. (WT %) = 40
 AIR TEMPERATURE (°C) = 78.3
 AIR VELOCITY (m/s) = 1

<u>TIME(sec)</u>	<u>VOLTAGE(mV)</u>	<u>TEMP (°C)</u>
.00	.3300	17.30
2.40	.3126	16.55
4.80	.3126	16.55
9.60	.3107	16.46
12.00	.4737	23.52
16.80	.5457	26.63
21.60	.5872	28.43
28.80	.6138	29.58
33.60	.6120	29.50
38.40	.5969	28.85
45.60	.5648	27.46
57.60	.6707	32.04
69.60	.7086	33.68
81.60	.7996	37.62
93.60	.8886	41.47
105.60	.8867	41.39
117.60	.9531	44.26
122.40	.9796	45.41
124.80	1.1368	53.04
127.20	1.6295	71.74
129.60	1.7924	77.92
132.00	1.7987	78.16
136.80	1.8024	78.30
148.80	1.8024	78.30
160.80	1.8024	78.30

APPENDIX D

- D.1 VARIABLES USED IN MODEL
- D.2 COMPUTER PROGRAM LISTINGS
Program Filename: REI MODEL
- D.3 TABULATION OF MODEL PREDICTIONS

APPENDIX D

D.1 VARIABLES USED IN MODEL

Initial Concentration of Sodium Sulphate Decahydrate	= 40 wt.%
Core density (113)	= 1221.8 kg m ⁻³
Heat capacity of core (110)	= 4180 J kg ⁻¹ K ⁻¹
Heat of crystallisation per kg. of water evaporated (114)	= 152 J kg ⁻¹
Latent heat of fusion (110)	= +239 x 10 ³ J kg ⁻¹
Thermal conductivity of crust	= 0.015 W m ⁻¹ K ⁻¹
Partial pressure of drying medium	= 1.61 x 10 ⁻⁴ atm.

Variation of vapour pressure with absolute temperature (113),

$$\log_e p_c = - \frac{5104.05}{T_s} + 20.21 \quad (D.1)$$

where p_c = vapour pressure (mm Hg.)

Porosity function:

$$\epsilon = 1 - 2.4 (\psi/R)$$

Effective diffusivity,

$$D_{\text{eff}} = D_v \epsilon^{1.5}$$

D.2 COMPUTER PROGRAM LISTING

Program Filename: REI MODEL

```

100 REM RECEDING EVAPORATION INTERFACE MODEL
110 REM
120 REM VARIABLES
130 REM R = INITIAL PARTICLE RADIUS (M)
140 REM DC= CORE DENSITY (KG/M3)
150 REM CP= HEAT CAPACITY OF CORE (J/KG/K)
160 REM MW= MOLECULAR WT
170 REM RC= UNI. GAS CONST. (ATM M3/KGMOLE/K)
180 REM CO= PARTIAL PRESS OF AIR (ATM)
190 REM TA= AIR TEMP (K)
200 REM MF= MASS FRACT. OF WATER
210 REM E = POROSITY
220 REM V = VELOCITY OF AIR (M/S)
230 REM CA= HEAT CAPACITY OF AIR (J/KG/K)
240 REM KC= THERMAL COND. OF CRUST (W/M/K)
250 REM HC= HEAT OF CRYSTALLISATION (J/KG)
260 REM RE= REYNOLDS NO.
270 REM PR= PRANDTL NO.
280 REM SC= SCHMIDT NO.
290 REM DA= AIR DENSITY (KG/M3)
300 REM VA= AIR VISCOSITY (KG/M/S)
310 REM DF= DIFFUS. OF VAP. IN AIR (M2/S)
320 REM CH= HEAT TRANSFER COEFF (W/M2/K)
330 REM CM= MASS TRANSFER COEFF (M/S)
340 REM ED= EFFECTIVE DIFFUSIVITY (M2/S)
345 REM KA= THERMAL COND. OF AIR (W/M/K)
346 REM LT= LATENT HEAT OF VAPORISATION (J/KG)
347 REM LF= LATENT HEAT OF FUSION (J/KG)
348 REM H = STEP LENGTH
350 REM A1-A4 = CONSTANTS
360 REM B1-B3 = CONSTANTS
370 REM
500 REM INPUT VARIABLES
505 PI=3.14159:CT=0
510 READ R,DC,CP,MW,RC,CO,TA,MF,V,CA,KC,HC,LF
515 REM
520 REM INPUT INITIAL CONDITIONS
530 READ X1,T1,W1,H
532 WT=W1
535 REM
540 REM SET TIME TO ZERO
542 T=0
543 REM
545 REM OPEN FILES FOR PRINTER
547 OPEN1,4:OPEN2,4,1:OPEN3,4,2
549 F#="" 999.9 99.99 9.999"
551 B#="" 9.999"
559 PRINT#3,F#+B#
560 REM
561 GOSUB 7000
562 REM
564 REM INITIATE INTERGRATION
565 FOR I=0 TO 1000 STEP 25

```

```

570 IF T=I THEN 900
575 REM
580 REM EVALUATE PHYSICAL PROPS
590 GOSUB 7000
595 E=1-2.4*(R-X1)/R
600 RE=R*2*V*DA/VA
610 PR=CA*VA/KA
620 SC=VA/DA/DF
630 CH=KA/2/R*(2+.185*(LT/CA/(TA-T1))†.244*RE†.5*PR†.33)
640 CM=DF/2/R*(2+.185*(LT/CA/(TA-T1))†.244*RE†.5*SC†.33)
645 REM
650 REM CONSTANTS FOR DIFF EQN.
660 A1=R†2*CH*KC/DC/MF/(LT-HC)
670 A2=KC-R*CH
680 A3=R†2*CH
690 A4=CP/3/MF/(LT-HC)
700 REM
710 ED=E†1.5*DF
720 B1=R†2*ED*MW*CM/DC/MF/RC
730 B2=ED-R*CM
740 B3=R†2*CM
750 REM
760 T=T+H
780 GOSUB1000
790 GOSUB2000
800 GOSUB3000
810 X1=X
820 T1=Y
830 W1=Z
835 IF T1>=306.15 THEN GOSUB 7500
840 GOTO 570
850 REM
900 REM PRINT RESULTS
940 T2=T1-273.15
945 X2=(R-X1)
946 W2=(WT-W1)/WT
950 X2=INT(X2*1E6+.5)/1E3
951 T2=INT(T2*1E2+.5)/1E2
952 W2=INT(W2*1E3+.5)/1E3
955 PRINT#2,T;T2;X2;W2
970 NEXT I
980 END
1000 REM
1010 REM RUNGE KUTTA ROUTINE TO INTEGRATE FOR CRUST THICKNESS
1020 GOSUB4000
1030 X2=X1
1040 J1=H*D1
1050 X1=X2+J1/2:GOSUB4000
1060 J2=H*D1

```

```

1070 X1=X2+J2/2:GOSUB4000
1080 J3=H*D1
1090 X1=X2+J3:GOSUB4000
1100 J4=H*D1
1110 X=X2+(J1+2*J2+2*J3+J4)/6
1120 X1=X2
1130 RETURN
2000 REM
2010 REM RUNGE KUTTA ROUTINE TO INTEGRATE FOR CORE TEMP.
2020 GOSUB5000
2030 T2=T1
2040 L1=H*D2
2050 T1=T2+L1/2:GOSUB5000
2060 L2=H*D2
2070 T1=T2+L2/2:GOSUB5000
2080 L3=H*D2
2090 T1=T2+L3:GOSUB5000
2100 L4=H*D2
2110 Y=T2+(L1+2*L2+2*L3+L4)/6
2120 T1=T2
2130 RETURN
3000 REM
3010 REM RUNGE KUTTA ROUTINE TO INTEGRATE FOR WEIGHT OF DROP
3020 GOSUB6000
3030 W2=W1
3040 G1=H*D3
3050 W1=W2+G1/2:GOSUB6000
3060 G2=H*D3
3070 W1=W2+G2/2:GOSUB6000
3080 G3=H*D3
3090 W1=W2+G3:GOSUB6000
3100 G4=H*D3
3110 Z=W2+(G1+2*G2+2*G3+G4)/6
3120 W1=W2
3130 RETURN
4000 REM
4010 REM DIFF. EQN D1
4020 CC=(EXP(-5104.054/T1+20.207))/760
4030 D1=(CC-CC)/T1*(B1/(B2*X112+B3*X1))
4040 RETURN
5000 REM
5010 REM DIFF. EQN D2
5020 GOSUB4000
5030 D2=A1/A4/(A2*X112+A3*X1)*(TA-T1)/X1+(D1/A4/X1)
5040 RETURN
6000 REM
6010 REM DIFF. EQN D3
6020 GOSUB4000
6030 D3=4*PI*DC*MF*X112*D1

```

```

6040 RETURN
7000 REM
7010 REM PHYSICAL PROPS.
7015 TM=((TA-273.15)+(T1-273.15))/2
7020 KA=(4.2956E-5*TM+.014)*1.7307
7030 LT=(1075.95-1.0246*(T1-273.15))*1.326*1E3
7040 VA=4.568E-8*TM+1.7199E-5
7050 DA=1.2929*273.15/(TA+T1)*2
7060 DF=.22*((TA+T1)/2/273.15)1.75/1E4
7070 RETURN
7500 REM
7510 REM LATENT HEAT OF FUSION AT 33 C
7520 IF CT=1 THEN 7560
7530 HF=LF*4/3*PI*R3*DC*(1-MF)
7540 TF=HF/W1/CP
7550 T1=T1-TF
7555 CT=1
7560 RETURN
7570 REM
7700 REM
7800 REM EXP. CONDITIONS LISTING
7805 T7=INT((TA-273.15)*1E2+.5)/1E2
7806 M1=INT((1-MF)*1E2+.5)
7807 R7=INT(2*R*1E6+.5)/1E3
7809 PRINT#1:PRINT#1
7810 PRINT#1,TAB(12);"RECEDING EVAPORATION INTERFACE MODEL"
7820 PRINT#1,TAB(11);"_____""
7830 PRINT#1:PRINT#1
7840 PRINT#1,TAB(8);"AIR TEMPERATURE (C)           =";T7
7850 PRINT#1,TAB(8);"AIR VELOCITY (MM/SEC)         =";V
7860 PRINT#1,TAB(8);"AQ. SOD. SULPH. DECAHYD. (WT %) =";M1
7870 PRINT#1,TAB(8);"INITIAL WT. OF DROP (MG)        =";WT*1E6
7880 PRINT#1,TAB(8);"INITIAL DROP DIAMETER (MM)       =";R7
7900 PRINT#1:PRINT#1
7906 PRINT#1,TAB(33);"CRUST           FRACT. OF INITIAL"
7910 PRINT#1,TAB(8);"TIME(SEC)    CORE TEMP(C)  THICKNESS(MM)";
7920 PRINT#1,"  WT. EVAPORATED" _____";
7930 PRINT#1,TAB(8);"_____""
7940 PRINT#1," _____""
7950 RETURN

```

D.3 TABULATION OF MODEL PREDICTIONS

<u>Tables</u>	<u>Initial Conc. (wt.%)</u>	<u>Air Temp (°C)</u>
D1	40	20
D2	40	40.7
D3	40	59.3
D4	40	78.3

TABLE D 1

RECEDING EVAPORATION INTERFACE MODEL

AIR TEMPERATURE (C) = 20
 AIR VELOCITY (m/s) = 1
 AQ. SOD. SULPH. DECAHYD. (WT %) = 40
 INITIAL WT. OF DROP (mg) = 3.391
 INITIAL DROP DIAMETER (mm) = 1.744

<u>TIME(sec)</u>	<u>CORE TEMP(C)</u>	<u>CRUST THICKNESS(mm)</u>	<u>FRACT. OF INITIAL WT. EVAPORATED</u>
.0	15.00	.000	.000
25.0	8.98	.035	.071
50.0	8.58	.061	.119
75.0	8.61	.084	.160
100.0	8.82	.106	.195
125.0	9.16	.125	.226
150.0	9.58	.143	.253
175.0	10.06	.160	.277
200.0	10.59	.175	.298
225.0	11.14	.189	.316
250.0	11.69	.202	.332
275.0	12.25	.214	.347
300.0	12.79	.225	.359
325.0	13.32	.236	.371
350.0	13.83	.245	.381
375.0	14.31	.253	.390
400.0	14.77	.261	.398
425.0	15.19	.268	.405
450.0	15.59	.275	.412
475.0	15.95	.281	.418
500.0	16.29	.287	.423
525.0	16.60	.292	.427
550.0	16.89	.296	.432
575.0	17.15	.301	.435
600.0	17.38	.305	.439
625.0	17.60	.308	.442
650.0	17.80	.311	.445
675.0	17.97	.314	.448
700.0	18.14	.317	.450
725.0	18.28	.320	.452
750.0	18.42	.322	.454
775.0	18.54	.324	.456
800.0	18.65	.327	.457

TABLE D 2

RECEDING EVAPORATION INTERFACE MODEL

AIR TEMPERATURE (C) = 40.7
 AIR VELOCITY (m/s) = 1
 AQ. SOD. SULPH. DECAHYD. (WT %) = 40
 INITIAL WT. OF DROP (mg) = 2.958
 INITIAL DROP DIAMETER (mm) = 1.666

<u>TIME(sec)</u>	<u>CORE TEMP(C)</u>	<u>CRUST THICKNESS(mm)</u>	<u>FRACT. OF INITIAL WT. EVAPORATED</u>
.0	16.84	.000	.000
25.0	18.95	.048	.100
50.0	18.90	.092	.181
75.0	19.65	.130	.244
100.0	20.97	.163	.293
125.0	22.64	.191	.331
150.0	24.52	.216	.362
175.0	26.50	.237	.387
200.0	28.46	.256	.407
225.0	30.34	.271	.423
250.0	32.06	.284	.435
275.0	34.19	.291	.442
300.0	31.83	.297	.447
325.0	34.94	.305	.454
350.0	36.20	.311	.460
375.0	37.09	.317	.464
400.0	37.80	.321	.468
425.0	38.36	.325	.471
450.0	38.80	.328	.474
475.0	39.15	.330	.475
500.0	39.42	.332	.477
525.0	39.64	.334	.478
550.0	39.81	.336	.479
575.0	39.95	.337	.480
600.0	40.07	.338	.481
625.0	40.16	.339	.482
650.0	40.23	.340	.482

TABLE D 3

RECEDING EVAPORATION INTERFACE MODEL

AIR TEMPERATURE (C) = 59.3
 AIR VELOCITY (m/s) = 1
 AQ. SO₂. SULPH. DECAHYD. (WT %) = 40
 INITIAL WT. OF DROP (mg) = 3.184
 INITIAL DROP DIAMETER (mm) = 1.708

<u>TIME(sec)</u>	<u>CORE TEMP(C)</u>	<u>CRUST THICKNESS(mm)</u>	<u>FRACT. OF INITIAL WT. EVAPORATED</u>
.0	17.09	.000	.000
25.0	25.87	.061	.122
50.0	26.26	.121	.226
75.0	28.23	.170	.299
100.0	31.31	.211	.353
125.0	20.35	.235	.381
150.0	36.25	.258	.406
175.0	40.90	.284	.431
200.0	45.02	.303	.449
225.0	48.72	.318	.462
250.0	51.80	.329	.471
275.0	54.14	.336	.477
300.0	55.81	.341	.480
325.0	56.93	.345	.483
350.0	57.67	.347	.485
375.0	58.16	.349	.486
400.0	58.48	.350	.487

TABLE D 4

RECEDING EVAPORATION INTERFACE MODEL

AIR TEMPERATURE (C) = 78.3
 AIR VELOCITY (m/s) = 1
 AQ. SOD. SULPH. DECAHYD. (WT %) = 40
 INITIAL WT. OF DROP (mg) = 3.184
 INITIAL DROP DIAMETER (mm) = 1.702

<u>TIME(sec)</u>	<u>CORE TEMP(C)</u>	<u>CRUST THICKNESS(mm)</u>	<u>FRACT. OF INITIAL WT. EVAPORATED</u>
.0	17.30	.000	.000
10.0	30.20	.023	.048
20.0	31.55	.059	.118
30.0	31.51	.093	.180
40.0	31.93	.125	.232
50.0	32.92	.153	.274
60.0	16.67	.168	.295
70.0	31.15	.180	.312
80.0	35.65	.201	.339
90.0	38.27	.222	.364
100.0	40.84	.241	.386
110.0	43.63	.259	.405
120.0	46.61	.274	.421
130.0	49.76	.288	.435
140.0	53.02	.301	.446
150.0	56.30	.311	.455
160.0	59.53	.320	.462
170.0	62.62	.327	.468
180.0	65.47	.333	.473
190.0	68.02	.337	.476
200.0	70.21	.341	.479
210.0	72.03	.344	.481
220.0	73.49	.346	.483
230.0	74.64	.348	.484
240.0	75.52	.349	.485
250.0	76.18	.350	.485
260.0	76.68	.351	.486
270.0	77.05	.351	.486
280.0	77.32	.352	.487
290.0	77.53	.352	.487
300.0	77.68	.352	.487

NOMENCLATURE

NOMENCLATURE

The meaning of the symbols are listed below unless otherwise stated in the pertinent text.

<u>Symbol</u>	<u>Meaning</u>
A	Surface area of spherical droplet (m^2)
A_f	Projected area of filament (m^2)
A_p	Projected area of spherical droplet (m^2)
A_m	Mass transfer area
A_h	Heat transfer area
C	Concentration
C_0	Initial concentration (wt.%)
C_1	Integrating constant
C_c	Heat of crystallisation per unit mass of water evaporated ($J\ kg^{-1}$)
C_p	Heat capacity of air ($J\ kg^{-1}\ K^{-1}$)
C_d	Drag coefficient on drop
C_f	Drag coefficient on filament
C_A	Concentration of component A
C_s	Concentration on droplet surface
C_∞	Concentration at infinite distance
C_{pf}	Heat capacity of diffusing vapour
C_{pc}	Heat capacity of core ($J\ kg^{-1}\ K^{-1}$)
D_{AB}	Diffusion coefficient of A in a mixture of A and B
D_v	Molecular diffusivity ($m^2\ s^{-1}$)
D_{eff}	Effective diffusivity ($m^2\ s^{-1}$)

SymbolMeaning

d_p	Drop diameter (m)
d_f	Diameter of filament (m)
d_w	Diameter of wire (m)
d_{pm}	Mean drop diameter (m)
e	Emissivity of water drop
e_g	Emissivity of glass filament
e_w	Emissivity of nickel wire
e_s	Emissivity of slurry droplet
F_a	Geometry factor
F_t	Total drag force (N)
F_d	Drag force on drop (N)
F_f	Drag force on filament (N)
g	Gravitational constant ($m\ s^{-2}$)
H	Henry's Constant
h_g	Gas film heat transfer coefficient ($W\ m^2\ K^{-1}$)
h_f	Heat transfer coefficient for glass filament ($W\ m^2\ K^{-1}$)
i_t	Interfacial tension
J_r	Mass flux
K	Overall mass transfer coefficient ($m\ s^{-1}$)
k	Thermal conductivity of air ($W\ m^{-1}\ K^{-1}$)
k_c	Crust coefficient ($m\ s^{-1}$)
k_g	Gas film mass transfer coefficient ($m\ s^{-1}$)
k_f	Thermal conductivity of diffusing vapour ($W\ m^{-1}\ K^{-1}$)
k_t	Thermal conductivity of glass filament ($W\ m^{-1}\ K^{-1}$)
k_w	Thermal conductivity of nickel wire ($W\ m^{-1}\ K^{-1}$)
k_{tc}	Thermal conductivity of crust ($W\ m^{-1}\ K^{-1}$)

SymbolMeaning

M_w	Molecular weight (kg/kgmole)
\dot{m}	Evaporation rate
\dot{m}_0	Evaporation rate in stagnant medium
\dot{m}_0'	Evaporation rate in stagnant medium neglecting radiation
N_A	Rate of mass transfer per unit area
P_t	Total pressure
p_X	Partial pressure at $r = X$
p_R	Partial pressure at $r = R$
p_c	Vapour pressure on surface of core
p_s	Saturated vapour pressure
p_g	Partial pressure of air
Q	Total heat transferred
Q_e	Total heat transferred by radiation
Q_f	Total heat conducted through glass filament
Q_r	Heat flux
q	Rate of heat transfer
q_e	Rate of heat transfer by radiation
q_f	Rate of heat transfer to a drop through the filament
q_w	Rate of heat transfer to a drop through the nickel wire
R	Outer radius of crust
R_l	Correlation coefficient
R_c	Universal gas constant ($\text{Atm m}^3 \text{ kgmole}^{-1} \text{ K}^{-1}$)
R_f	Outer radius of gas film surrounding a droplet
r_0	Initial radius of evaporating droplet
r_1	Radius of evaporating droplet

<u>Symbol</u>	<u>Meaning</u>
S_s	Rate of production of fresh surface
T'	Temperature (K)
T_g, T_g'	Gas temperature in $^{\circ}\text{C}$ and K respectively
T_s, T_s'	Drop temperature in $^{\circ}\text{C}$ and K respectively
ΔT	Temperature driving force
T_f	Average film temperature ($^{\circ}\text{C}$)
T_c	Core temperature ($^{\circ}\text{C}$)
T_R	Temperature at $r = R$ ($^{\circ}\text{C}$)
T_X	Temperature at $r = X$ ($^{\circ}\text{C}$)
T_w'	Temperature of nickel wire (K)
ΔT_s	Fall in drop temperature
T_{sm}'	Mean drop temperature (K)
V	Voltage (mV)
v	Velocity (m s^{-1})
W	Weight of drop (kg)
W_i	Length of exposed nickel wire
W_c	Weight correction for radiation and conduction
X	Interface between crust and core
x_w	Mass fraction of water

DIMENSIONLESS GROUPS

B	Transfer No. = $C_p \Delta T / \lambda$
B'	Spalding No. = $C_p \Delta T (\lambda - q/\dot{m})$
Bo	Bond No. = $(\rho_c - \rho_d) d_p^2 g \cdot i_t$

<u>Symbol</u>	<u>Meaning</u>
Gr	Grashof No. = $d_p^3 \rho^2 g \cdot \beta_1 \Delta T / \mu^2$
Nu	Nusselt No. = $h_g d_p / k$
Nu ₀	Nusselt No. under stagnant conditions
Nu _A	Nusselt No. under elevated temperatures
Pr	Prandtl No. = $C_p \mu / k$
Re	Reynolds No. = $v d_p \rho / \mu$
Re _g	Reynolds No. of gas stream
Re _f	Reynolds No. for glass filament
Sh	Sherwood No. = $k_g d_p / D_v$
Sh ₀	Sherwood No. under stagnant conditions
Sc	Schmidt No. = $\mu \cdot D_v / \rho$

GREEK SYMBOLS

β	Coefficient in Frössling's equation
β_1	Coefficient of expansion
ϵ	Porosity
λ	Latent heat of vaporisation ($J \text{ kg}^{-1}$)
λ_f	Latent heat of fusion ($J \text{ kg}^{-1}$)
μ	Viscosity of air ($\text{kg m}^{-1} \text{ s}^{-1}$)
μ_c	Viscosity of continuous phase ($\text{kg m}^{-1} \text{ s}^{-1}$)
μ_d	Viscosity of dispersed phase ($\text{kg m}^{-1} \text{ s}^{-1}$)
ρ	Density of air (kg m^{-2})
ρ_c	Density of continuous phase (kg m^{-3})
ρ_d	Drop density (kg m^{-3})

SymbolMeaning

ρ_{co}	Core density (kg m^{-3})
σ	Stefan-Boltzmann Constant
ψ	Crust thickness
\emptyset	Constant in Nusselt equation
θ	Time (sec)
$\Delta\theta$	Time interval
η	Index in Nusselt equation
π	Constant = 3.1416

REFERENCES

REFERENCES

1. Fick, A., Ann. Phys., 94, 59 (1855).
2. Whitman, W.G., Chem. Met. Eng., 29, 147 (1923).
3. Higbie, R., Trans. Am. Inst. Chem. Eng., 31, 365 (1935).
4. Danckwerts, P.V., Ind. Eng. Chem., 43, 1460 (1951).
5. Toor, H.L., Marchello, J.M., A.I.Ch.E. Journal, 4, 97 (1958).
6. Frössling, N., Gerlands Beitr. zur Geophysik, 52, 170 (1938).
7. Maxwell, J.C., Collected Scientific Papers, Cambridge, 11, 625 (1890).
8. Sreznevskii, V., Zh. R. Ph. Kh. O., 14, 420, 483 (1882).
9. Morse, H.W., Proc. Am. Acad. Sci., 45, 363 (1910).
10. Langmuir, I., Phys. Rev., 12, 368 (1918).
11. Whytlaw-Gray, R., Patterson, H., Smoke (Dym.), Goskhimizdat, M, 149 (1934).
12. Topley, B., Whytlaw-Gray, R., Phil. Mag., 4, 873 (1927).
13. Houghton, H.G., Physics, 4, 419 (1933).
14. Langstroth, G.O., Diehl, C.H., Winhold, E.J., Canad. J. Res., 28A, 574 (1950).
15. Ranz, W.E., Marshall, W.R., Chem. Eng. Prog., 48, 141, 173 (1952).
16. Mathers, W.G., Madden, A.J., Piret, E.L., Ind. Eng. Chem., 49, 961 (1957).

17. Steinberger, R.L., Treybal, R.E., A.I.Ch.E. Journal, 6, 227 (1960).
18. Yuge, T., Trans. A.S.M.E., 82, Series C, 214 (1960).
19. Woodland, D.J., Mack, E., J. Am. Chem. Soc., 55, 3149 (1933).
20. Nestle, R., Z. Physik, 77, 174 (1932).
21. Gudris, N., Kulikova, L., Z. Physik, 25, 121 (1924).
22. Majama, Togino, Bull. Inst. Phys. Chem. Res. (Tokyo), 9, 339 (1930).
23. Vyrubov, D.N., The Mechanism of the Internal Combustion Engine and its Ancillary Parts, Mashgiz, 5 (1946).
24. Johnstone, H.F., Eades, D.K., Ind. Eng. Chem., 42, 2293 (1950).
25. Kinzer, G.D., Gunn, R., J. Meteor., 81, 71 (1951).
26. Hsu, N.T., Sato, K., Sage, B.H., Ind. Eng. Chem., 46, 870 (1954).
27. Ingebo, R.D., Chem. Eng. Prog., 48, 403 (1952).
28. Maisel, D.S., Sherwood, T.K., Chem. Eng. Prog., 46, 131, 172 (1950).
29. Garner, F.H., Grafton, R.W., Proc. Roy. Soc. (London), A224, 64 (1954).
30. Garner, F.H., Suckling, R.D., A.I.Ch.E. Journal, 4, 114 (1958).

31. Evnochides, S., Thodos, G., A.I.Ch.E. Journal, 7, 78 (1961).
32. Pasternak, I.S., Gauvin, W.H., Canad. J. Chem. Eng., 38, 35 (1960).
33. Pasternak, I.S., Gauvin, W.H., A.I.Ch.E. Journal, 7, 254 (1961).
34. Fuchs, N.A., Evaporation and droplet growth in gaseous media, Pergamon Press, London (1959).
35. Ward, D.M., Trass, O., Johnson, A.I., Canad. J. Chem. Eng., 40, 164 (1962).
36. Jones, S.J.R., Smith, W., Proc. Symp. Interaction between fluid and particles, Inst. Chem. Eng., London, 190 (1962).
37. Kinard, G.E., Manning, F.S., Manning, W.P., Brit. Chem. Eng., 8, 326 (1963).
38. Locheil, A.C., Calderbank, P.H., Chem. Eng. Sci., 19, 471 (1964).
39. Hoffman, T.W., Ross, L.L., Int. J. Heat Mass Transfer, 15, 599 (1972).
40. Silbulkin, M.J., J. Aero. Sci., 19, 570 (1952).
41. Aksel'rud, G.A., Zh.Fiz. Khim, 27, 1445 (1953).
42. Ranz, W.E., Trans. A.S.M.E., 78, 909 (1956).
43. Audu, T.O.K., Ph.D. Thesis, University of Aston in Birmingham, England, (1973).
44. Frazier, G.C., Chang, H.W., Canad. J. Chem. Eng., 55, 678 (1977).
45. Frazier, G.C., Chang, H.W., Canad. J. Chem. Eng., 55, 736 (1977).

46. Hoffman, T.W., Gauvin, W.H., *Canad. J. Chem. Eng.*, 35, 129 (1960).
47. Miura, K., Miura, T., Ohtani, S., *A.I.Ch.E. Symp. Ser.*, 73, 95 (1977).
48. Garner, F.H., Kendrick, P., *Trans. Inst. Chem. Eng.*, 37, 155 (1959).
49. Davis, E.J., Ray, A.K., Chang, R., *A.I.Ch.E. Symp. Ser.*, 74, 190 (1978).
50. Sandoval-Robles, J.G., Riba, J.P., Couderc, J.P., *Trans. Inst. Chem. Eng.*, 58, 132 (1980).
51. Büttner, K., *Veröff preuss. met. Inst.*, 10, No.5, (1934).
52. Williams, G.C., D.Sc. Thesis, Massachusetts Inst. Tech., (1942).
53. Vyubov, D.N., *J. Tech. Phys. Moscow*, 9, 1923 (1939). (Canadian Defence Res. Board Translation, Sept. 1949).
54. Johnstone, H.F., Pigford, R.L., Chapin, J.H., *Trans. Am. Inst. Chem. Eng.*, 37, 95 (1941).
55. Kramers, H., *Physica's Grav.*, 12, 61 (1946).
56. Rowe, P.N., Claxton, K.T., Lewis, J.B., *Trans. Inst. Chem. Eng.*, 43, T14 (1965).
57. Tsubouchi, T., Sato, S., *Chem. Eng. Prog. Symp. Ser.*, 56, 269, 285 (1960)
58. Adams, A.E.S., Pinder, K.L., *Canad. J. Chem. Eng.*, 50, 707 (1972).

59. Marshall, W.R., Trans. A.S.M.E., 77, 1377 (1955).
60. Pei, D.C.T., Gauvin, W.H., A.I.Ch.E. Journal,
9, 375 (1963).
61. Pei, D.C.T., Narasimhan, C., Gauvin, W.H., Proc.
Symp. Interaction between fluid and particles,
Inst. Chem. Eng. London, 243 (1962).
62. Downing, C.G., A. I. Ch. E. Journal, 12, 760
(1966).
63. Spalding, D.B., 4th Int. Symp. on Combustion, 847,
Williams and Williams, Baltimore, Maryland,
(1953).
64. Toei, R., Okazaki, M., Kubota, K., Ohaski, K.,
Mizata, K., Chem. Eng. (Japan), 30, 43 (1966).
65. Lee, K., Ryley, D.J., J. Heat Transfer, Trans. A.S.M.E.,
90, 445 (1968).
66. Frazier, G.C., Hellier, W.W., Ind. Eng. Chem.
Fundam., 8, 807 (1969).
67. Crosby, E.J., Stewart, W.E., Ind. Eng. Chem.,
Fundam., 9, 515 (1970).
68. Trommelen, A.M., Crosby, E.J. A.I.Ch.E. Journal
16, 857 (1970).
69. Matlosz, R.L., Leipziger, S., Torda, T.P., Inst.
J. Heat Mass Transfer, 15, 831 (1972).
70. Kadota, T., Hiroyasu, H., Bull. J.S.M.E., 19,
1515 (1976).
71. Hiroyasu, H., et al., Trans. J.S.M.E., 40,
3147 (1974).

72. Charlesworth, D.H., Marshall, W.R., A.I.Ch.E. Journal, 6, 9 (1960).
73. Lewis, W.K., Ind. Eng. Chem., 13, 427 (1921).
74. Sherwood, T.K., Ind. Eng. Chem., 21, 12, 976 (1929).
75. Buckingham, E., U.S. Dept. Agr. Bur. Solids, Bull., 38 (1907).
76. Ceaglske, N.H., Hougen, O.A., Trans. Am. Inst. Chem. Eng., 33, 283 (1937).
77. Gurr, C.G., Marshall, T.K., Hutton, J.T., Soil Sci., 74, 335 (1952).
78. Hutcheon, W.L., Highw. Res. Bd. Spec. Rep., 40, 113 (1958).
79. Kuzmak, J.M., Sereda, P.J., Soil Sci., 84, 419 (1957).
80. Harmathy, T.Z., Ind. Eng. Chem. Fundam., 8, 92 (1969).
81. Lykov, A.V., Mikhailov, Y.A., Theory of Energy and Mass Transfer, Pergammon Press, Oxford, (1965).
82. Duffie, J.A., Marshall, W.R., Chem. Eng. Prog. 49, 417 (1953).
83. Miura, K., Atarashiya, K., Ouchi, I., Ohtani, S., Kagaku Kogaku, 35, 643 (1971) - Translation:- Heat Transfer, Jap. Res., 1, 11 (1972).
84. Audu, T.O.K., Jeffreys, G.V., Trans. Inst. Chem. Eng., 53, 165 (1975).

85. Joffre, G., Prunet-Foch, B., Cloupeau, M., C.R.
Hebd. Seances Acad. Sci. Ser., B., 284, 81
(1977).
86. El Golli, S., Bricard, J., Treiner, C., J. Aerosol
Sci., 10, 177 (1979).
87. Wijlhuizen, A.E., Kerkhof, R.J.A.M., Bruin, S., Chem.
Eng. Sci., 34, 651 (1979).
88. Van der Lijn, J., Ph.D. Thesis, Agricultural University
Wageningen, Netherlands, (1976).
89. Haertling, M., Drying '80, Vol 1., Hemisphere Publ.
Corp., N.Y. (1980).
90. Esubiyi, A.O., Ph.D. Thesis, University of Aston in
Birmingham, England (1980).
91. Coulson, J.M., Richardson, J.F., Chemical Engineering,
Vol. 2., 2nd Edition, Pergammon Press, Oxford (1968).
92. Sano, Y., Keey, R.B., Chem. Eng. Sci., 37, 881 (1982).
93. Sano, Y., Yamamoto, S., Proc. Third Inst. Drying
Symp., 1, 535 (1982).
94. Masters, K., Spray Drying, 2nd Edition, John
Wiley and Sons, N.Y. (1976).
95. Probert, R.P., Phil. Mag., 37, 94 (1946).
96. Rosin, P., Rammler, E., J. Inst. Fuel, 7, 29
(1933).
97. Fledderman, R.G., Hanson, A.R., Univ. Michigan
Res. Dept. CM 667 (1951).

98. Nukiyama, S., Tanasawa, Y., Trans. Soc. Mech. Eng., (Japan), 4, 86 (1937)
99. Manning, W.P., Gauvin, W.H., A.I.Ch. E. Journal, 6, 184 (1960).
100. Bose, A.K., Pei, D.C.T., Canad. J. Chem. Eng., 42, 259 (1964).
101. Dlouhy, J., Gauvin, W.H., A.I.Ch.E. Journal, 6, 29 (1960).
102. Dickinson, D.R., Marshall, W.R., A.I.Ch.E. Journal, 14, 541 (1968).
103. Miura, T., Ohtani, S., Kagaku Kogaku Ronbunshu, 5, 130 (1979).
104. Baltas, L., Gauvin, W.H., A.I.Ch.E. Journal, 15, 764, 772 (1969).
105. Katta, S., Gauvin, W.H., A.I.Ch.E. Journal, 21, 143 (1975).
106. Miura, T., Ohtani, S., Maeda, S., Drying '80, Vol 1, Hemisphere Publ. Corp., N.Y. (1980).
107. Williams, G.C., Schmitt, R.O., Ind. Eng. Chem. 38, 967 (1946).
108. Holland, L., Vacuum Deposition of Thin Films, Chapman and Hall Limited, London (1956).
109. Perry, R.H., Chilton, C.H., Chemical Engineers' Handbook, 5th Ed., McGraw-Hill Kogakusha Ltd., Tokyo (1973).
110. International Critical Tables, Vol 5, 1st ed., McGraw-Hill Ltd., N.Y. (1933).

111. Kaye, G.W.C., Laby, T.H., Tables of Physical and Chemical Constants, 13th Edition, Longmans, London, (1966).
112. Glasstone, S., Text Book of Physical Chemistry, 1st ed., Macmillan Ltd., London (1940).
113. International Critical Tables, Vol 3, 1st ed., McGraw-Hill Ltd., N.Y. (1933).
114. Kirk-Othmer Encyclopaedia of Chemical Technology, Vol 21, 248, 3rd ed., John Wiley and Sons, N.Y. (1983).